Oxidative Medicine and Cellular Longevity

Mitochondrial Health in Aging and Age-Related Metabolic Disease

Guest Editors: David Sebastián, Rebeca Acín-Pérez, and Katsutaro Morino

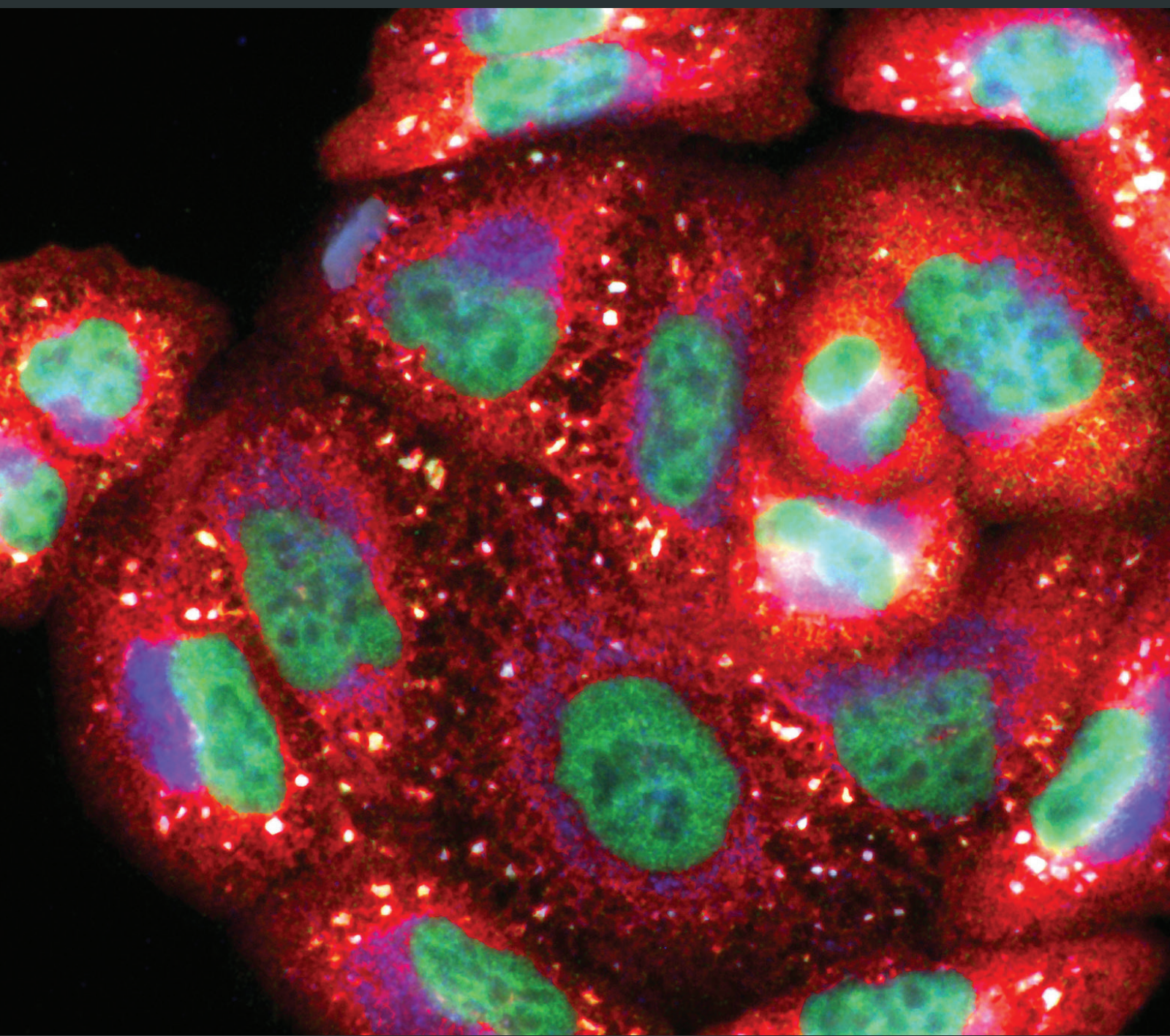

Mitochondrial Health in Aging and Age-Related Metabolic Disease

Oxidative Medicine and Cellular Longevity

Mitochondrial Health in Aging and Age-Related Metabolic Disease

Guest Editors: David Sebastián, Rebeca Acín-Pérez, and Katsutaro Morino

Copyright © 2016 Hindawi Publishing Corporation. All rights reserved.

This is a special issue published in "Oxidative Medicine and Cellular Longevity." All articles are open access articles distributed under the Creative Commons Attribution License, which permits unrestricted use, distribution, and reproduction in any medium, provided the original work is properly cited.

Editorial Board

Mohammad Abdollahi, Iran
Antonio Ayala, Spain
Neelam Azad, USA
Peter Backx, Canada
Damian Bailey, UK
Consuelo Borrás, Spain
Vittorio Calabrese, Italy
Angel Catalá, Argentina
Shao-Yu Chen, USA
Zhao Zhong Chong, USA
Giuseppe Cirillo, Italy
Massimo Collino, Italy
Mark J. Crabtree, UK
Manuela Curcio, Italy
Andreas Daiber, Germany
Felipe Dal Pizzol, Brazil
Francesca Danesi, Italy
Domenico D'Arca, Italy
Yolanda de Pablo, Sweden
James Duce, UK
Grégory Durand, France
Javier Egea, Spain
Amina El Jamali, USA
Ersin Fadillioglu, Turkey
Qingping Feng, Canada
Giuseppe Filomeni, Italy
Swaran J. S. Flora, India
Rodrigo Franco, USA
José Luís García-Giménez, Spain
Janusz Gebicki, Australia
Husam Ghanim, USA
Laura Giamperi, Italy
Daniela Giustarini, Italy
Saeid Golbidi, Canada
Tilman Grune, Germany
Hunjoo Ha, Republic of Korea
Nikolas Hodges, UK
Tim Hofer, Norway
Silvana Hrelia, Italy
Maria G. Isaguliants, Sweden
Vladimir Jakovljevic, Serbia
Peeter Karihtala, Finland
Raouf A. Khalil, USA
Kum Kum Khanna, Australia
Neelam Khaper, Canada
Thomas Kietzmann, Finland
Mike Kingsley, UK
Ron Kohen, Israel
Werner Koopman, Netherlands
Jean-Claude Lavoie, Canada
Christopher Horst Lillig, Germany
Paloma B. Liton, USA
Nageswara Madamanchi, USA
Kenneth Maiese, USA
Tullia Maraldi, Italy
Reiko Matsui, USA
Steven McAnulty, USA
Bruno Meloni, Australia
Trevor A. Mori, Australia
Ryuichi Morishita, Japan
Ange Mouithys-Mickalad, Belgium
Hassan Obied, Australia
Pál Pacher, USA
Valentina Pallottini, Italy
David Pattison, Australia
Serafina Perrone, Italy
Tiziana Persichini, Italy
Vincent Pialoux, France
Chiara Poggi, Italy
Aurel Popa-Wagner, Germany
Ada Popolo, Italy
José L. Quiles, Spain
Walid Rachidi, France
Kota V. Ramana, USA
Pranela Rameshwar, USA
Sidhartha D. Ray, USA
Alessandra Ricelli, Italy
Francisco J. Romero, Spain
Vasantha Rupasinghe, Canada
Gabriele Saretzki, UK
Honglian Shi, USA
Cinzia Signorini, Italy
Dinender K. Singla, USA
Richard Siow, UK
Shane Thomas, Australia
Rosa Tundis, Italy
Giuseppe Valacchi, Italy
Jeannette Vasquez-Vivar, USA
Victor M. Victor, Spain
Michal Wozniak, Poland
Sho-ichi Yamagishi, Japan
Liang-Jun Yan, USA
Guillermo Zalba, Spain
Jacek Zielonka, USA

Contents

Hindawi Publishing Corporation
Oxidative Medicine and Cellular Longevity
Volume 2016, Article ID 5831538, 2 pages
http://dx.doi.org/10.1155/2016/5831538

Editorial

Mitochondrial Health in Aging and Age-Related Metabolic Disease

David Sebastián,[1,2,3] Rebeca Acín-Pérez,[4] and Katsutaro Morino[5]

[1]*Institute for Research in Biomedicine (IRB Barcelona), The Barcelona Institute of Science and Technology, Baldiri Reixac 10-12, 08028 Barcelona, Spain*
[2]*Departament de Bioquímica i Biomedicina Molecular, Facultat de Biologia, Universitat de Barcelona, 08028 Barcelona, Spain*
[3]*Instituto de Salud Carlos III, Centro de Investigación Biomédica en Red de Diabetes y Enfermedades Metabólicas Asociadas (CIBERDEM), Madrid, Spain*
[4]*Centro Nacional de Investigaciones Cardiovasculares (CNIC), 28029 Madrid, Spain*
[5]*Division of Endocrinology and Metabolism, Department of Medicine, Shiga University of Medical Science, Tsukinowa, Seta, Otsu, Shiga 520-2192, Japan*

Correspondence should be addressed to David Sebastián; david.sebastian@irbbarcelona.org

Received 15 June 2016; Accepted 16 June 2016

Copyright © 2016 David Sebastián et al. This is an open access article distributed under the Creative Commons Attribution License, which permits unrestricted use, distribution, and reproduction in any medium, provided the original work is properly cited.

Aging is a biological process characterized by a progressive accumulation of damage that finally leads to disrupted metabolic homeostasis leading to cell damage. One of the hallmarks of aging is the presence of mitochondrial dysfunction translated in a decline in mitochondrial respiration and oxidative capacity, reduced mitochondrial mass, morphological alterations of mitochondria, and increase in oxidative stress. Therefore, preservation of mitochondrial health is crucial for maintaining tissue homeostasis during aging. Several mitochondrial quality control mechanisms have been identified, such as pathways related to protein folding and degradation, also known as mitochondrial unfolding protein response (mtUPR), as well as pathways involved in the turnover of mitochondria (mitophagy). However the direct link between quality control mechanisms and loss of mitochondrial health observed during aging and age-related alterations is still unknown. In this special issue, different research articles, performed by independent groups, address the role of mitochondrial function in the frame of aging or age-related pathologies using different experimental approaches and models. Although mitochondrial fitness is declined due to different pathological alterations, most of them converge in two critical hotspots: increase of reactive oxygen species leading to oxidative damage and metabolic maladaptation as leading causes of unhealthy aging.

H. Yamamoto et al. investigated the effects of a traditional Indian medicinal plant, Amla, on mitochondrial function. Amla has been shown to improve age-related pathology by decreasing oxidative stress. In their article, H. Yamamoto et al. show that Amla increases mitochondrial function and biogenesis, together with an activation of Nrf2, which together explain the antioxidant actions of Amla.

In their research article, A. V. Lokhmatikov et al. study the capacity of several natural antioxidants in the maintenance of mitochondrial health. Mitochondrial cardiolipin (CL) oxidation is increased in aging and age-related pathologies and is considered one of the first signaling elements of the mitochondrial apoptotic pathway. By using a chemical model resembling the mitochondrial membrane, they show that amphiphilic antioxidants can prevent oxidation of CL trapped within the respiratory supercomplexes and then preserve mitochondrial function.

Mitochondrial dysfunction has been also associated with coronary heart disease (CHD) and diabetes. O. M. Duicu et al. have found a more severe mitochondrial dysfunction in patients with CHD and diabetes than in patients with only CHD, characterized by a lower mitochondrial respiration. Importantly, this mitochondrial dysfunction is associated with increase in oxidative stress which was reduced when monoamine oxidase (MAO) was inhibited, pointing out to MAO as an important contributor to oxidative stress in CHD.

Neurodegeneration is also associated with aging and mitochondrial dysfunction. In this special issue, two research articles address the role of mitochondria in neurodegenerative diseases. F. Zhao et al. study the role of AP39, a new hydrogen sulphide donor with beneficial effects in Alzheimer's disease (AD). They found that AP39 sustains mitochondrial bioenergetics in neurons coming from an AD mouse model, leading to a decrease in ROS and an increase in cell viability. Moreover, administration of this compound to a mouse model of AD inhibited brain atrophy and ameliorated the alterations seen in AD. K. Peng et al. address the protective effect of resveratrol on a rotenone-induced model of Parkinson's disease (PD). They demonstrate that resveratrol increases mitochondrial mass and fusion and decreases ROS levels, leading to neurotoxicity protection, increased survival rate, and motor ability.

Finally, R. Pääsuke et al. evaluate the alterations in energy metabolism in muscle satellite cells during aging. By using myoblasts isolated from biopsies from young and old subjects, they show that both aging *in vitro* (increase in passages) and aging *in vivo* (myoblasts from young and old subjects) are associated with a reduced mitochondrial respiration and increased glycolysis.

Taken altogether, the data presented in the different research articles of this special issue suggest that manipulations aimed at preserving mitochondrial function and health, mainly targeting oxidative damage and metabolic adaptations, could contribute to the amelioration of aging and age-related pathologies and could help in the development of novel therapeutic approaches.

David Sebastián
Rebeca Acín-Pérez
Katsutaro Morino

Hindawi Publishing Corporation
Oxidative Medicine and Cellular Longevity
Volume 2016, Article ID 1735841, 11 pages
http://dx.doi.org/10.1155/2016/1735841

Research Article

Amla Enhances Mitochondrial Spare Respiratory Capacity by Increasing Mitochondrial Biogenesis and Antioxidant Systems in a Murine Skeletal Muscle Cell Line

Hirotaka Yamamoto,[1,2] Katsutaro Morino,[2] Lemecha Mengistu,[2] Taishi Ishibashi,[1] Kohei Kiriyama,[1] Takao Ikami,[1] and Hiroshi Maegawa[2]

[1]*Institute for Health Science, MIKI Corporation, 3-12-4, Naruohama, Nishinomiya, Hyogo 663-8142, Japan*
[2]*Department of Medicine, Division of Endocrinology and Metabolism, Shiga University of Medical Science, Tsukinowa, Seta, Otsu, Shiga 520-2192, Japan*

Correspondence should be addressed to Katsutaro Morino; morino@belle.shiga-med.ac.jp

Received 26 December 2015; Revised 25 March 2016; Accepted 4 May 2016

Academic Editor: Thomas Kietzmann

Copyright © 2016 Hirotaka Yamamoto et al. This is an open access article distributed under the Creative Commons Attribution License, which permits unrestricted use, distribution, and reproduction in any medium, provided the original work is properly cited.

Amla is one of the most important plants in Indian traditional medicine and has been shown to improve various age-related disorders while decreasing oxidative stress. Mitochondrial dysfunction is a proposed cause of aging through elevated oxidative stress. In this study, we investigated the effects of Amla on mitochondrial function in C2C12 myotubes, a murine skeletal muscle cell model with abundant mitochondria. Based on cell flux analysis, treatment with an extract of Amla fruit enhanced mitochondrial spare respiratory capacity, which enables cells to overcome various stresses. To further explore the mechanisms underlying these effects on mitochondrial function, we analyzed mitochondrial biogenesis and antioxidant systems, both proposed regulators of mitochondrial spare respiratory capacity. We found that Amla treatment stimulated both systems accompanied by AMPK and Nrf2 activation. Furthermore, we found that Amla treatment exhibited cytoprotective effects and lowered reactive oxygen species (ROS) levels in cells subjected to t-BHP-induced oxidative stress. These effects were accompanied by increased oxygen consumption, suggesting that Amla protected cells against oxidative stress by using enhanced spare respiratory capacity to produce more energy. Thus we identified protective effects of Amla, involving activation of mitochondrial function, which potentially explain its various effects on age-related disorders.

1. Introduction

Amla is one of the most important botanical materials in Indian traditional medicine, "Ayurveda." It has been used for many diseases including diabetes, osteoporosis, liver dysfunction, and anemia, not only in India but also in other countries [1, 2]. Recently, the chemical composition of Amla was analyzed, showing relatively high levels of phenolic compounds [2]. A recent clinical study showed that Amla extract improved endothelial function in patients with type 2 diabetes mellitus [3]. Furthermore, its antioxidant [4], hepatoprotective [5], nephroprotective [6], hypolipidemic [7, 8], cardioprotective [9, 10], and antidiabetic effects [11] were demonstrated in *in vivo* animal models. One potential mechanism for these effects was reduction of oxidative stress, based on observations of decreased oxidative stress with Amla treatment. However, the detailed mechanisms have not yet been fully identified.

Accumulating evidence suggested a central role for mitochondria in aging through production of both energy and reactive oxygen species (ROS). Mitochondria can produce substantial energy through aerobic metabolism, though they also produce ROS as unwanted byproducts, causing serious damage to various cellular components. Because mitochondria are the major ROS producing organelle, they are also vulnerable to injury by ROS. Damaged mitochondria produce more ROS, leading to further mitochondrial damage [12]. These defective mitochondria exhibit impaired energy

production and increased oxidative stress, both negatively impacting cellular function. Numerous reports implicated mitochondrial dysfunction in many pathologies or disorders related to the aging process [13, 14]. Mitochondrial spare respiratory capacity is regarded as an important aspect of mitochondrial function and is defined as the difference between basal ATP production and its maximal activity. When cells are subjected to stress, energy demand increases, with more ATP required to maintain cellular functions. A cell with a larger spare respiratory capacity can produce more ATP and overcome more stress, including oxidative stress [15]. Therefore, we hypothesized that Amla could improve mitochondrial function, especially spare respiratory capacity, and exert positively effects on various disorders related to oxidative stress.

To explore the effects of Amla on mitochondrial function, we used a skeletal muscle cell known to contain abundant mitochondria. Using this model, we investigated the molecular mechanisms of Amla's beneficial effects.

2. Materials and Methods

2.1. Plant Materials. A commercial product of Amla fruit juice extract (SunAmla) was obtained from Taiyo Kagaku Co., Ltd. (Mie, Japan). It is a dried powder of water extract from fresh Amla fruit and was previously shown to contain ~30% polyphenols and 2% vitamin C [6]. To confirm the equivalence of Amla used in this study, total polyphenol was analyzed by a colorimetric method using gallic acid as a standard [6], and vitamin C content was analyzed by high-performance liquid chromatography (HPLC) as previously reported [16]. Glucose and fructose in Amla were analyzed by HPLC as previously reported [17]. To prepare Amla extract stock solution, the extract was dissolved in distilled water at a concentration of 200 mg/mL and then sterilized using a polyvinylidene difluoride membrane filter (Merck Millipore, Darmstadt, Germany).

2.2. Reagents. Oligomycin, carbonyl cyanide-p-trifluoromethoxyphenylhydrazone (FCCP), rotenone, and antimycin A were obtained from Seahorse Bioscience (North Billerica, MA, USA) in XF Cell Mito Stress Test kit (#103015-100). Water soluble tetrazolium salts for the MTT assay were from Kishida Chemical Co., Ltd. (Osaka, Japan). 2′,7′-Dichlorofluorescein diacetate (D6883) and *tert*-butyl hydroperoxide (t-BHP; 458139) were obtained from Sigma-Aldrich (St. Louis, MO, USA).

2.3. Cell Culture. C2C12 myoblasts were obtained from the American Type Culture Collection (ATCC; Manassas, VA, USA) and grown in Dulbecco's modified Eagle's medium (DMEM) supplemented with 10% (v/v) fetal bovine serum (FBS), 100 units/mL penicillin, and 100 mg/mL streptomycin in a humidified atmosphere of 95% air and 5% CO_2 at 37°C. At confluence, myoblasts were induced to differentiate in DMEM with 2% FBS, 100 units/mL penicillin, and 100 mg/mL streptomycin. Differentiation medium was replaced every 48 h. Human embryonic kidney 293 (HEK293) cells were obtained from the Japanese Collection of Research Bioresources cell bank (Osaka, Japan) and grown in Eagle's minimum essential medium with 10% (v/v) FBS, 100 units/mL penicillin, and 100 mg/mL streptomycin in a humidified atmosphere of 95% air and 5% CO_2 at 37°C. For Amla treatment, Amla stock solution was diluted with medium to final concentrations of 100 μg/mL and 200 μg/mL.

2.4. Measurement of Mitochondrial Function. Mitochondrial function in C2C12 myotubes was analyzed using the XFe24 flux analyzer with XF Cell Mito Stress Test kit according to manufacturer instructions (Seahorse Bioscience). Briefly, differentiated C2C12 myotubes were prepared on Seahorse 24-well plates and treated with or without Amla (100 μg/mL or 200 μg/mL) for 48 h. The culture medium was changed at least 40 min prior to the assay to unbuffered DMEM supplemented with 5 mM glucose. The oxygen consumption ratio (OCR, pmol/min) was monitored in real time, with sequential treatments with oligomycin (ATP synthase inhibitor), FCCP (mitochondrial uncoupler), and rotenone/antimycin A (respiration inhibitor) to evaluate OCR from proton leak, maximum respiration capacity, and nonmitochondrial respiration, respectively. OCR was measured multiple times at 8 min intervals at each stage, and average values were determined. Nonmitochondrial respiration was subtracted from OCR at each stage to calculate the net OCR for Basal, Leak, and Max values. Mitochondrial respiratory spare capacity and ATP-transratio were calculated by the formula shown in Figure 1(a), left panel.

2.5. Nucleic Acid and Protein Isolation. Total DNA was isolated using a Qiamp DNA mini kit (Qiagen, Mississauga, ON, Canada) according to manufacturer instructions. RNA and total protein were isolated using a PARIS kit (AM1921; Thermo Fisher Scientific, Waltham, MA, USA). Nuclear lysates were isolated using a nuclear/cytosol-fractionation kit (K266; Biovision, Inc., Milpitas, CA, USA) according to manufacturer protocol. Isolated protein samples were denatured by boiling in sodium dodecyl sulfate (SDS) sample buffer.

2.6. Western Blot. Proteins were separated by SDS-polyacrylamide gel electrophoresis and transferred onto polyvinylidene fluoride membranes. Immunoblotting was performed with primary antibodies against phosphorylated AMPKα (#2531; Cell Signaling Technology, Danvers, MA, USA), AMPKα (#2603; Cell Signaling Technology), Nrf2 (SC-722; Santa Cruz Biotechnology, Dallas, TX, USA), and YY-1 (ab109237; Abcam, Tokyo, Japan), with horseradish peroxidase-conjugated secondary antibodies (GE Healthcare Japan, Tokyo, Japan). YY-1 was used as a nuclear-loading control. The intensity of protein bands was visualized using a chemiluminescence detection reagent (PerkinElmer, Inc., Waltham, MA, USA) and a WSE-6100 luminograph system (ATTO, Tokyo, Japan).

2.7. Quantitative PCR for Mitochondrial DNA (mtDNA) Content. mtDNA content was analyzed as previously described

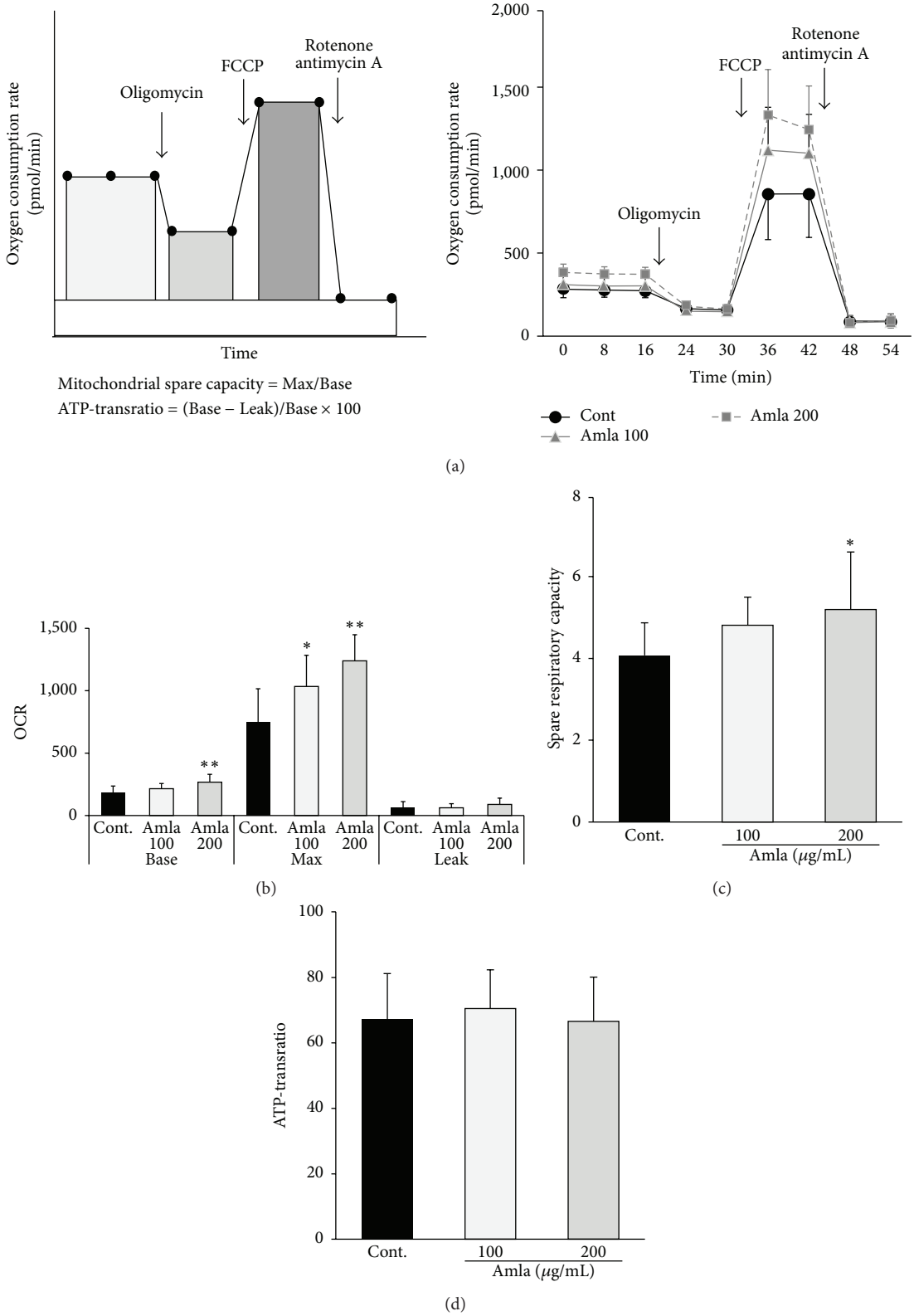

Figure 1: Amla treatment stimulated mitochondrial bioenergetic function. C2C12 myotubes were pretreated with two doses of Amla (100 μg/mL or 200 μg/mL) for 48 h and subjected to mitochondrial function analysis. ((a), left panel) Schematic figure analyzing mitochondrial function using an extracellular flux analyzer. After measuring basal OCR, oligomycin, FCCP, and rotenone/antimycin A were sequentially injected to measure OCR from proton leak, maximal respiratory capacity, and nonmitochondrial respiration, respectively. OCR from nonmitochondrial respiration was subtracted from OCR at each stage to calculate the net OCR for basal (Base), proton leak (Leak), and maximal respiratory capacity (Max) values. Mitochondrial spare respiratory capacity and ATP-transratio were calculated by the formula shown. ((a), right panel) OCR measurements over time (n = 10 or 11). (b) Basal, Max, and Leak OCRs represented as average values from multiple measurements. (c) Mitochondrial spare respiratory capacity was calculated from Max and Basal OCRs. (d) ATP-transratio was calculated from Basal and Leak OCRs. $^{*}p < 0.05$; $^{**}p < 0.01$ as compared with control (n = 10 or 11).

Table 1: Primer sets used for RT-qPCR.

Gene name	F/R	Sequence (5′ to 3′)
Internal standard		
18S rRNA	F	TTCCGATAACGAACGAGACTCT
	R	TGGCTGAACGCCACTTGTC
Mitochondrial biogenesis		
PGC1α	F	CCAAACCCACAGAAAACAGG
PPAR-gamma coactivator 1-alpha	R	TGGGGTCATTTGGTGACTCT
NRF1	F	GAACTGCCAACCACAGTCAC
Nuclear respiratory factor 1	R	TCGTCTGGATGGTCATTTCA
mtTFA	F	CCGAAGTGTTTTTCCAGCAT
Mitochondrial transcriptional factor A	R	GGCTGCAATTTTCCTAACCA
Antioxidant system		
Nrf2	F	GGGAGAAAACGACAGAAACC
Nuclear factor erythroid 2 related factor 2	R	TGGGAGAGTAAGGCTTTCCA
HO-1	F	TGACACCTGAGGTCAAGCAC
Heme oxygenase-1	R	TCCTCTGTCAGCATCACCTG
NQO1	F	AAACGTCTGGAAACCGTCTG
Nadph dehydrogenase quinone 1	R	TTCTGCTCCTCTTGAACTTCC
Cat	F	GGACGCTCAGCTTTTCATTC
Catalase	R	TTGTCCAGAAGAGCCTGGAT
GPx	F	CTCATGACCGACCCCAAGTA
Glutathione peroxidase	R	CCCACCAGGAACTTCTCAAA
Mn-SOD	F	TCTGTGGGAGTCCAAGGTTC
Manganese superoxide dismutase	R	TAAGGCCTGTTGTTCCTTGC
Cu-SOD	F	GAGACCTGGGCAATGTGACT
Copper superoxide dismutase	R	TCATGGACCACCATTGTACG

[18]. DNA primers were designed to detect cytochrome oxidase 2 (COX2) and uncoupling protein 2 (UCP2) for mtDNA and nuclear DNA, respectively (COX2-F: 5′-TTTTCAGGCTTCACCCTAGATGA-3′ COX2-R: 5′-GAAGAATGTTATGTTATGTTTACTCCTA-3′ UCP2-F: 5′-GCGACCAGCCCATTGTAGA-3′ UCP2-R: 5′-GCGTTCTGGGTACCATCCTAAC-3′). The ratio of COX2 to UCP2 within each sample was used to calculate mtDNA content.

2.8. mRNA Quantification. Complementary DNA was prepared using the PrimeScript2 1st strand cDNA synthesis kit (Takara, Otsu, Japan). RT-qPCR was performed in a StepOnePlus Real-Time PCR system (Thermo Fisher Scientific) using Fast SYBR Green Master Mix (Thermo Fisher Scientific) and primer pair sets described in Table 1. The 18S rRNA was used as a housekeeping gene and served as an endogenous control.

2.9. Antioxidant Response Element (ARE) Luciferase Assay. The luciferase reporter plasmid (pGL4.26 luc2/minP/Hygro, E8441) and internal control plasmid (pRL-CMV, E2271) were from Promega (Madison, WI, USA). The DNA sequence for the ARE was obtained from the National Center for Biotechnology Information (GenBank: JQ858521.1), and a synthetic ARE polynucleotide was inserted into the *Hin*dIII site in multicloning site of pGL4.26 using the In-Fusion HD cloning kit (Takara). The ARE-loaded reporter and internal control vectors were cotransfected into HEK293 cells using lipofectamine-transfection reagent (Thermo Fisher Scientific). After a 24 h incubation, cells were treated with Amla (200 μg/mL) for another 48 h, and luciferase activity was measured using the Dual-Luciferase Reporter Assay System (Promega).

2.10. MTT Measurements of Cell Viability under Oxidative Stress. C2C12 cells were seeded on 96-well plates and differentiated to myotubes as previously described in Section 2.3. To evaluate the cytoprotective effects of Amla on t-BHP-induced oxidative stress, cells were pretreated with or without Amla (200 μg/mL) for 48 h, then with t-BHP (250 μM or 500 μM) for 6 h. Cell viability was determined using a cell-viability kit based on MTT reduction. Briefly, after treatment with t-BHP, cells were incubated with MTT assay reagents in culture medium for 20 min, and absorbance at 495 nm was measured using an ARVO SX 1420 multilabel counter (PerkinElmer, Inc., Waltham, MA, USA). Cell viability was expressed as the percentage of values obtained with control cells not treated with t-BHP.

2.11. ROS Measurement. Intracellular ROS levels were analyzed using the fluorescent probe 2′,7′-dichlorofluorescein diacetate. Differentiated C2C12 myotubes in 96-well

Table 2: Components of Amla extract.

	Content, %	
	Mean	SD
Total polyphenols	23.9	0.6
Vitamin C	1.32	0.2
Glucose	3.5	0.2
Fructose	4.3	0.4

Values are means of three replicate samples.

culture plates were pretreated with Amla (200 μg/mL) for 48 h. Myotubes were incubated with 10 μM 2′,7′-dichlorofluorescein diacetate for 30 min following t-BHP treatment (0 μM, 250 μM, or 500 μM) for 2 h. The fluorescence in cells, which was increased by ROS, was analyzed at 485 nm/535 nm (excitation/emission) in an ARVO SX 1420 multilabel counter.

2.12. Oxygen Consumption Analysis in Response to Oxidative Stress. Amla (200 μg/mL) treated or untreated C2C12 myotubes in 24-well plates (Seahorse Bioscience) were prepared as described in Section 2.4. Basal OCR was measured three times at 8 min intervals prior to treatment. After administration of t-BHP (0 μM, 250 μM, or 500 μM), OCR was then measured at 8 min intervals for 160 min. Data are expressed as relative-OCR values normalized to basal OCR values.

2.13. Statistical Analysis. Results are means ± standard deviation. Significance was assessed using Student's t-test and one-way analysis of variance. Differences among groups were determined using Tukey's multiple range test. A $p < 0.05$ was considered significant.

3. Results

3.1. Amla Extract Components. The total polyphenol and vitamin C contents of Amla extract were 23.9% and 1.32%, respectively (Table 2), and the extract contained low levels of glucose and fructose (3.5% and 4.3%, resp.). Because Amla extract was applied to cells at a concentration of 200 μg/mL, extract-derived sugars (~0.8 mg/dL each) were regarded as negligible.

3.2. Amla Treatment Enhanced Mitochondrial Spare Respiratory Capacity. To evaluate the effects of Amla treatment on mitochondrial function, we analyzed the OCR in C2C12 myotubes with or without Amla pretreatment (100 μg/mL or 200 μg/mL). Nonmitochondrial respiration (Figure 1(a), right panel) and Leak (Figure 1(a), right panel, and Figure 1(b)) were unchanged by Amla treatment; however, Base and Max OCRs increased in a dose-dependent manner following Amla treatment (Figure 1(a), right panel, and Figure 1(b)). Mitochondrial spare respiratory capacity also increased in a dose-dependent manner following Amla treatment, though the effects were not significant at lower Amla doses (Figure 1(c)). The ATP-transratio was unchanged by Amla treatment (Figure 1(d)). In order to clarify the mechanisms associated with Amla treatment, we conducted further experiments using the higher dosage (200 μg/mL).

3.3. Amla Treatment Stimulated Mitochondrial Biogenesis by AMPK Activation. To elucidate how Amla treatment enhanced OCR and mitochondrial spare respiratory capacity, we evaluated its effects on mitochondrial biogenesis in C2C12 myotubes. mtDNA copy number increased 1.5-fold following Amla treatment (Figure 2(a)). To evaluate the molecular effects associated with Amla treatment, we analyzed activation of the AMPKα/PGC1α/NRF1/mtTFA pathway, a key regulatory pathway involved in mitochondrial biogenesis. In cells treated with Amla, AMPKα-phosphorylation levels increased dramatically (Figure 2(b)), NRF1 and mtTFA mRNA expression increased significantly, and PGC1α mRNA exhibited trends indicating increased expression levels (Figure 2(c)).

3.4. Amla Treatment Stimulated Antioxidant Systems. In order to maintain mitochondrial function, ROS reduction and mitochondrial biogenesis are important. Therefore, we assessed the effects of Amla treatment on antioxidant systems in C2C12 myotubes. The activity of Nrf2, a key transcriptional factor involved in cellular antioxidant systems, was analyzed by luciferase reporter assay using a vector containing an ARE. As shown in Figure 3(a), Amla treatment dramatically increased ARE-driven luciferase activity. To further evaluate Nrf2 activation, we analyzed translocation of Nrf2 and observed that Amla treatment significantly increased Nrf2 translocation to the nucleus in C2C12 myotubes (Figure 3(b)). Furthermore, we found that several antioxidant enzymes that are Nrf2 target genes, such as HO-1, NQO-1, Cat, Mn-SOD, and Cu-SOD, were significantly upregulated at the transcriptional level following Amla treatment (Figure 3(c)).

3.5. Amla Treatment Exhibited Cytoprotective Effects on Cells Subjected to Oxidative Stress. To evaluate the cytoprotective effects of Amla treatment against oxidative stress, we first evaluated cell viability using the MTT assay in cells treated with t-BHP for 6 h to induce oxidative stress (Figure 4(a)). As shown in Figure 4(b), t-BHP treatment (250 μM and 500 μM) induced cytotoxicity in a dose-dependent manner, whereas this was significantly attenuated by pretreatment with Amla for 48 h. Next, to evaluate oxidative stress status, we analyzed ROS levels in C2C12 myotubes treated with t-BHP for 2 h (Figure 4(a)). Without t-BHP treatment, Amla pretreatment significantly reduced ROS levels, whereas t-BHP treatment increased ROS levels in a dose-dependent manner, which was significantly suppressed by pretreatment with Amla for 48 h (Figure 4(c)). We then evaluated oxygen consumption under oxidative stress conditions in C2C12 myotubes with or without Amla pretreatment (Figure 4(a)). In control myotubes, t-BHP at high doses caused a time-dependent increase in oxygen consumption, followed by a gradual decline, exhibiting a maximum OCR of 109.5 ± 7.3% that of basal OCR. Amla pretreatment increased maximum OCR in the presence of t-BHP (113.7±9.7% and 120.6±10.0% that of basal OCR at 250 μM and 500 μM t-BHP, resp.). OCRs

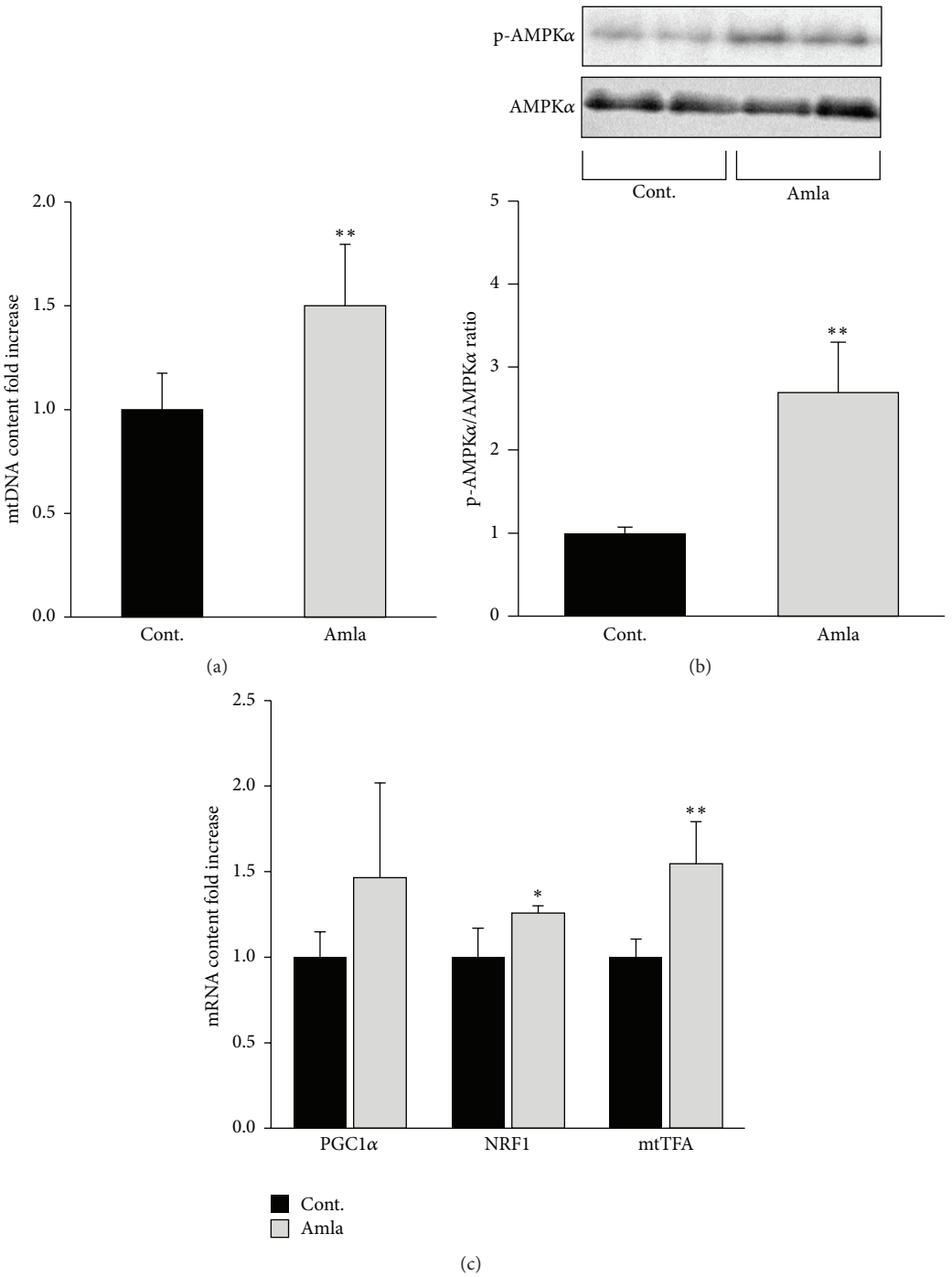

Figure 2: Amla treatment stimulated mitochondrial biogenesis by AMPK activation. C2C12 myotubes were incubated with Amla (200 μg/mL) for 48 h. Cell lysates were prepared for western blotting, RT-qPCR, and mtDNA analysis. (a) Relative mtDNA content was determined by qPCR using specific primer sets for the mitochondrial and nuclear genome. $^{**}p < 0.01$; $n = 8$. (b) Phosphorylated AMPKα to total AMPKα ratios were determined by western blot. $^{**}p < 0.01$; $n = 6$. (c) Relative contents of PGC1α, NRF1, and mtTFA mRNAs were determined by RT-qPCR. $^{*}p < 0.05$ and $^{**}p < 0.01$; $n = 5$. 18S rRNA was used as an internal control for RT-qPCR.

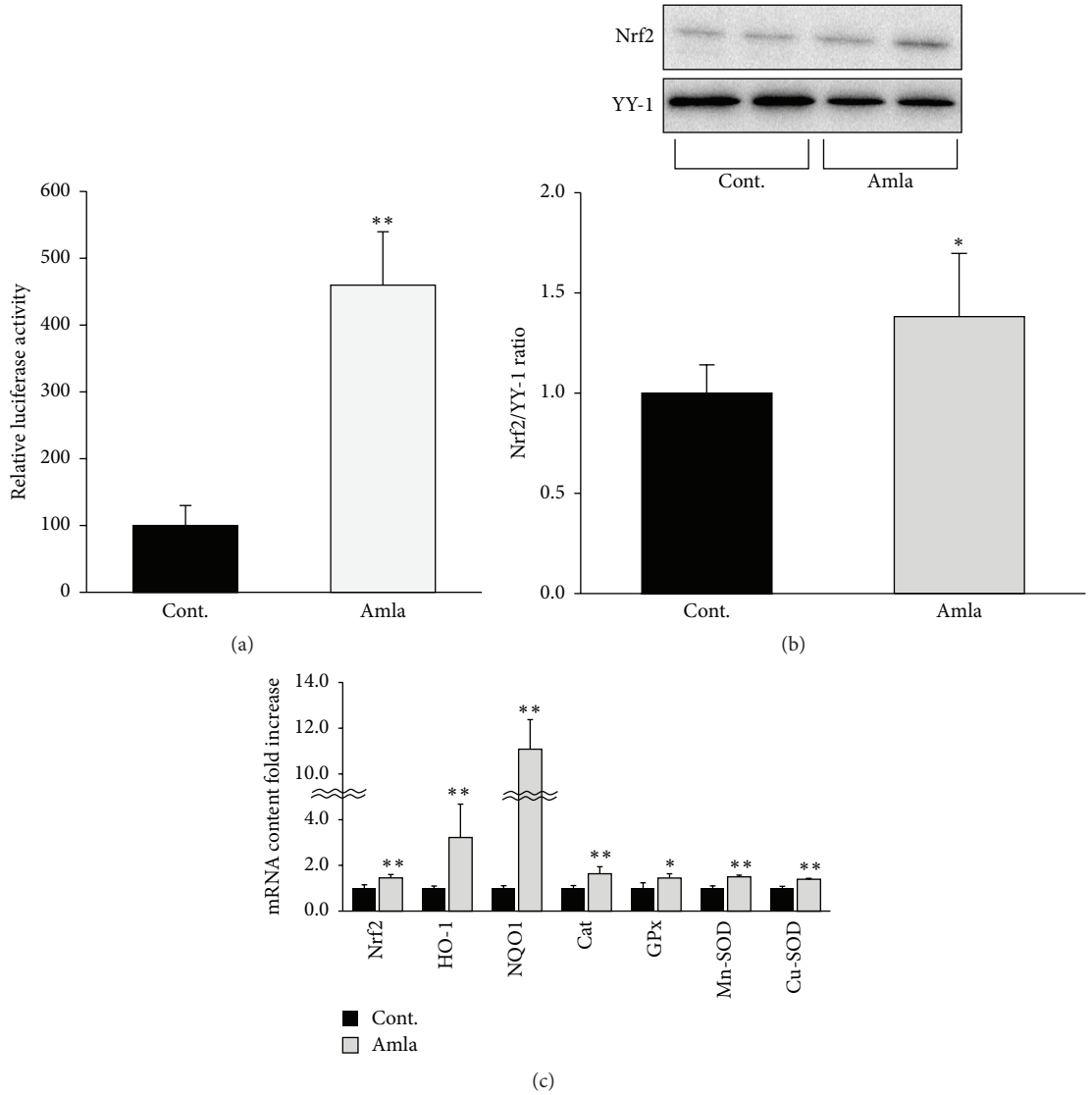

Figure 3: Amla treatment stimulated antioxidant systems by Nrf2 activation. (a) Activation of Nrf2 was analyzed using an ARE luciferase assay. Data are expressed as relative activities (reporter luciferase activity/control luciferase activity) as compared with data from control cells. $^{**}p < 0.01$; $n = 5$. (b and c) C2C12 myotubes were incubated with Amla (200 μg/mL) for 48 h. (b) Nuclear lysates were analyzed by western blot, and YY-1 was used an internal control for nuclear protein. $^{*}p < 0.05$; $n = 6$. (c) Relative levels of mRNA for antioxidant system related genes were analyzed by RT-qPCR. $^{*}p < 0.05$; $^{**}p < 0.01$; $n = 5$. 18S rRNA was used as an internal control for RT-qPCR.

were unchanged following Amla pretreatment in the absence of t-BHP treatment (Figure 4(d)).

4. Discussion

In this study, we made three observations relevant to the beneficial effects of Amla treatment in murine skeletal muscle cells. First, Amla treatment stimulated mitochondrial function, specifically increasing mitochondrial spare respiratory capacity. Second, Amla treatment stimulated mitochondrial biogenesis and antioxidant systems along with activation of the AMPK and Nrf2 pathways. Third, Amla treatment protected cells against oxidative stress accompanied by increased oxygen consumption.

Amla treatment stimulated mitochondrial function by increasing mitochondrial spare respiratory capacity (Figure 1). There have been few studies reporting the ability of food ingredients to enhance mitochondrial spare respiratory capacity. In mouse cortical neuronal cultures, epicatechin and quercetin, both major polyphenols in plant-derived food materials, enhanced mitochondrial spare respiratory capacity and protected cells against oxygen-glucose deprivation stress [19]. Additionally, pharmaceutical approaches, such as administering thyroid hormones, can positively regulate mitochondrial spare respiratory capacity in skeletal muscle [20]. Decreased mitochondrial spare respiratory capacity was also reported in aging [21], and its depletion was implicated in various pathologies in high energy-requiring tissues, such

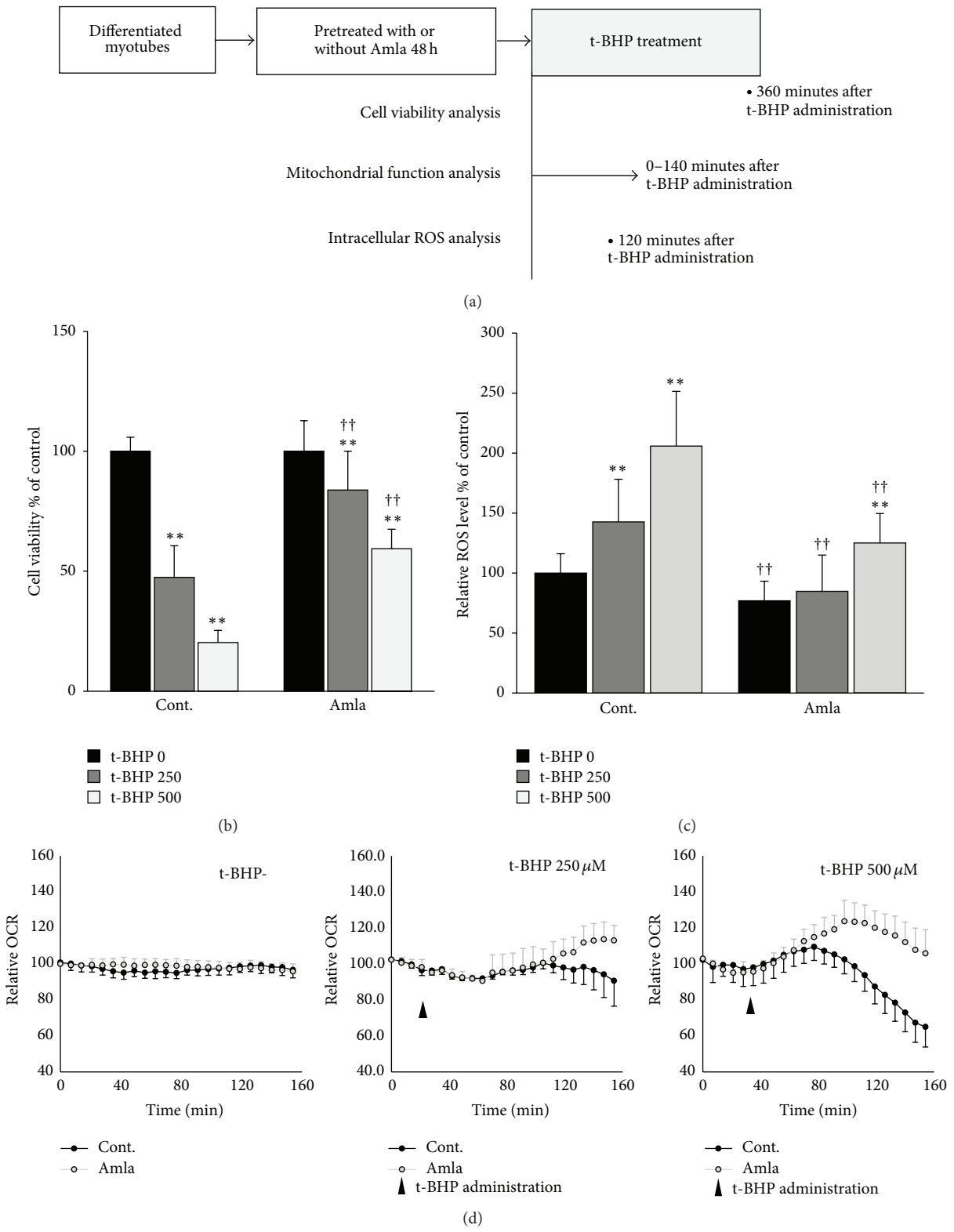

Figure 4: Amla treatment exhibited a cytoprotective effect against oxidative stress and concomitantly increased oxygen consumption. C2C12 myotubes were pretreated with Amla (200 μg/mL) for 48 h and then treated with t-BHP (250 μM or 500 μM). (a) Schematic showing the time points for three experiments performed to evaluate the cytoprotective effects of Amla treatment. (b) Cell viability was analyzed by MTT assay at 6 h after t-BHP treatment. $^{**}p < 0.01$ versus t-BHP-untreated cells; $^{\dagger\dagger}p < 0.01$ versus Amla-untreated cells treated with each t-BHP concentration; $n = 20$. (c) Relative ROS levels in cells were analyzed at 2 h after t-BHP stimulation. $^{**}p < 0.01$ versus t-BHP-untreated cells; $^{\dagger\dagger}p < 0.01$ versus Amla-untreated cells treated with each t-BHP concentration; $n = 12$. (d) OCR after t-BHP stimulation was analyzed following t-BHP injection after three basal OCR measurements. OCR was measured every 8 min for a total of 160 min. Data are represented as relative-OCR values divided by the basal OCR values measured prior to t-BHP treatment ($n = 10$).

as the heart, brain, and skeletal muscle [22–24]. Our findings suggested that Amla and other food ingredients are potentially novel approaches to improving age-related disorders in skeletal muscle by enhancing mitochondrial spare respiratory capacity. We confirmed that polyphenol rich Amla fractions prepared by adsorption chromatography stimulated mitochondrial respiratory spare capacity (see Supplemental Figures 1(A)–1(C) in Supplementary Material available online at http://dx.doi.org/10.1155/2016/1735841). These results indicated that the polyphenols were the functional components responsible for the observed effects, and given that Amla was reported to contain higher polyphenol content [6], it was expected to be superior to other fruits in mitochondrial maintenance.

Amla treatment stimulated mitochondrial biogenesis and antioxidant systems along with activation of the AMPKα and Nrf2 pathways (Figures 2 and 3). Studies showed that both mitochondrial biogenesis and antioxidant systems could regulate mitochondrial spare respiratory capacity. Increased mitochondrial biogenesis and energy production caused by thyroid hormone treatment leads to stimulation of mitochondrial spare respiratory capacity in skeletal muscle [20]. In striatal neurons, decreased mitochondrial density accompanying mutant huntingtin expression indicated reduced mitochondrial spare respiratory capacity [25]. Furthermore, depletion of an antioxidant enzyme impaired mitochondrial spare respiratory capacity in cortical synaptosomes isolated from *SOD2* null mice [26]. These reports were consistent with our findings, and we speculated that the effects of Amla treatment on mitochondrial spare respiratory capacity were related to activation of mitochondrial biogenesis and antioxidant systems. AMPKα and Nrf2 activation reportedly play key roles in mitochondrial biogenesis and antioxidant systems, and there are many studies showing that plant-derived polyphenols activate AMPKα or Nrf2 [27, 28]. In an animal model, dietary gallic acid protected mice from diet-induced obesity by stimulating the AMPKα/Sirt1/PGC1α pathway in liver, muscle, and brown adipose tissues [29]. Furthermore, ellagic acid consumption improved oxidant-induced endothelial dysfunction through Nrf2 activation [30]. These reports supported our findings, because the major polyphenols in Amla include gallic and ellagic acid [6]. Therefore, we proposed that gallic acid and ellagic acid were key factors involved in AMPK and Nrf2 activation following Amla treatment in our experiments.

Amla treatment protected cells against oxidative stress accompanied by increased oxygen consumption (Figure 4). Many reports showed that activation of antioxidant systems could increase cell survival in the presence of oxidative stress [31, 32]. In our study, we observed that Amla treatment protected cells against t-BHP-induced cell death, likely by reducing ROS levels through activation of the Nrf2 pathway (Figures 4(b) and 4(c)). Various oxidative stresses led to increased oxygen consumption, suggesting a critical role for mitochondrial spare respiratory capacity in cell survival and maintenance of biological functions under oxidative stress [15, 33]. We observed that t-BHP treatment increased OCR and that this was likely mediated by the spare respiratory capacity against oxidative stress. Additionally, pretreatment with Amla elevated the maximum OCR against t-BHP treatment (Figure 4(d)). Therefore, we speculated that not only activation of antioxidant systems but also increased mitochondrial function contributed to the cytoprotective effects of Amla treatment against oxidative stress.

In addition to being toxic, ROS are involved in various physiological processes as messenger molecules [34]. Signaling by insulin, several growth factors, and transcriptional factors can be mediated by physiological ROS levels [35, 36]. Because of these multiple roles, ROS homeostasis is regulated by numerous systems [37]. In our experiments, the magnitude by which Amla treatment decreased ROS increased with t-BHP concentration (Figure 4(c)). Therefore, our findings suggested that Amla treatment might remove excessive and damaging levels of ROS without neutralizing the ROS required for physiological function.

One limitation of our study was that it only demonstrated the effects of Amla treatment *in vitro*. Component analysis and previous research strongly suggested that polyphenols contributed to the effects of Amla treatment [29, 30] and that Amla contained various kinds of polyphenols, with gallic acid as a major component [6]. In one report, gallic acid was absorbed better in humans as compared to other polyphenols [38], and a previous clinical study investigating the bioavailability of gallic acid from red wine showed that glucuronidated and intact forms of gallic acid were detected in plasma [39]. These findings indicated that gallic acid in Amla may partially account for the biological relevance of our findings. Further experiments will be needed to clarify whether the effects of Amla treatment reported here can be reproduced *in vivo*.

Our results indicated that Amla treatment enhanced mitochondrial spare respiratory capacity, which was supported by its effect on mitochondrial biogenesis and antioxidant systems, through activation of the AMPKα and Nrf2 pathways, respectively. Furthermore, we found that Amla treatment decreased ROS levels and increased cell viability in the presence of t-BHP induced oxidative stress. We attributed the cytoprotective effects of Amla treatment not only to activation of antioxidant systems, but also to enhancement of the mitochondrial spare respiratory capacity (Figure 5).

5. Conclusions

In conclusion, our study demonstrated that Amla enhanced mitochondrial spare respiratory capacity through activation of mitochondrial biogenesis and antioxidant systems. Furthermore, we showed that these effects of Amla resulted in decreased ROS levels and increased cell viability under oxidative stress conditions. Therefore, our findings suggested novel potential mechanisms for the beneficial effects associated with Amla intake, including decreased oxidative stress.

Competing Interests

Hirotaka Yamamoto, Takao Ikami, Kohei Kiriyama, and Taishi Ishibashi are employees of Miki Corporation. Miki

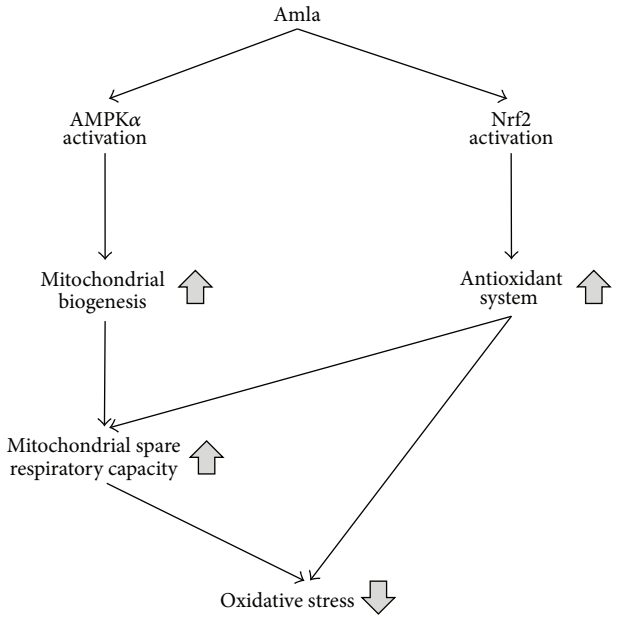

Figure 5: Schematic figure showing the effects of Amla treatment resulting in reduced oxidative stress.

Corporation has a food product containing Amla extract. This work was conducted in collaboration with Shiga University of Medical Science (SUMS). Hirotaka Yamamoto is a Visiting Assistant Professor at SUMS.

Authors' Contributions

Hirotaka Yamamoto and Katsutaro Morino conceived and designed the research; Hirotaka Yamamoto, Katsutaro Morino, Taishi Ishibashi, and Kohei Kiriyama performed experiments; Hirotaka Yamamoto and Katsutaro Morino analyzed data; Hirotaka Yamamoto, Katsutaro Morino, and Lemecha Mengistu interpreted the experimental results; Hirotaka Yamamoto and Katsutaro Morino prepared the figures and drafted the paper; Hirotaka Yamamoto, Katsutaro Morino, Takao Ikami, and Hiroshi Maegawa edited, revised, and approved the final version of paper.

Acknowledgments

The authors thank Misako Kitano, Takahiro Okuda, Yuichiro Mori, and Takashi Fujii for their technical assistance. The Department of Medicine, SUMS, received research promotion grants (Shougaku Kifukin) from Astellas, AstraZeneca, Bayer, Boehringer-Mannheim, Bristol-Myers Squibb, Chugai Pharma, Daiichi-Sankyo, Dainippon Sumitomo, Eisai, Eli Lilly, Fuji Yakuhin, Glaxo Smithkline, Kaken Pharmaceutical, Kaneka Medix, Kissei, Kowa Pharmaceuticals, Kyowa-hakko-Kirin, Miki Corporation, Mitsubishi Tanabe, Mochida, MSD, Nihon Medi-Physics, Nipro, Novartis, Novo Nordisk, Ono Pharmaceutical, Otsuka Pharmaceutical, Pfizer, Sanofi, Sanwa Kagaku Kenkyusho, Shionogi, Sunstar, Taisho-Toyama, Takeda, Teijin Pharma, Terumo, and Torii Pharmaceutical. The research topics funded by these grants are unrestricted.

References

[1] S. S. Patel and R. K. Goyal, "*Emblica officinalis* Geart.: a comprehensive review on phytochemistry, pharmacology and ethnomedicinal uses," *Research Journal of Medicinal Plant*, vol. 6, no. 1, pp. 6–16, 2012.

[2] P. Bhandari and M. Kamdod, "*Emblica officinalis* (Amla): a review of potential therapeutic applications," *International Journal of Green Pharmacy*, vol. 6, no. 4, pp. 257–269, 2012.

[3] P. Usharani, N. Fatima, and N. Muralidhar, "Effects of *Phyllanthus emblica* extract on endothelial dysfunction and biomarkers of oxidative stress in patients with type 2 diabetes mellitus: a randomized, double-blind, controlled study," *Diabetes, Metabolic Syndrome and Obesity: Targets and Therapy*, vol. 6, pp. 275–284, 2013.

[4] A. Bhattacharya, A. Chatterjee, S. Ghosal, and S. K. Bhattacharya, "Antioxidant activity of active tannoid principles of *Emblica officinalis* (amla)," *Indian Journal of Experimental Biology*, vol. 37, no. 7, pp. 676–680, 1999.

[5] V. Damodara Reddy, P. Padmavathi, S. Gopi, M. Paramahamsa, and N. C. Varadacharyulu, "Protective effect of *Emblica officinalis* against alcohol-induced hepatic injury by ameliorating oxidative stress in rats," *Indian Journal of Clinical Biochemistry*, vol. 25, no. 4, pp. 419–424, 2010.

[6] T. Yokozawa, H. Y. Kim, L. R. Juneja et al., "Amla (*Emblica officinalis* Gaertn.) attenuates age-related renal dysfunction by oxidative stress," *Journal of Agricultural and Food Chemistry*, vol. 55, no. 19, pp. 7744–7752, 2007.

[7] T. Yokozawa, H. Y. Kim, H. J. Kim, T. Okubo, D.-C. Chu, and L. R. Juneja, "Amla (*Emblica officinalis* Gaertn.)prevents dyslipidaemia and oxidative stress in the ageing process," *British Journal of Nutrition*, vol. 97, no. 6, pp. 1187–1195, 2007.

[8] H. Y. Kim, T. Okubo, L. R. Juneja, and T. Yokozawa, "The protective role of amla (*Emblica officinalis* Gaertn.) against fructose-induced metabolic syndrome in a rat model," *British Journal of Nutrition*, vol. 103, no. 4, pp. 502–512, 2010.

[9] S. Ojha, M. Golechha, S. Kumari, and D. S. Arya, "Protective effect of *Emblica officinalis* (amla) on isoproterenol-induced cardiotoxicity in rats," *Toxicology and Industrial Health*, vol. 28, no. 5, pp. 399–411, 2012.

[10] S. S. Patel and R. K. Goyal, "Prevention of diabetes-induced myocardial dysfunction in rats using the juice of the *Emblica officinalis* fruit," *Experimental and Clinical Cardiology*, vol. 16, no. 3, pp. 87–91, 2011.

[11] M. S. Akhtar, A. Ramzan, A. Ali, and M. Ahmad, "Effect of amla fruit (*Emblica officinalis* Gaertn.) on blood glucose and lipid profile of normal subjects and type 2 diabetic patients," *International Journal of Food Sciences and Nutrition*, vol. 62, no. 6, pp. 609–616, 2011.

[12] A. Bratic and N.-G. Larsson, "The role of mitochondria in aging," *The Journal of Clinical Investigation*, vol. 123, no. 3, pp. 951–957, 2013.

[13] A. Safdar, M. J. Hamadeh, J. J. Kaczor, S. Raha, J. deBeer, and M. A. Tarnopolsky, "Aberrant mitochondrial homeostasis in the skeletal muscle of sedentary older adults," *PLoS ONE*, vol. 5, no. 5, Article ID e10778, 2010.

[14] C. Mancuso, G. Scapagini, D. Currò et al., "Mitochondrial dysfunction, free radical generation and cellular stress response

in neurodegenerative disorders," *Frontiers in Bioscience*, vol. 12, pp. 1107–1123, 2007.

[15] B. G. Hill, B. P. Dranka, L. Zou, J. C. Chatham, and V. M. Darley-Usmar, "Importance of the bioenergetic reserve capacity in response to cardiomyocyte stress induced by 4-hydroxynonenal," *Biochemical Journal*, vol. 424, no. 1, pp. 99–107, 2009.

[16] D. B. Dennison, T. G. Brawley, and G. L. K. Hunter, "Rapid high-performance liquid chromatographic determination of ascorbic acid and combined ascorbic acid-dehydroascorbic acid in beverages," *Journal of Agricultural and Food Chemistry*, vol. 29, no. 5, pp. 927–929, 1981.

[17] S. Kim, J. M. Park, and C. H. Kim, "Ethanol production using whole plant biomass of Jerusalem artichoke by *Kluyveromyces marxianus* CBS1555," *Applied Biochemistry and Biotechnology*, vol. 169, no. 5, pp. 1531–1545, 2013.

[18] H. Yamamoto, K. Morino, Y. Nishio et al., "MicroRNA-494 regulates mitochondrial biogenesis in skeletal muscle through mitochondrial transcription factor A and Forkhead box j3," *American Journal of Physiology—Endocrinology and Metabolism*, vol. 303, no. 12, pp. E1419–E1427, 2012.

[19] M. Nichols, J. Zhang, B. M. Polster et al., "Synergistic neuroprotection by epicatechin and quercetin: activation of convergent mitochondrial signaling pathways," *Neuroscience*, vol. 308, pp. 75–94, 2015.

[20] R. Lesmana, R. A. Sinha, B. K. Singh et al., "Thyroid hormone stimulation of autophagy is essential for mitochondrial biogenesis and activity in skeletal muscle," *Endocrinology*, vol. 157, no. 1, pp. 23–38, 2016.

[21] B. Rohrer, M. Bandyopadhyay, and C. Beeson, "Reduced metabolic capacity in aged primary retinal pigment epithelium (RPE) is correlated with increased susceptibility to oxidative stress," *Advances in Experimental Medicine and Biology*, vol. 854, pp. 793–798, 2016.

[22] C. Desler, T. L. Hansen, J. B. Frederiksen, M. L. Marcker, K. K. Singh, and L. Juel Rasmussen, "Is there a link between mitochondrial reserve respiratory capacity and aging?" *Journal of Aging Research*, vol. 2012, Article ID 192503, 9 pages, 2012.

[23] B. E. Sansbury, S. P. Jones, D. W. Riggs, V. M. Darley-Usmar, and B. G. Hill, "Bioenergetic function in cardiovascular cells: the importance of the reserve capacity and its biological regulation," *Chemico-Biological Interactions*, vol. 191, no. 1–3, pp. 288–295, 2011.

[24] N. Yadava and D. G. Nicholls, "Spare respiratory capacity rather than oxidative stress regulates glutamate excitotoxicity after partial respiratory inhibition of mitochondrial complex I with rotenone," *The Journal of Neuroscience*, vol. 27, no. 27, pp. 7310–7317, 2007.

[25] A. Siddiqui, S. R. Sánchez, M. D. R. Castro et al., "Mitochondrial DNA damage is associated with reduced mitochondrial bioenergetics in Huntington's disease," *Free Radical Biology and Medicine*, vol. 53, no. 7, pp. 1478–1488, 2012.

[26] J. M. Flynn, S. W. Choi, N. U. Day, A. A. Gerencser, A. Hubbard, and S. Melov, "Impaired spare respiratory capacity in cortical synaptosomes from *Sod2* null mice," *Free Radical Biology and Medicine*, vol. 50, no. 7, pp. 866–873, 2011.

[27] M. Zang, S. Xu, K. A. Maitland-Toolan et al., "Polyphenols stimulate AMP-activated protein kinase, lower lipids, and inhibit accelerated atherosclerosis in diabetic LDL receptor-deficient mice," *Diabetes*, vol. 55, no. 8, pp. 2180–2191, 2006.

[28] H. Erlank, A. Elmann, R. Kohen, and J. Kanner, "Polyphenols activate Nrf2 in astrocytes via H_2O_2, semiquinones, and quinones," *Free Radical Biology and Medicine*, vol. 51, no. 12, pp. 2319–2327, 2011.

[29] K. V. Doan, C. M. Ko, A. W. Kinyua et al., "Gallic acid regulates body weight and glucose homeostasis through AMPK activation," *Endocrinology*, vol. 156, no. 1, pp. 157–168, 2015.

[30] Y. Ding, B. Zhang, K. Zhou et al., "Dietary ellagic acid improves oxidant-induced endothelial dysfunction and atherosclerosis: role of Nrf2 activation," *International Journal of Cardiology*, vol. 175, no. 3, pp. 508–514, 2014.

[31] R.-Z. Zhong, Y. Fang, G.-X. Qin, H.-Y. Li, and D.-W. Zhou, "Tea catechins protect goat skeletal muscle against H_2O_2-induced oxidative stress by modulating expression of phase 2 antioxidant enzymes," *Journal of Agricultural and Food Chemistry*, vol. 63, no. 36, pp. 7921–7928, 2015.

[32] J. S. Kang, M. H. Han, G.-Y. Kim et al., "Schisandrae semen essential oil attenuates oxidative stress-induced cell damage in C2C12 murine skeletal muscle cells through Nrf2-mediated upregulation of HO-1," *International Journal of Molecular Medicine*, vol. 35, no. 2, pp. 453–459, 2015.

[33] B. P. Dranka, B. G. Hill, and V. M. Darley-Usmar, "Mitochondrial reserve capacity in endothelial cells: the impact of nitric oxide and reactive oxygen species," *Free Radical Biology and Medicine*, vol. 48, no. 7, pp. 905–914, 2010.

[34] H. Sies, "Role of metabolic H_2O_2 generation: redox signaling and oxidative stress," *The Journal of Biological Chemistry*, vol. 289, no. 13, pp. 8735–8741, 2014.

[35] D. Heffetz, L. Bushkin, R. Dror, and Y. Zick, "The insulinomimetic agents H_2O_2 and vanadate stimulate protein tyrosine phosphorylation in intact cells," *The Journal of Biological Chemistry*, vol. 265, no. 5, pp. 2896–2902, 1990.

[36] M. Sundaresan, Z.-X. Yu, V. J. Ferrans, K. Irani, and T. Finkel, "Requirement for generation of H_2O_2 for platelet-derived growth factor signal transduction," *Science*, vol. 270, no. 5234, pp. 296–299, 1995.

[37] A. Rahal, A. Kumar, V. Singh et al., "Oxidative stress, prooxidants, and antioxidants: the interplay," *BioMed Research International*, vol. 2014, Article ID 761264, 19 pages, 2014.

[38] M. Daglia, A. Di Lorenzo, S. F. Nabavi, Z. S. Talas, and S. M. Nabavi, "Polyphenols: well beyond the antioxidant capacity: gallic acid and related compounds as neuroprotective agents: you are what you eat!," *Current Pharmaceutical Biotechnology*, vol. 15, no. 4, pp. 362–372, 2014.

[39] E. Cartron, G. Fouret, M.-A. Carbonneau et al., "Red-wine beneficial long-term effect on lipids but not on antioxidant characteristics in plasma in a study comparing three types of wine—description of two *O*-methylated derivatives of gallic acid in humans," *Free Radical Research*, vol. 37, no. 9, pp. 1021–1035, 2003.

Hindawi Publishing Corporation
Oxidative Medicine and Cellular Longevity
Volume 2016, Article ID 8679469, 19 pages
http://dx.doi.org/10.1155/2016/8679469

Research Article

Impact of Antioxidants on Cardiolipin Oxidation in Liposomes: Why Mitochondrial Cardiolipin Serves as an Apoptotic Signal?

Alexey V. Lokhmatikov,[1,2] Natalia Voskoboynikova,[1] Dmitry A. Cherepanov,[3,4] Maxim V. Skulachev,[5] Heinz-Jürgen Steinhoff,[1] Vladimir P. Skulachev,[2,3] and Armen Y. Mulkidjanian[1,2,3]

[1]*School of Physics, University of Osnabrueck, 49069 Osnabrueck, Germany*
[2]*School of Bioengineering and Bioinformatics, Lomonosov Moscow State University, Moscow 119991, Russia*
[3]*A.N. Belozersky Institute of Physico-Chemical Biology, Lomonosov Moscow State University, Moscow 119991, Russia*
[4]*A.N. Frumkin Institute of Physical Chemistry and Electrochemistry of the Russian Academy of Sciences, Leninsky Prospect 31, Moscow 119991, Russia*
[5]*Institute of Mitoengineering, Lomonosov Moscow State University, Moscow 119991, Russia*

Correspondence should be addressed to Armen Y. Mulkidjanian; amulkid@uni-osnabrueck.de

Received 25 December 2015; Revised 29 February 2016; Accepted 17 March 2016

Academic Editor: Rebeca Acín-Pérez

Copyright © 2016 Alexey V. Lokhmatikov et al. This is an open access article distributed under the Creative Commons Attribution License, which permits unrestricted use, distribution, and reproduction in any medium, provided the original work is properly cited.

Molecules of mitochondrial cardiolipin (CL) get selectively oxidized upon oxidative stress, which triggers the intrinsic apoptotic pathway. In a chemical model most closely resembling the mitochondrial membrane—liposomes of pure bovine heart CL—we compared ubiquinol-10, ubiquinol-6, and alpha-tocopherol, the most widespread naturally occurring antioxidants, with man-made, quinol-based amphiphilic antioxidants. Lipid peroxidation was induced by addition of an azo initiator in the absence and presence of diverse antioxidants, respectively. The kinetics of CL oxidation was monitored via formation of conjugated dienes at 234 nm. We found that natural ubiquinols and ubiquinol-based amphiphilic antioxidants were equally efficient in protecting CL liposomes from peroxidation; the chromanol-based antioxidants, including alpha-tocopherol, were 2-3 times less efficient. Amphiphilic antioxidants, but not natural ubiquinols and alpha-tocopherol, were able, additionally, to protect the CL bilayer from oxidation by acting from the water phase. We suggest that the previously reported therapeutic efficiency of mitochondrially targeted amphiphilic antioxidants is owing to their ability to protect those CL molecules that are inaccessible to natural hydrophobic antioxidants, being trapped within respiratory supercomplexes. The high susceptibility of such occluded CL molecules to oxidation may have prompted their recruitment as apoptotic signaling molecules by nature.

1. Introduction

During last decades, the pathophysiological aspects of redox homeostasis came into focus of cell research; it has been shown that many diseases lead to oxidative imbalance and an increase in the level of reactive oxygen species (ROS) [1–6]. The ROS comprise the superoxide anion radical ($O_2^{\bullet-}$), hydroperoxide (H_2O_2), and the extremely reactive hydroxyl radical ($^{\bullet}OH$), as well as nitrogen-containing compounds: nitroxide (NO) and peroxynitrite ($ONOO^-$) [7–9]. Interaction of ROS with organic molecules could yield organic radicals, such as alkoxyl ($RO^{\bullet}$) and peroxyl ($ROO^{\bullet}$) radicals, which can be involved in further oxidation processes [10].

The oxidative damage to nucleic acids, proteins, and lipids, as caused by ROS, is usually considered to be a major factor in the general functional decline of tissues upon aging and age-associated degenerative diseases [2]. In case of *Metazoa*, the means to limit the ROS-induced damage seem to invoke apoptosis—the programmed cell death via activation of executor caspases and digestion of the cell from the inside [11]. Apparently, when the ROS level in a particular cell reaches a certain threshold, apoptosis is activated to eliminate

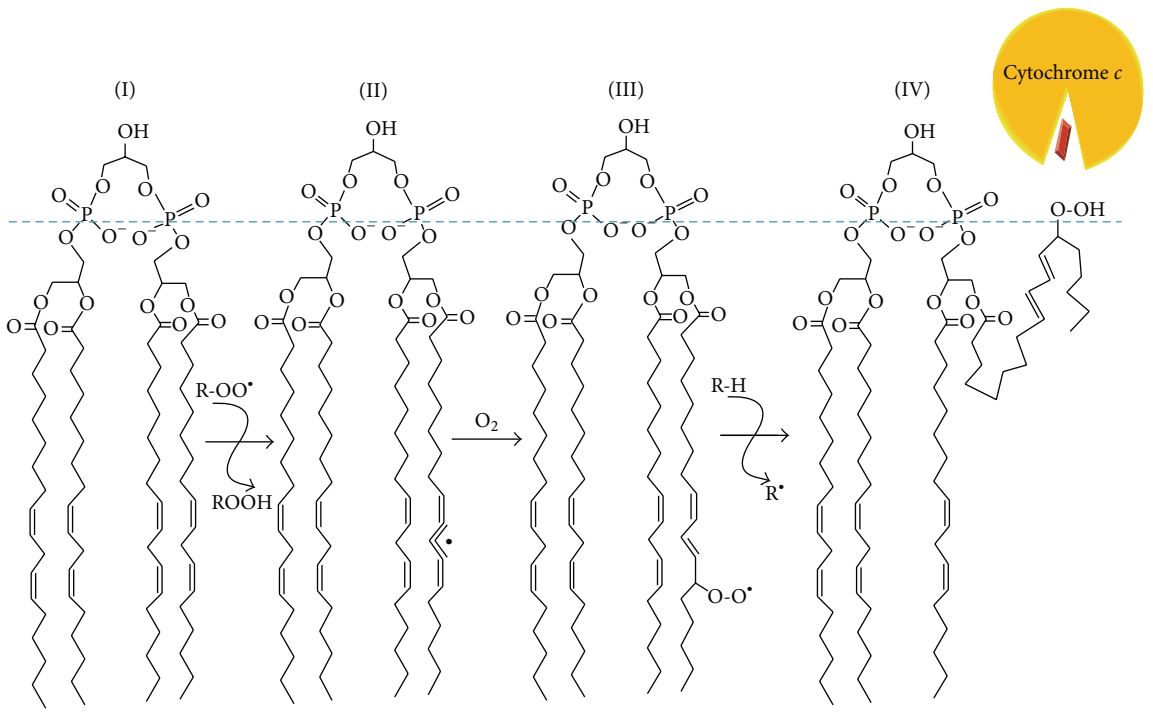

Figure 1: Schematic representation of the initial steps of CL peroxidation as based on [4, 10, 15–17]. The mammalian heart CL is mostly found in the form of tetralinoleoyl-CL, that is, with four polyunsaturated residues of linoleic acid (I). A bis-allylic hydrogen atom of CL may be abstracted by a peroxyl radical (ROO•) yielding peroxide (ROOH) and a lipid-centered radical (II). The latter is involved in a fast reaction with molecular oxygen and turns into another peroxyl radical, which may consequently attack another polyunsaturated lipid in a chain process. This reaction is accompanied by rearrangement of double bonds of the fatty acid residue, which ultimately leads to the accumulation of conjugated dienes (III). Peroxide of CL exposes its nascent hydrophilic moiety at the surface of the membrane, where it may interact with cytochrome *c* and turn it into a peroxidase, thus forcing amplification of the oxidation cascade (IV).

the ROS-producing cell, which prevents damaging of the whole tissue; see [5, 12–14] for reviews. Apoptosis, generally useful in protecting an organism from oxidative damage, could, however, become counterproductive under conditions of an acute—although potentially reversible—oxidative stress that accompanies such pathological states as stroke and trauma. In such cases, apoptosis could lead to undesirable cell loss, cumulative tissue degradation, and ultimately even to the death of the whole organism. Therefore, a controlled prevention of apoptotic reactions under conditions of acute oxidative stress might save lives.

One of the first signals of the apoptotic pathway within mitochondria is oxidized cardiolipin [5, 13, 20, 21]. A cardiolipin (CL) molecule is built of two glycerophosphate moieties, each carrying two fatty acid tails, which are connected via one more glycerol molecule (see Figure 1). Bound CL molecules are seen in the crystal structures of many membrane energy-converting complexes; see [22, 23] for reviews. Because of their four fatty acid tails, CL molecules were proposed to promote the interaction between mitochondrial respiratory enzymes [24]. Later, it was shown that CL, indeed, stabilizes supercomplexes formed of the NADH dehydrogenase (mitochondrial complex I), quinol:cytochrome *c* oxidoreductase (cytochrome bc_1 complex; complex III), and cytochrome *c* oxidase (complex IV) [25–28]; a large fraction of loosely bound CL was shown to be affiliated with these supercomplexes [26–28]. Supposedly, CL molecules facilitate the integration of respiratory complexes into dynamic functional units [29, 30]. In eukaryotes, ROS are produced in mitochondria as byproducts of respiration [31, 32]; the major sources of ROS are the NADH : quinone oxidoreductase [33–35] and cytochrome bc_1 complex [9, 36–40], which form CL-rich supercomplexes.

The animal variant of CL, which is closely associated with the respiratory complexes and carries polyunsaturated fatty acid chains, can be regarded as an easily "ignitable" compound. The selective peroxidation of CL in mitochondria in response to the oxidative stress was demonstrated with various experimental models [20, 41–45]. Hence, those drugs that protect CL from oxidation might postpone or prevent the cell death.

Recent years have shown notable progress in development and investigation of such drugs; see [15, 46] for reviews. It has been shown that some antioxidants can prevent both the oxidation of CL and the development of pathology. Specifically, idebenone, or 6-(10-hydroxydecyl)ubiquinone, was shown to protect the mitochondrial membrane against lipid peroxidation and improve vascular disorders—owing to strokes or experimental cerebral ischemia—as well as improve the overall brain function [47–50]. Decylubiquinone (decUQ) was shown to block ROS accumulation and prevented activation of the MPT and the cell death in

the glutathione-depleted cells [51]. Treatment by propofol, a phenolic anaesthetic, was shown to protect against mitochondrial dysfunction [52].

Among others, several mitochondrially targeted antioxidants were developed; see [15, 46] for reviews. Antioxidants based on mitochondrially targeted peptides could concurrently prevent the oxidation of CL, cytochrome *c* release to the cytoplasm, and the cell death [44, 53–55].

Another way to target drugs to mitochondria is based on a covalent binding of an antioxidant to a penetrating cation. Such cations, termed "Skulachev ions" by Green [56], penetrate through biological membranes in the charged state and get distributed according to the transmembrane difference of electrical potentials [57]. Due to the ability to selectively accumulate in energized mitochondria, which are negatively charged with respect to the cell cytoplasm, such compounds can be used as "locomotives" for delivery of drugs into mitochondria [58]. Since the interior of mitochondria is by approximately 200 mV more negative than the cytosol, penetrating cations can accumulate by a factor of 1000, at least [20, 58]. A mitochondrially targeted ubiquinol analogue 10-(6′-ubiquinonyl)decyltriphenylphosphonium (MitoQ), with a triphenylphosphonium group [57] as a penetrating cation, was shown to prevent lipid peroxidation and apoptotic reactions [59, 60].

At the Lomonosov University, a series of mitochondrially targeted antioxidants comprised of a penetrating cation and an antioxidant, usually a plastoquinol group, separated by a C-10 linker, have been synthesized and tested. Such compounds were dubbed SkQ ions, that is, conjugates of penetrating Skulachev ions (Sk) and quinols (Q); these constructs were tested *in vitro* and *in vivo* [20, 61–74]. SkQs prolonged life of different organisms [68], helped animals to survive after brain and kidney ischemia [69], stroke, and heart attack [64], and decelerated the development of many age-related pathological states, such as cataract and some other eye diseases, balding, achromotrichia, lordokyphosis, and myeloid shift of the blood [20]. Owing to their ability to accumulate in mitochondria [20, 58], the SkQ ions were already efficient when added at concentrations of tens of nanomoles per kg of body weight.

Upon these studies, it has been shown that CL molecules were specifically peroxidized in mitochondria under oxidative stress, whereas other phospholipids remained more or less intact, and that 10-(6′-plastoquinonyl)decyltriphenylphosphonium (SkQ1) protected the mitochondrial CL from oxidation [20, 63, 67].

While the physiological protective effects of SkQs and some other mitochondrially targeted antioxidants are well documented (see [46] for a recent review), the mechanism of their action has remained obscure. Indeed, mitochondria possess high levels of powerful natural antioxidants, such as ubiquinols and tocopherols. The concentration of ubiquinol in the mitochondrial membrane is especially high comprising about 1% of the total lipid content [75], which corresponds to a molar concentration in the order of 10 mM. The high level of natural antioxidants in mitochondrial membranes brings us to the conundrum: why the natural stock of ubiquinol and α-tocopherol does not fully protect the mitochondrial CL from oxidation, whereas the artificial antioxidants, being externally added in nanomolar amounts [20], could do that?

In an attempt to answer this question, we have established a chemically defined system to quantitatively study the oxidation of CL in the membrane as a function of different antioxidants [19]. We chose pure CL membranes as an object for our kinetic studies and established production of extrusion-derived liposomes of a uniform size of about 100 nm, as confirmed by dynamic light scattering measurements and electron microscopy. The CL liposomes were impermeable for small organic molecules such as 5(6)-carboxyfluorescein [19]. To avoid protein-due effects, we initiated the oxidation of CL by an azo initiator 2,2′-azobis(4-methoxy-2,4-dimethylvaleronitrile), or MeO-AMVN [18]. The formation of primary oxidation products, conjugated dienes (see Figure 1), was followed, in real time, by measuring their accumulation at 234 nm [18, 76, 77]. The high efficiency of the hydrophobic initiator MeO-AMVN at low temperatures [18] allowed us to use low amounts of the initiator, which decreased the possible influence of the initiator on the structure of the liposomes. Our method is a direct method, and, along with polarography [10, 78], enables continuous tracing of the lipid peroxidation. However, the advantage of the spectrophotometric approach is the ability to simultaneously trace not only the accumulation of the reaction products but also the depletion of the antioxidant, which is essential for kinetic analysis of peroxidation; see Section 2 and [19] for further details on the method used.

With this experimental setup, we have already shown that the amphiphilic quinol-based antioxidants, when added to a solution of CL liposomes, were effective in protecting cardiolipin liposomes from peroxidation even in submicromolar range, with their relative effectiveness depending on the type of antioxidant group and on the nature of the membrane-targeted moiety [19].

Here, we have compared natural, hydrophobic antioxidants with artificial, amphiphilic antioxidants in a somewhat amended experimental setup. We have found that natural hydrophobic ubiquinols, when preincubated in liposomes, were as efficient as artificial amphiphilic quinol-containing antioxidants and much more efficient than chromanol-based compounds. The artificial amphiphilic antioxidants, unlike the hydrophobic ubiquinol and α-tocopherol, could almost fully inhibit the CL oxidation also when acting from the aqueous phase. We suggest that amphiphilic antioxidants specifically protect those CL molecules which are tightly bound within the enzymes of the respiratory chain, accounting thus for the observed therapeutic effects.

2. Materials and Methods

2.1. Chemicals. CL from bovine heart and 1-palmitoyl-2-oleoyl-phosphatidylglycerol (POPG) were derived from Avanti Polar Lipids Inc. (Alabaster, AL, US) in the form of lyophilized powder. Yeast ubiquinone-6 was also from Avanti. Ubiquinone-10 and α-tocopherol were bought from Sigma-Aldrich (St. Louis, MO, US). Sodium borohydride and chloroform (99.8%) were purchased from Roth (Karlsruhe, Germany). Chemicals for buffer solutions were

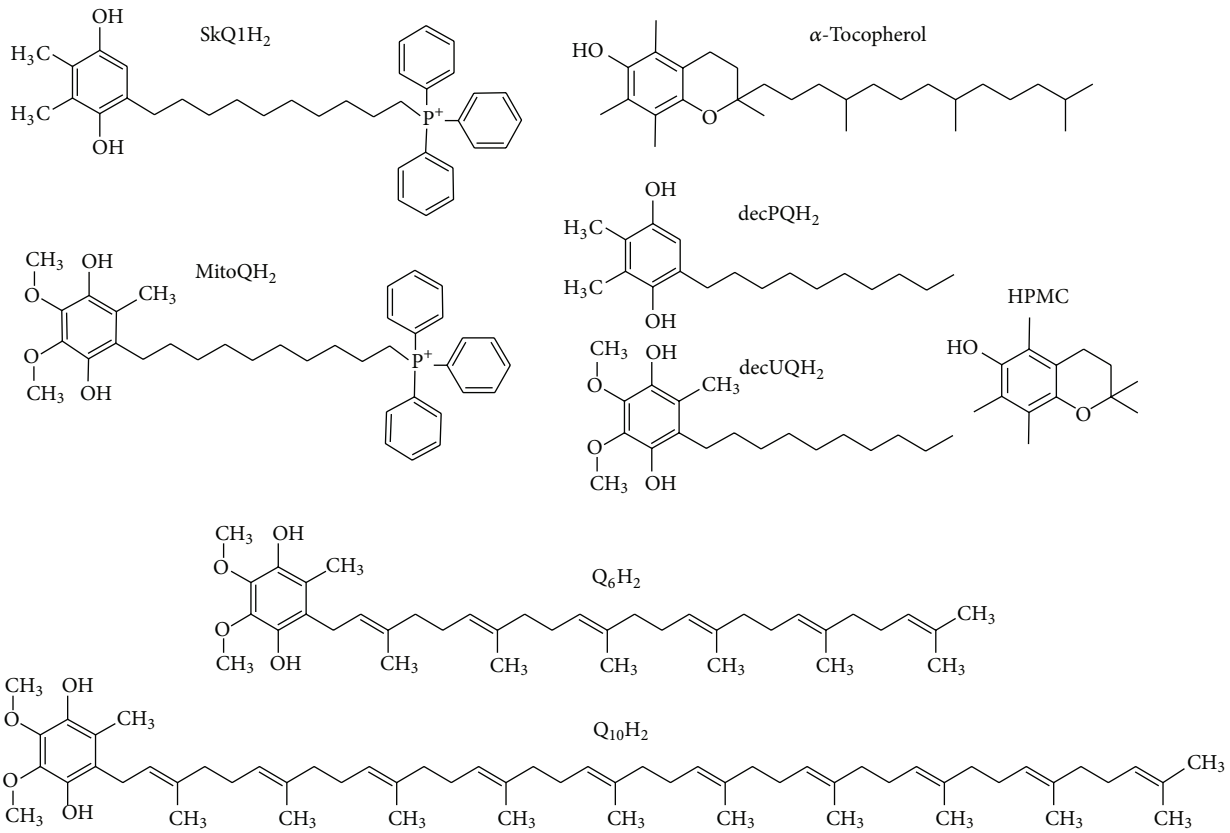

Figure 2: Chemical structures of the tested antioxidants. Quinone-based antioxidants are depicted in their reduced forms (i.e., as quinols).

ordered from Sigma-Aldrich or Roth. Mini-Extruder and the porous membranes were supplied by Avanti. Azo initiator 2,2′-azobis(4-methoxy-2,4-dimethylvaleronitrile), or MeO-AMVN, was delivered by Wako Pure Chemical Industries (Osaka, Japan). HPMC was a gift of Dr. Vitaly Roginsky. Diverse triphenylphosphonium-containing quinone-based antioxidants (see Figure 2) were synthesized in their oxidized (quinone) forms as previously described [63].

2.2. Preparation of Liposomes. The liposomes were produced by extrusion, based on the method of Cullis and coworkers [79, 80], similarly to our previous study [19]. Liposomes were prepared by suspending lipid powder in 50 mM sodium phosphate buffer (pH 7.4) containing 100 μM diethylene-triaminepentaacetic acid (buffer A) to bind possible traces of transition metals, followed by 5 minutes of vortexing to obtain a 3 mg/mL homogeneous lipid suspension. Whenever an antioxidant was incorporated into liposomes, the lipid powder was mixed with the respective antioxidant in chloroform in a glass beaker and the mixture was dried under a stream of nitrogen for at least 2 hours. Then the lipid film was hydrated by buffer A with a short series of ultrasonication followed by 3 freeze-thawing cycles to obtain lipid suspension consisting of large multilamellar vesicles (3 mg/mL). In either case large unilamellar vesicles were formed from lipid suspensions by passing them through a 100 nm pore filter using Mini-Extruder for 19 times. Kinetic studies with liposomes were performed within the day of preparation.

2.3. Converting Quinones to Quinols. Reduction of quinones to corresponding quinols was performed by adding a small amount (2-3 mg) of dry sodium borohydride to 1-2 mM quinone solution in ethanol. The reaction was complete within a minute of intensive mixing. The excess of reductant was removed by a small volume of fuming HCl followed by at least two centrifugations at 15800 g (5 minutes each) to remove the sodium borate pellet. Reduced quinones were stored at −80°C until use. The final quinol concentration was determined from the absorbance maximum at 290 nm. The molar absorptivity coefficients used for ubiquinol-6, ubiquinol-10, plastoquinol-based antioxidants ($SkQ1H_2$ and $decPQH_2$), and amphiphilic ubiquinol-based antioxidants ($MitoQH_2$ and $decUQH_2$) were 4890, 3940 $M^{-1}\,cm^{-1}$ [81], 3540 $M^{-1}\,cm^{-1}$ [82], and 4140 $M^{-1}\,cm^{-1}$ [83], respectively. Under acidic conditions the reduced state of quinols was preserved for months. The list of all antioxidants in their reduced forms is presented in Figure 2.

2.4. Oxidation of HPMC. The oxidized form of HPMC (the respective quinone or other products) was achieved by

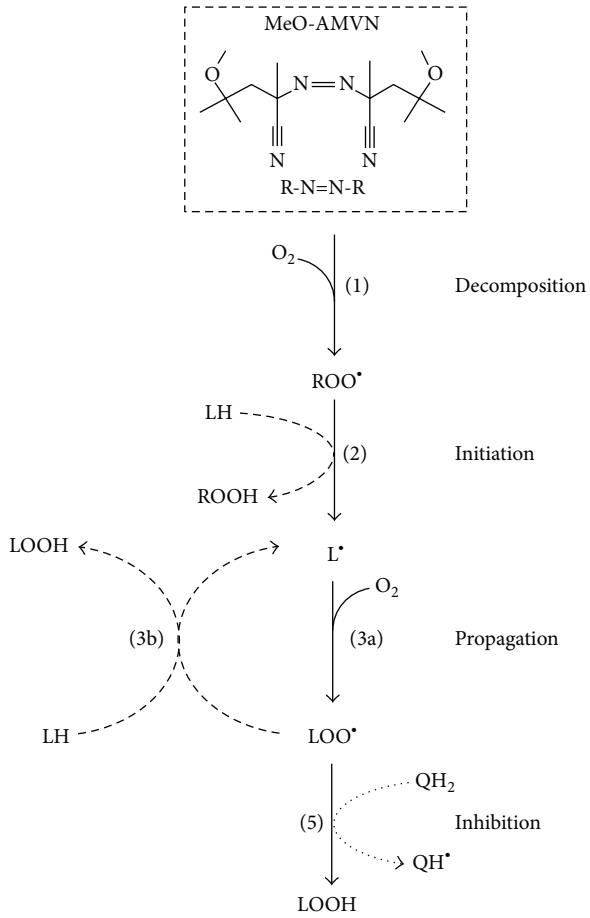

Figure 3: Scheme of a chain radical reaction in a system containing an azo initiator MeO-AMVN, CL molecules, and a chain-breaking inhibitor of quinol nature (based on [4, 10, 15–18]). The main stages of the process are indicated by numbers corresponding to the respective reactions, as described in Section 2. The radical products of the initiator decomposition (1) ROO• initiate the oxidative cycle via formation of an alkyl (L•) radical (2). The reaction propagates ((3a) and (3b)) as this alkyl radical consumes molecular oxygen to form peroxyl (LOO•) radical (3a), which abstracts a hydrogen atom from another lipid molecule (LH) to yield another L• radical (3b). An inhibitor, such as quinol (QH_2), may break the reaction chain by quenching a LOO• radical (5).

overnight incubation of 5 μM HPMC with 10 μM of $CuCl_2$ at 40°C in 50 mM sodium phosphate pH-buffer, pH 7.4.

2.5. Experimental Setup for Lipid Peroxidation Assays. As shown in Figure 3, the lipid peroxidation was initiated by an azo initiator, based on approaches described in [18, 76, 77], similarly as in our previous study [19].

Following Noguchi et al. [18], we launched the peroxidation of CL by adding the peroxyl radical azo initiator MeO-AMVN. This substance spontaneously decomposes, with a rate that is constant at a given temperature, into two carbon-centered radicals, which promptly become peroxyl radicals in an oxygen-rich medium (Figure 3).

Decomposition:

$$\begin{aligned} \text{R-N=N-R} &\longrightarrow 2\text{R}^{\bullet} + \text{N}_2 \\ \text{R}^{\bullet} + \text{O}_2 &\longrightarrow \text{ROO}^{\bullet} \end{aligned} \quad (1)$$

The peroxyl radical (ROO•) may abstract a bis-allylic hydrogen atom from a polyunsaturated lipid molecule, thus initiating the chain.

Initiation:

$$\text{ROO}^{\bullet} + \text{LH} \longrightarrow \text{L}^{\bullet} + \text{ROOH} \quad (2)$$

The resulting carbon-centered lipid radical L• will further react with oxygen molecules to give a peroxyl radical of a lipid (LOO•). This radical, in turn, may attack other polyunsaturated lipids, thereby accounting for the propagation of the oxidation chain.

Propagation:

$$\text{L}^{\bullet} + \text{O}_2 \longrightarrow \text{LOO}^{\bullet} \quad (3a)$$

$$\text{LOO}^{\bullet} + \text{LH} \longrightarrow \text{L}^{\bullet} + \text{LOOH} \quad (3b)$$

The process continues until two radicals terminate in a bimolecular reaction.

Termination:

$$2\,\text{LOO}^{\bullet} \longrightarrow \text{nonradical products} \quad (4)$$

These first stages of polyunsaturated fatty acid peroxidation lead to formation of monohydroperoxide accompanied by the rearrangement of double bonds to form conjugated dienes [4, 84, 85] (see Figures 1 and 3). Conjugated dienes have a broad absorption band with a maximum at 234 nm, which can be monitored spectroscopically. If the majority of polyunsaturated fatty acid residues represent linoleic acid, as in the case of bovine heart CL, the number of peroxides formed would be stoichiometrically equal to the number of conjugated dienes formed [10, 86]. Since we used a mild initiator only capable of producing peroxyl radicals, and the medium was purged from transition metal ions with a chelator, the reaction would halt at the first diene-peroxide stage. This method is both direct, as it quantifies the primary reaction product [10], and precise in terms of the signal to noise ratio.

Chain-breaking antioxidants, such as tocopherols or quinols, react with peroxyl radicals much faster than the bis-allylic hydrogen atom of a fatty acid, and thereby can prevent the chain propagation.

Inhibition:

$$\text{QH}_2 + \text{LOO}^{\bullet} \longrightarrow \text{QH}^{\bullet} + \text{LOOH} \quad (5)$$

The product of such reaction, a semiquinone (QH•) or an α-tocopheroxyl (α-toc•) radical, can either quench another lipid radical species

$$\text{QH}^{\bullet} + \text{LOO}^{\bullet} \longrightarrow \text{Q} + \text{LOOH} \quad (6)$$

or be quenched by another radical species of the same antioxidant. In case of semiquinone, this will partly regenerate the initial quinol molecule via disproportionation:

$$2\,QH^{\bullet} \longrightarrow Q + QH_2 \quad (7)$$

The products of collision of two α-tocopheroxyl radicals may give rise to different substances; see [10].

In the ideal case, when an antioxidant and its oxidation-derived radical form both participate in the quenching of lipid peroxyl radicals, the stoichiometry of the inhibition would correspond to two quenched radicals per one consumed antioxidant molecule. In reality, the stoichiometry is usually lower because of losses. For instance, a semiquinone radical can be oxidized by molecular oxygen yielding a superoxide anion and a fully oxidized quinone molecule as products:

$$QH^{\bullet} + O_2 \longrightarrow Q + O_2^{\bullet -} + H^{+} \quad (8)$$

Ultimately, if the extent of the autooxidation is very high, the stoichiometry of the quenching of peroxyl radicals by quinols may be even close to zero [78, 87]. Unlike quinols, both α-tocopherol and its α-tocopheroxyl radical are practically nonreactive towards oxygen [88], which implies that α-tocopherol and its analogues have an inhibitory stoichiometry of two, being often viewed as reference antioxidants.

Oxidation assays were performed in buffer A at final CL concentration of 100 μM. The sample was incubated in a 3 mL quartz cuvette inside a UV-2450 spectrophotometer (Shimadzu, Tokyo, Japan) equipped with a Peltier element at 40°C. The experiment was initiated by addition of 50 μM MeO-AMVN.

Oxidation of CL was monitored by changes in absorbance at 234 nm which corresponds to formation of conjugated dienes [18, 89, 90]. The value taken for the molar absorptivity of conjugated dienes was 27400 $M^{-1}\,cm^{-1}$. Antioxidants themselves also absorbed in the UV range; however their difference "oxidized minus reduced" spectra had isosbestic points close to 234 nm (Figure 4) and therefore could not notably contribute to the absorbance changes as monitored at 234 nm. Spectra at the wavelengths of 210–300 nm were recorded every 5 minutes against a reference cuvette containing all the same components, except for MeO-AMVN. The noise produced by the setup was always in the range of 0.002 absorbance units at 230–300 nm. Antioxidants were introduced to both cuvettes either initially, when incorporated into CL liposomes, or 30 minutes after the start of the experiment, when incorporated into POPG liposomes, or added as ethanol solutions. The POPG stock suspension used for antioxidant delivery usually contained 20 or 100 μM of antioxidant incorporated into 4 mM of POPG.

2.6. Statistical Analysis of the Data. The statistical analysis was performed with MATLAB software. The data for pure CL oxidation were obtained from five experiments when no antioxidants were incorporated. The data for natural and amphiphilic antioxidants were derived from the plateau region by averaging three runs for each antioxidant incorporated into CL or POPG liposomes, and two runs for $MitoQH_2$. The data for HPMC were averaged from five separate runs including experiments with CL incorporation, POPG incorporation, and external addition to CL liposomes in ethanol, as described in our previous publication [19]. The duration of inhibition phase for each antioxidant was determined as a time point of intersection of the lines corresponding to the average kinetics of inhibited and non-inhibited oxidation.

3. Results

3.1. Preincorporation of Antioxidants into Cardiolipin Liposomes. In the first set of experiments, we incorporated the antioxidants into the hydrophobic lipid phase as described in Materials and Methods. Figures 5(a) and 5(b) show the UV absorbance changes during the MeO-AMVN-induced CL peroxidation in the sample that contained 1 μM $Q_{10}H_2$ incorporated into 100 μM of liposomal CL. The most remarkable changes occurred around 234 nm and 281 nm (Figure 5(c)), which correspond to the absorption maxima of conjugated dienes and "oxidized *minus* reduced" ubiquinone (Figure 4), respectively. First, in response to the addition of MeO-AMVN, the fast formation of ubiquinone was observed (Figure 5(c)). Concurrently, a small dip was observed at 290 nm (Figure 5(b)), which reflected the disappearance of ubiquinol. Only after ubiquinol got exhausted in approximately 100 minutes, a broad peak of conjugated dienes with a maximum at 234 nm appeared and started to grow (Figure 5(c)). The start of absorbance rise at 234 nm correlated well with a plateau in the A_{281} kinetics (at a time point of ~100 minutes). Thus, the protective action of $Q_{10}H_2$ was not compromised until the full expenditure of the antioxidant.

Figures 6(a) and 6(b) show the kinetics of CL oxidation in the presence of three natural antioxidants, namely, $Q_{10}H_2$, Q_6H_2, and α-tocopherol, as well as artificial antioxidants, amphiphilic plastoquinol-based $SkQ1H_2$, and 6-hydroxy-2,2,5,7,8-pentamethylbenzochroman (HPMC), a synthetic α-tocopherol analogue lacking the hydrophobic tail (see Figure 2 for the structures). The initial slopes of the kinetic curves (see the insert in Figure 6(b)) correspond to the effectiveness of the tested substances as antioxidants. Apparently, the quinol-based antioxidants almost fully protected CL from oxidation, unlike α-tocopherol, in the presence of which a notable oxidation of CL still took place. All the quinols, both natural and synthetic, demonstrated equal antioxidant activity, but the duration of the inhibitory action was almost twice longer for $Q_{10}H_2$ and Q_6H_2 as compared with $SkQ1H_2$. The duration of the antioxidant activity of α-tocopherol was the longest. The antioxidant potency of HPMC was lower than that of the quinols and slightly higher than that of α-tocopherol, although the duration of the induction period was much shorter.

We have also examined other amphiphilic analogues of ubiquinol (see Figure 2 for the structures) using the same experimental setup. Namely, we tested the aforementioned $MitoQH_2$, a compound similar to $SkQ1H_2$ but with an ubiquinol group instead of the plastoquinol moiety of $SkQ1H_2$ (Figure 7(a)), and amphiphilic short-tail quinols

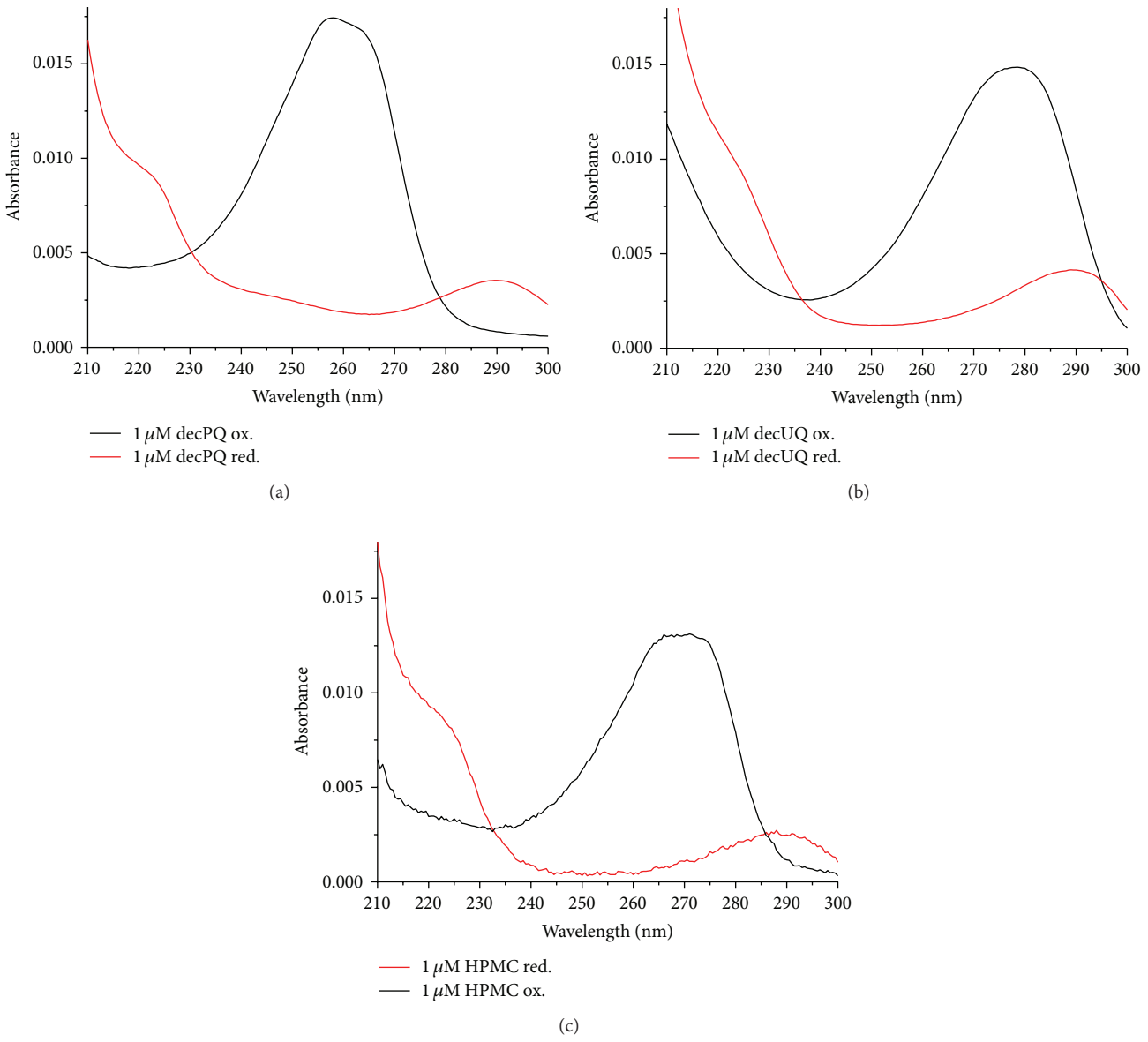

Figure 4: Spectra of oxidized (black line) and reduced (red line) forms of (a) decPQ, (b) decUQ, and (c) HPMC (see text). The spectra were normalized to 1 μM of the substance to assess the impact of oxidation of these compounds into total absorbance changes during the experiment. All the three redox pairs have isosbestic points at 230–240 nm suggesting a minimal interference with the robust signal of conjugated dienes. The ubiquinone/ubiquinol pair also has an "oxidized *minus* reduced" difference absorption maximum at ~275 nm, which does not strongly overlap with the spectrum of conjugated dienes.

lacking penetrating cation moieties, $decPQH_2$ and $decUQH_2$ (Figure 7(b)). In both cases, the antioxidant efficiency of all tested compounds was high, but the duration of protection was almost twice as long in the case of ubiquinol-based antioxidants.

The quantitative comparison of different antioxidants incorporated into CL or POPG liposomes (see also Section 3.2) is given in Figure 8 and Table 1. The data correlate with our previous study where the amphiphilic quinol-based antioxidants were potent inhibitors of CL peroxidation when added externally as ethanol solutions [19].

3.2. Preincorporation of Antioxidants into Nonoxidizable Liposomes. The data in Figures 6–8 and Table 1 indicate that all tested quinol-based antioxidants efficiently protected liposomal CL from oxidation; still with this approach we could not compare the kinetics of CL oxidation in the absence and in the presence of an antioxidant, respectively, because antioxidants were added already upon the preparation of liposomes. In our previous study [19], we added antioxidants as an ethanol solution after liposomes underwent MeO-AMVN-initiated peroxidation for 30 minutes. This approach, however, is of little use with hydrophobic, water-insoluble

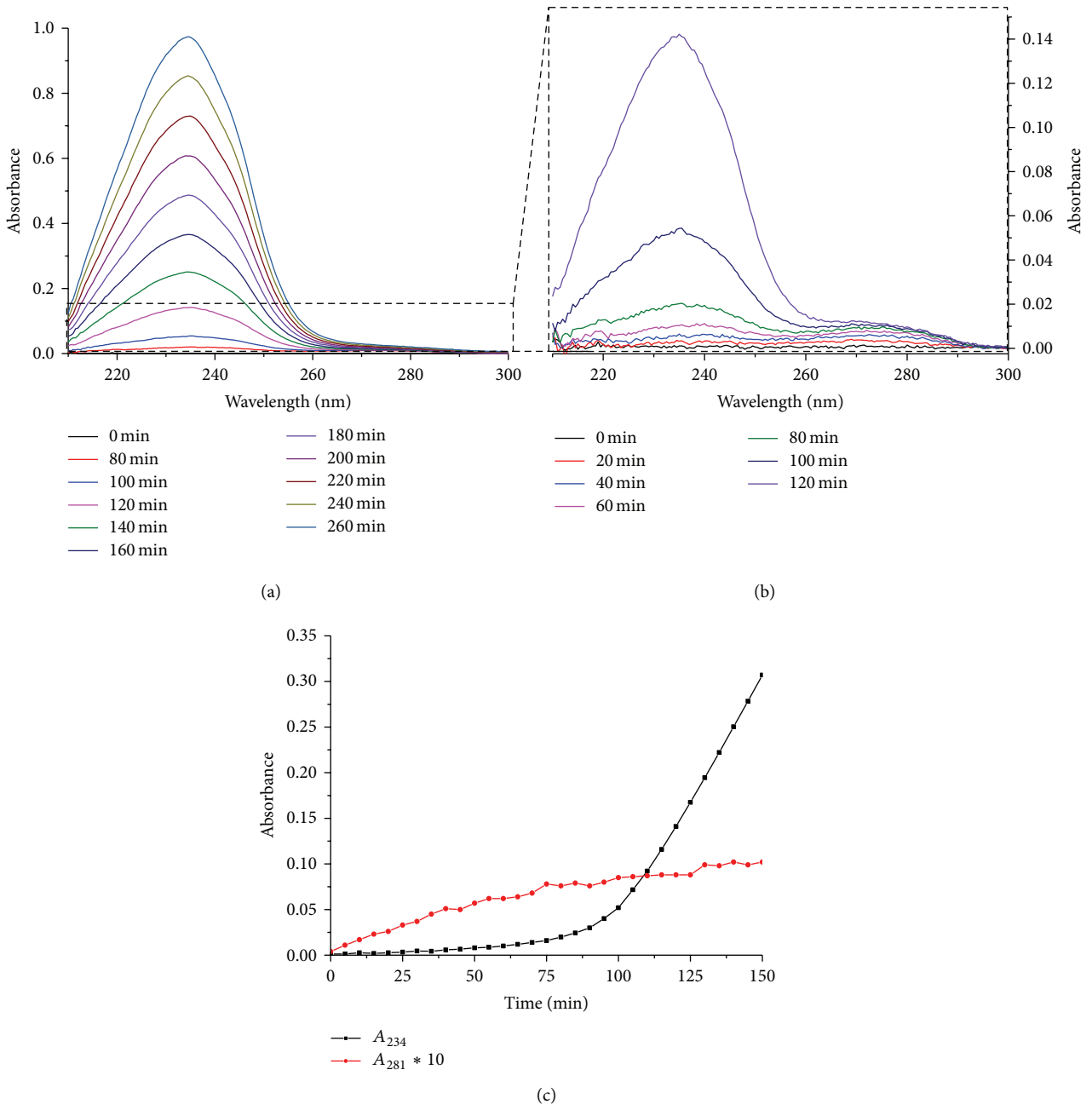

Figure 5: Prevention of the MeO-AMVN-induced oxidation in CL liposomes by 1 μM $Q_{10}H_2$. Conditions: pH-buffer A (see Section 2), 100 μM CL, 50 μM MeO-AMVN, and 40°C. (a, b) Spectral changes of the liposome suspension over the whole time range (a) and during the induction phase (b). (c) Kinetics of absorbance changes at 234 nm (accumulation of conjugated dienes) and at 281 nm ("oxidized *minus* reduced" absorption difference for Q_{10}, cf with Figure 4(b)) show that lipid peroxidation did not start before the antioxidant $Q_{10}H_2$ was exhausted.

antioxidants. Therefore, we combined preincorporation of hydrophobic antioxidants into lipid bilayer with an external way of their supplementation to CL liposomes. For this purpose, antioxidants were incorporated into liposomes made of an inert, nonoxidizable lipid 1-palmitoyl-2-oleoyl-phosphatidylglycerol (POPG), and these antioxidant-loaded liposomes were added to a suspension of CL liposomes that underwent MeO-AMVN-driven peroxidation for 30 minutes (Figures 9(a) and 9(b)). In this setup we tested the antioxidant potency of $Q_{10}H_2$, Q_6H_2, and α-tocopherol, as well as of $SkQ1H_2$ (Figure 9(a)). The generation of conjugated dienes was essentially blocked by the addition of liposomes that contained $SkQ1H_2$; the duration of the lag period was similar to that observed earlier when the same antioxidant was added in an ethanol solution (~60 min, see [19]). Natural hydrophobic antioxidants, being added, within liposomes, to the same final concentration of 1 μM, retarded the oxidation of CL only slightly, and to the same extent. To understand

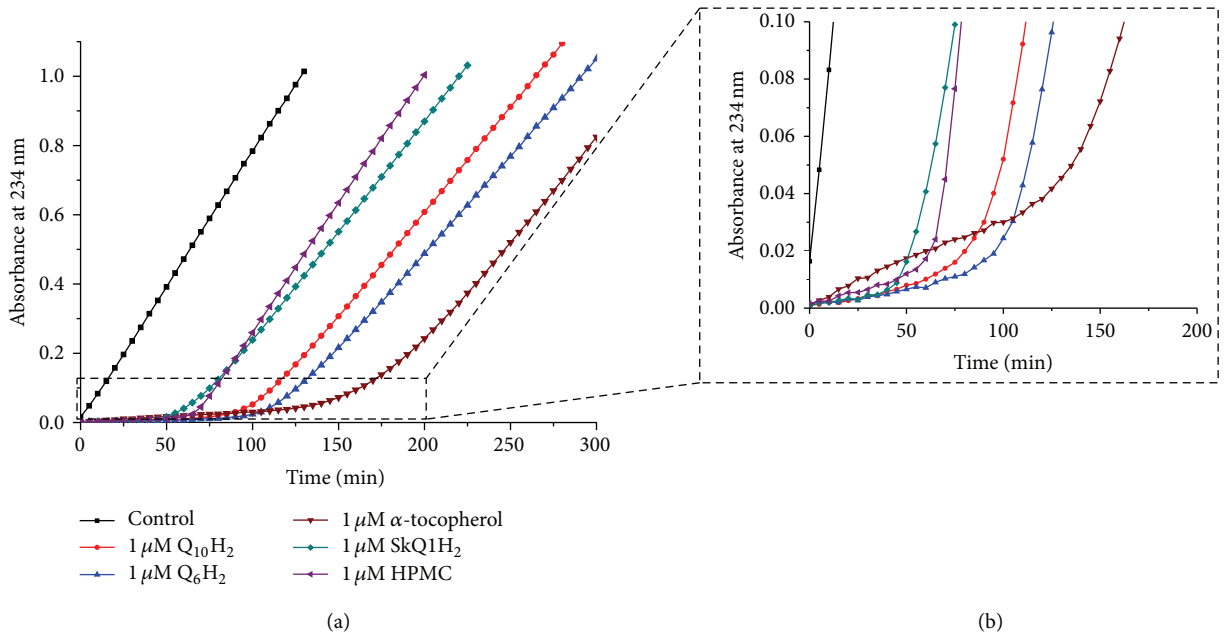

Figure 6: Prevention of the MeO-AMVN-induced oxidation of CL liposomes by incorporated natural antioxidants, $SkQ1H_2$ and HPMC. Conditions: pH-buffer A (see Section 2), 100 μM CL, 50 μM MeO-AMVN, and 40°C. (a, b) Kinetics of absorbance changes at 234 nm in the presence of 1 μM of tested incorporated antioxidants and in their absence (black line) over the whole time range (a) and only during the induction phase (b).

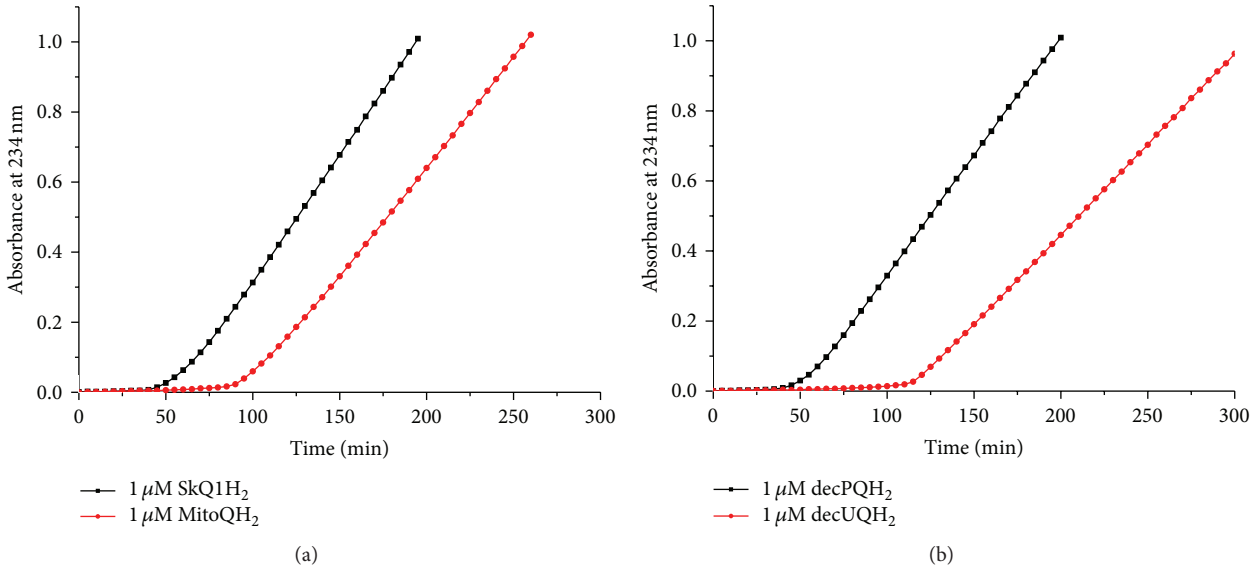

Figure 7: Prevention of the MeO-AMVN-induced oxidation in CL liposomes by incorporated amphiphilic, quinol-based antioxidants. Conditions: pH-buffer A (see Section 2), 100 μM CL, 50 μM MeO-AMVN, and 40°C. (a, b) Absorbance changes at 234 nm in the presence of decyl-containing antioxidants (a) and decyltriphenylphosphonium-containing antioxidants (b).

the reason of this retardation, we have studied the impact of $Q_{10}H_2$ in some more detail (Figure 9(b)). The effect of $Q_{10}H_2$ was found to be concentration-dependent, as 5 μM of $Q_{10}H_2$ retarded the peroxidation more efficiently than 1 μM of $Q_{10}H_2$. In contrast, the efficiency was independent of the lipid : antioxidant ratio in the added POPG suspension. 1 μM of $Q_{10}H_2$ introduced with 200 μM POPG was almost as efficient as 1 μM of $Q_{10}H_2$ added within 40 μM POPG (Figure 9(b)). Apparently, only the final concentration of $Q_{10}H_2$ determined the efficiency, but not the amount of externally added POPG. It is noteworthy that in both experiments (Figures 9(a) and 9(b)) the addition of POPG liposomes without antioxidants (the control sample) did not affect the rate of CL peroxidation.

Table 1: Relative efficiencies of various antioxidants in CL liposomes (note the split y-axis). The values for oxidation rates were obtained from the data in Figures 6, 7, and 10 and analogous repetitive experiments as described in Section 2. The chain propagation length for pure CL and each antioxidant was calculated using the radical production rate of 11.8 nM/min, as derived from the α-tocopherol run; see Section 4. The inhibition efficiencies were calculated as ratios of the respective uninhibited and inhibited oxidation rates. The inhibition duration rates were determined from the data in Figures 5–7 and 10.

Antioxidant	CL oxidation rate, nM/min	Chain propagation length	Inhibition efficiency	Inhibition duration (min)
Pure CL	334 ± 32	28	—	—
$decPQH_2$	3.28 ± 1.1	0.28	102	48.7 ± 2.1
$SkQ1H_2$	3.87 ± 0.6	0.33	86	58.7 ± 5.7
$decUQH_2$	4.49 ± 1.2	0.38	74	114 ± 4.4
$MitoQH_2$	6.70 ± 2.0	0.57	50	91 ± 8.9
Q_6H_2	4.05 ± 0.5	0.34	82	124 ± 9
$Q_{10}H_2$	4.55 ± 0.4	0.39	73	104 ± 1
α-Tocopherol	10.6 ± 0.5	0.90	32	171 ± 1
HPMC	8.62 ± 1.8	0.73	39	N.A.*

*The duration of action varied dramatically in the case of HPMC because of its variable loss upon the incorporation into liposomes; see Section 4.

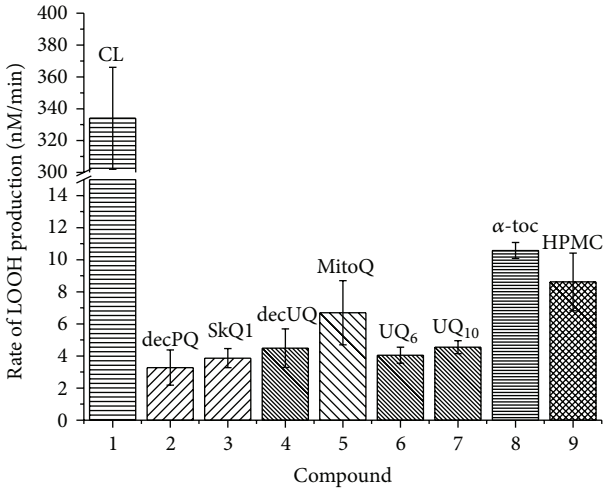

Figure 8: The rate of oxidation of liposomal CL in the presence of various antioxidants (data from Figures 5–7 and 10; see also Table 1). 1 μM of hydrophobic or amphiphilic antioxidants was added to 100 μM of CL liposomes in the presence of 50 μM of MeO-AMVN (40°C). The mean values are represented as bars, and the standard deviations are shown as ticks (see Section 2).

With externally added liposomes we delivered also some further analogues of natural antioxidants, namely, HPMC, $MitoQH_2$, $decPQH_2$, and $decUQH_2$, to CL liposomes (Figure 10(a)). All these amphiphilic antioxidants were able to diffuse between liposomes via the water phase and prevent the oxidation of CL. Similarly to the CL-incorporated antioxidants (Figures 6 and 7) and the antioxidants introduced as ethanol solutions [19], the ubiquinol-based antioxidants ($decUQH_2$, $MitoQH_2$) showed an approximately twice as long inhibitory period compared to plastoquinol-based antioxidants ($decPQH_2$, $SkQ1H_2$). Here, HPMC was again barely able to incorporate into the POPG liposomes upon their preparation accounting for the shortest lag period, as compared to other tested antioxidants (Figure 10(a)). Figure 10(b) shows the antioxidant action of compounds that were delivered to the suspension of CL liposomes being dissolved in ethanol, using the approach from our previous study [19]. In this case, HPMC provided a much longer protection with a stoichiometry close to two trapped radicals per one antioxidant molecule.

4. Discussion

The present work complements our previous study of quenching the peroxidation of CL liposomes by amphiphilic antioxidants dissolved in ethanol [19]. Here, we tested natural hydrophobic antioxidants such as α-tocopherol and ubiquinols, by preincorporating them into the hydrophobic environment of liposomes.

The relative antioxidant efficiency of ubiquinols and tocopherols was earlier assessed in numerous natural and artificial systems and was shown to depend on the nature of the system tested [16, 91–100].

In homogeneous systems, such as hexane [91, 92] or acetonitrile [92], α-tocopherol was shown to be more efficient than ubiquinol-10 in protecting fatty acid esters from oxidation.

In heterogeneous systems containing polar/nonpolar interfaces, the affinity of both the antioxidant and substrate—the lipid peroxyl radical—to the interfaces could affect the kinetics of radical quenching. In simplest biphasic micellar systems the antioxidant potencies of quinols and α-tocopherol were shown to be comparable [78, 92, 101]. In the case of low density lipoprotein (LDL) particles, the carriers of fatty acids in the blood, the literature data on relative antioxidant capacities of ubiquinol and α-tocopherol indicate a higher protective effect of ubiquinol [93, 97].

Unilamellar liposomes represent a good model for quantitative studying of antioxidants [102]. While liposomes share many traits with physiological systems, their oxidation kinetics can be described by the law of mass action [103, 104]. However, liposomal phospholipid membranes are even more complex than micelles or LDL particles because of the complex nature of their interfaces formed of polar

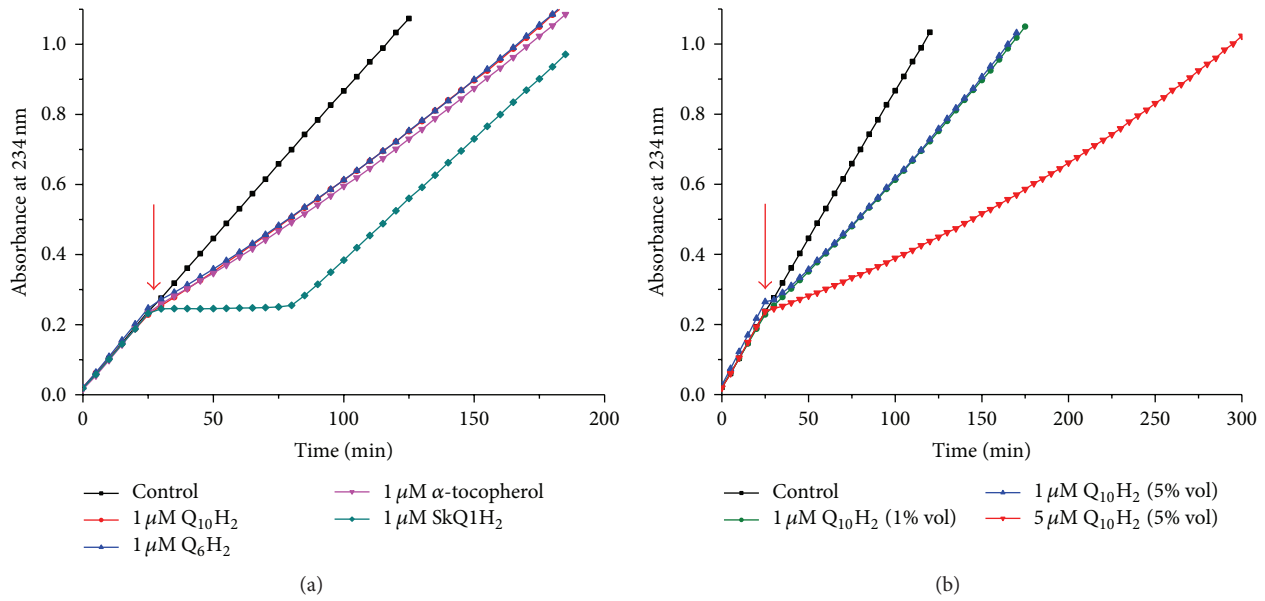

Figure 9: Prevention of MeO-AMVN-induced oxidation of CL liposomes by antioxidants added externally within POPG liposomes. Peroxidation was started by addition of 50 μM MeO-AMVN to 100 μM CL liposomes at 40°C in buffer A. Antioxidant-containing POPG liposomes were added 30 minutes after the start of the experiment, as indicated by arrows. (a) Comparison of $SkQ1H_2$ with natural hydrophobic antioxidants. In each case the final concentrations were 1 μM of antioxidants and 40 μM of POPG. (b) Radical quenching efficiency of ubiquinol-10 as function of its concentration and the extent of dilution. The amount of added POPG stock suspension was 1% (30 μL) or 5% (150 μL) of the total system volume, which accounts for 40 or 200 μM POPG, respectively.

lipid heads that are connected to the hydrophobic tails via glycerol moieties and phosphate groups. The redox active moieties of tocopherols [105] and natural ubiquinols [106–108] are expected to dwell on the level of these phosphate groups. Therefore, interactions of antioxidants with these membrane embedded polar groups may additionally affect the antioxidant efficiency and other properties of tocopherols and ubiquinols. Furthermore, the exact position of the polar "phosphate" layer might depend on the nature of the phospholipid; molecular dynamics simulations showed that the phosphate to phosphate distances increased from about 3.8 nm to about 4.7 nm when the CL content of a POPC membrane changed from 0% to 100% [109]. Therefore, the relative antioxidant efficiency of tocopherols and ubiquinols, as well as their other properties, may depend on the nature of phospholipids and should be determined experimentally for different lipid membranes.

According to the here presented data, all the tested quinols were equally highly effective in protecting CL from peroxidation, as indicated by negligible slopes of absorbance increase at 234 nm in their presence; see Figures 5–8 and 10, as well as the Table 1. In agreement with previous observations [19], even minute, residual amounts of the antioxidant were sufficient to protect CL from peroxidation. At the same time, α-tocopherol and its hydrophilic analogue HPMC were less effective (Figures 6 and 10). These results were rather unexpected, since some of the previous data on concurrent measurements of antioxidant activities of α-tocopherol and ubiquinols in lipid bilayers were interpreted as indicating α-tocopherol to be either an equally potent [94], or even a better [91] antioxidant than ubiquinol. In these experiments, where both α-tocopherol and ubiquinol-10 were present as antioxidants, ubiquinol was consumed before α-tocopherol [91, 92, 94, 97, 110, 111]. Building on the previously observed kinetic superiority of α-tocopherol over ubiquinol in homogenous model systems [16, 91, 92] and the observed ability of ubiquinol to recover the α-tocopheroxyl radical [92, 112], it was generally implied that the faster expenditure of ubiquinol was only apparent, being due to repletion of the promptly oxidized α-tocopherol by ubiquinol; see [113, 114] for reviews. Our kinetically resolved data clarify this conundrum, at least, for CL membranes. It follows from our data that all the tested quinol-based antioxidants distinctly outperformed α-tocopherol and its hydrophilic analogue HPMC. The faster oxidation of ubiquinol in the presence of α-tocopherol in the earlier experiments with liposomes [91, 92, 94, 97, 110, 111] was, most likely, due to the genuinely faster interaction of ubiquinol with radical species. To what extent our results could be extrapolated to multicomponent mitochondrial membranes, where the potency of different antioxidants is constrained by the rate of their "recycling" by components of the electron transfer chain [63, 110, 111], is yet to be established.

The radical-scavenging stoichiometry for α-tocopherol equals two trapped peroxyl radicals per antioxidant molecule under most of the experimental conditions [10]; the same should be true for its hydrophilic analogue HPMC. Indeed, when HPMC was added as ethanol solution (Figure 10(b)) the duration of its action was almost as long as that of ubiquinol-based antioxidants. The shorter duration of action

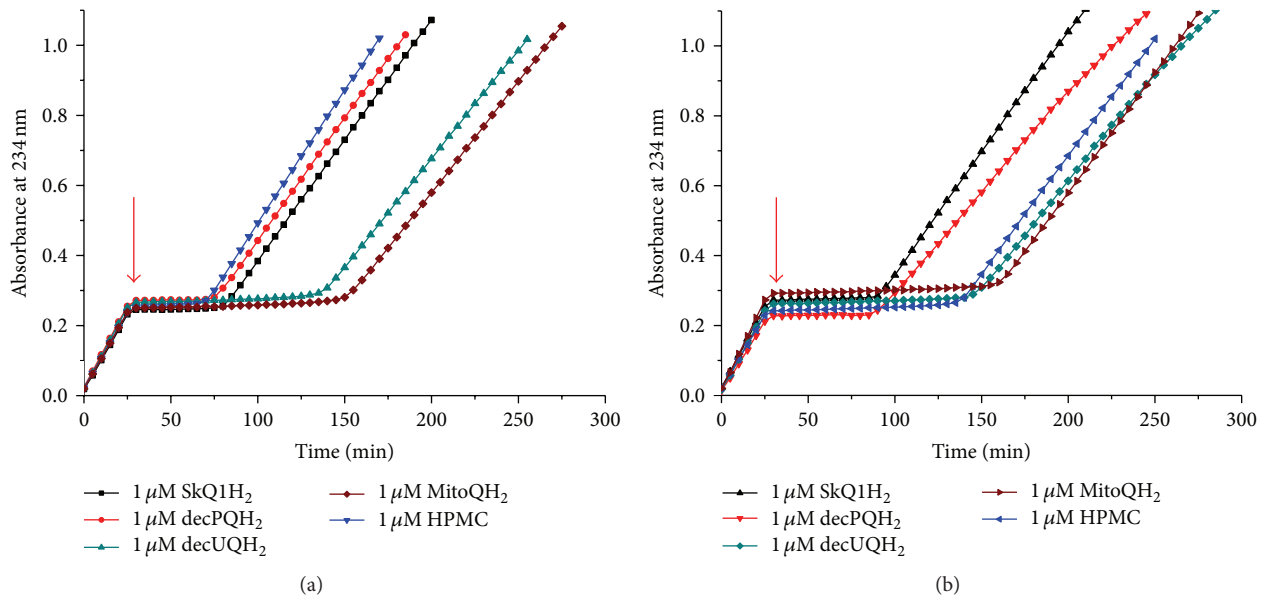

Figure 10: Prevention of MeO-AMVN-induced oxidation in CL liposomes by various antioxidants added externally within POPG liposomes (a) or as ethanol solutions (b). Peroxidation was started by addition of 50 μM MeO-AMVN to 100 μM CL liposomes at 40°C in buffer A. The moments of addition of the antioxidants (30 minutes after the start of the experiment) are marked by arrows. (a) Effects of 1 μM $SkQ1H_2$, 1 μM $decPQH_2$, 1 μM $decUQH_2$, 1 μM $MitoQH_2$, or 1 μM HPMC added in POPG liposomes to CL liposomes within 40 μM POPG (1% volume). (b) Effects of 1 μM $SkQ1H_2$, 1 μM $decPQH_2$, 1 μM $decUQH_2$, 1 μM $MitoQH_2$, or 1 μM HPMC added as ethanol solutions, see also [19].

of HPMC upon its addition into liposomes (Figures 6 and 10(a)) might reflect the loss of hydrophilic HPMC upon the sample preparation.

From our data, we could approximately estimate the chain propagation length of CL peroxidation in the membrane, that is, the number of peroxidized fatty acid chains per one radical as generated upon thermal decomposition of MeO-AMVN (see Figure 3). Typically, this value could be obtained from an experiment where the oxidation is inhibited by an antioxidant with known stoichiometry, for example, α-tocopherol, for which the number of trapped radicals has been estimated as two [10]. During the lag phase caused by the addition of a potent antioxidant, all the radicals generated are assumed to be eventually quenched, so that the total number of generated radicals should match the concentration of the added antioxidant.

In our experiments, α-tocopherol, a reference antioxidant for such calculations, could not block the oxidation of CL completely, unlike quinols.

According to the data in Figure 6, the duration of plateau due to the oxidation of 1 μM α-tocopherol was about 170 minutes. Assuming that all radicals produced by the MeO-AMVN decomposition were finally trapped by α-tocopherol, and two radicals were taken per one α-tocopherol molecule, the rate of radical generation within this system would be 1 μM/170 min × 2 = 11.8 nM/min. At the end of plateau the absorbance at 234 nm (A_{234}) reached approx. 0.04; this corresponded to ~1.5 μM of peroxidized lipid tails (given that the molar extinction of conjugated dienes is about 27400 M^{-1} cm^{-1}); that is, the oxidation rates of α-tocopherol and CL coincided under such conditions. Thus, α-tocopherol managed to trap directly about half of the radicals that would otherwise attack CL molecules in the absence of the antioxidant.

To calculate the rate of lipid oxidation, R_{ox}, as caused by this radical flux, we calculated the rate of lipid oxidation without inhibitors (the first 25 minutes of the experiment in Figure 10(a)). This value may be derived from the accumulation of conjugated dienes as followed at 234 nm, assuming that the molar extinction coefficient for conjugated dienes is 27400 M^{-1} cm^{-1}:

$$R_{ox} = \frac{c\,(\text{lipid})}{t} = \frac{\left(A_{234}\,(25\text{ min}) - A_{234}\,(0\text{ min})\right)}{(27400 \times 25\text{ min})} = 3.3 \times 10^{-7}\,\text{M} \times \text{min}^{-1}. \quad (9)$$

Hence, the rate of uninhibited CL oxidation was ~ 330 nM/min, resulting in a chain propagation length of the CL peroxidation cycle of approximately 28. In the case of natural ubiquinols as antioxidants the chain propagation length was less than 0.4 (see Table 1), which indicates that the quenching of radicals by the antioxidant (see (5)) was approx. three times faster than the formation of a fatty acid peroxide (see (3a)). Hence, almost all radicals were quenched before getting the opportunity to oxidize a fatty acid, so that quinols essentially prevented the propagation of lipid oxidation. In the presence of α-tocopherol, the chain propagation length was about 0.9, which roughly corresponds to the quenching of only each second radical (see also above).

The duration of the inhibitory effect, as tested here and in the previous study [19], was, in both cases, related to the nature of the antioxidant moiety, decreasing in the series

α-tocopherol ~ ubiquinol > plastoquinol, independently of the rest of the structure of the antioxidant; compare Figures 5–7, 9, and 10, Table 1, and [19]. Hence, although all the quinols got fully oxidized at the end of the lag phase, the duration of the inhibitory action of plastoquinols (this work) and several other quinols [19] was approximately two times shorter than the respective duration for ubiquinols, which, in turn, was almost as long as the duration of the protective effect of α-tocopherol. Since α-tocopherol is known to quench stoichiometrically two peroxyl radicals per molecule [10, 16, 92], the number of quenched radicals could be estimated as slightly less than two for ubiquinols and as about one for other tested quinols.

As discussed elsewhere [10, 115, 116], the decrease in the number of quenched radicals in the case of quinols might be due to the competition of radical species with oxygen for the semiquinones of the antioxidant (see (8)). Most likely, the shorter oxidation time of quinols as compared to α-tocopherol was due to the partial oxidation of semiquinones by the oxygen; see the discussion below and [115, 116]. The slower expenditure of methoxy-substituted ubiquinols, as compared to other quinols, was earlier noted in experiments where oxidation of styrene and methyl linoleate in micelles was induced by a water-soluble azo initiator [78, 87]; the difference was attributed to the slower oxidation of methoxy-substituted semiquinones by oxygen (see (8)) as compared to other semiquinones.

The slower oxidation of methoxy-substituted ubisemiquinones by oxygen (Figures 6, 7, 9, and 10) may have several reasons. Some of the available estimates of the standard redox potential at neutral pH ($E_o{}^7$) for the ubiquinone/ubisemiquinone redox pair for protic solvents, such as methanol or water, are higher (up to 90 mV [117]) than the estimates for $E_o{}^7$ for the oxygen/superoxide pair under the same conditions (approx. −150 mV) [116, 118]. Conversely, the available estimates for $E_o{}^7$ of the plastoquinone/plastosemiquinone pair are lower, for example, −165 mV [115]. With these numbers taken at a face value, the equilibrium of the reaction

$$O_2 + SQ \longleftrightarrow O_2^{\bullet -} + Q \quad (10)$$

should be shifted to the left in case of ubiquinone and to the right in case of plastoquinone, in agreement with our observations and also the earlier reports on the long life of pulse-generated ubiquinone radicals in the presence of oxygen [117, 119].

Still, the case might be not so simple. In fact, the potentials of redox pairs that involve radical states strongly depend on the environment and the measurement conditions. Generally, any interaction that would selectively stabilize the polar semiquinone molecule should increase the respective $E_o{}^7$ value [37, 115, 120]. Therefore, for semiquinone-involving redox pairs the very term "standard redox potential" (E_o) is meaningful only in relation to particular homogeneous solvents such as water, methanol, or *n*-hexane [115]. For micelles or phospholipid bilayers it is more appropriate to use a "working" term "midpoint redox potential" (E_m) for the efficient redox potential; a term being applicable only to the given system and only under given conditions. No systematic determination of midpoint potentials of quinones in CL bilayers has been done so far. Therefore, the thermodynamics of quinol oxidation in CL membranes awaits its investigators. In addition, the methoxy groups of ubisemiquinones can kinetically hamper the interaction with oxygen, as discussed in more detail in [19]. Particularly, a methoxy group might render the addition of dioxygen molecule to the benzene ring of the semiquinone, which seems to precede the subsequent elimination of superoxide [121].

Hence, as it follows from our data, ubisemiquinone radicals were much less susceptible to oxygen than radicals of other semiquinones when studied within a CL bilayer, which modeled the mitochondrial environment of respiratory complexes. The relative contributions of thermodynamic and kinetic factors in rendering the oxidation of ubisemiquinones by oxygen deserve further clarification. The physiological and evolutionary implications of the poor oxidizability of ubisemiquinones by oxygen are discussed elsewhere [122].

As it follows from Figures 5–8 and 10 as well as from Table 1, the quinols of the same type (ubiquinols, plastoquinols) but differing in the side chain structure (with decyl, decyltriphenylphosphonium, or prenyl tails) protected CL liposomes from oxidation with similar efficiency. This is also true for α-tocopherol and its hydrophilic analogue HPMC (see Figures 6 and 10). This finding correlates with the previous studies where the antioxidants bearing the same active group were equally efficient in protecting liposomes made of two-tail lipids [76, 123].

In experiments with two types of liposomes, namely, oxidizable CL liposomes and antioxidant-containing, nonoxidizable POPG liposomes (Figure 9), all the three tested natural hydrophobic antioxidants (Q_6H_2, $Q_{10}H_2$, and α-tocopherol), being much less efficient than $SkQ1H_2$, slowed down the peroxidation of CL to the same extent (Figure 9(a)). Although we used a hydrophobic azo initiator MeO-AMVN with the oil/water distribution coefficient of about 1000 [124], the prevalence of the aqueous phase in our system over the lipid phase and the more hydrophilic nature of the MeO-AMVN-derived peroxyl radicals as compared to MeO-AMVN suggest that lipid peroxidation would be almost exclusively induced from the water phase, which agrees with the fact that the MeO-AMVN radicals can be removed by size exclusion gel filtration [124]. In this case, the extent of radical quenching would not depend on the amount of nonoxidizable lipid. Indeed, a fivefold increase in the amount of nonoxidizable lipid did not affect the rate of CL oxidation (Figure 9(b)).

The rate of CL peroxidation decreased, however, when the total amount of incorporated ubiquinol-10 was increased; see Figure 9(b). It is unlikely that highly hydrophobic antioxidants could escape the POPG membrane and relocate into the CL liposomes to protect them. The exchange of α-tocopherol between liposomes was estimated to be in the order of hours [125, 126]; for more hydrophobic Q_6H_2 and $Q_{10}H_2$ the exchange time should be even longer. In all likelihood, the antioxidants in POPG liposomes "competed" with CL molecules for the water-dissolved MeO-AMVN radicals. In Figure 9, 1 μM of hydrophobic antioxidant in

POPG liposomes slowed down the oxidation of CL liposomes only by a factor of 3, although the rate constant of radical quenching by an antioxidant (about 3×10^5 M^{-1} s^{-1}) is 5000 times larger than the rate constant of hydrogen abstraction from polyunsaturated linoleate acid (60 M^{-1} s^{-1}; see [122] and the references therein). One has to consider, however, that 1 μM of antioxidant competed with 100 μM of CL. Taking into account four polyunsaturated tails per 1 CL molecule and the chain reaction length of 28 (see above), one gets acceptable correspondence with the experimental data. In the framework of the suggested rational, one would expect that a 5-fold increase in the amount of antioxidant would decrease the rate of lipid peroxidation also fivefold. We have observed only a threefold drop in the rate (Figure 9(b)); the reason for this minor discrepancy with the expectations should be yet clarified.

While ubiquinols were more efficient than α-tocopherol in experiments where antioxidants were added to CL upon preparation of liposomes, the efficiency of natural ubiquinols and α-tocopherol was similarly low when they were incorporated in the POPG liposomes (Figure 9(a)). In the latter case, the rate of CL oxidation should slow proportionally to the fraction of the MeO-AMVN radicals that were quenched in the hydrophobic phase of the antioxidant-containing POPG liposomes. Under the assumption that the fraction of MeO-AMVN radicals that got into the hydrophobic phase of POPG liposomes was independent of the nature of the antioxidant, the data obtained indicate that almost all MeO-AMVN radicals that got into the hydrophobic phase of the POPG liposomes could be quenched, independently of the nature of incorporated hydrophobic antioxidant.

In contrast to hydrophobic antioxidants, the amphiphilic antioxidants, when added with POPG liposomes, fully blocked the oxidation of CL (Figures 9 and 10(a)). Apparently, amphiphilic antioxidants could easily escape the POPG liposomes to interact with the CL liposomes or the MeO-AMVN radicals in the solution.

As noted in Introduction, SkQ ions and other amphiphilic antioxidants exhibited pronounced therapeutic effects *in vivo* [20, 44, 52, 54, 55, 61–74, 127–129], in spite of high levels of hydrophilic and hydrophobic antioxidants present in the cells, even when added in minute amounts. The mechanism of this specific therapeutic action has remained obscure. Here we show that natural ubiquinols extremely efficiently protect CL from oxidation within membrane bilayer, so that their failure *in vivo* cannot be attributed to poor antioxidant qualities. The reported particular efficiency of amphiphilic antioxidants [20, 44, 52, 54, 55, 61–74, 127–129] might be related to our observation that amphiphilic antioxidants, unlike the hydrophobic ones, can protect CL molecules from the water phase (Figure 9). Indeed, given that many CL molecules are trapped within respiratory enzymes [22], as well as between respiratory enzymes of supercomplexes [26–28], that is, close to locations where ROS are generated [9, 33–40, 45], it is tempting to anticipate that these trapped CL molecules might be the first to become accessible to ROS. This fraction of CL molecules, however, might be secluded both from the bulky ubiquinol-10 molecules with their large isoprenoid tails confined between the membrane leaflets [130] and from the highly polar water-soluble antioxidants, such as glutathion. Earlier we have suggested that these secluded CL molecules could be still accessible to small, nimble, and amphiphilic artificial antioxidants [19, 122]. The data in Figure 9 indicate that a further advantage of amphiphilic antioxidants over natural ubiquinols and tocopherols is the ability to reach their "occluded" CL targets from the water phase, without the need to get through tightly packed α-helices of respiratory supercomplexes. Such a scenario would explain the ability of amphiphilic antioxidants to prevent the CL oxidation *in vivo*.

Hence, those CL molecules that are occluded within respiratory complexes are close to the sources of ROS and should be the first targets of oxidation in response to a redox imbalance in the respiratory chain. The same secluded CL molecules should be hardly accessible to natural antioxidants. Taken together, these two factors may explain why CL molecules are those preferably oxidized upon oxidative stress [20, 43, 44]. An interaction with cytochrome *c* molecules at the membrane surface would result in a further oxidation of CL and release of cytochrome *c* into the cytoplasm [41–44]. Hence, the very susceptibility of CL molecules to oxidation should accelerate the delivery of the message on a redox disaster within mitochondria to the cytoplasmic apoptotic machinery, which might explain the recruiting of CL as the primary sensor of the apoptotic cascade by nature.

In sum, amphiphilic, positively charged antioxidants targeted to mitochondria might specifically protect the occluded CL "sensors" from oxidation and postpone thereby apoptosis. Such postponement might be life-saving in case of acute but transient oxidative stress, such as upon traumas or strokes. Therefore amphiphilic antioxidants, even being added in minute amounts over a huge background of natural ubiquinol and tocopherol, might be efficient in preventing irreversible damage and death.

5. Conclusions

We found that natural ubiquinols were as efficient in protecting CL liposomes from peroxidation as ubiquinol-based amphiphilic antioxidants, whereas chromanol-based antioxidants were 2-3 times less efficient. The amphiphilic antioxidants, but not the natural ubiquinols and α-tocopherol, could, additionally, interact with the CL bilayer from the water phase. Building on these data, we suggest that the therapeutic efficiency of mitochondrially targeted amphiphilic antioxidants is owing to their ability to protect those CL molecules that are inaccessible to natural hydrophobic antioxidants, being trapped within respiratory supercomplexes. The high susceptibility of such occluded CL molecules may have prompted their recruitment as the sensors of oxidative stress by nature.

Abbreviations

CL: Cardiolipin
$decPQH_2$: Decylplastoquinol
$decUQH_2$: Decylubiquinol

HPMC:	6-Hydroxy-2,2,5,7,8-pentamethylbenzochroman
MeO-AMVN:	2,2′-Azobis(4-methoxy-2,4-dimethylvaleronitrile)
$MitoQH_2$:	10-(6′-Ubiquinonyl)decyltriphenylphosphonium
MPT:	Mitochondrial permeability transition
LDL:	Low density lipoprotein
POPG:	1-Palmitoyl-2-oleoyl-phosphatidylglycerol
Q_6H_2:	Ubiquinol-6
$Q_{10}H_2$:	Ubiquinol-10
ROS:	Reactive oxygen species
SkQ:	Compounds composed of penetrating cation and quinone
$SkQH_2$:	Reduced (quinol or hydroquinone) forms of SkQ
$SkQ1H_2$:	10-(6′-Plastoquinonyl)decyltriphenylphosphonium
SQ or $QH^{\bullet}$:	Semiquinone.

Competing Interests

The authors declare that there are no competing interests regarding the publication of this paper.

Acknowledgments

The authors gratefully acknowledge many useful pieces of advice from Dr. V. A. Roginsky and helpful discussions with Drs. B. V. Chernyak, R. A. Simonyan, and M. Y. Vyssokikh. This work was supported by grants from the Russian Science Foundation (14-14-00592), Institute of Mitoengineering of the Moscow State University, the *Deutsche Forschungsgemeinschaft* (DFG), the Federal Ministry of Education and Research of Germany, the German Academic Exchange Service (DAAD), and the Open Access Publishing Fund of Osnabrück University.

References

[1] B. Halliwell and J. M. C. Gutteridge, "Role of free radicals and catalytic metal ions in human disease: an overview," *Methods in Enzymology*, vol. 186, pp. 1–85, 1990.

[2] V. P. Skulachev, "Membrane-linked systems preventing superoxide formation," *Bioscience Reports*, vol. 17, no. 3, pp. 347–366, 1997.

[3] G. Lenaz, "The mitochondrial production of reactive oxygen species: mechanisms and implications in human pathology," *IUBMB Life*, vol. 52, no. 3–5, pp. 159–164, 2001.

[4] E. Niki, "Lipid peroxidation: physiological levels and dual biological effects," *Free Radical Biology and Medicine*, vol. 47, no. 5, pp. 469–484, 2009.

[5] C.-C. Wu and S. B. Bratton, "Regulation of the intrinsic apoptosis pathway by reactive oxygen species," *Antioxidants and Redox Signaling*, vol. 19, no. 6, pp. 546–558, 2013.

[6] E. Niki, Y. Yoshida, Y. Saito, and N. Noguchi, "Lipid peroxidation: mechanisms, inhibition, and biological effects," *Biochemical and Biophysical Research Communications*, vol. 338, no. 1, pp. 668–676, 2005.

[7] M. L. Circu and T. Y. Aw, "Reactive oxygen species, cellular redox systems, and apoptosis," *Free Radical Biology and Medicine*, vol. 48, no. 6, pp. 749–762, 2010.

[8] P. Pacher, J. S. Beckman, and L. Liaudet, "Nitric oxide and peroxynitrite in health and disease," *Physiological Reviews*, vol. 87, no. 1, pp. 315–424, 2007.

[9] A. W. Rutherford, A. Osyczka, and F. Rappaport, "Back-reactions, short-circuits, leaks and other energy wasteful reactions in biological electron transfer: redox tuning to survive life in O_2," *FEBS Letters*, vol. 586, no. 5, pp. 603–616, 2012.

[10] L. R. C. Barclay and M. R. Vinqvist, "Phenols as antioxidants," in *The Chemistry of Phenols*, Z. Rappoport, Ed., pp. 839–908, John Wiley & Sons, New York, NY, USA, 2003.

[11] J. F. Kerr, A. H. Wyllie, and A. R. Currie, "Apoptosis: a basic biological phenomenon with wide-ranging implications in tissue kinetics," *British Journal of Cancer*, vol. 26, no. 4, pp. 239–257, 1972.

[12] V. P. Skulachev, "Why are mitochondria involved in apoptosis? Permeability transition pores and apoptosis as selective mechanisms to eliminate superoxide-producing mitochondria and cell," *FEBS Letters*, vol. 397, no. 1, pp. 7–10, 1996.

[13] V. E. Kagan, G. G. Borisenko, Y. Y. Tyurina et al., "Oxidative lipidomics of apoptosis: redox catalytic interactions of cytochrome c with cardiolipin and phosphatidylserine," *Free Radical Biology and Medicine*, vol. 37, no. 12, pp. 1963–1985, 2004.

[14] C. Wang and R. J. Youle, "The role of mitochondria in apoptosis," *Annual Review of Genetics*, vol. 43, pp. 95–118, 2009.

[15] A. T. Hoye, J. E. Davoren, P. Wipf, M. P. Fink, and V. E. Kagan, "Targeting mitochondria," *Accounts of Chemical Research*, vol. 41, no. 1, pp. 87–97, 2008.

[16] L. R. C. Barclay, M. R. Vinqvist, K. Mukai, S. Itoh, and H. Morimoto, "Chain-breaking phenolic antioxidants: steric and electronic effects in polyalkylchromanols, tocopherol analogs, hydroquinones, and superior antioxidants of the polyalkylbenzochromanol and naphthofuran class," *Journal of Organic Chemistry*, vol. 58, no. 26, pp. 7416–7420, 1993.

[17] E. Niki, "Antioxidants in relation to lipid peroxidation," *Chemistry and Physics of Lipids*, vol. 44, no. 2–4, pp. 227–253, 1987.

[18] N. Noguchi, H. Yamashita, N. Gotoh, Y. Yamamoto, R. Numano, and E. Niki, "2,2′-azobis (4-methoxy-2,4-dimethylvaleronitrile), a new lipid-soluble azo initiator: application to oxidations of lipids and low-density lipoprotein in solution and in aqueous dispersions," *Free Radical Biology and Medicine*, vol. 24, no. 2, pp. 259–268, 1998.

[19] A. V. Lokhmatikov, N. E. Voskoboynikova, D. A. Cherepanov et al., "Prevention of peroxidation of cardiolipin liposomes by quinol-based antioxidants," *Biochemistry*, vol. 79, no. 10, pp. 1081–1100, 2014.

[20] V. P. Skulachev, V. N. Anisimov, Y. N. Antonenko et al., "An attempt to prevent senescence: a mitochondrial approach," *Biochimica et Biophysica Acta—Bioenergetics*, vol. 1787, no. 5, pp. 437–461, 2009.

[21] Z. T. Schug and E. Gottlieb, "Cardiolipin acts as a mitochondrial signalling platform to launch apoptosis," *Biochimica et Biophysica Acta (BBA)—Biomembranes*, vol. 1788, no. 10, pp. 2022–2031, 2009.

[22] C. Hunte and S. Richers, "Lipids and membrane protein structures," *Current Opinion in Structural Biology*, vol. 18, no. 4, pp. 406–411, 2008.

[23] R. Arias-Cartin, S. Grimaldi, P. Arnoux, B. Guigliarelli, and A. Magalon, "Cardiolipin binding in bacterial respiratory complexes: structural and functional implications," *Biochimica et Biophysica Acta*, vol. 1817, no. 10, pp. 1937–1949, 2012.

[24] K. Mikel'saar, I. I. Severina, and V. P. Skulachev, "Phospholipids and oxidative phosphorylation," *Uspekhi Sovremennoi Biologii*, vol. 78, no. 3, pp. 348–370, 1974.

[25] M. Zhang, E. Mileykovskaya, and W. Dowhan, "Gluing the respiratory chain together: cardiolipin is required for supercomplex formation in the inner mitochondrial membrane," *Journal of Biological Chemistry*, vol. 277, no. 46, pp. 43553–43556, 2002.

[26] S. Bazán, E. Mileykovskaya, V. K. P. S. Mallampalli, P. Heacock, G. C. Sparagna, and W. Dowhan, "Cardiolipin-dependent reconstitution of respiratory supercomplexes from purified *Saccharomyces cerevisiae* complexes III and IV," *The Journal of Biological Chemistry*, vol. 288, no. 1, pp. 401–411, 2013.

[27] E. Mileykovskaya, P. A. Penczek, J. Fang, V. K. P. S. Mallampalli, G. C. Sparagna, and W. Dowhan, "Arrangement of the respiratory chain complexes in *Saccharomyces cerevisiae* supercomplex III_2IV_2 revealed by single particle cryo-electron microscopy," *Journal of Biological Chemistry*, vol. 287, no. 27, pp. 23095–23103, 2012.

[28] T. Althoff, D. J. Mills, J.-L. Popot, and W. Kühlbrandt, "Arrangement of electron transport chain components in bovine mitochondrial supercomplex $I_1III_2IV_1$," *The EMBO Journal*, vol. 30, no. 22, pp. 4652–4664, 2011.

[29] K. B. Busch, G. Deckers-Hebestreit, G. T. Hanke, and A. Y. Mulkidjanian, "Dynamics of bioenergetic microcompartments," *The Biological Chemistry*, vol. 394, no. 2, pp. 163–188, 2013.

[30] E. Lapuente-Brun, R. Moreno-Loshuertos, R. Aciń-Pérez et al., "Supercomplex assembly determines electron flux in the mitochondrial electron transport chain," *Science*, vol. 340, no. 6140, pp. 1567–1570, 2013.

[31] A. Boveris and B. Chance, "The mitochondrial generation of hydrogen peroxide. General properties and effect of hyperbaric oxygen," *Biochemical Journal*, vol. 134, no. 3, pp. 707–716, 1973.

[32] S. S. Korshunov, V. P. Skulachev, and A. A. Starkov, "High protonic potential actuates a mechanism of production of reactive oxygen species in mitochondria," *FEBS Letters*, vol. 416, no. 1, pp. 15–18, 1997.

[33] J. F. Turrens and A. Boveris, "Generation of superoxide anion by the NADH dehydrogenase of bovine heart mitochondria," *Biochemical Journal*, vol. 191, no. 2, pp. 421–427, 1980.

[34] L. Kussmaul and J. Hirst, "The mechanism of superoxide production by NADH:ubiquinone oxidoreductase (complex I) from bovine heart mitochondria," *Proceedings of the National Academy of Sciences of the United States of America*, vol. 103, no. 20, pp. 7607–7612, 2006.

[35] V. G. Grivennikova and A. D. Vinogradov, "Partitioning of superoxide and hydrogen peroxide production by mitochondrial respiratory complex I," *Biochimica et Biophysica Acta (BBA)—Bioenergetics*, vol. 1827, no. 3, pp. 446–454, 2013.

[36] M. Ksenzenko, A. A. Konstantinov, G. B. Khomutov, A. N. Tikhonov, and E. K. Ruuge, "Effect of electron transfer inhibitors on superoxide generation in the cytochrome bc_1 site of the mitochondrial respiratory chain," *FEBS Letters*, vol. 155, no. 1, pp. 19–24, 1983.

[37] A. Y. Mulkidjanian, "Ubiquinol oxidation in the cytochrome bc_1 complex: reaction mechanism and prevention of short-circuiting," *Biochimica et Biophysica Acta*, vol. 1709, no. 1, pp. 5–34, 2005.

[38] D. Malinska, B. Kulawiak, A. P. Kudin et al., "Complex III-dependent superoxide production of brain mitochondria contributes to seizure-related ROS formation," *Biochimica et Biophysica Acta*, vol. 1797, no. 6-7, pp. 1163–1170, 2010.

[39] M. Sarewicz, M. Dutka, S. Pintscher, and A. Osyczka, "Triplet state of the semiquinone-Rieske cluster as an intermediate of electronic bifurcation catalyzed by cytochrome bc_1," *Biochemistry*, vol. 52, no. 37, pp. 6388–6395, 2013.

[40] L. Bleier and S. Dröse, "Superoxide generation by complex III: from mechanistic rationales to functional consequences," *Biochimica et Biophysica Acta*, vol. 1827, no. 11-12, pp. 1320–1331, 2013.

[41] V. E. Kagan, V. A. Tyurin, J. Jiang et al., "Cytochrome *c* acts as a cardiolipin oxygenase required for release of proapoptotic factors," *Nature Chemical Biology*, vol. 1, no. 4, pp. 223–232, 2005.

[42] V. E. Kagan, P. Wipf, D. Stoyanovsky et al., "Mitochondrial targeting of electron scavenging antioxidants: regulation of selective oxidation vs random chain reactions," *Advanced Drug Delivery Reviews*, vol. 61, no. 14, pp. 1375–1385, 2009.

[43] V. A. Tyurin, Y. Y. Tyurina, W. Feng et al., "Mass-spectrometric characterization of phospholipids and their primary peroxidation products in rat cortical neurons during staurosporine-induced apoptosis," *Journal of Neurochemistry*, vol. 107, no. 6, pp. 1614–1633, 2008.

[44] J. Ji, A. E. Kline, A. Amoscato et al., "Lipidomics identifies cardiolipin oxidation as a mitochondrial target for redox therapy of brain injury," *Nature Neuroscience*, vol. 15, no. 10, pp. 1407–1413, 2012.

[45] A. Musatov and N. C. Robinson, "Susceptibility of mitochondrial electron-transport complexes to oxidative damage. Focus on cytochrome c oxidase," *Free Radical Research*, vol. 46, no. 11, pp. 1313–1326, 2012.

[46] H. Jin, A. Kanthasamy, A. Ghosh, V. Anantharam, B. Kalyanaraman, and A. G. Kanthasamy, "Mitochondria-targeted antioxidants for treatment of Parkinson's disease: preclinical and clinical outcomes," *Biochimica et Biophysica Acta—Molecular Basis of Disease*, vol. 1842, no. 8, pp. 1282–1294, 2014.

[47] T. Koyama, M.-Y. Zhu, M. Kinjo, and T. Araiso, "Protective effects of idebenone against alterations in dynamic microstructure induced by lipid peroxidation in rat cardiac mitochondria," *Japanese Heart Journal*, vol. 32, no. 1, pp. 91–100, 1991.

[48] U. Senin, L. Parnetti, G. Barbagallo-Sangiorgi et al., "Idebenone in senile dementia of Alzheimer type: a multicentre study," *Archives of Gerontology and Geriatrics*, vol. 15, no. 3, pp. 249–260, 1992.

[49] M. Suno and A. Nagaoka, "Inhibition of lipid peroxidation by a novel compound, idebenone (CV-2619)," *Japanese Journal of Pharmacology*, vol. 35, no. 2, pp. 196–198, 1984.

[50] I. Zs-Nagy, "Chemistry, toxicology, pharmacology and pharmacokinetics of idebenone: a review," *Archives of Gerontology and Geriatrics*, vol. 11, no. 3, pp. 177–186, 1990.

[51] J. S. Armstrong, M. Whiteman, P. Rose, and D. P. Jones, "The Coenzyme Q10 analog decylubiquinone inhibits the redox-activated mitochondrial permeability transition: role of mitcohondrial [correction mitochondrial] complex III," *The Journal of Biological Chemistry*, vol. 278, no. 49, pp. 49079–49084, 2003.

[52] H. Shao, J. Li, Y. Zhou et al., "Dose-dependent protective effect of propofol against mitochondrial dysfunction in ischaemic/reperfused rat heart: role of cardiolipin," *British Journal of Pharmacology*, vol. 153, no. 8, pp. 1641–1649, 2008.

[53] K. Zhao, G.-M. Zhao, D. Wu et al., "Cell-permeable peptide antioxidants targeted to inner mitochondrial membrane inhibit mitochondrial swelling, oxidative cell death, and reperfusion injury," *The Journal of Biological Chemistry*, vol. 279, no. 33, pp. 34682–34690, 2004.

[54] J. Jiang, N. A. Belikova, A. T. Hoye et al., "A mitochondria-targeted nitroxide/hemigramicidin S conjugate protects mouse embryonic cells against gamma irradiation," *International Journal of Radiation Oncology Biology Physics*, vol. 70, no. 3, pp. 816–825, 2008.

[55] M. P. Fink, C. A. Macias, J. Xiao et al., "Hemigramicidin-TEMPO conjugates: novel mitochondria-targeted anti-oxidants," *Biochemical Pharmacology*, vol. 74, no. 6, pp. 801–809, 2007.

[56] D. E. Green, "The electromechanochemical model for energy coupling in mitochondria," *Biochimica et Biophysica Acta*, vol. 346, no. 1, pp. 27–78, 1974.

[57] E. A. Liberman, V. P. Topaly, L. M. Tsofina, A. A. Jasaitis, and V. P. Skulachev, "Mechanism of coupling of oxidative phosphorylation and the membrane potential of mitochondria," *Nature*, vol. 222, no. 5198, pp. 1076–1078, 1969.

[58] D. O. Levitsky and V. P. Skulachev, "Carnitine: the carrier transporting fatty acyls into mitochondria by means of an electrochemical gradient of H^+," *Biochimica et Biophysica Acta*, vol. 275, no. 1, pp. 33–50, 1972.

[59] M. L. Jauslin, T. Meier, R. A. Smith, and M. P. Murphy, "Mitochondria-targeted antioxidants protect Friedreich Ataxia fibroblasts from endogenous oxidative stress more effectively than untargeted antioxidants," *The FASEB Journal*, vol. 17, no. 13, pp. 1972–1974, 2003.

[60] G. F. Kelso, C. M. Porteous, C. V. Coulter et al., "Selective targeting of a redox-active ubiquinone to mitochondria within cells: antioxidant and antiapoptotic properties," *The Journal of Biological Chemistry*, vol. 276, no. 7, pp. 4588–4596, 2001.

[61] L. S. Agapova, B. V. Chernyak, L. V. Domnina et al., "Mitochondria-targeted plastoquinone derivatives as tools to interrupt execution of the aging program. 3. Inhibitory effect of SkQ1 on tumor development from p53-deficient cells," *Biochemistry*, vol. 73, no. 12, pp. 1300–1316, 2008.

[62] V. N. Anisimov, L. E. Bakeeva, P. A. Egormin et al., "Mitochondria-targeted plastoquinone derivatives as tools to interrupt execution of the aging program. 5. SkQ1 prolongs lifespan and prevents development of traits of senescence," *Biochemistry*, vol. 73, no. 12, pp. 1329–1342, 2008.

[63] Y. N. Antonenko, A. V. Avetisyan, L. E. Bakeeva et al., "Mitochondria-targeted plastoquinone derivatives as tools to interrupt execution of the aging program. 1. Cationic plastoquinone derivatives: synthesis and *in vitro* studies," *Biochemistry*, vol. 73, no. 12, pp. 1273–1287, 2008.

[64] L. E. Bakeeva, I. V. Barskov, M. V. Egorov et al., "Mitochondria-targeted plastoquinone derivatives as tools to interrupt execution of the aging program. 2. Treatment of some ROS- and age-related diseases (heart arrhythmia, heart infarctions, kidney ischemia, and stroke)," *Biochemistry (Moscow)*, vol. 73, no. 12, pp. 1288–1299, 2008.

[65] V. V. Neroev, M. M. Archipova, L. E. Bakeeva et al., "Mitochondria-targeted plastoquinone derivatives as tools to interrupt execution of the aging program. 4. Age-related eye disease. SkQ1 returns vision to blind animals," *Biochemistry*, vol. 73, no. 12, pp. 1317–1328, 2008.

[66] F. F. Severin, I. I. Severina, Y. N. Antonenko et al., "Penetrating cation/fatty acid anion pair as a mitochondria-targeted protonophore," *Proceedings of the National Academy of Sciences of the United States of America*, vol. 107, no. 2, pp. 663–668, 2010.

[67] V. P. Skulachev, Y. N. Antonenko, D. A. Cherepanov et al., "Prevention of cardiolipin oxidation and fatty acid cycling as two antioxidant mechanisms of cationic derivatives of plastoquinone (SkQs)," *Biochimica et Biophysica Acta (BBA)—Bioenergetics*, vol. 1797, no. 6-7, pp. 878–889, 2010.

[68] V. N. Anisimov, M. V. Egorov, M. S. Krasilshchikova et al., "Effects of the mitochondria-targeted antioxidant SkQ1 on lifespan of rodents," *Aging*, vol. 3, no. 11, pp. 1110–1119, 2011.

[69] E. Y. Plotnikov, A. A. Chupyrkina, S. S. Jankauskas et al., "Mechanisms of nephroprotective effect of mitochondria-targeted antioxidants under rhabdomyolysis and ischemia/reperfusion," *Biochimica et Biophysica Acta—Molecular Basis of Disease*, vol. 1812, no. 1, pp. 77–86, 2011.

[70] E. Y. Plotnikov, M. A. Morosanova, I. B. Pevzner et al., "Protective effect of mitochondria-targeted antioxidants in an acute bacterial infection," *Proceedings of the National Academy of Sciences of the United States of America*, vol. 110, no. 33, pp. E3100–E3108, 2013.

[71] E. E. Genrikhs, E. V. Stelmashook, O. V. Popova et al., "Mitochondria-targeted antioxidant SkQT1 decreases trauma-induced neurological deficit in rat and prevents amyloid-β-induced impairment of long-term potentiation in rat hippocampal slices," *Journal of Drug Targeting*, vol. 23, no. 4, pp. 347–352, 2015.

[72] E. N. Iomdina, I. P. Khoroshilova-Maslova, O. V. Robustova et al., "Mitochondria-targeted antioxidant SkQ1 reverses glaucomatous lesions in rabbits," *Frontiers in Bioscience*, vol. 20, pp. 892–901, 2015.

[73] V. N. Manskikh, O. S. Gancharova, A. I. Nikiforova et al., "Age-associated murine cardiac lesions are attenuated by the mitochondria-targeted antioxidant SkQ1," *Histology and Histopathology*, vol. 30, no. 3, pp. 353–360, 2015.

[74] I. A. Demyanenko, E. N. Popova, V. V. Zakharova et al., "Mitochondria-targeted antioxidant SkQ1 improves impaired dermal wound healing in old mice," *Aging*, vol. 7, no. 7, pp. 475–485, 2015.

[75] S. Fleischer, H. Klouwen, and G. Brierley, "Studies of the electron transfer system. 38. Lipid composition of purified enzyme preparations derived from beef heart mitochondria," *The Journal of Biological Chemistry*, vol. 236, pp. 2936–2941, 1961.

[76] L. R. C. Barclay, S. J. Locke, J. M. MacNeil, J. Vankessel, G. W. Burton, and K. U. Ingold, "Autoxidation of micelles and model membranes. Quantitative kinetic measurements can be made by using either water-soluble or lipid-soluble initiators with water-soluble or lipid-soluble chain-breaking antioxidants," *Journal of the American Chemical Society*, vol. 106, no. 8, pp. 2479–2481, 1984.

[77] M. Cipollone, D. Fiorentini, M. C. Galli, A. M. Sechi, and L. Landi, "Autoxidation and antioxidant activity of ubiquinol homologues in large unilamellar vesicles," *Chemistry and Physics of Lipids*, vol. 69, no. 1, pp. 87–94, 1994.

[78] V. Roginsky, T. Barsukova, D. Loshadkin, and E. Pliss, "Substituted *p*-hydroquinones as inhibitors of lipid peroxidation," *Chemistry and Physics of Lipids*, vol. 125, no. 1, pp. 49–58, 2003.

[79] L. D. Mayer, M. J. Hope, and P. R. Cullis, "Vesicles of variable sizes produced by a rapid extrusion procedure," *Biochimica et Biophysica Acta (BBA)—Biomembranes*, vol. 858, no. 1, pp. 161–168, 1986.

[80] M. J. Hope, M. B. Bally, G. Webb, and P. R. Cullis, "Production of large unilamellar vesicles by a rapid extrusion procedure. Characterization of size distribution, trapped volume and ability to maintain a membrane potential," *Biochimica et Biophysica Acta (BBA)—Biomembranes*, vol. 812, no. 1, pp. 55–65, 1985.

[81] R. M. C. Dawson, D. C. Elliott, W. H. Elliott, and K. M. Jones, *Data for Biochemical Research*, Clarendon Press, Oxford, UK, 2nd edition, 1969.

[82] R. M. C. Dawson, D. C. Elliott, W. H. Elliott, and K. M. Jones, *Data for Biochemical Research*, Clarendon Press, Oxford, UK, 3rd edition, 1986.

[83] P. R. Rich, "Electron and proton transfers through quinones and cytochrome *bc* complexes," *Biochimica et Biophysica Acta*, vol. 768, no. 1, pp. 53–79, 1984.

[84] W. Liu, N. A. Porter, C. Schneider, A. R. Brash, and H. Yin, "Formation of 4-hydroxynonenal from cardiolipin oxidation: intramolecular peroxyl radical addition and decomposition," *Free Radical Biology and Medicine*, vol. 50, no. 1, pp. 166–178, 2011.

[85] H. Yin and M. Zhu, "Free radical oxidation of cardiolipin: chemical mechanisms, detection and implication in apoptosis, mitochondrial dysfunction and human diseases," *Free Radical Research*, vol. 46, no. 8, pp. 959–974, 2012.

[86] E. Niki, "Assessment of antioxidant capacity in vitro and in vivo," *Free Radical Biology and Medicine*, vol. 49, no. 4, pp. 503–515, 2010.

[87] D. Loshadkin, V. Roginsky, and E. Pliss, "Substituted p-hydroquinones as a chain-breaking antioxidant during the oxidation of styrene," *International Journal of Chemical Kinetics*, vol. 34, no. 3, pp. 162–171, 2002.

[88] T. Doba, G. W. Burton, K. U. Ingold, and M. Matsuo, "α-Tocopheroxyl decay—lack of effect of oxygen," *Journal of the Chemical Society, Chemical Communications*, no. 7, pp. 461–462, 1984.

[89] R. C. R. M. Vossen, M. C. E. van Dam-Mieras, G. Hornstra, and R. F. A. Zwaal, "Continuous monitoring of lipid peroxidation by measuring conjugated diene formation in an aqueous liposome suspension," *Lipids*, vol. 28, no. 9, pp. 857–861, 1993.

[90] H. Esterbauer, G. Striegl, H. Puhl, and M. Rotheneder, "Continuous monitoring of *in vztro* oxidation of human low density lipoprotein," *Free Radical Research Communications*, vol. 6, no. 1, pp. 67–75, 1989.

[91] Y. Yamamoto, E. Komuro, and E. Niki, "Antioxidant activity of ubiquinol in solution and phosphatidylcholine liposome," *Journal of Nutritional Science and Vitaminology*, vol. 36, no. 5, pp. 505–511, 1990.

[92] H. Shi, N. Noguchi, and E. Niki, "Comparative study on dynamics of antioxidative action of α-tocopheryl hydroquinone, ubiquinol, and α-tocopherol against lipid peroxidation," *Free Radical Biology and Medicine*, vol. 27, no. 3-4, pp. 334–346, 1999.

[93] K. U. Ingold, V. W. Bowry, R. Stocker, and C. Walling, "Autoxidation of lipids and antioxidation by α-tocopherol and ubiquinol in homogeneous solution and in aqueous dispersions of lipids: unrecognized consequences of lipid particle size as exemplified by oxidation of human low density lipoprotein," *Proceedings of the National Academy of Sciences of the United States of America*, vol. 90, no. 1, pp. 45–49, 1993.

[94] B. Frei, M. C. Kim, and B. N. Ames, "Ubiquinol-10 is an effective lipid-soluble antioxidant at physiological concentrations," *Proceedings of the National Academy of Sciences of the United States of America*, vol. 87, no. 12, pp. 4879–4883, 1990.

[95] J. Kruk, M. Jemioła-Rzemińska, and K. Strzałka, "Plastoquinol and α-tocopherol quinol are more active than ubiquinol and α-tocopherol in inhibition of lipid peroxidation," *Chemistry and Physics of Lipids*, vol. 87, no. 1, pp. 73–80, 1997.

[96] D. Fiorentini, L. Cabrini, and L. Landi, "Ubiquinol-3 and ubiquinol-7 exhibit similar antioxidant activity in model membranes," *Free Radical Research*, vol. 18, no. 4, pp. 201–209, 1993.

[97] R. Stocker, V. W. Bowry, and B. Frei, "Ubiquinol-10 protects human low density lipoprotein more efficiently against lipid peroxidation than does α-tocopherol," *Proceedings of the National Academy of Sciences of the United States of America*, vol. 88, no. 5, pp. 1646–1650, 1991.

[98] V. W. Bowry and R. Stocker, "Tocopherol-mediated peroxidation. The prooxidant effect of vitamin E on the radical-initiated oxidation of human low-density lipoprotein," *Journal of the American Chemical Society*, vol. 115, no. 14, pp. 6029–6044, 1993.

[99] V. W. Bowry, D. Mohr, J. Cleary, and R. Stocker, "Prevention of tocopherol-mediated peroxidation in ubiquinol-10-free human low density lipoprotein," *Journal of Biological Chemistry*, vol. 270, no. 11, pp. 5756–5763, 1995.

[100] S. R. Thomas, J. Neužil, and R. Stocker, "Cosupplementation with coenzyme Q prevents the prooxidant effect of alpha-tocopherol and increases the resistance of LDL to transition metal-dependent oxidation initiation," *Arteriosclerosis, Thrombosis, and Vascular Biology*, vol. 16, no. 5, pp. 687–696, 1996.

[101] W. A. Pryor, T. Strickland, and D. F. Church, "Comparison of the efficiencies of several natural and synthetic antioxidants in aqueous sodium dodecyl sulfate micelle solutions," *Journal of the American Chemical Society*, vol. 110, no. 7, pp. 2224–2229, 1988.

[102] D. Fiorentini, M. Cipollone, M. C. Galli, A. Pugnaloni, G. Biagini, and L. Landi, "Characterization of large unilamellar vesicles as models for studies of lipid peroxidation initiated by azocompounds," *Free Radical Research*, vol. 21, no. 5, pp. 329–339, 1994.

[103] L. R. C. Barclay and K. U. Ingold, "Autoxidation of biological molecules. 2. The autoxidation of a model membrane—a comparison of the autoxidation of egg lecithin phosphatidylcholine in water and in chlorobenzene," *Journal of the American Chemical Society*, vol. 103, no. 21, pp. 6478–6485, 1981.

[104] L. R. C. Barclay and K. U. Ingold, "Autoxidation of a model membrane. A comparison of the autoxidation of egg lecithin phosphatidylcholine in water and in chlorobenzene," *Journal of the American Chemical Society*, vol. 102, no. 26, pp. 7792–7794, 1980.

[105] J. Atkinson, T. Harroun, S. R. Wassall, W. Stillwell, and J. Katsaras, "The location and behavior of α-tocopherol in membranes," *Molecular Nutrition and Food Research*, vol. 54, no. 5, pp. 641–651, 2010.

[106] J. A. Nilsson, A. Lyubartsev, L. A. Eriksson, and A. Laaksonen, "Molecular dynamics simulations of ubiquinone; a survey over torsional potentials and hydrogen bonds," *Molecular Physics*, vol. 99, no. 21, pp. 1795–1804, 2001.

[107] R. Fiorini, L. Ragni, S. Ambrosi, G. P. Littarru, E. Gratton, and T. Hazlett, "Fluorescence studies of the interactions of ubiquinol-10 with liposomes," *Photochemistry and Photobiology*, vol. 84, no. 1, pp. 209–214, 2008.

[108] A. Ausili, A. Torrecillas, F. Aranda et al., "Redox state of coenzyme Q10 determines its membrane localization," *Journal of Physical Chemistry B*, vol. 112, no. 40, pp. 12696–12702, 2008.

[109] M. Dahlberg and A. Maliniak, "Molecular dynamics simulations of cardiolipin bilayers," *Journal of Physical Chemistry B*, vol. 112, no. 37, pp. 11655–11663, 2008.

[110] A. Lass and R. S. Sohal, "Electron transport-linked ubiquinone-dependent recycling of α-tocopherol inhibits autooxidation of mitochondrial membranes," *Archives of Biochemistry and Biophysics*, vol. 352, no. 2, pp. 229–236, 1998.

[111] V. Kagan, E. Serbinova, and L. Packer, "Antioxidant effects of ubiquinones in microsomes and mitochondria are mediated by tocopherol recycling," *Biochemical and Biophysical Research Communications*, vol. 169, no. 3, pp. 851–857, 1990.

[112] D. A. Stoyanovsky, A. N. Osipov, P. J. Quinn, and V. E. Kagan, "Ubiquinone-dependent recycling of vitamin E radicals by superoxide," *Archives of Biochemistry and Biophysics*, vol. 323, no. 2, pp. 343–351, 1995.

[113] P. J. Quinn, J. P. Fabisiak, and V. E. Kagan, "Expansion of antioxidant function of vitamin E by coenzyme Q," *BioFactors*, vol. 9, no. 2–4, pp. 149–154, 1999.

[114] V. E. Kagan, J. P. Fabisiak, and P. J. Quinn, "Coenzyme Q and vitamin E need each other as antioxidants," *Protoplasma*, vol. 214, no. 1-2, pp. 11–18, 2000.

[115] Y. Song and G. R. Buettner, "Thermodynamic and kinetic considerations for the reaction of semiquinone radicals to form superoxide and hydrogen peroxide," *Free Radical Biology and Medicine*, vol. 49, no. 6, pp. 919–962, 2010.

[116] V. Roginsky and T. Barsukova, "Kinetics of oxidation of hydroquinones by molecular oxygen. Effect of superoxide dismutase," *Journal of the Chemical Society, Perkin Transactions 2*, no. 7, pp. 1575–1582, 2000.

[117] K. B. Patel and R. L. Willson, "Semiquinone free radicals and oxygen. Pulse radiolysis study of one electron transfer equilibria," *Journal of the Chemical Society, Faraday Transactions 1: Physical Chemistry in Condensed Phases*, vol. 69, no. 4, pp. 814–825, 1973.

[118] A. Maroz, R. F. Anderson, R. A. J. Smith, and M. P. Murphy, "Reactivity of ubiquinone and ubiquinol with superoxide and the hydroperoxyl radical: implications for in vivo antioxidant activity," *Free Radical Biology and Medicine*, vol. 46, no. 1, pp. 105–109, 2009.

[119] R. Pethig, P. R. C. Gascoyne, J. A. McLaughlin, and A. Szent-Gyorgyi, "Ascorbate-quinone interactions: electrochemical, free radical, and cytotoxic properties," *Proceedings of the National Academy of Sciences of the United States of America*, vol. 80, no. 1 I, pp. 129–132, 1983.

[120] W. A. Cramer and D. B. Knaff, *Energy Transduction in Biological Membranes: A Textbook of Bioenergetics*, Springer, 1990.

[121] L. Valgimigli, R. Amorati, M. G. Fumo et al., "The unusual reaction of semiquinone radicals with molecular oxygen," *Journal of Organic Chemistry*, vol. 73, no. 5, pp. 1830–1841, 2008.

[122] D. V. Dibrova, D. A. Cherepanov, M. Y. Galperin, V. P. Skulachev, and A. Y. Mulkidjanian, "Evolution of cytochrome *bc* complexes: from membrane-anchored dehydrogenases of ancient bacteria to triggers of apoptosis in vertebrates," *Biochimica et Biophysica Acta—Bioenergetics*, vol. 1827, no. 11-12, pp. 1407–1427, 2013.

[123] E. Niki, A. Kawakami, M. Saito, Y. Yamamoto, J. Tsuchiya, and Y. Kamiya, "Effect of phytyl side chain of vitamin E on its antioxidant activity," *The Journal of Biological Chemistry*, vol. 260, no. 4, pp. 2191–2196, 1985.

[124] S. M. Culbertson, M. R. Vinqvist, L. R. C. Barclay, and N. A. Porter, "Minimizing tocopherol-mediated radical phase transfer in low-density lipoprotein oxidation with an amphiphilic unsymmetrical azo initiator," *Journal of the American Chemical Society*, vol. 123, no. 37, pp. 8951–8960, 2001.

[125] L. R. C. Barclay, K. A. Mclaughlin, and M. R. Vinqvist, "The transfer of antioxidants between liposomes," *Journal of Liposome Research*, vol. 5, no. 4, pp. 955–979, 1995.

[126] L. R. C. Barclay, F. Antunes, Y. Egawa et al., "The efficiency of antioxidants delivered by liposomal transfer," *Biochimica et Biophysica Acta*, vol. 1328, no. 1, pp. 1–12, 1997.

[127] J. Jiang, D. A. Stoyanovsky, N. A. Belikova et al., "A mitochondria-targeted triphenylphosphonium-conjugated nitroxide functions as a radioprotector/mitigator," *Radiation Research*, vol. 172, no. 6, pp. 706–717, 2009.

[128] J. Jiang, I. Kurnikov, N. A. Belikova et al., "Structural requirements for optimized delivery, inhibition of oxidative stress, and antiapoptotic activity of targeted nitroxides," *Journal of Pharmacology and Experimental Therapeutics*, vol. 320, no. 3, pp. 1050–1060, 2007.

[129] Z. Huang, J. Jiang, N. A. Belikova, D. A. Stoyanovsky, V. E. Kagan, and A. H. Mintz, "Protection of normal brain cells from γ-irradiation-induced apoptosis by a mitochondria-targeted triphenyl-phosphonium-nitroxide: a possible utility in glioblastoma therapy," *Journal of Neuro-Oncology*, vol. 100, no. 1, pp. 1–8, 2010.

[130] T. Haußß, S. Dante, T. H. Haines, and N. A. Dencher, "Localization of coenzyme Q10 in the center of a deuterated lipid membrane by neutron diffraction," *Biochimica et Biophysica Acta (BBA)—Bioenergetics*, vol. 1710, no. 1, pp. 57–62, 2005.

Hindawi Publishing Corporation
Oxidative Medicine and Cellular Longevity
Volume 2016, Article ID 8470394, 12 pages
http://dx.doi.org/10.1155/2016/8470394

Research Article

Assessment of Mitochondrial Dysfunction and Monoamine Oxidase Contribution to Oxidative Stress in Human Diabetic Hearts

O. M. Duicu,[1,2] R. Lighezan,[2,3] A. Sturza,[1,2] R. Balica,[4] A. Vaduva,[5] H. Feier,[6] M. Gaspar,[6] A. Ionac,[7] L. Noveanu,[1,2] C. Borza,[1,2] D. M. Muntean,[1,2] and C. Mornos[7]

[1]*Department of Pathophysiology, "Victor Babeş" University of Medicine and Pharmacy, 2 Eftimie Murgu Square, 300041 Timişoara, Romania*
[2]*Center for Translational Research and Systems Medicine, "Victor Babeş" University of Medicine and Pharmacy, 2 Eftimie Murgu Square, 300041 Timişoara, Romania*
[3]*Department of Parasitology, "Victor Babeş" University of Medicine and Pharmacy, 2 Eftimie Murgu Square, 300041 Timişoara, Romania*
[4]*Department of Histology, "Victor Babeş" University of Medicine and Pharmacy, 2 Eftimie Murgu Square, 300041 Timişoara, Romania*
[5]*Department of Morphopathology, "Victor Babeş" University of Medicine and Pharmacy, 2 Eftimie Murgu Square, 300041 Timişoara, Romania*
[6]*Department of Cardiovascular Surgery, "Victor Babeş" University of Medicine and Pharmacy, 2 Eftimie Murgu Square, 300041 Timişoara, Romania*
[7]*Department of Cardiology, 2nd Cardiology Clinic, "Victor Babeş" University of Medicine and Pharmacy, 2 Eftimie Murgu Square, 300041 Timişoara, Romania*

Correspondence should be addressed to D. M. Muntean; daninamuntean@umft.ro

Received 25 September 2015; Revised 26 January 2016; Accepted 11 February 2016

Academic Editor: Katsutaro Morino

Copyright © 2016 O. M. Duicu et al. This is an open access article distributed under the Creative Commons Attribution License, which permits unrestricted use, distribution, and reproduction in any medium, provided the original work is properly cited.

Mitochondria-related oxidative stress is a pathomechanism causally linked to coronary heart disease (CHD) and diabetes mellitus (DM). Recently, mitochondrial monoamine oxidases (MAOs) have emerged as novel sources of oxidative stress in the cardiovascular system and experimental diabetes. The present study was purported to assess the mitochondrial impairment and the contribution of MAOs-related oxidative stress to the cardiovascular dysfunction in coronary patients with/without DM. Right atrial appendages were obtained from 75 patients randomized into 3 groups: (1) Control (CTRL), valvular patients without CHD; (2) CHD, patients with confirmed CHD; and (3) CHD-DM, patients with CHD and DM. Mitochondrial respiration was measured by high-resolution respirometry and MAOs expression was evaluated by RT-PCR and immunohistochemistry. Hydrogen peroxide (H_2O_2) emission was assessed by confocal microscopy and spectrophotometrically. The impairment of mitochondrial respiration was substrate-independent in CHD-DM group. MAOs expression was comparable among the groups, with the predominance of MAO-B isoform but no significant differences regarding oxidative stress were detected by either method. Incubation of atrial samples with MAOs inhibitors significantly reduced the H_2O_2 in all groups. In conclusion, abnormal mitochondrial respiration occurs in CHD and is more severe in DM and MAOs contribute to oxidative stress in human diseased hearts with/without DM.

1. Introduction

Coronary heart disease (CHD) represents the most important cause of mortality and morbidity attributable to heart failure worldwide. Progression of the disease is aggravated by diabetes mellitus (DM), a major independent risk factor, whose prevalence is alarmingly high [1]. It is widely accepted that oxidative stress is a major contributor to the pathogenesis of both cardiovascular and metabolic disorders and mitochondria are the principal sources of reactive oxygen species (ROS) (recently reviewed in [2]). In this respect, the role of the electron transport chain (ETC) at the inner mitochondrial

membrane as the critical site for ROS production in the failing rat myocardium has been already reported in the late 90s. Indeed, these authors reported a decrease in complex I activity as the major reason responsible for the deleterious ROS production [3] that has been further correlated with left ventricular contractile dysfunction [4]. Since then, a substantial body of research has been carried out in order to shed light on the impairment of mitochondrial function in experimental models of heart failure and the failing human heart (recently reviewed in [5–8]).

Similarly, in type 2 diabetes mellitus (T2DM), mitochondrial abnormalities have been reported to accelerate the progression of insulin resistance *via* ROS overproduction (reviewed in [9–11]). Interestingly, in a recent study, the impairment of mitochondrial function and dynamics has been associated with contractile dysfunction in diabetic (but not obese) patients [12]. However, despite the widely reported role of mitochondria-related oxidative stress in diabetes [13, 14], the sources of ROS generation in the heart remain elusive. In particular, the membrane permeable hydrogen peroxide (H_2O_2) has been regarded both as signalling molecule and harmful ROS in several pathologies, including diabetes [15, 16].

In the past decade, monoamine oxidases (MAOs) with 2 isoforms (A and B) at the outer mitochondrial membrane have emerged as sources for constant H_2O_2 generation in heart and vessels (for a recent comprehensive review see [17]). These flavoproteins catalize the transfer of electrons from the endogenous and dietary amines to O_2 according to the general reaction: R-CH_2-NH_2 + O_2 + H_2O → R-CHO + NH_3 + H_2O_2 [18, 19]. Both isoforms are present in the cardiovascular system, MAO-A being largely considered the predominant enzyme in rodents and humans [17]. MAOs-derived H_2O_2 contributes to the oxidative stress associated with ischemia/reperfusion injury [20, 21], maladaptive left ventricular hypertrophy [22–24], and endothelial dysfunction in normal and diabetic vessels in rodents [25, 26].

Despite the unequivocal role of MAOs as mitochondrial contributors to the obligatory ROS production in the cardiovascular system in experimental settings [17], the role of these enzymes in coronary patients with diabetes, the most frequent chronic metabolic disease associated with increased oxidative stress, has not been addressed so far [5]. Thus, the aims of the present study were to investigate the status of mitochondrial function and the contribution of MAOs to oxidative stress in coronary patients with and without diabetes.

2. Material and Methods

The study is in accordance with the ethical principles for medical research involving human subjects from the Declaration of Helsinki. Approval for this study was granted by the Committee for Research Ethics of the University of Medicine and Pharmacy Timisoara, Romania. Seventy-five patients undergoing heart surgery were randomized into 3 groups: (1) Control (CTRL), valvular patients without documented CHD; (2) CHD, patients with documented CHD; and (3) CHD-DM, patients with documented CHD and DM. All patients gave informed consent prior to surgery. Demographic and clinical data and preoperative medication were collected from medical records and are presented in Table 1. Echocardiography was performed with an ultrasonographic system (Vivid 9 General Electric, Milwaukee, WI) and analyzed using commercially available software (EchoPAC; GE Vingmed Ultrasound AS). LVEF was calculated from apical two- and four-chamber views using a modified Simpson's rule [27].

Atrial myocardium was sampled from patients subjected to open-heart surgery once cardiopulmonary bypass was established, by resecting the tip of the right atrial appendage (approximately 20 mg). The atrial samples were further placed in ice-cold buffer A containing 10 mM Ca-EGTA (ethylene glycol tetra-acetic acid) buffer, 0.1 μM free calcium, 20 mM imidazole, 20 mM taurine, 50 mM K-MES (2-(*N*-morpholino)-ethanesulfonic acid), 0.5 mM DTT (dithiothreitol), 6.56 mM $MgCl_2$, 5.77 mM ATP (adenosine-5′-triphosphate), and 15 mM phosphocreatine (pH 7.1 adjusted with 5 N KOH at 0°C) and immediately transferred to the laboratory for further experimental procedures. When needed, parts of the atrial biopsies were snap-frozen.

2.1. Atrial Tissue Permeabilization Procedure. Dissection and permeabilization of myocardial fibers were performed according to a previously described method [28]. Briefly, after atrial appendage was trimmed by vascular and connective tissue, myocardial muscle bundles were isolated and immersed in ice-cold buffer A. Fiber bundles were further separated mechanically under a microscope, transferred into ice-cold buffer A supplemented with 50 μg/mL of saponin stock solution (5 mg/mL) and shaken by gentle agitation on ice for 30 min. Following saponin permeabilization, samples were quickly transferred into the incubation buffer B (0.5 mM EGTA, 3 mM $MgCl_2 \cdot 6H_2O$, 60 mM K-lactobionate, 20 mM taurine, 10 mM KH_2P0_4, 20 mM HEPES (4-(2-hydroxyethyl)-1-piperazineethanesulfonic acid), 110 mM sucrose, 1 g/L BSA (bovine serum albumin), essentially fatty acid free, pH = 7.1, at 30°C + 280 U/mL catalase lyophilized powder, and 2000–5000 units/mg protein), shaken by gentle agitation for 10 min on ice. Permeabilized fibers were kept in buffer B on ice throughout the respirometry measurements (~4 hours).

2.2. Assessment of Mitochondrial Respiration. Mitochondrial measurements were performed for 1–3 mg (wet weight) of permeabilized fibers at 37°C using the Oxygraph-2k system (Oroboros Instruments Corp., Innsbruck, Austria) as previously described [28]. The Substrate-Uncoupler-Inhibitor Titration (SUIT) protocol was as follows: (1) $GM_{STATE\,2}$ and $S(Rot)_{STATE\,2}$: addition of glutamate (10 mM) + Malate (2 mM) and Succinate (10 mM) + Rotenone (0.5 μM): STATE 2 evaluation for complex I and complex II dependent respiration; (2) D_{OXPHOS}: addition of adenosine diphosphate (ADP, D: 5 mM), OXPHOS capacity measurement; (3) c: addition of cytochrome c (10 μM) to evaluate the intactness of the outer mitochondrial membrane; (4) $Atr_{STATE\,4}$: addition of atractyloside (0.75 mM), an ADP/ATP mitochondrial translocase inhibitor, STATE 4 measurement; (5) $FCCP_{ETS}$: FCCP (carbonyl cyanide p-(trifluoromethoxy) phenylhydrazone) titrations (0.5 μM/step) in order to measure uncoupled

respiration: ETS (electron transport system) capacity; (6) Ama*ROX*: addition of antimycin A (2.5 μM), and a complex III inhibitor: residual oxygen consumption, subtracted from total flux, ROX state. Mitochondrial respiration was corrected for oxygen flux due to instrumental background and ROX.

Citrate synthase (CS) activity was quantified by measuring the rate of 5,5′-dithiobis-(nitrobenzoic acid) reactive reduced coenzyme A at 37°C with a Hitachi F-7000 spectrofluorometer, according to a previously described method (monitoring the reaction of sodium oxaloacetate, acetylcoenzyme A, and 5,5′-dithiobis-(2 nitrobenzoic) acid at 412 nm) [29].

2.3. Evaluation of Oxidative Stress. The spatial distribution of hydrogen peroxide (H_2O_2) throughout the atrial sample was determined using the 2′,7′-dichlorofluorescein diacetate (DCF, Sigma-Aldrich D6882) probe according to a previously described technique [30]. Briefly, the atrial fragments were embedded in OCT and snap-frozen. The frozen fragments were cut in 8 μm thick cryosections and put on glass slides. After 3 washes with PBS, 5 minutes each, the cryosections were incubated in the dark with DCF for 30 minutes at room temperature. Excess DCF was washed away by 3 additional washes with PBS. The slides were mounted with Vectashield (Vector Laboratories) and immediately analyzed with the confocal microscope (Olympus Fluoview FV1000). Images were obtained using laser excitation at 488 nm, detection at 519 nm, with a 40x UPLSAPO objective (NA = 0.95). Image analysis was performed using the Icy Bioimage Analysis software [31].

Hydrogen peroxide production was also assessed in atrial samples in the presence versus the absence of MAO inhibitors (30 min preincubation with clorgyline and selegiline, 10 μM) by means of the ferrous iron xylenol orange oxidation (FOX) assay (PeroxiDetect Kit, Sigma-Aldrich) as previously described [25]. The principle of the assay is that peroxides oxidize Fe^{2+} to Fe^{3+} ions at acidic pH; the Fe^{3+} ion will further form a coloured adduct with xylenol orange (XO,3,3′-bis[N,N-bis-(carboxymethyl) aminomethyl]-o-cresolsulfonephthalein, sodium salt) that is measured at 560 nm.

2.4. MAO Gene Expression. MAO-A and MAO-B genes expression was evaluated by quantitative real time polymerase chain reaction (RT-PCR), as previously described [26]. The sequence information of the NCBI database (5′-> 3′: human MAO-A fw AGG ACT ATC TGC TGC CAA AC; human MAO-A rev AAG CTC CAC CAA CAT CTA CG; human MAO-B fw GAA GAG TGG GAC AAC ATG AC; and human MAO-B rev CTC CAC ACT GCT TCA CAT AC) was used to design the primers against MAO isoforms. The housekeeping gene and its primers were as follows: EEF2 (fw): 5′-GAC ATC ACC AAG GGT GTG CAG-3′ and EEF2 (rv): 5′-GCG GTC AGC ACA CTG GCA TA-3′, respectively. Total RNA was isolated from atrial samples with the "Total RNA Mini SI Isolation Spin-Kit, Applichem" and used for reverse transcription (Superscript III RT, Invitrogen). The PCR conditions consisted of initial denaturation (95°C, 10 minutes), 40 cycles of denaturation (95°C, 30 seconds), annealing (55°C, 60 seconds), and elongation (72°C, 60 seconds).

2.5. MAO Protein Expression. The immunohistochemistry assay was performed as previously described [32]. Briefly, atrial samples were fixed in 4% buffered formalin, embedded in paraffin, and sectioned at 3–5 μm. The slides were then dewaxed and rehydrated and either stained with the usual Hematoxylin-Eosin (HE) or pretreated for immunohistochemistry. A heat-induced epitope retrieval was performed with Novocastra Bond Epitope Retrieval Solution 1, a ready-to-use, citrate based pH 6.0 solution (Leica Biosystems, UK) for 20 minutes. Endogenous peroxidase blocking was realised with 3% hydrogen peroxide for 5 minutes. This step was followed by the 30-minute incubation with the primary antibodies (Novus Biologicals, USA): anti-MAO-A (mouse monoclonal, 1D6, dilution 1 : 300) and anti-MAO-B (rabbit polyclonal, dilution 1 : 50). The Bond Polymer Refine Detection System was applied for visualisation, and 3,3-diamino-benzidine dihydrochloride was applied as chromogen for 10 minutes. The nuclei were counterstained with hematoxylin for 5 minutes. The immunohistochemistry assay was performed with Leica Bond-Max autostainer (Leica Biosystems, Newcastle uponTyne, UK). After staining, the slides were dehydrated and mounted with Canada balsam. Image acquisition and analysis were performed using a Nikon Eclipse E-600 microscope.

2.5.1. Semi-Quantitative Immunohistochemical Analysis. The immunoreactivity was quantified using the hot-spot method from 3 consecutive areas at the magnification of ×200 with a corresponding area of 0.267 mm^2, at the microscopic scale of 50 μm. The protein expression was scored using a semiquantitative scale for intensity: absent = 0, week = 1, moderate = 2, and strong = 3. The score for each probe was expressed as a mean score after the quantification of protein expression in the muscular layer, endothelial cells of intramyocardial vessels, and the mesothelium of the atrial sample.

2.6. Chemicals. All reagents were purchased from Sigma-Aldrich.

2.7. Data Analysis. Data analysis was performed by GraphPad Prism version 6.0 for Windows (GraphPad Software, USA). Data were expressed as means ± SEM. For multiple comparisons, one-way ANOVA followed by Bonferroni post hoc analysis was used, differences between groups being considered significant at $p < 0.05$.

3. Results and Discussion

Atrial samples were collected from 75 patients with comparable clinical and demographic data, except for hypertension which was more frequent in CHD patients (Table 1). Fasting plasma glucose (FPG) and body mass index (BMI) were significantly higher in diabetic patients as compared to both CTRL and CHD patients, respectively (Table 1). One of the exclusion criteria in our study was heart failure with reduced ejection fraction where mitochondrial dysfunction has been reported [33]. However, despite the fact that we recruited patients with preserved ejection fraction, a lower mean value

Table 1: Patients' demographic, clinical data, and preoperative medication.

Study groups	CTRL ($n = 25$)	CHD ($n = 30$)	CHD-DM ($n = 20$)
Demographics			
Age	63 ± 9.5	63 ± 8.5	61 ± 9
Sex, M/F (male/female)	15/10	26/4	16/4
Clinical characteristics			
BMI	26.7 ± 5.7	27 ± 4	30 ± 3.2*†
Cholesterol (mg/dL)	184.8 ± 49.1	153.2 ± 33*	148 ± 23*
FPG	103.3 ± 20.2	105 ± 16	192 ± 64*†
LVEF	55.7 ± 7.8	48.5 ± 8.4*	48 ± 7.7*
HT	15 (60)	30 (100)*	20 (100)*
AF	3 (12)	2 (6.67)	0
Preoperative medication			
Aspirin	5 (20)	30 (100)	20 (100)
β-blockers	20 (80)	30 (100)	20 (100)
Anticoagulants	25 (100)	30 (100)	20 (100)
Statins	18 (72)	30 (100)	20 (100)
Nitrates	8 (32)	21 (70)	15 (75)
Calcium channel blockers	5 (20)	8 (26.67)	7 (35)
ACE inhibitors	0	30 (100)	20 (100)
Diuretics	25 (100)	30 (100)	20 (100)
Insulin	0	0	5 (25)
Oral antidiabetics	0	0	20 (75)
Antibiotherapy	25 (100)	30 (100)	20 (100)

Data are means ± SEM. In parentheses the percentages of the corresponding variable are mentioned. * $p < 0.05$ versus CTRL; † $p < 0.05$: CHD versus CHD-DM. BMI: body mass index, FPG: fasting plasma glucose, LVEF: left ventricular ejection fraction, HT: hypertension, AF: atrial fibrillation, and ACEI: angiotensin-converting-enzyme inhibitors.

of LVEF in CHD patients with/without diabetes as compared to the valvular ones was present (Table 1).

Due to different biopsy amount and/or quality, mitochondrial respiration, MAO gene expression, MAO protein expression, and oxidative stress evaluation have been performed on 60, 30, 30, and 45 samples, respectively.

3.1. Complex I-Supported Respiration Is Depressed in CHD Patients with and without Diabetes. To characterize mitochondrial dysfunction in coronary patients with and without diabetes, we performed a high-resolution respirometry study in permeabilized atrial fibers using two different SUIT protocols (see Methods). Thus, in mitochondria energized with glutamate + malate we found a significant decrease of OXPHOS and uncoupled respiration (ETS) in coronary patients regardless of the presence of diabetes, whereas STATES 2 and 4 were decreased only in CHD-DM group (Figure 1).

3.2. Complex II-Supported Respiration Is Depressed Only in CHD Patients with Diabetes. At variance from the previous findings, in mitochondria energized with succinate (+rotenone) a significant decrease in all respiratory parameters (STATES 2 and 4, OXPHOS, and ETS capacities) was found only in CHD-DM group, suggesting a more significant impairment of mitochondrial function in the presence of diabetes (Figure 2).

We further measured citrate synthase activity (a marker for the content of intact mitochondria) in atrial samples and found comparable values among the three groups (CTRL: 210.2 ± 32.3, CHD: 209.6 ± 21.5, and CHD-DM: 208.8 ± 43.4 $nmol \cdot min^{-1} \cdot mg^{-1}$ protein), suggesting that the reduced oxidative phosphorylation in atrial tissue of CHD patients with/without diabetes is not a consequence of the reduction in mitochondrial content.

In the past decades mitochondrial dysfunction and subcellular remodelling associated with heart failure have been systematically characterized in several animal models (reviewed in [34, 35]). Subsequently, an increasing number of studies also described the occurrence of the impairment in mitochondrial oxygen consumption as well as of the increase in ROS production in the hypertrophic/failing human heart [6, 28, 36]. However, it was not clear until recently whether mitochondrial dysfunction is also causally related to the contractile dysfunction in humans. Accordingly, Dela's group reported that left ventricular systolic dysfunction (ejection fraction < 45%) was associated with markedly reduced mitochondrial oxidative phosphorylation when fatty acids were used as substrate [33]. In our previous study performed in patients with preserved ejection fraction (≥50%), we reported the early impairment of complex I-supported respiration without considering the possible contribution of diabetes (since both patients with and without DM were included) [28]. In the present study, we showed that both CI-dependent and CII-dependent respiration is decreased in coronary patients with diabetes and preserved ejection fraction. Our results are in agreement with the study of Anderson et al. who reported a marked decrease in the oxidative capacity for glutamate and fatty acid-supported respiration together with an increased content of myocardial triglycerides in the atrial tissue of diabetic *versus* nondiabetic patients [14]. More recently, in an elegant and comprehensive study performed in 141 patients with/without DM and no sign of cardiomyopathy, Montaigne et al. reported an association between impaired mitochondrial function/dynamics and contractile dysfunction in diabetic (but not in nondiabetic) obese patients and indicated that chronic hyperglycemia is mainly responsible for mitochondrial dysfunction in the diabetic heart [12].

3.3. H_2O_2 Emission Was Not Increased in Diabetic versus Nondiabetic Patients. To assess the oxidative stress, a classic feature of DM, we measured in atrial samples the H_2O_2 release by two methods, confocal microscopy (with the DCF probe) and FOX assay. However, we could not identify a significant increase in hydrogen peroxide in atrial samples isolated from diabetic versus the other 2 groups (Figures 3 and 4(a)). This finding is rather surprising, considering the large body of evidence suggestive for the role of oxidative stress in the evolution of diabetes [37]. Moreover, two recent studies performed in the same model (human atrial samples) reported higher rates of H_2O_2 production derived from the

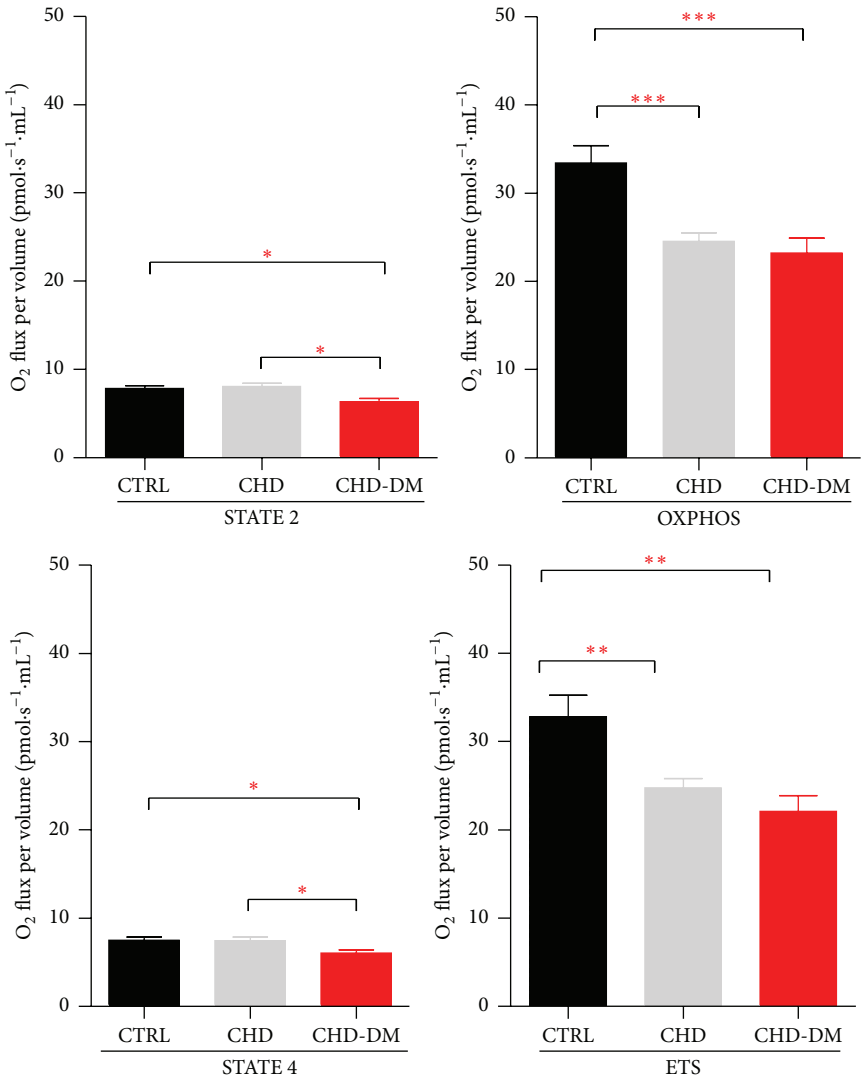

Figure 1: Respiratory parameters for CI-supported respiration (n = 20/CTRL group, n = 25/CHD group, and n = 15/CHD-DM group; values are means ± SEM; $^{*}p < 0.05$, $^{**}p < 0.01$, and $^{***}p < 0.001$).

mitochondrial electron transport chain (ETC) in diabetic versus nondiabetic patients [13, 14]. These authors estimated the rate of H_2O_2 originating from ETC as being at least 10-fold lower than the one derived from either MAOs or the NADPH-oxidases alone [38]. A possible explanation for our unexpected result could be that we included in the CHD-DM group both obese and nonobese patients; whether the diabetic nonobese patients are less prone to develop oxidative stress it is not known. Another possible explanation might be related to the preoperative medication in coronary patients (versus the control group), statins, and angiotensin-converting enzyme inhibitors being known to be able to mitigate the oxidative stress [39].

3.4. Ex Vivo Inhibition of MAOs Attenuated Atrial H_2O_2 Generation in All Groups. In order to assess the possible contribution of MAOs to oxidative stress, we further measured by FOX assay the atrial H_2O_2 production in the presence of two irreversible MAO inhibitors: selegiline for MAO-B and clorgyline for MAO-A. As shown in Figures 4(b1), 4(b2), and 4(b3), H_2O_2 production was significantly reduced in the presence of both MAOs inhibitors in all groups, an observation that is highly suggestive for the role of MAOs as important sources of oxidative stress in diseased atrial myocardium.

3.5. MAO mRNA Expression Was Comparable among the Groups and MAO-B Was the Predominant Isoform. To evaluate the potential induction of MAOs, we further assessed the expression of MAO-A and MAO-B in human atrial samples by RT-PCR. Interestingly, the expression of MAO-B isoform mRNA (by analyzing the computed threshold value difference of the RT-PCR) was more abundant as compared to the one of MAO-A isoform (Figures 5(a)–5(c)) in all groups. However, no difference in mRNA expression of both MAO isoforms could be detected among the groups (Figure 5(d)).

Despite the fact that MAO-A is considered the predominant isoform in cardiovascular system [17], relatively increased amounts of the MAO-B isoform have been

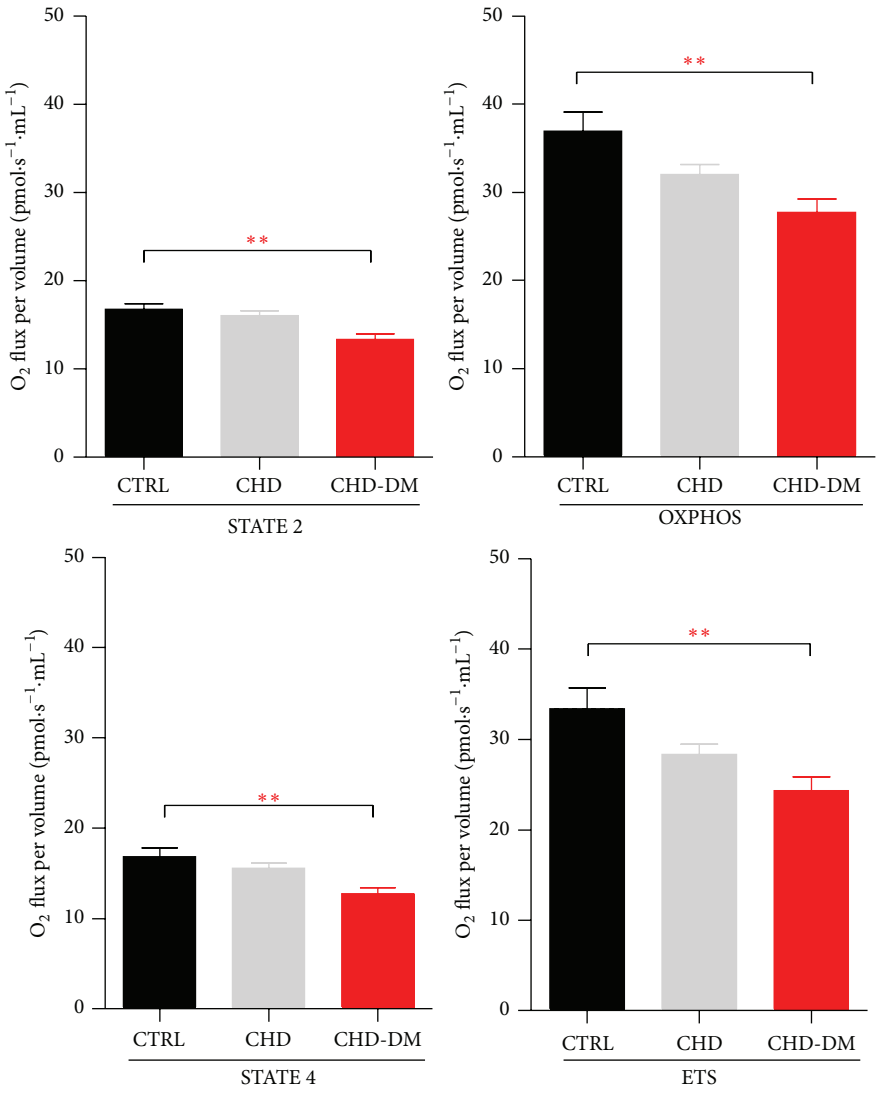

Figure 2: Respiratory parameters for CII-supported respiration (n = 20/CTRL group, n = 25/CHD group, and n = 15/CHD-DM group; values are means ± SEM; $^{**}p < 0.01$).

reported in both rodent and human hearts (reviewed by Wang et al. [40]). In line with this observation, Kaludercic et al. were the first to demonstrate that an increased activity of MAO-B elicited mitochondrial dysfunction and structural/functional cardiac alterations in mice with experimentally induced heart failure [41]. Recently, we have also demonstrated the predominant expression of MAO-B in hearts and aortic rings harvested from diabetic animals [26].

3.6. MAO Protein Expression Was Comparable among the Groups. In order to assess whether mRNA induction also translates into changes in protein expression we further performed immunohistochemistry of the atrial samples. We observed the colocalization of MAO-A and MAO-B in the sarcoplasm of cardiomyocytes, fibroblasts, endothelial cells, and mesothelial cells, and the absence of the immunostaining in the collagen fibers of the connective tissue (Figure 6(a)). Both MAO isoforms were better expressed within the cardiac muscle cells, and again the MAO-B isoform was strongly expressed as compared to MAO-A in all three groups (Figure 6(a)). Thus, the previous results at gene level have been also confirmed at protein level (Figure 6(b)). Of note, we also found an increased expression of MAO-B protein in rodent hearts with streptozotocin-induced diabetes as compared to the nondiabetic animals [26].

The present study was purported to assess mitochondrial respiratory function and characterize the contribution of myocardial MAOs to the oxidative stress in diabetic coronary patients as compared to a group of nondiabetic coronary patients and of valvular patients with no documented CHD, respectively. Our findings confirm that diabetes elicits the impairment of mitochondrial respiratory function, regardless of the substrates used. A decreased oxidative phosphorylation and energy production in diabetic patients are suggestive for the hypothesis that mitochondrial dysfunction represents the underlying cause of diabetic cardiomyopathy

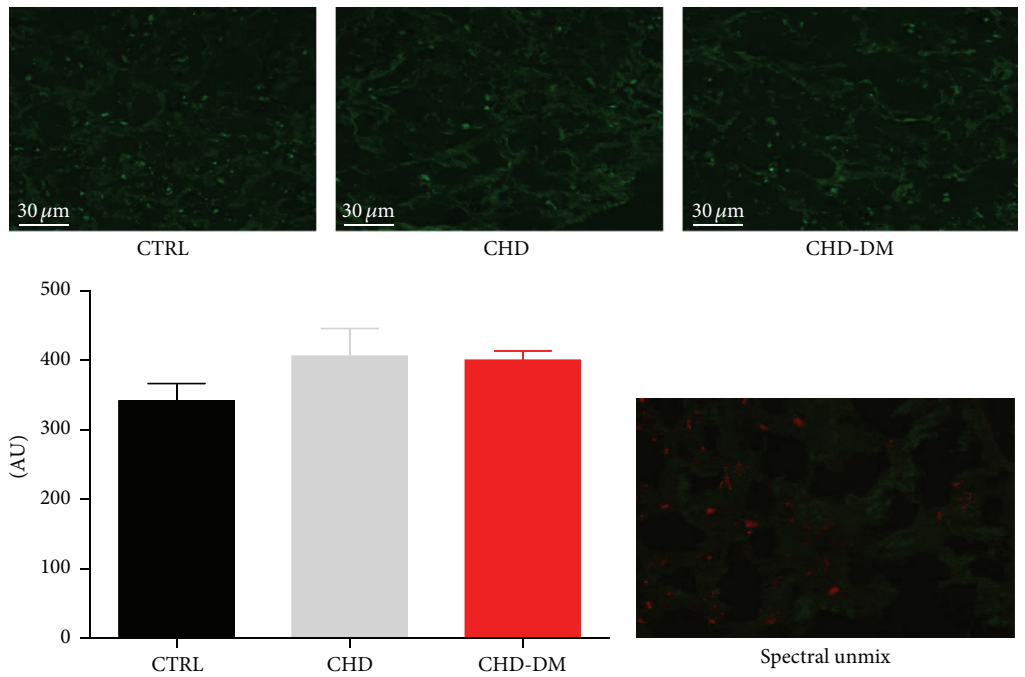

FIGURE 3: Atrial H_2O_2 emission detected with DCF fluorescence production. Fluorescent green positive staining was measured by confocal microscopy in the dichlorofluorescein- (DCF-) treated images. Levels of H_2O_2 detected with DCF fluorescence were similar in the studied groups (n = 10/group). Spectral unmixing was done using Lambda scan acquisition mode, range 490–600 nm, step 10 nm. The resulting composite image shows the real DCF component (red channel) on the autofluorescent background (green channel).

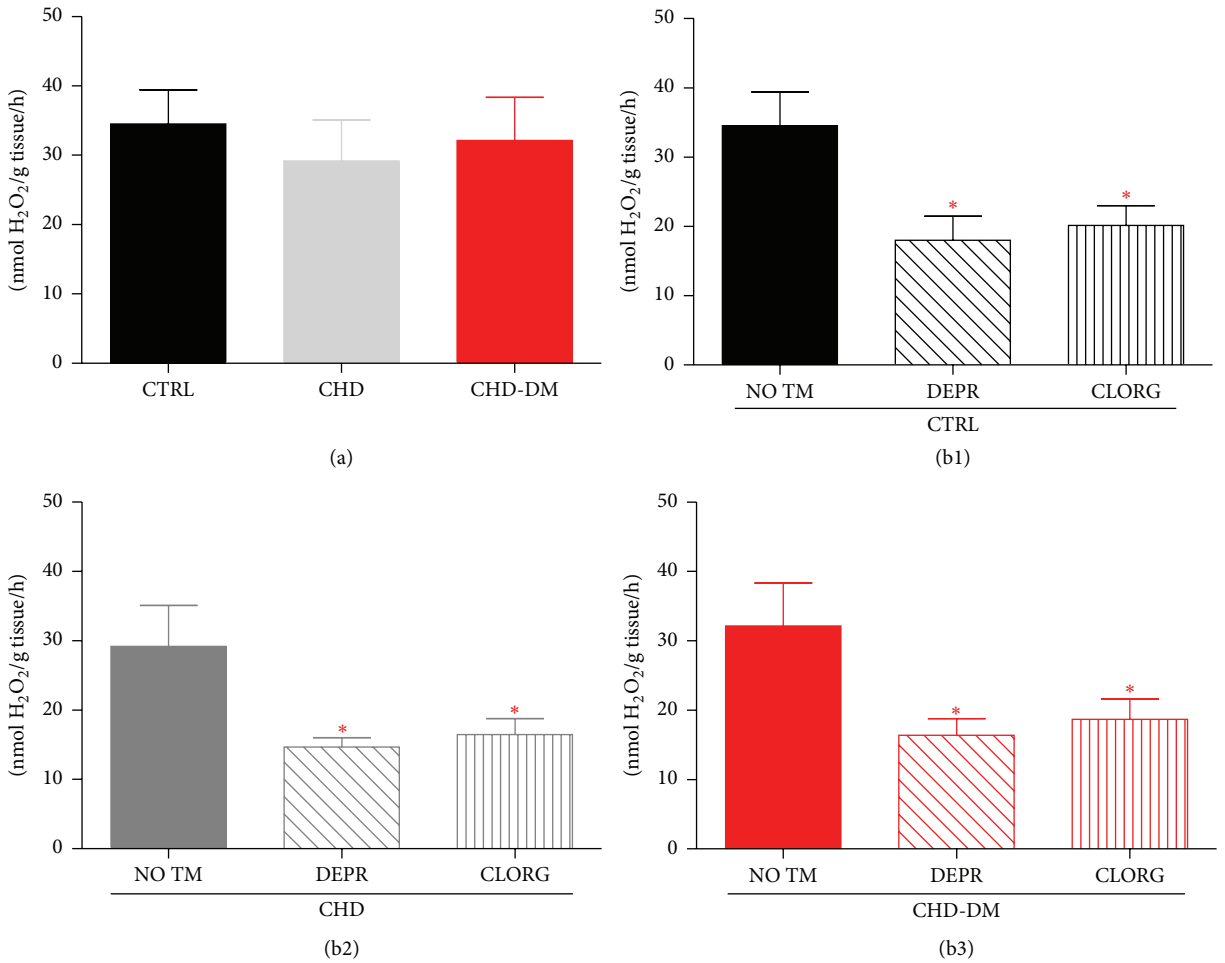

FIGURE 4: Atrial H_2O_2 emission detected with FOX assay. (a) Levels of H_2O_2 were similar in all groups (n = 5/group). (b1)–(b3) H_2O_2 level in the presence of selegiline and clorgyline (10 μM each) versus their corresponding controls (i.e., not treated atrial samples: NO TM) in each of the studied groups (n = 5/group; values are means ± SEM; $^*p < 0.05$ versus not treated atrial samples).

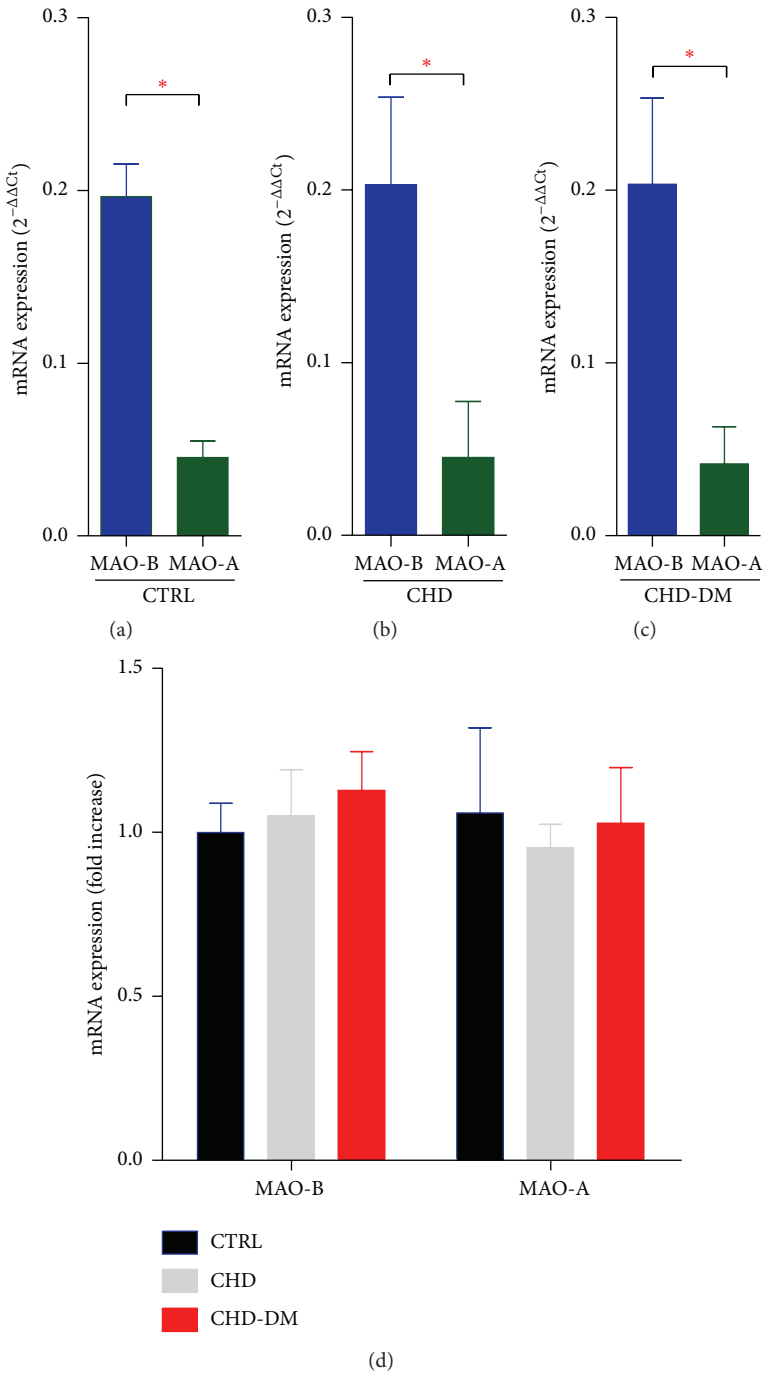

Figure 5: MAO mRNA expression in human atrial samples. (a)–(c) RT-PCR (mRNA expression: $2^{-\Delta\Delta Ct}$) for MAO-A and MAO-B relative to the housekeeping gene EEF2α in atrial samples from CTRL group (a), CHD group (b), CHD-DM (c), $n = 10$, $^{*}p < 0.05$, and (d) RT-PCR (fold increase) for MAO-A and MAO-B relative to the housekeeping gene EEF2α in atrial samples ($n = 10$/group).

(DCM) [42]. We showed here that both isoforms of MAO are expressed in atrial appendages harvested from patients with cardiovascular pathology regardless of the underlying disease, with the predominance of the MAO-B isoform. However, an important limitation of this study is that we did not investigate a possible link between mitochondrial dysfunction and MAOs activation. Indeed, Kaludercic et al. have recently demonstrated that MAO-B activation and inhibition of aldehyde dehydrogenase 2 activity contributed to altered mitochondrial bioenergetics [41].

We have also showed that *ex vivo* MAO-A and MAO-B inhibition significantly reduced ROS production, which strongly suggests a role for MAOs as contributors to oxidative stress in diseased atrial myocardium (namely, valvular

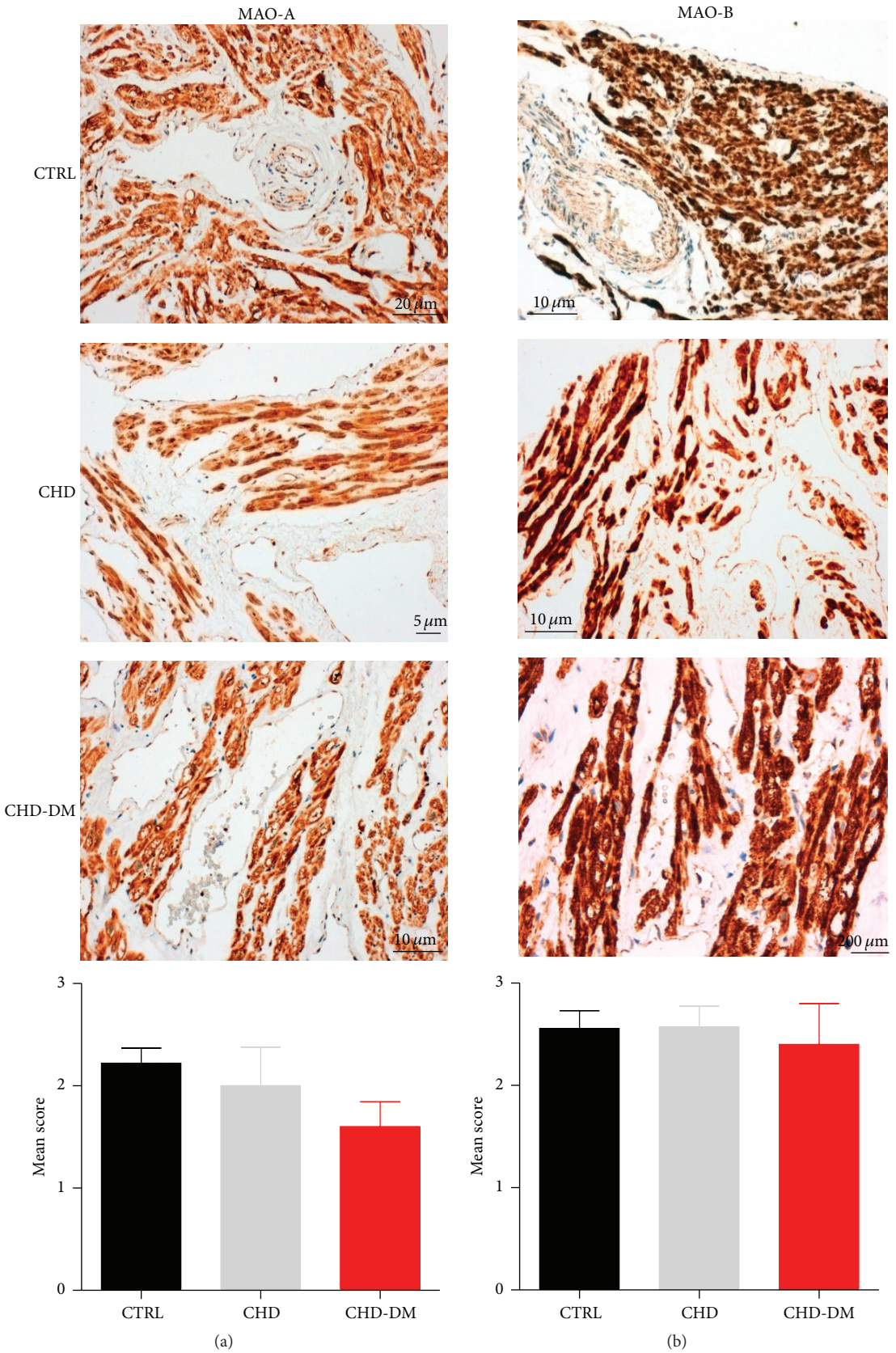

FIGURE 6: MAO protein expression in human atrial samples. The immunohistochemistry assay for MAO-A and MAO-B in atrial samples (a) and the corresponding results expressed as a mean score of intensity (b) (n = 10/group).

diseases and coronary heart disease with/without diabetes). The subcellular targets of MAO-derived ROS have not been identified so far. This issue is particularly important, in light of the novel concepts of functional repair of oxidatively damaged proteins [43] and compartmentalization of oxidative stress [44].

Several other enzymatic systems, such as NADPH-oxidases (Nox) and xanthine oxidase, are recognized cellular sources of oxidative stress [45, 46]. In an early study we have shown that MAO inhibitors had no effect on xanthine oxidase-dependent H_2O_2 formation, and Nox activity in cells overexpressing Nox1, Nox2, and Nox4 was not affected by MAO inhibition [25]. Another relevant question is whether MAO inhibitors are not antioxidants *per se*. However, in the above-mentioned study, no significant antioxidant effect of MAO inhibitors was observed by two different H_2O_2 assays (Amplex red and FOX assay) [25].

We do acknowledge as further limitations of our study that (i) the antioxidant defence systems in the heart were not assessed (as possible reason for the lack of high oxidative stress in the setting of diabetes) and (ii) data from coronary patients were compared with those obtained from valvular patients (since a true "control group" is obviously difficult to recruit).

To date, there is only one study that identified MAO as an important determinant of redox balance in human atrial myocardium and associated MAO overexpression with an increased risk for postoperative atrial fibrillation [38]. However, experimental evidence available so far unequivocally demonstrated that monoamine oxidases contribute to mitochondrial and endothelial dysfunction, both widely investigated pathomechanisms and valuable therapeutic targets in cardiometabolic diseases. MAO inhibitors (MAOI) are currently used mainly in psychiatry and neurology. Given their already wide prescription for mood disorders, depression, and Parkinson's disease, the use of MAO inhibitors for cardiac disorders and diabetic cardiomyopathy should not present with major issues in terms of safety, at least at certain dosages. Nevertheless, translating basic science's predictions on the beneficial role of MAOI in the setting of heart failure and diabetes is likely to encounter resistance from medical community; the major concern is related to the risk for hypertensive crisis reported to occur with the first generation of irreversible MAOI when dietary tyramine is ingested. Of note, selegiline (the selective and irreversible MAO-B inhibitor) is also available as a transdermal patch; this type of administration clearly prevents the side-effects related to MAOI ingestion. However, whether this administration will achieve the circulating concentration relevant for the protective effects of the drugs in cardiovascular system remains to be investigated. Moreover, the novel selective and reversible MAOI (such as moclobemide) are reported to be both well-tolerated compounds and free from the above-mentioned interaction included in the elderly [47]. Of note, we have recently reported that moclobemide improved endothelial function impaired by *in vitro* incubation of isolated canine carotid arteries with angiotensin-II [48]. Whether this effect can be recapitulated after the *in vivo* administration of the drug remains to be demonstrated.

4. Conclusion

We report here the impairment of mitochondrial respiratory function in diabetic coronary patients regardless of the substrate used and the contribution of MAOs, in particular of the MAO-B isoform, to oxidative stress in human coronary hearts with and without DM. Further studies addressing the role of the novel selective and reversible MAO inhibitors in mitigating oxidative stress in cardiometabolic diseases are warranted.

Conflict of Interests

The authors declare that there is no conflict of interests regarding the publication of this paper.

Acknowledgment

This study was supported by the university Grant PIII-C1-PCFI-2014/2015-04.

References

[1] L. Rydén, P. J. Grant, S. D. Anker et al., "ESC Guidelines on diabetes, pre-diabetes, and cardiovascular diseases developed in collaboration with the EASD: the Task Force on diabetes, pre-diabetes, and cardiovascular diseases of the European Society of Cardiology (ESC) and developed in collaboration with the European Association for the Study of Diabetes (EASD)," *European Heart Journal*, vol. 34, no. 39, pp. 3035–3087, 2013.

[2] Y.-R. Chen and J. L. Zweier, "Cardiac mitochondria and reactive oxygen species generation," *Circulation Research*, vol. 114, no. 3, pp. 524–537, 2014.

[3] T. Ide, H. Tsutsui, S. Kinugawa et al., "Mitochondrial electron transport complex I is a potential source of oxygen free radicals in the failing myocardium," *Circulation Research*, vol. 85, no. 4, pp. 357–363, 1999.

[4] T. Ide, H. Tsutsui, S. Kinugawa et al., "Direct evidence for increased hydroxyl radicals originating from superoxide in the failing myocardium," *Circulation Research*, vol. 86, no. 2, pp. 152–157, 2000.

[5] O. M. Duicu, R. Lighezan, A. Sturza et al., "Monoamine oxidases as potential contributors to oxidative stress in diabetes: time for a study in patients undergoing heart surgery," *BioMed Research International*, vol. 2015, Article ID 515437, 9 pages, 2015.

[6] M. G. Rosca and C. L. Hoppel, "Mitochondrial dysfunction in heart failure," *Heart Failure Reviews*, vol. 18, no. 5, pp. 607–622, 2013.

[7] H. Lemieux, S. Semsroth, H. Antretter, D. Höfer, and E. Gnaiger, "Mitochondrial respiratory control and early defects of oxidative phosphorylation in the failing human heart," *International Journal of Biochemistry and Cell Biology*, vol. 43, no. 12, pp. 1729–1738, 2011.

[8] A. M. Cordero-Reyes, A. A. Gupte, K. A. Youker et al., "Freshly isolated mitochondria from failing human hearts exhibit preserved respiratory function," *Journal of Molecular and Cellular Cardiology*, vol. 68, pp. 98–105, 2014.

[9] J. Szendroedi, E. Phielix, and M. Roden, "The role of mitochondria in insulin resistance and type 2 diabetes mellitus," *Nature Reviews Endocrinology*, vol. 8, no. 2, pp. 92–103, 2012.

[10] S. Boudina, S. Sena, H. Theobald et al., "Mitochondrial energetics in the heart in obesity-related diabetes: direct evidence for increased uncoupled respiration and activation of uncoupling proteins," *Diabetes*, vol. 56, no. 10, pp. 2457–2466, 2007.

[11] R. Blake and I. A. Trounce, "Mitochondrial dysfunction and complications associated with diabetes," *Biochimica et Biophysica Acta—General Subjects*, vol. 1840, no. 4, pp. 1404–1412, 2014.

[12] D. Montaigne, X. Marechal, A. Coisne et al., "Myocardial contractile dysfunction is associated with impaired mitochondrial function and dynamics in type 2 diabetic but not in obese patients," *Circulation*, vol. 130, no. 7, pp. 554–564, 2014.

[13] E. J. Anderson, E. Rodriguez, C. A. Anderson, K. Thayne, W. R. Chitwood, and A. P. Kypson, "Increased propensity for cell death in diabetic human heart is mediated by mitochondrial-dependent pathways," *American Journal of Physiology—Heart and Circulatory Physiology*, vol. 300, no. 1, pp. H118–H124, 2011.

[14] E. J. Anderson, A. P. Kypson, E. Rodriguez, C. A. Anderson, E. J. Lehr, and P. D. Neufer, "Substrate-specific derangements in mitochondrial metabolism and redox balance in the atrium of the type 2 diabetic human heart," *Journal of the American College of Cardiology*, vol. 54, no. 20, pp. 1891–1898, 2009.

[15] O. Lorenzo, E. Ramírez, B. Picatoste, J. Egido, and J. Tuñón, "Alteration of energy substrates and ROS production in diabetic cardiomyopathy," *Mediators of Inflammation*, vol. 2013, Article ID 461967, 11 pages, 2013.

[16] H. Sies, "Role of metabolic H_2O_2 generation: redox signaling and oxidative stress," *Journal of Biological Chemistry*, vol. 289, no. 13, pp. 8735–8741, 2014.

[17] N. Kaludercic, J. Mialet-Perez, N. Paolocci, A. Parini, and F. Di Lisa, "Monoamine oxidases as sources of oxidants in the heart," *Journal of Molecular and Cellular Cardiology*, vol. 73, pp. 34–42, 2014.

[18] J. C. Shih, K. Chen, and M. J. Ridd, "Monoamine oxidase: from genes to behavior," *Annual Review of Neuroscience*, vol. 22, pp. 197–217, 1999.

[19] D. E. Edmondson, "Hydrogen peroxide produced by mitochondrial monoamine oxidase catalysis: biological implications," *Current Pharmaceutical Design*, vol. 20, no. 2, pp. 155–160, 2014.

[20] P. Bianchi, D. R. Pimentel, M. P. Murphy, W. S. Colucci, and A. Parini, "A new hypertrophic mechanism of serotonin in cardiac myocytes: receptor-independent ROS generation," *The FASEB Journal*, vol. 19, no. 6, pp. 641–643, 2005.

[21] P. Bianchi, O. Kunduzova, E. Masini et al., "Oxidative stress by monoamine oxidase mediates receptor-independent cardiomyocyte apoptosis by serotonin and postischemic myocardial injury," *Circulation*, vol. 112, no. 21, pp. 3297–3305, 2005.

[22] N. Kaludercic, E. Takimoto, T. Nagayama et al., "Monoamine oxidase A-mediated enhanced catabolism of norepinephrine contributes to adverse remodeling and pump failure in hearts with pressure overload," *Circulation Research*, vol. 106, no. 1, pp. 193–202, 2010.

[23] C. Villeneuve, C. Guilbeau-Frugier, P. Sicard et al., "p53-PGC-1α pathway mediates oxidative mitochondrial damage and cardiomyocyte necrosis induced by monoamine oxidase-A upregulation: role in chronic left ventricular dysfunction in mice," *Antioxidants & Redox Signaling*, vol. 18, no. 1, pp. 5–18, 2013.

[24] A. Carpi, R. Menabò, N. Kaludercic, P. Pelicci, F. Di Lisa, and M. Giorgio, "The cardioprotective effects elicited by $p66^{Shc}$ ablation demonstrate the crucial role of mitochondrial ROS formation in ischemia/reperfusion injury," *Biochimica et Biophysica Acta (BBA)—Bioenergetics*, vol. 1787, no. 7, pp. 774–780, 2009.

[25] A. Sturza, M. S. Leisegang, A. Babelova et al., "Monoamine oxidases are mediators of endothelial dysfunction in the mouse aorta," *Hypertension*, vol. 62, no. 1, pp. 140–146, 2013.

[26] A. Sturza, O. M. Duicu, A. Vaduva et al., "Monoamine oxidases are novel sources of cardiovascular oxidative stress in experimental diabetes," *Canadian Journal of Physiology and Pharmacology*, vol. 93, no. 7, pp. 555–561, 2015.

[27] R. M. Lang, M. Bierig, R. B. Devereux et al., "Recommendations for chamber quantification," *European Journal of Echocardiography*, vol. 7, no. 2, pp. 79–108, 2006.

[28] O. Duicu, C. Juşcă, L. Falniţă et al., "Substrate-specific impairment of mitochondrial respiration in permeabilized fibers from patients with coronary heart disease versus valvular disease," *Molecular and Cellular Biochemistry*, vol. 379, no. 1-2, pp. 229–234, 2013.

[29] M. A. Birch-Machin and D. M. Turnbull, "Assaying mitochondrial respiratory complex activity in mitochondria isolated from human cells and tissues," *Methods in Cell Biology*, vol. 65, pp. 97–117, 2001.

[30] J. D. Miller, Y. Chu, R. M. Brooks, W. E. Richenbacher, R. Peña-Silva, and D. D. Heistad, "Dysregulation of antioxidant mechanisms contributes to increased oxidative stress in calcific aortic valvular stenosis in humans," *Journal of the American College of Cardiology*, vol. 52, no. 10, pp. 843–850, 2008.

[31] F. de Chaumont, S. Dallongeville, N. Chenouard et al., "Icy: an open bioimage informatics platform for extended reproducible research," *Nature Methods*, vol. 9, no. 7, pp. 690–696, 2012.

[32] A. Alexa, F. Baderca, R. Lighezan, D. E. Zăhoi, and D. Izvernariu, "The diagnostic value of EMA expression in the renal parenchyma tumors," *Romanian Journal of Morphology and Embryology*, vol. 52, no. 3, pp. 1019–1025, 2012.

[33] N. Stride, S. Larsen, M. Hey-Mogensen et al., "Decreased mitochondrial oxidative phosphorylation capacity in the human heart with left ventricular systolic dysfunction," *European Journal of Heart Failure*, vol. 15, no. 2, pp. 150–157, 2013.

[34] H. Lemieux and C. L. Hoppel, "Mitochondria in the human heart," *Journal of Bioenergetics and Biomembranes*, vol. 41, no. 2, pp. 99–106, 2009.

[35] N. S. Dhalla, N. Takeda, D. Rodriguez-Leyva, and V. Elimban, "Mechanisms of subcellular remodeling in heart failure due to diabetes," *Heart Failure Reviews*, vol. 19, no. 1, pp. 87–99, 2014.

[36] V. G. Sharov, A. V. Todor, N. Silverman, S. Goldstein, and H. N. Sabbah, "Abnormal mitochondrial respiration in failed human myocardium," *Journal of Molecular and Cellular Cardiology*, vol. 32, no. 12, pp. 2361–2367, 2000.

[37] S. D. Martin and S. L. McGee, "The role of mitochondria in the aetiology of insulin resistance and type 2 diabetes," *Biochimica et Biophysica Acta (BBA)—General Subjects*, vol. 1840, no. 4, pp. 1303–1312, 2014.

[38] E. J. Anderson, J. T. Efird, S. W. Davies et al., "Monoamine oxidase is a major determinant of redox balance in human atrial myocardium and is associated with postoperative atrial fibrillation," *The Journal of the American Heart Association*, vol. 3, no. 1, Article ID e000713, 2014.

[39] G. Nickenig, "Should angiotensin II receptor blockers and statins be combined?" *Circulation*, vol. 110, no. 8, pp. 1013–1020, 2004.

[40] C. C. Wang, E. Billett, A. Borchert, H. Kuhn, and C. Ufer, "Monoamine oxidases in development," *Cellular and Molecular Life Sciences*, vol. 70, no. 4, pp. 599–630, 2013.

[41] N. Kaludercic, A. Carpi, T. Nagayama et al., "Monoamine oxidase B prompts mitochondrial and cardiac dysfunction in pressure overloaded hearts," *Antioxidants and Redox Signaling*, vol. 20, no. 2, pp. 267–280, 2014.

[42] O.-J. How, E. Aasum, D. L. Severson, W. Y. A. Chan, M. F. Essop, and T. S. Larsen, "Increased myocardial oxygen consumption reduces cardiac efficiency in diabetic mice," *Diabetes*, vol. 55, no. 2, pp. 466–473, 2006.

[43] V. T. Dao, A. I. Casas, G. J. Maghzal et al., "Pharmacology and clinical drug candidates in Redox medicine," *Antioxidants & Redox Signaling*, vol. 23, no. 14, pp. 1113–1129, 2015.

[44] N. Kaludercic, S. Deshwal, and F. Di Lisa, "Reactive oxygen species and redox compartmentalization," *Frontiers in Physiology*, vol. 5, Article ID 00285, 2014.

[45] R. P. Brandes, "Vascular functions of NADPH oxidases," *Hypertension*, vol. 56, no. 1, pp. 17–21, 2010.

[46] Y. Ohara, T. E. Peterson, H. S. Sayegh, R. R. Subramanian, J. N. Wilcox, and D. G. Harrison, "Dietary correction of hypercholesterolemia in the rabbit normalizes endothelial superoxide anion production," *Circulation*, vol. 92, no. 4, pp. 898–903, 1995.

[47] H.-P. Volz and C. H. Gleiter, "Monoamine oxidase inhibitors. A perspective on their use in the elderly," *Drugs and Aging*, vol. 13, no. 5, pp. 341–355, 1998.

[48] A. Sturza, L. Noveanu, O. Duicu, M. Danila, N. Jost, and D. Muntean, "Reversible monoamine oxidase—a inhibition improves vascular dysfunction in canine carotid arteries exposed to angiotensin II," *Revista de Chimie*, vol. 66, no. 6, pp. 851–854, 2015.

Hindawi Publishing Corporation
Oxidative Medicine and Cellular Longevity
Volume 2016, Article ID 8360738, 19 pages
http://dx.doi.org/10.1155/2016/8360738

Research Article

AP39, a Mitochondria-Targeted Hydrogen Sulfide Donor, Supports Cellular Bioenergetics and Protects against Alzheimer's Disease by Preserving Mitochondrial Function in APP/PS1 Mice and Neurons

Feng-li Zhao,[1] Fang Fang,[1] Pei-feng Qiao,[1] Ning Yan,[2] Dan Gao,[1] and Yong Yan[1]

[1]*Experimental Research Center, Department of Neurology, The First Affiliated Hospital of Chongqing Medical University, Chongqing Medical University, Chongqing 400016, China*
[2]*Department of Neurology, The University-Town Hospital of Chongqing Medical University, Chongqing 400016, China*

Correspondence should be addressed to Yong Yan; yanyongzflh@163.com

Received 10 November 2015; Revised 11 December 2015; Accepted 15 December 2015

Academic Editor: David Sebastián

Copyright © 2016 Feng-li Zhao et al. This is an open access article distributed under the Creative Commons Attribution License, which permits unrestricted use, distribution, and reproduction in any medium, provided the original work is properly cited.

Increasing evidence suggests that mitochondrial functions are altered in AD and play an important role in AD pathogenesis. It has been established that H_2S homeostasis is balanced in AD. The emerging mitochondrial roles of H_2S include antioxidation, antiapoptosis, and the modulation of cellular bioenergetics. Here, using primary neurons from the well-characterized APP/PS1 transgenic mouse model, we studied the effects of AP39 (a newly synthesized mitochondrially targeted H_2S donor) on mitochondrial function. AP39 increased intracellular H_2S levels, mainly in mitochondrial regions. AP39 exerted dose-dependent effects on mitochondrial activity in APP/PS1 neurons, including increased cellular bioenergy metabolism and cell viability at low concentrations (25–100 nM) and decreased energy production and cell viability at a high concentration (250 nM). Furthermore, AP39 (100 nM) increased ATP levels, protected mitochondrial DNA, and decreased ROS generation. AP39 regulated mitochondrial dynamics, shifting from fission toward fusion. After 6 weeks, AP39 administration to APP/PS1 mice significantly ameliorated their spatial memory deficits in the Morris water maze and NORT and reduced Aβ deposition in their brains. Additionally, AP39 inhibited brain atrophy in APP/PS1 mice. Based on these results, AP39 was proposed as a promising drug candidate for AD treatment, and its anti-AD mechanism may involve protection against mitochondrial damage.

1. Introduction

Alzheimer's disease (AD) is the most universal age-related neurodegenerative disease and form of dementia, affecting approximately 5.3 million American people. Of those, 5.1 million are over the age of 65 years [1]. AD initially causes memory impairment, and as the disease progresses, patients exhibit motor aberrancies, personality changes, language deficiencies, and other neuropsychiatric symptoms. Because AD is a complex and multifaceted disease involving various mechanisms, including energy metabolism [2], inflammation, and abnormal cell cycle control [3], the currently available treatments include a combination treatment regimen targeting two or more aspects of AD pathology [4]. For example, drug treatment for AD is primarily based on the acetylcholine hypothesis or the amyloid-β (Aβ) accumulation hypothesis, but none of these drugs can stop or reverse the progression of AD.

Swerdlow first proposed the "AD mitochondrial cascade hypothesis" in 2004 [5]. Recently, increasing evidence has shown that mitochondrial dysfunction is a prominent factor in AD pathogenesis [6], as either a cause or a consequence of Aβ toxicity. Severe structural and functional abnormalities of the mitochondria were observed in the immediate vicinity of Aβ plaques [7]. Moreover, Aβ gradually accumulates within the mitochondria of both living mouse models of AD and human AD brain sections, and Aβ has been found to directly interact with several mitochondrial proteins, for example,

cyclophilin D (CypD), amyloid-β binding alcohol (ABAD) dehydrogenase, and dynamin-related protein 1 (Drp1) [8]. These interactions impair the physiological functions of mitochondria, resulting in limited electron transfer, abnormal adenosine 5′-triphosphate (ATP) production, increased production of reactive oxygen species (ROS), and altered mitochondrial morphology and mobility in AD transgenic models [9, 10]. Furthermore, a growing body of research suggests that mitochondrial biogenesis is considerably decreased in the brains of both AD patients and AD model mice [9, 11–13]. Impaired mitochondrial biogenesis is conducive to mitochondrial dysfunction in AD [13].

Hydrogen sulfide (H_2S) has recently been recognized as an endogenous gaseous mediator that plays multiple regulatory roles in humans and mammals [14]. Increasing evidence has demonstrated that the dysregulation of H_2S homeostasis is implicated in the pathological processes of AD. Recently, our experimental research has revealed that the level of H_2S is decreased in AD patients and that this change in the H_2S levels may be related to the severity of AD. The emerging mitochondrial roles of H_2S include antioxidant, antiapoptotic, and anti-inflammatory effects [15]. Tang revealed that H_2S modulates Aβ-induced damage to PC12 cells by ameliorating the decrease in the mitochondrial membrane potential (MMP, $\Delta\Psi m$) and attenuating the increase in intracellular ROS levels [16]. Moreover, Xuan et al. found that H_2S may attenuate spatial memory impairment and neuroinflammation within the hippocampus of AD model mice [17]. With regard to the regulatory role of H_2S in cellular bioenergy metabolism, recent studies have shown that H_2S can serve as a physiological electron donor and as an inorganic energy source in mammalian cells. Recently, Módis et al. reported that an endogenous intramitochondrial H_2S-producing pathway, which is governed by 3-mercaptopyruvate sulfurtransferase (3-MST), complements and balances the bioenergetic activity of Krebs cycle-derived electron donors in the Hepa1c1c7 cell line [18].

Taken together, these findings indicate that the potential effects of H_2S on mitochondrial dysfunction in AD models are significant. Therefore, to clarify whether the new H_2S donor AP39, which contains the mitochondria-targeting compound triphenylphosphonium (TPP+) coupled to an H_2S-donating moiety (dithiolethione) via an aliphatic linker, regulates mitochondrial function and cellular bioenergetics is of great interest. Using APP/PS1 neurons and mice, we first detected the overall viability of the neurons and evaluated the effects of AP39 on cellular bioenergetics and mitochondrial function. In addition, we examined the effects of AP39 on spatial memory deficits and on magnetic resonance imaging (MRI) characteristics of the mouse brains.

2. Materials and Methods

2.1. Materials. AP39, a novel mitochondria-targeted H_2S donor, was designed and synthesized by Medicilon Inc., as described previously [19, 20]. Antimycin A, 0.25% trypsin, 2-deoxyglucose, oligomycin, carbonyl cyanide-4-(trifluoromethoxy)phenylhydrazone (FCCP), trichloroacetic acid, rotenone, 7-azido-4-methylcoumarin (AzMC), monobasic potassium phosphate, dibasic sodium succinate hexahydrate, adenosine 5′-triphosphate (ATP) disodium salt hydrate, fatty acid-free BSA, sodium hydrosulfide hydrate ($NaSH{\cdot}xH_2O$), N,N-diethyl-p-phenylenediamine sulfate, magnesium chloride, and iron(III) chloride ($FeCl_3$) were purchased from Sigma-Aldrich Company. The monoclonal anti-Aβ antibody 6E10 was obtained from Covance Inc. (Princeton, NJ, USA). Drp1 was purchased from Novus Biologicals, Inc. Fis1 was purchased from Proteintech Group. Mfn1 and Mfn2 antibodies were purchased from Santa Cruz Biotech, and OPA-1 antibody was purchased from BD Transduction Laboratories. The secondary antibodies goat anti-mouse-HRP and donkey anti-rabbit-HRP antibodies were purchased from GE Healthcare. The Pierce BCA protein assay kit was purchased from Thermo Fisher Scientific (Waltham, MA, USA). Dulbecco's modified Eagle's medium (DMEM), 1% glutamine, and 1% penicillin were obtained from Invitrogen. All other chemicals were purchased from Amresco (Solon, OH, USA).

2.2. Animals and Treatments. This experiment was performed as described previously [21]. All animal protocols were approved by the Animal Research Committee of Chong Qing Medical University. Heterozygous APP/PS1 double-transgenic mice (APPswe-PS1dE9) were crossed with non-transgenic female mice (the Model Animal Research Center of Nanjing University, Jiangsu, China) to produce hemizygous transgenic mice and nontransgenic littermates. In the double-transgenic mice that coexpressed the Swedish mutation of APP (APPswe) and two FAD-PS1 variants, Aβ plaques accumulated in the brain, and learning and memory ability declined over time [22]. The mice were housed at 23–25°C with 60% humidity under 12 : 12 h light-dark cycles and were provided with free access to food and water throughout the experiment. Pregnant females were sacrificed at gestational days 15-16 (E15-16), and the embryos were removed for the preparation of brain neuronal cultures. The genotyping for APP and PS1 was performed according to the literature to assign cultures to transgenic and nontransgenic groups according to the PCR results with genomic DNA. For the Morris water maze test and the novel object recognition task (NORT), these 12-month-old mice were divided into four groups of fifteen mice in each group: wild-type (WT) mice treated with deionized water or 100 nM/kg AP39 and AD model mice treated with deionized water or 100 nM/kg AP39. The mice were treated once daily via intraperitoneal injection for 6 weeks prior to the experiments. After the behavioral tests, the mice were scanned by MRI and then sacrificed for the collection of their blood and brains. The blood was collected into heparinized tubes and then centrifuged at 1000 g for 10 min at 4°C. The plasma (supernatant) was collected to detect $A\beta_{40}$ and $A\beta_{42}$ by ELISA. The brains were removed and collected to examine Aβ deposition by immunohistochemistry.

2.3. Primary Neuron Culture. Primary cultures of cortical neurons were generated from the brains of individual embryos at E15-16. Briefly, the brains were removed and then placed in Hank's balanced salt solution at 4°C. The cortex was dissected from the brain, chopped, and digested

in 0.25% trypsin for 16 min at 37°C with gentle shaking. For the mixed neuronal cultures, after cell counting, the dissociated cells were plated at a density of 2×10^5 cells/cm^2 in a 35 mm dish on poly-d-lysine-coated cover slips in DMEM containing 10% F-12 and 10% fetal bovine serum (FBS) and were maintained at 37°C in a humidified atmosphere of 95% air and 5% CO_2. After culturing for 24 h in vitro, the medium was replaced with serum-free neurobasal medium containing 2% B27 serum-free supplement, 1% glutamine, and 1% penicillin. Thereafter, half of the medium was replaced with neurobasal medium every three days. Pure neuronal cultures were supplemented with glia-conditioned medium (GCM). These neurons were prepared in a similar manner, except that cytosine arabinoside (5 μM) was added to the culture media at DIV 4 to block the proliferation of glia, and the cultures were maintained in GCM. After 16 days, the neurons were treated with different concentrations of AP39 diluted in the appropriate medium for 24 h.

2.4. Measurement of H_2S Production

2.4.1. H_2S Production in Neurons and Brain Tissue (Methylene Blue Assay). This experiment was performed based on previous literature [23, 24]. Neurons were scraped, collected, and then washed 3 times with phosphate-buffered saline (PBS). The neurons were suspended in ice-cold 50 mM Tris-HCl buffer and homogenized by sonication. Homogenized samples were centrifuged at 10,000 g for 10 min at 4°C, and the supernatants were collected as cell lysates. The protein concentrations of the supernatants were determined using the Quick Start Protein Assay Kit.

We used spectrophotometric measurements based on the formation of methylene blue by H_2S to detect H_2S production. We performed all reactions in duplicate. Cell lysates (310 μL, 1 mg/mL) in 1.5-mL tubes were mixed with trichloroacetic acid (20% w/v, 60 μL), zinc acetate (2% w/v, 30 μL), and N, N-dimethyl-p-phenylenediamine sulfate (NNDPD) (20 mM; 40 μL) in 7.2 M HCl and $FeCl_3$ (30 mM; 30 μL) in 1.2 M HCl. The optical absorbance of the resulting solution (670 nm) was measured after 15 min using a 96-well microplate reader (Tecan Systems Inc., Switzerland). H_2S was calculated against a calibration curve of NaHS.

To explore the effect of AP39 on the generation of H_2S in mice, these 12-month-old WT or APP/PS1 mice were treated with different concentrations of AP39 (25 nM/kg–250 nM/kg). The mice were treated once daily via intraperitoneal injection for 6 weeks prior to determining H_2S concentration. In brief, mice from each group were anesthetized with chloral hydrate and euthanized by decapitation. Tissues from the hippocampus and cerebral cortex were immediately removed and then homogenized in ice-cold 50 mM potassium phosphate buffer (12% wt./vol, pH 8.0) with a Polytron homogenizer. The homogenates were centrifuged at 47,000 ×g for 10 min at 4°C and supernatants were collected. Then the H_2S production was measured as above described via methylene blue assay.

2.4.2. H_2S Detection in Mitochondria. Neurons were seeded at a density of 5×10^4 cells/well in a Lab-Tek II chamber coverglass system and were maintained at 37°C in a humidified atmosphere of 95% air and 5% CO_2. The H_2S-sensitive fluorescent dye AzMC was incorporated into a cell-based assay to detect H_2S production [19, 25]. The neurons were loaded with the fluorogenic dyes 10 μM AzMC and 200 nM MitoTracker Red CMXRos (Invitrogen) at 37°C for 30 min. Different concentrations of AP39 were added to fresh media, and the neurons were further incubated for 2 h, after which H_2S imaging was performed. After washing 3 times with PBS, the specific fluorescence from the various dyes was examined using a confocal laser scanning microscope.

2.5. Bioenergetic Analysis in Neurons. We used the XF24 Extracellular Flux Analyzer (Seahorse Bioscience, Billerica, MA, USA) to measure cellular bioenergetic function as previously described [26]. Neurons were treated with different concentrations of AP39 in medium. Neurons were seeded at the optimal density of 3.5×10^4 cells per well and were maintained at 37°C in a humidified atmosphere of 95% air and 5% CO_2. Next, the indices of mitochondrial function were measured according to the following protocol. After recording the basal OCR and PPR levels, oligomycin (1.5 μg/mL) was used to assess the mitochondrial ATP production rate, and FCCP (0.5 μM) was used to assess the maximal mitochondrial respiratory capacity (a parameter that characterizes overall mitochondrial function in neurons) via the measurement of the oxygen consumption rate (OCR). Finally, antimycin A (2 μg/mL) and rotenone (2 μM) were used to inhibit the flux of electrons through complexes III and I and to detect the residual nonmitochondrial OCR, which is considered to be mediated by cytosolic oxidase enzymes. Bioenergetic parameters were normalized to the neuron count, as the same number of neurons was seeded in each well.

2.6. MTT Assay. Cell viability was determined by the MTT reduction assay method as follows. The neurons were cultured and treated with different concentration of AP39 for 24 h in 96-well plates. MTT was added to each well with a final concentration of 0.5 mg/mL for 4 h. After a 4-h incubation at 37°C, the MTT solution was removed and the insoluble formazan crystal was dissolved in DMSO. The absorbance of the colored solution was measured at 570 nm using a microplate reader (Tecan, USA).

2.7. LDH Assay. Lactate dehydrogenase (LDH) release, an indirect measurement of cell death, was determined using a cytotoxicity assay according to the manufacturer's instructions. Briefly, 30 μL of supernatant was saved before the addition of MTT and mixed with 100 μL of freshly prepared LDH assay reagent. LDH release into the culture medium was detected using a colorimetric reaction reading of absorbance at 490 nm according to manufacturer's protocol for the LDH assay kit (Beyotime, Jiangsu, China). LDH activity values are shown as V_{max} for kinetic assays in mOD/min.

2.8. Cellular ATP Measurements. Neurons were plated at a density of 0.5×10^4 cells/well in 96-well plates before the experiment. WT and APP/PS1 neurons were treated with

water or 100 nMAP39, and the samples were measured in triplicate. After incubation for 24 h, the ATP levels were assessed using the ATP Bioluminescent Assay Kit (Sigma-Aldrich). The fluorescence intensity, which was linearly related to the ATP concentration, was measured using a microplate luminometer [27].

2.9. Measurement of Mitochondrial and Nuclear DNA Integrity. DNA integrity was assessed using gene-specific semiquantitative PCR assays as described previously [28]. Briefly, total DNA from experimental neurons was isolated using the DNase Blood and Tissue Kit. Quantification of a PCR-amplified 9-kb nuclear-specific DNA fragment using PicoGreen fluorescent dye to measure double-stranded DNA was used to estimate damage to nuclear DNA. Quantification of a PCR-amplified 10-kb mitochondrial-specific DNA fragment using PicoGreen dye was used to detect damage to mitochondrial DNA. The obtained data were normalized by the PCR amplification of a 117-bp mitochondrial genome-specific fragment to correct for multiple copies of the mitochondrial genome. Preliminary assays were performed to ensure the linearity of PCR amplification with respect to the number of cycles and DNA concentration.

2.10. Measurement of Intracellular ROS. The fluorescent dye 2′, 7′-dichlorofluorescein diacetate (DCFH-DA) was used to assess the intracellular production of ROS according to the manufacturer's instructions. Following the indicated treatment, the neurons were harvested, washed twice with PBS, and centrifuged at 1000 g for 10 min. Then, the cells were resuspended in 10 μM DCFH-DA (Beyotime, Jiangsu, China) solution and incubated in a CO_2 incubator at 37°C for 30 min in the dark, followed by three washes with PBS. Finally, the cells were resuspended in 0.5 mL of PBS, and the fluorescence intensity of the samples was analyzed by flow cytometry.

2.11. Western Blot. Approximately 1×10^7 neurons were collected for each experiment. The cell samples were lysed with Western and IP lysis buffer (Beyotime, Jiangsu, China) and centrifuged at 12,000 g for 15 min. The protein concentrations were determined using the BCA protein assay kit. A total of 20 μg protein was loaded per lane and subjected to electrophoretic separation in a 10% SDS-PAGE gel. After separation, the proteins were electrically transferred to a nitrocellulose transfer membrane (PerkinElmer Life Sciences) for 1 h. After blocking with 5% nonfat milk in Tris-buffered saline containing Tween-20 (TBST), the membranes were incubated in primary antibodies against Mitofusin-1 (Mfn-1, 1 : 200, rabbit polyclonal), Mitofusin-1 (Mfn-2, 1 : 200, rabbit polyclonal), Optic Atrophy-1 (OPA-1, 1 : 400, mouse monoclonal), Fission-1 (Fis-1, 1 : 1500, rabbit polyclonal), Drp-1 (1 : 200, rabbit polyclonal), or VDAC (1 : 500 to 1 : 1000) overnight at 4°C. The membranes were subsequently incubated in donkey anti-rabbit or goat anti-mouse antibodies for 1 h at 37°C. Chemiluminescent detection was performed using the Pierce ECL Western blotting substrate, and the signals were analyzed using Quantity One software.

2.12. Behavioral Testing

2.12.1. Morris Water Maze Test. The Morris water maze test was performed according to the protocols of a previous study [29]. Animals were randomly assigned to different treatment groups and then were pretreated with once-daily administration of either water or AP39 for 6 weeks prior to testing. Briefly, the mice were put into each quadrant in a random order to locate a hidden platform within 1 min, and the experimenter would guide them to the platform if the mice failed to find the platform. Then, the mice were left on the platform for 30 s to help them remember the platform location. The mice were trained to locate the platform using a two-trial-per-day regimen, and the training was divided into two blocks of four trials. The first block of four trials was performed in the morning, and the second block of four trials was performed in the afternoon. In the probe trial, the platform was removed, and the mice were placed in the water for a single 60-s period. The latency to reach the platform was recorded for both the training and probe trials, and the parameters were analyzed using an EthoVision 3.1 analysis system by an observer who was blinded to the treatment status of the mice.

2.12.2. Novel Object Recognition Task (NORT). The novel object recognition task (NORT), which is based on the natural instinct of rodents to interact more with a novel object than a familiar object, was performed to assess the memory of the experimental mice as described in the literature [30]. Briefly, on the first day of acclimation, each mouse was provided with 10 min to interact with either object for combined 30 s. The total distance traveled was recorded and analyzed to evaluate the motor ability of the mice. On the following day, the mice were exposed to two identical objects (A1 and A2) for 10 min for familiarization. Both objects A1 and A2 had identical textures, colors, and sizes and were positioned in two adjacent corners from the walls. After a 24-h delay in the mice cages, the mice were again placed into the same arena used before for 10 min and then exposed to the field for 5 min in the presence of the old familiar (A1) and a new different novel (B) object. We determined the amount of time spent at both familiar and novel objects through video analysis using a "within object area" scoring method. A mouse was scored as interacting with the object when its nose was in contact with the object or directed at the object within $\leq$ 2 cm. Time spent standing, sitting, or leaning on the secured object was not scored. The exploratory preference was defined as the percentage of total time that the animal spent investigating the novel object and calculated for each animal by the following ratio: TB/(TA + TB) × 100% [TA: time spent exploring the familiar object A; TB: time spent exploring the novel object B].

2.13. Mouse Brain MRI. The mice were scanned by MRI after treatment with water or AP39 for 6 weeks as described previously in the literature [31]. The MRI experiment was conducted in Da Ping Hospital, Research Institute of Surgery, Third Military Medical University, China. The mice were anesthetized with 10% chloral hydrate-saline and then placed

in the prone position. Their chests were connected to a life signal detector to monitor their physiological status. The heads of the mice were scanned using a 7.0 T ultrahigh field animal MRI scanner (7.0 T ClinScan system, Bruker BioSpin, Ettlingen, Germany). T2-weighted images of the mouse heads were acquired from the sagittal plane, axial direction, and coronal plane according to the following conditions: TR = 3200 ms, TE = 45 ms, field of view (FOV) = 22 × 22 mm, slice thickness = 0.5 mm, a scan matrix = 384 × 384, and repetitions (NEX) = 5.

2.14. ELISA for $A\beta_{40}$ and $A\beta_{42}$. A commercially available ELISA kit for $A\beta_{40}$ and $A\beta_{42}$ was purchased from Invitrogen. The plasma from samples was collected by centrifugation (1,000 g at 4°C for 10 min), and 100 μL of plasma was used for $A\beta_{40}$ and $A\beta_{42}$ measurement. The secreted levels of $A\beta_{40}$ and $A\beta_{42}$ in blood were quantitatively measured according to the manufacturer's instructions.

2.15. Immunohistochemistry. After the behavioral tests, the mice were deeply anaesthetized with chloral hydrate (400 mg/kg body weight) and sacrificed for the preparation of brain slices [32]. The brains were removed from the skull, postfixed overnight in 4% paraformaldehyde at 4°C, and transferred to 30% sucrose solution for dehydration. Subsequently, the brains were frozen and sliced into 30-mm thick sections using a Leica CM3050 S cryostat. After multiple washes in PBS, the slices were incubated with a 6E10 primary antibody (1 : 1,000 diluted) in 10% goat serum overnight at 4°C. The tissue sections were washed 3 times for 10 min in PBS and then incubated with a TRITC-conjugated goat anti-mouse IgG antibody at room temperature for 1 h followed by PBS washing. The slides were subsequently stained with diaminobenzidine and counterstained with hematoxylin. The images were acquired using a 10x objective on a Carl Zeiss LSM780 confocal microscope (Olympus BX60, Tokyo, Japan). The Aβ plaque areas were quantified using Image-Pro Plus 6.0 software.

2.16. Statistical Analysis. All statistical analyses were performed using SPSS 22.0 software. All data were presented as the means ± SEM. The data in the Morris water maze were analyzed using two-way ANOVA coupled with a post hoc Fisher's LSD test using GraphPad Prism 6.0 software. The data from other experiments were analyzed by one-way ANOVA coupled with Dunnett's posttest using GraphPad Prism 6.0 software, and $P \leq 0.05$ was considered to be statistically significant.

3. Results

3.1. AP39 Increased the Generation of H_2S in Neurons and Mitochondria. H_2S levels were comparable between WT neurons treated with different concentrations of AP39 for 2 h. AP39 (25–250 nM) induced a concentration-dependent increase in H_2S generation and in the fluorescence of the H_2S-detecting dye AzMC, and the signal was significantly colocalized with the mitochondria (Figures 1(a) and 1(b)). Notably, baseline fluorescent signal was detectable in the neurons. In this study, the low basal levels of H_2S did not indicate a mitochondrial preference (Figure 1(b)). In conclusion, the data in Figure 1 indicate that AP39 contributes to the synthesis of H_2S in neurons, especially in the mitochondria.

3.2. Biphasic Effects of AP39 on Cellular Bioenergetics. Similar to the responses previously noted for authentic H_2S [25, 33, 34], exposure of WT neurons to AP39 induced a significant increase in the basal OCR at 100 nM but induced a decrease in the basal OCR at 250 nM (Figure 2(a)). Additionally, AP39 caused a dose-dependent increase in the FCCP-stimulated OCR at 25 and 100 nM but caused a decrease in the FCCP-stimulated OCR at 250 nM (Figure 2(b)). The FCCP-induced increase in the OCR represents the "maximal respiration." Thus, AP39 acts as a supplemental bioenergetic stimulator at low concentrations. The pattern of the effects of AP39 is consistent with the previously established bell-shaped pharmacological properties of H_2S [19, 35]. These results demonstrated that this inhibitory effect is only conspicuous at higher concentrations (Figure 2(b)).

3.3. AP39 Exerted Cytoprotective Effects on APP/PS1 Neurons. We cultured cortical neurons from the brains of embryonic APP/PS1 transgenic mice as an experimental model to study the effects of AP39. We detected the levels and time course of the release of $A\beta_{42}$ from these neurons into the culture media by ELISA. Figure 3(a) shows that at 3 DIV a small amount of $A\beta_{42}$ was released into the media of neurons cultured from APP/PS1 mice, but significant differences were observed between neurons cultured from APP/PS1 mice and their WT littermates (16.1±6.9 and 5.9±2.7 pg/mL, resp.). By 7 DIV, the level of $A\beta_{42}$ produced in the cultures from the APP/PS1 mice was significantly higher than that produced in the cultures from the WT mice (285.7 ± 38.6 versus 6.2 ± 0.7 pg/mL, $P < 0.01$), and this level was further increased at 16 DIV (898.3 ± 27.3 versus 6.8 ± 0.5 pg/mL, $P < 0.01$). The total protein from WT and APP/PS1 neurons was extracted separately and analyzed by Western blot. We observed that Aβ was overexpressed in the APP/PS1 primary neurons compared to the WT neurons (Figures 3(b) and 3(c)).

Exposure of WT neurons to AP39 for 24 h had no effect on cell viability, but treating the APP/PS1 neurons with AP39 (25,100 nM) for 24 h resulted in increase in cell viability (Figures 3(d) and 3(e)). To confirm this result, we measured the release of LDH in the supernatant of the primary neurons. AP39 had no effect on basal LDH release in WT neurons, but there was a significant increase in the amount of LDH in the APP/PS1 neuron culture medium. This result indicated a loss of cell membrane integrity and an increase in cell necrosis. In contrast, after treatment with AP39, particularly at 100 nM, the amount of LDH in the APP/PS1 neuron culture medium was decreased (Figures 3(f) and 3(g)).

3.4. AP39 Attenuated the Loss of Cellular Bioenergetics and Protected Mitochondrial Function in APP/PS1 Neurons. To investigate the effects of AP39 on mitochondrial dysfunction, we measured cellular bioenergetics using the XF24 Extracellular Flux Analyzer. Cellular bioenergetic parameters were significantly decreased in the mitochondria of APP/PS1

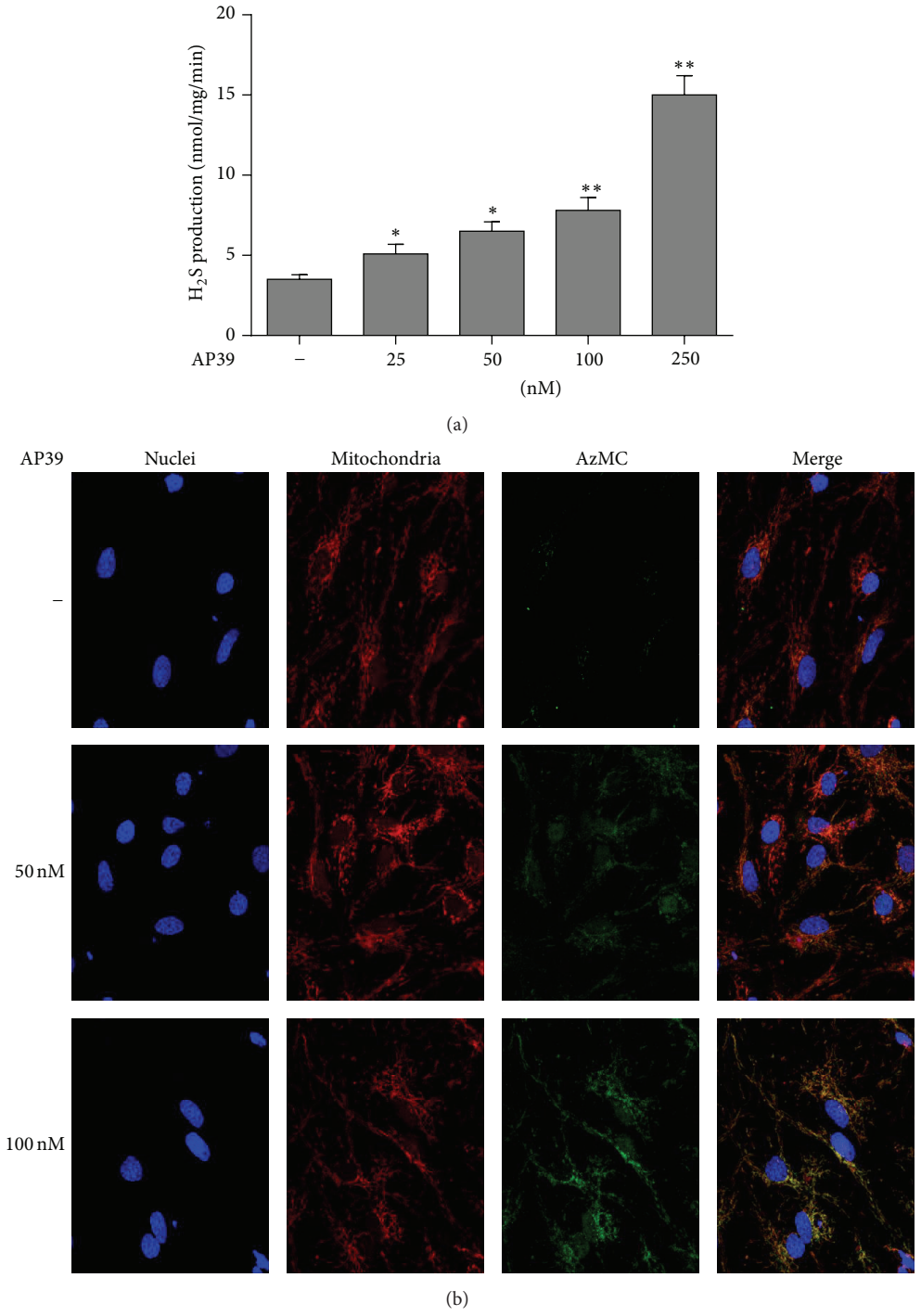

Figure 1: AP39 generates H_2S in WT neurons, primarily in the mitochondria. (a) The contribution of AP39 to H_2S production in neurons. Neurons from WT mice were treated with various concentrations of AP39 for 2 h, and H_2S production was detected by methylene blue assay. (b) Neurons were treated with different concentrations of AP39 for 2 h, and intracellular H_2S was detected using the fluorescent probe AzMC. DAPI was used to stain nuclei, and MitoTracker was used to stain mitochondria. The colocalization of H_2S with mitochondria was indicated by the overlapping of red (mitochondria) and green (H_2S) fluorescence in the merged image. Note the concentration-dependent increase in the H_2S signal in response to AP39 treatment. $^{*}P < 0.05$, $^{**}P < 0.01$ compared with control treatment (no AP39).

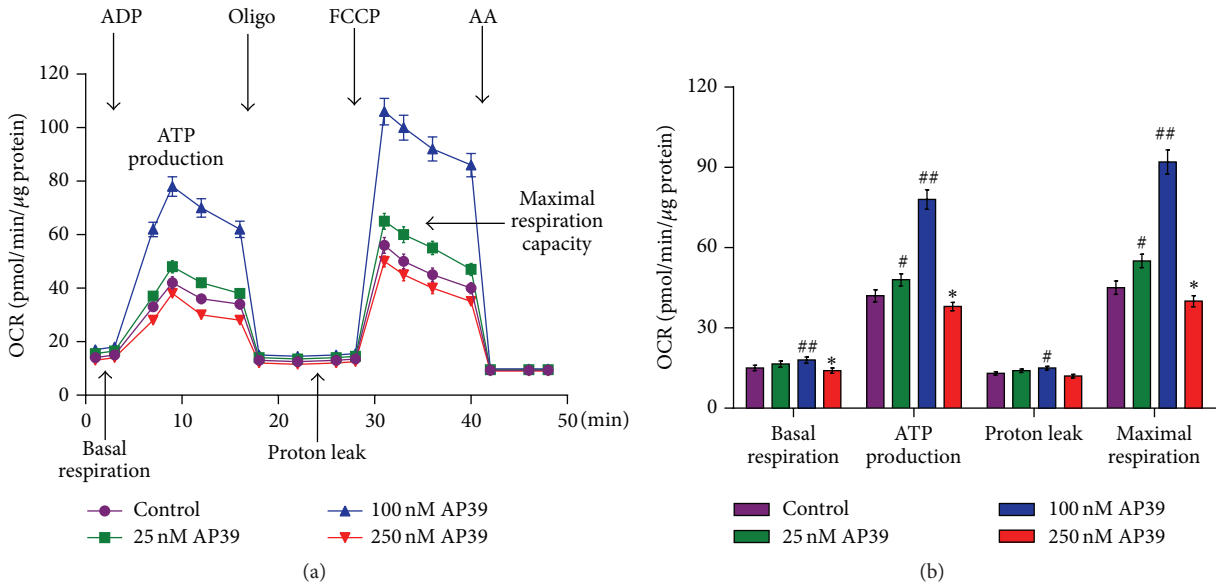

Figure 2: Biphasic effects of AP39 on the cellular bioenergetics of the WT neurons. Neurons from WT mice were incubated in AP39 (25-250 nM) for 2 h, and bioenergetic parameters were measured using an Extracellular Flux Analyzer. (a) Representative tracings. (b) The calculated bioenergetic parameters. # and ## indicate a significant enhancement in the bioenergetic parameter, compared to the control group (no AP39) ($P < 0.05$ and $P < 0.01$, resp.); ∗ indicates a significant reduction in the bioenergetic parameter, compared to the control group ($P < 0.05$).

neurons compared with those of WT neurons. Importantly, AP39 (100 nM) significantly increased the basal respiratory rate and the OCR-linked maximal respiratory capacity of the APP/PS1 neurons (Figure 4). These data indicated that AP39 may attenuate the loss of cellular bioenergetics in APP/PS1 neurons.

ATP production, mitochondrial DNA (mtDNA) integrity, and ROS production were measured to evaluate mitochondrial function. AP39 significantly increased the ATP production in WT and APP/PS1 neurons (Figure 5(a)). Next, mtDNA and nuclear genomic DNA integrity was assessed via PCR of long DNA fragments. We found that mtDNA but not nuclear DNA integrity was clearly reduced in APP/PS1 neurons, compared to WT neurons. However, AP39 significantly protected against mtDNA damage in APP/PS1 neurons by partially restoring mtDNA integrity (Figure 5(b)).

Intracellular ROS levels are a basic indicator of oxidative stress. A fluorescence assay using a DCFH-DA probe was performed to quantify the generation of ROS. AP39 (100 nM) effectively decreased ROS levels in APP/PS1 neurons (Figures 5(c) and 5(d)). In conclusion, these results suggested that AP39 protects against mitochondrial dysfunction in APP/PS1 neurons.

3.5. AP39 Shifted the Mitochondrial Dynamics toward Fission in APP/PS1 Neurons. The changes in the levels of proteins involved in mitochondrial dynamics (Drp1, Fis1, Mfn1, Mfn2, and OPA1) were determined via Western blot analysis (Figure 6). The levels of these mitochondrial dynamics-related proteins were shifted toward fission in APP/PS1 neurons. The levels of the mitochondrial fusion proteins Mfn1 and OPA1 were significantly reduced, and the level of the mitochondrial fission protein Fis1 was markedly increased in APP/PS1 neurons compared with WT neurons. The protein levels of Mfn2 and Drp1 were not significantly different between APP/PS1 and WT neurons. OPA1, Mfn1, and Mfn2 catalyze mitochondrial fusion. AP39 increased the levels of OPA1 and Mfn1 but not Mfn2. Moreover, AP39 decreased the levels of Fis1 but not Drp1. These findings suggested that AP39 may shift mitochondrial dynamics in APP/PS1 neurons from fission towards fusion.

3.6. AP39 Increased the Generation of H_2S in WT and APP/PS1 Mice. AP39 (25–250 nM) induced a dose-dependent increase in H_2S generation in the cortex and hippocampus of WT and APP/PS1 mice (Figures 7(a) and 7(b)). We also observed that H_2S levels in the cortex were lower than those of the hippocampus. However, the level of H_2S was significantly decreased in APP/PS1 mice compared to WT mice. In conclusion, the data indicate that AP39 contributes to the synthesis of H_2S in WT and APP/PS1 mice.

3.7. AP39 Reversed the Memory Deficits of APP/PS1 Transgenic Mice. The APP/PS1 transgenic mice developed a pronounced spatial learning and memory deficit and produced Aβ plaques by 12 months of age [22]. To test the ability of AP39 to ameliorate the spatial learning deficits of the AD model mice, we treated 12-month-old AD model mice and WT controls with 100 nM/kgAP39. Then, behavioral testing was initiated 6 weeks after the initiation of AP39 therapy using the Morris water maze and the NORT.

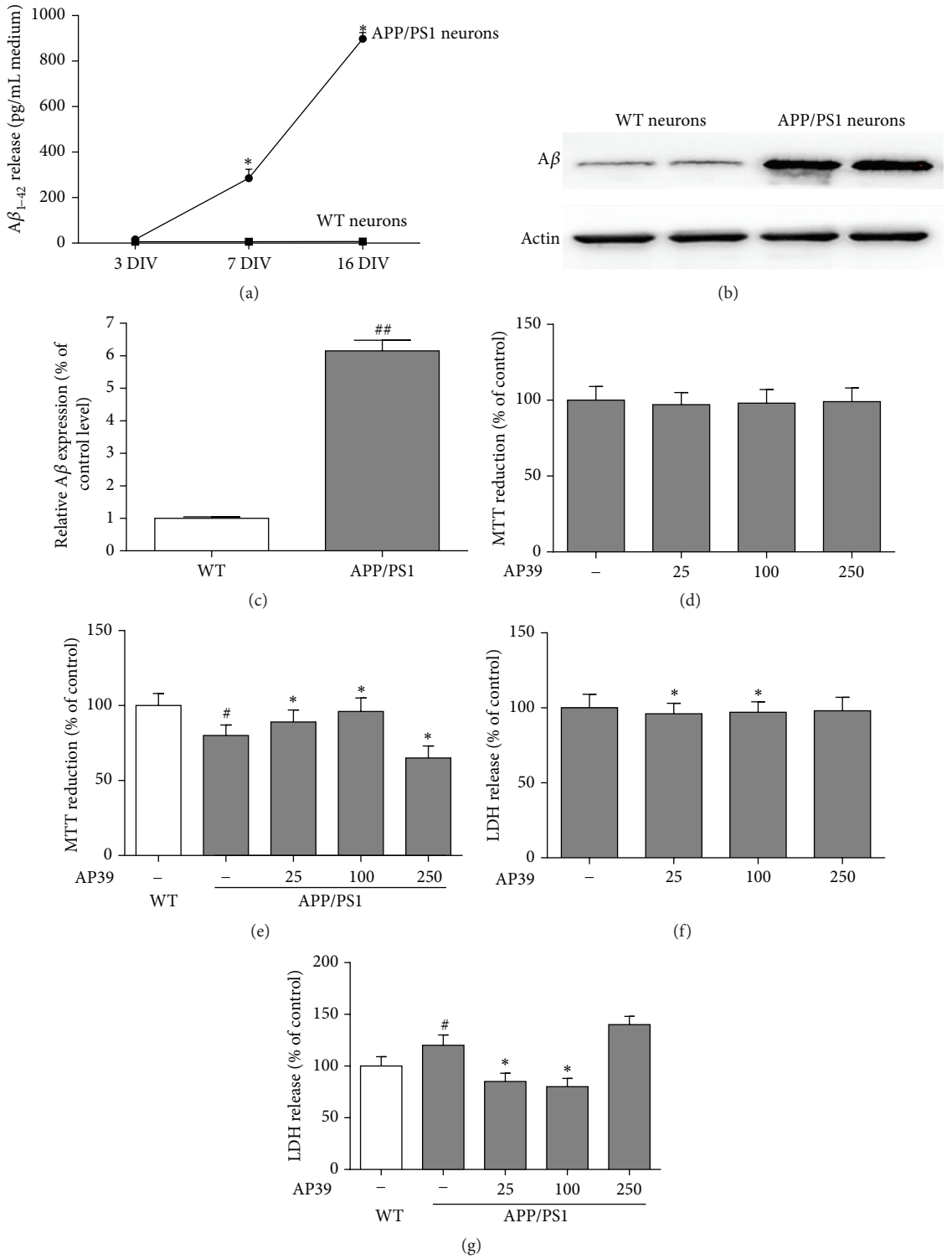

Figure 3: Cytoprotective effects of AP39 in APP/PS1 neurons. (a) A time course shows that increasing levels of $A\beta_{42}$ are released into the culture media of neurons from transgenic mice but not their WT littermates. (b) $A\beta$ was overexpressed in neurons from APP/PS1 mice compared to $A\beta$ expression in neurons from their WT littermates. (c) Representative of $A\beta$ blots is shown with quantification. (d) The effects of AP39 (25–250 nM) treatment for 24 h on cell viability in WT neurons. AP39 alone did not affect MTT conversion. (e) The effects of AP39 (25–250 nM) on MTT conversion in APP/PS1 neurons. There was a decrease in MTT conversion in the APP/PS1 neurons compared to the WT neurons; these effects were attenuated by AP39. (f) After treatment of WT neurons with AP39 for 24 h, AP39 alone did not affect LDH release in the cellular medium. (g) The effects of AP39 on LDH release from APP/PS1 neurons. $^{*}P < 0.05$, versus the APP/PS1 group; $^{\#}P < 0.05$, the APP/PS1 group versus the WT group.

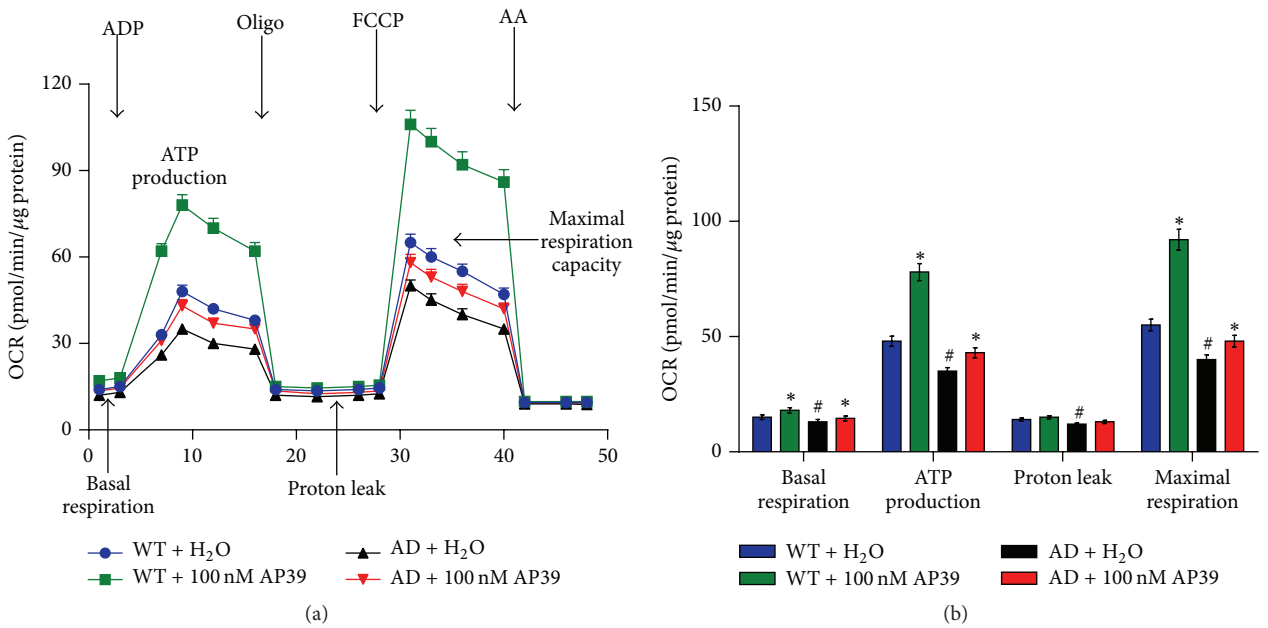

Figure 4: Protective effects of AP39 on the cellular bioenergetics of APP/PS1 neurons. APP/PS1 neurons were incubated in AP39 (100 nM) for 24 h, and bioenergetic parameters were measured using the Extracellular Flux Analyzer. (a) Representative tracings are shown. (b) The calculated bioenergetic parameters are shown. ∗ indicates a significant enhancement of the bioenergetic parameter compared to the control (H_2O) ($P < 0.05$); # indicates a significant reduction in the bioenergetic parameter compared to the control (WT + H_2O) ($P < 0.05$).

In the training trials, treatment with AP39 for 6 weeks eliminated the preexisting deficits of the transgenic mice, as demonstrated by a reduced latency to locate the hidden platform compared to the latency of the WT control with AP39 (Figure 8(a)). The WT mice with or without AP39 treatment preferred the target quadrant in the probe trial. In contrast, the AD model mice treated with H_2O spent much less time in the target quadrant, near the chance level of 15 s. The AD model mice treated with AP39 showed the same strong preference for the target quadrant as the WT mice. Thus, after 6 weeks, AP39 treatment reversed the spatial learning and memory deficits of the aged AD model mice (Figure 8(b)). This benefit was concentration-dependent, as 25 nM/kg AP39 treatment did not improve the water maze performance of the AD model mice (Figure 8(c)). Next, the same mice with 100 nM/kg AP39 or H_2O treatment were subjected to the NORT test (Figure 8(d)). The NORT test does not put stress on the animal and does not require spatial orientation. It has been used to measure deficits in learning and memory in various AD mouse models [36, 37]. Importantly, AD mice treated with water performed poorly and presented an impairment compared to the WT mice, indicated by a significant reduction in the percentage of time exploring the novel object; this behavior was consistent with an impairment in memory function for familiarization on the previous day. In contrast, the AP39-treated AD mice showed significantly improved performance levels compared to the water-treated AD mice level. Thus, treatment of aged APP/PS1 mice with 100 nM/kg AP39 for 6 weeks reversed the age-dependent memory impairment. All of these results indicated that appropriate doses of AP39 improved the learning and working memory ability of AD model mice.

3.8. AP39 Inhibited the Brain Atrophy of APP/PS1 Transgenic Mice. In addition to behavioral assessments, mice were randomly selected for intravital scanning to noninvasively study brain structure using MRI data. We studied the coronal and axial sections of the mouse brains (Figures 9(a)–9(f)). As expected, there were no apparent structural abnormalities in the WT mouse brains. For example, the sizes of the ventricle were symmetric between the two brain hemispheres, and the edges of the ventricle were clear and sharp (Figures 9(a) and 9(b)). However, we observed visible atrophy in the brains of the 12-month-old AD model mice treated with water (Figures 9(c) and 9(d)). Their ventricles were asymmetric, with a much larger size on the right than the left side, and had unclear edges. The MRI imaging data revealed that AP39 might alleviate brain atrophy and ventricle asymmetry in AD model mice (Figures 9(e) and 9(f)).

The apparent diffusion coefficient (ADC) value in parietal cortex and hippocampus of each group of mice was compared with diffusion weighted imaging (DWI) sequences. Figure 9(g) showed the ADC value in parietal cortex and hippocampus of APP/PS1 mice significantly declined compared to those in WT mice, whereas AP39 significantly increased the ADC values in parietal cortex and hippocampus of APP/PS1 mice ($P < 0.05$).

3.9. AP39 Reduced the Levels of Aβ and Aβ Deposition in APP/PS1 Transgenic Mice. After different treatments for 6 weeks, Aβ levels and plaque development were examined in vivo. The $A\beta_{40}$ and $A\beta_{42}$ levels in the 12-month-old AD transgenic model mouse brains were 925 and 532 pg/mL, respectively. Importantly, treatment with 100 nM/kg AP39 decreased the $A\beta_{40}$ and $A\beta_{42}$ levels in AD mice compared

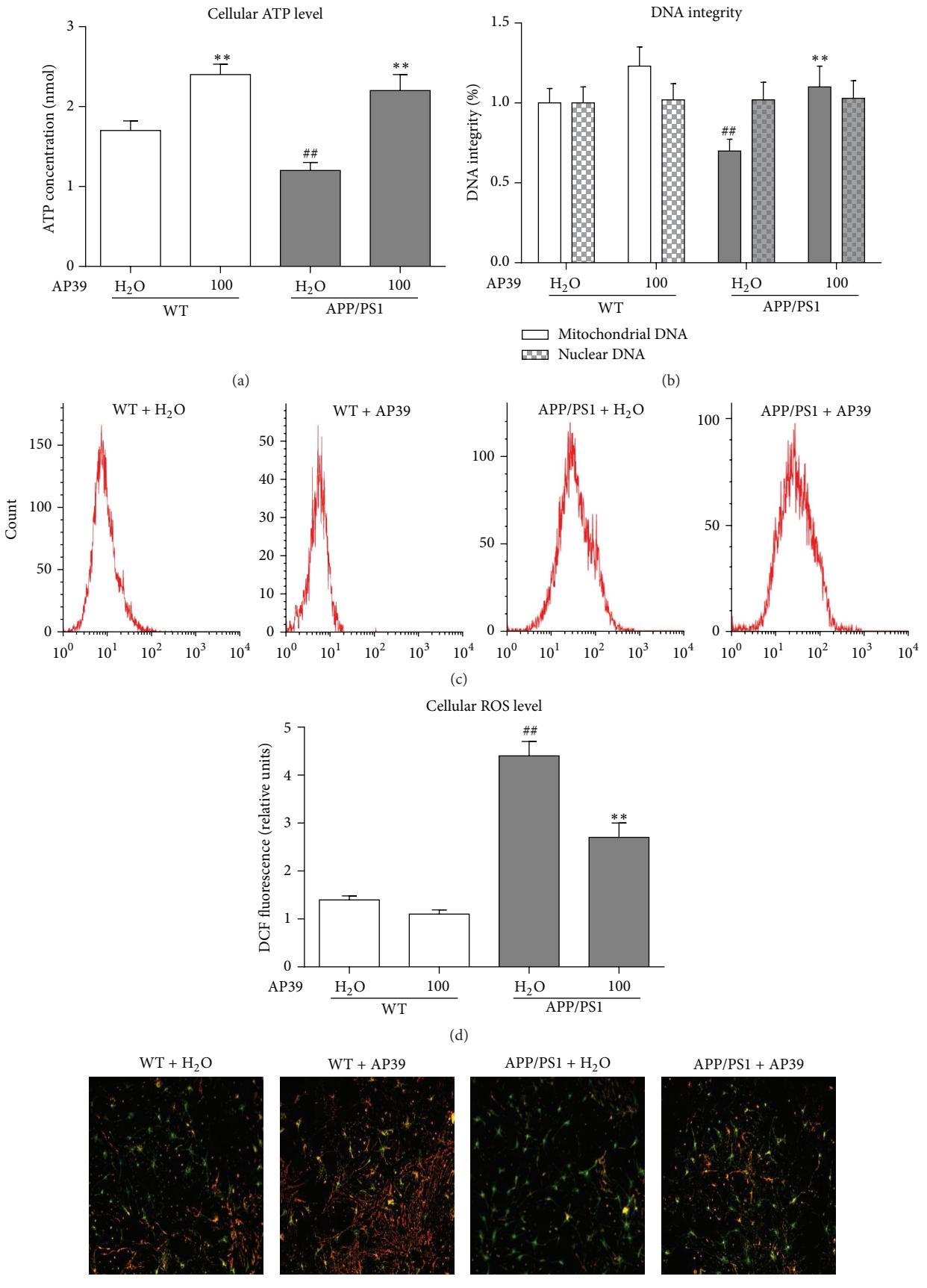

Figure 5: Continued.

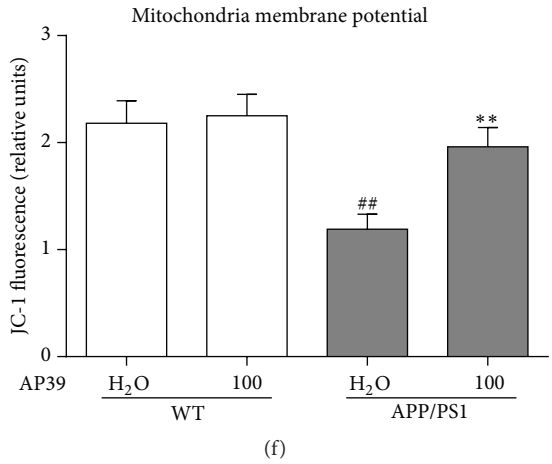

Figure 5: AP39 protected mitochondrial function in APP/PS1 neurons. (a) AP39 increased the cellular ATP levels. (b) AP39 protected mtDNA integrity. (c) ROS levels were detected by flow cytometry. (d) AP39 reduced ROS levels. $^{\#\#}P < 0.01$, compared with the WT group; $^{**}P < 0.01$, compared with the control group (H_2O).

to water treatment (Figures 10(a) and 10(b)). As expected, amyloid plaques were not observed in WT mice. However, intracellular amyloid in the hippocampal and cortical tissues of the AD model mice treated with water was remarkably increased compared with the WT control mice. This observation is consistent with those from a previous study [31]. Importantly, treatment with AP39 significantly reduced both the number and the size of intracellular amyloid plaques in the cortical and hippocampal tissues compared to treatment with water in the AD mice (Figure 10(c)). The amyloid plaque burden in the brains of AD model mice treated with AP39 was decreased compared with the brains of AD mice treated with water (Figure 10(c)). These results demonstrated the ability of AP39 to inhibit Aβ plaque deposition in the brains of AD mice.

4. Discussion

Our findings demonstrate that AP39, a newly synthesized mitochondrially targeted H_2S donor, maintains cellular bioenergetics and exerts mitochondrial protective effects in AD neurons and mice. First, AP39 exerted concentration-dependent modulatory effects on cell viability and cellular bioenergetic function. At 25 or 100 nM, AP39 enhanced cell viability and bioenergetics, but the highest AP39 concentration (250 nM) reduced these parameters in APP/PS1 neurons. In addition, treatment with an appropriately selected concentration of AP39 (100 nM) increased ATP levels, protected mtDNA integrity, decreased intracellular ROS levels, and regulated mitochondrial dynamics. Moreover, AP39 significantly inhibited brain atrophy and ameliorated the memory deficits and Aβ deposition in APP/PS1 mice.

H_2S, which has recently been determined to be the third most abundant gasotransmitter, plays a variety of physiological and pathological roles in the central nervous system and other systems [38, 39]. An increasing amount of evidence suggests that H_2S is a potential therapeutic drug for AD. Recently, it was reported that H_2S-modulating agents such as S-ally-l-cysteine (SAC) and Tabiano spa waters (enriched in H_2S) protected against impairments in learning and memory in AD transgenic mice by modulating inflammation and apoptosis [40–42]. In addition, our group reported that NaHS can promote the nonamyloidogenic processing of APP and improve spatial learning and memory acquisition in APP/PS1 mice [43]. However, due to technical limitations for H_2S detection, at present its biological roles and metabolites in vivo have remained elusive, resulting in considerable controversy [44]. Moreover, the use of sulfide salts such as NaHS is limited, although the solutions to these problems have recently become apparent [36]. Importantly, recent studies indicated that AP39 acts as an endogenous H_2S donor and exerts antioxidative and cytoprotective effects on bEnd.3 cells [19]. AP39 decreased blood pressure, heart rate, and pulse wave velocity in rats [37]. Based on these limitations and progress, we synthesized AP39 to evaluate its protective effects on mitochondrial function in APP/PS1 mice.

We observed that AP39 increased H_2S levels in neurons and mitochondria. Given that AP39 has the TPP+ group, which has been used to selectively target various molecules [45–47], this resulted in AP39 successfully and selectively delivering H_2S to mitochondria. This result is consistent with previous literature [19].

Previous research demonstrated that H_2S can act as an electron donor and as a potential inorganic source of energy in mammalian cells, resulting in an increase in cellular oxygen utilization and ATP production [48, 49]. Subsequently, studies reported opposing (stimulatory at lower concentrations; inhibitory at higher concentrations) effects of H_2S on cellular bioenergetics in HT-29 Glc(−/+) cells and some immune cells [50, 51]. However, owing to the various measurement methods used in experiment, the exact concentrations of H_2S reported to induce stimulation versus inhibition were different. Recently, Módis et al. reported that 3-MST-derived H_2S functions as an endogenous bioenergetic factor that donates electrons to SQR: the subsequent mitochondrial electron transport is coupled to aerobic ATP generation. In

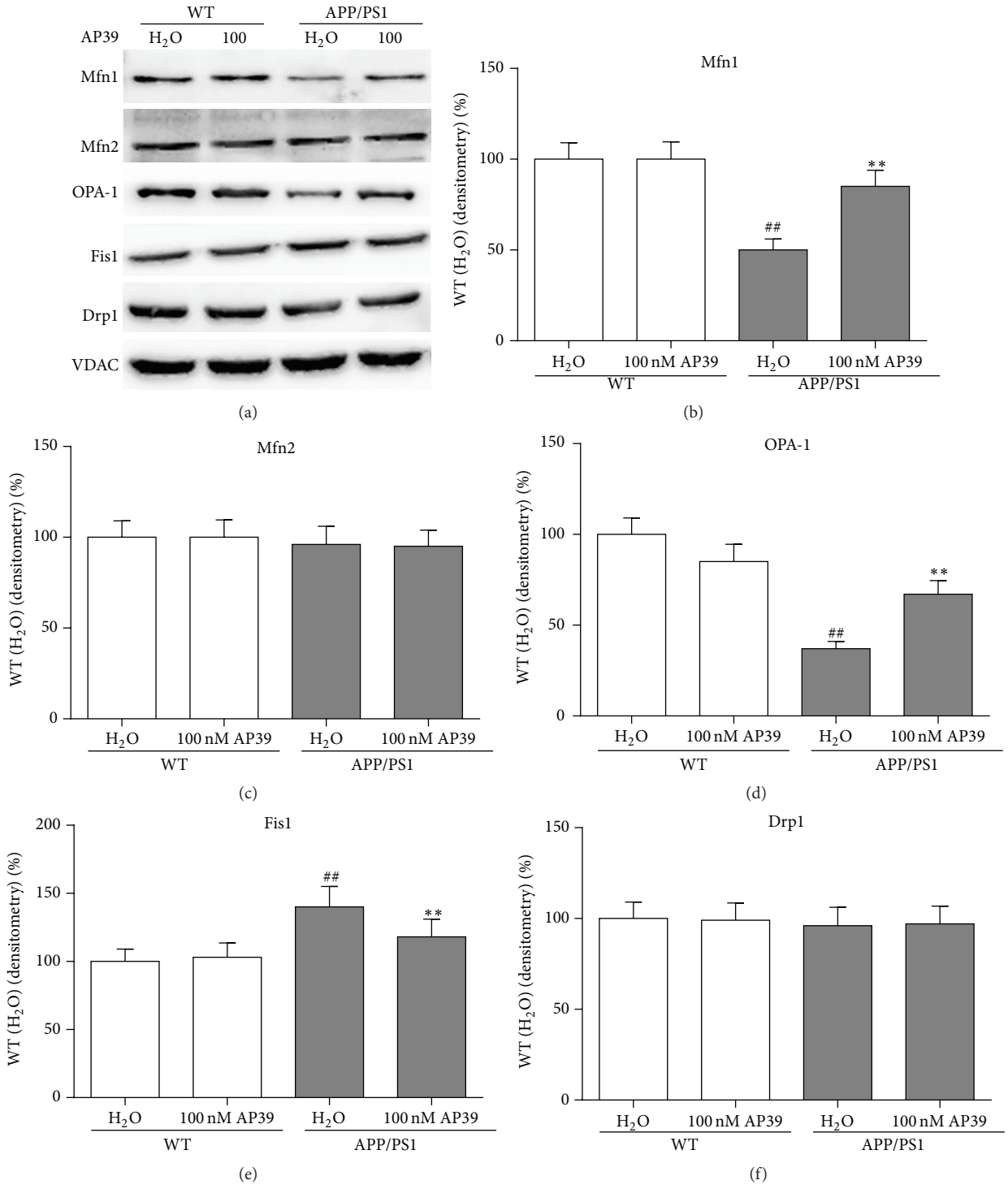

Figure 6: AP39 reduced the expression of proteins involved in mitochondrial fusion but increased the expression of a mitochondrial fission protein. (a) Protein samples were probed for Drp1, Fis1, Mfn1, Mfn2, OPA-1, and VDAC expression. (b–f) Representative blots are shown with quantification. $^{\#\#}P < 0.01$ AD mice receiving water compared to WT mice receiving water; $^{**}P < 0.01$ mice receiving AP39 compared with mice receiving water.

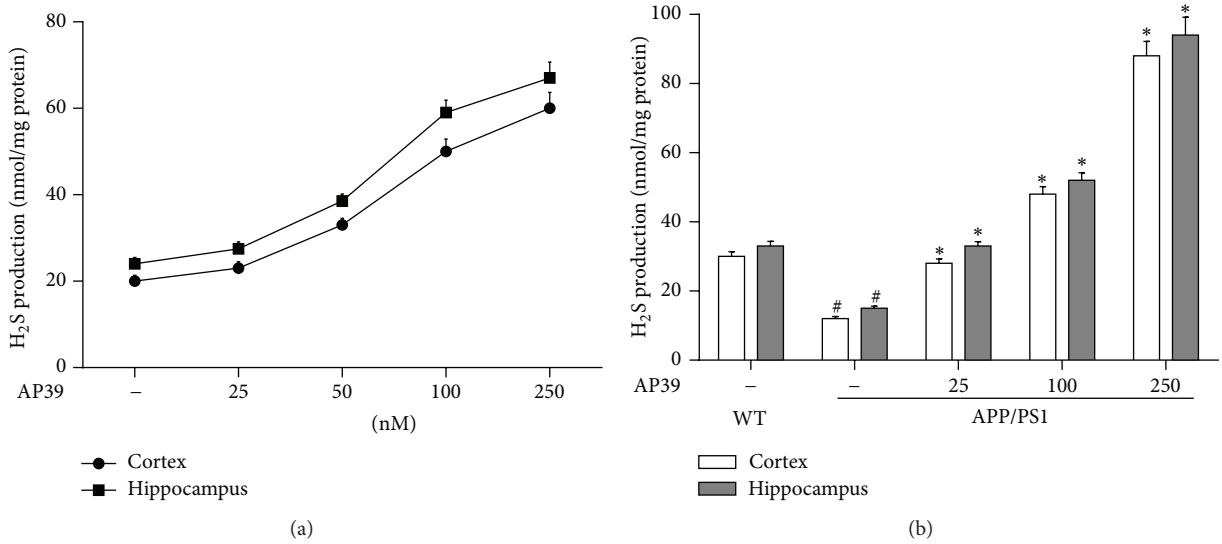

FIGURE 7: AP39 generates H_2S in WT mice and AP39 increased H_2S levels in APP/PS1 mice. (a) The contribution of AP39 to H_2S production in the cortex and hippocampus of WT mice. (b) AP39 increased H_2S levels in APP/PS1 mice. $^{\#\#}P < 0.01$, compared with the WT group; $^{**}P < 0.01$, compared with the control group (H_2O).

Hepa1c1c7, low concentrations of H_2S (0.1–1 μM) elicited a significant increase in mitochondrial electron transport and cellular bioenergetics and higher concentrations of H_2S (3–30 μM) were inhibitory [18]. In our experiments, AP39 (25–100 nM) induced the stimulation of cellular bioenergetics and AP39 (250 nM) induced marked inhibition in WT neurons. Moreover, APP/PS1 neurons exhibited higher "baseline" rates of oxygen consumption, electron transport, and cellular bioenergetic status than WT neurons. However, it is noted that AP39 (100 nM) increased the basal respiratory rate and exerted a protective effect on the cellular bioenergetics of the APP/PS1 neurons. These results are consistent with a previous study showing a stimulatory role for H_2S on bioenergetics but are opposed to the inhibitory effects of H_2S on mitochondrial electron transport at complex IV [52–54], which occurs at supraphysiological concentrations. Interestingly, the concentrations of AP39 (nM) that resulted in either stimulation or inhibition were lower than those previously reported using H_2S. We considered that AP39 accumulated in mitochondria, in which the AP39 concentration is likely substantially higher than the "nominal" concentration that was applied to the culture medium, resulting in this discrepancy. Overall, these data indicated that the stimulatory and inhibitory effects of H_2S occur in a narrow concentration range (in a specific concentration range to exert positive bioenergetic effects; exceeding this range produces inhibitory effects). However, the exact molecular mechanism underlying the protective effect of AP39 remains to be investigated in further experiments.

It has been reported that transgenic mouse strains harboring a single (APP) or double (APP and PSEN1) genetic mutation generate amyloid plaques [55]. In our experiments, $A\beta_{42}$ release was significantly decreased in neurons cultured from APP/PS1 mice compared to neurons from WT mice, and this result may be attributed to these two (APP and PSEN1) gene mutations. Previous reports have commonly used AβPP cultured primary neurons to evaluate AβPP processing and Aβ secretion [56, 57] and have shown that Aβ accumulates intracellularly in AβPP cultured neurons [58]. Our data are consistent with the reports of these previous studies.

We first evaluated the effects of AP39 on APP/PS1 neurons. In APP/PS1 neurons, cell viability was decreased and LDH release was improved compared to WT neurons. The results may be attributable to the fact that media from the AβPP primary neuronal cultures contained toxic components that led to neuritic degeneration [59]. However, AP39 improved the situation in a dose-dependent manner. These findings demonstrate the beneficial effects of AP39.

Recently, mtDNA damage and oxidative stress were found to play important roles in the pathogenesis of AD [60]. Aβ can decrease mitochondrial energy production, increase ROS levels within the mitochondria, and injure sensitive mtDNA [61]. In our study, treatment of APP/PS1 neurons with AP39 was shown to increase neuronal ATP production and reduce ROS levels. Interestingly, the APP/PS1 neurons showed significant damage to their mitochondrial DNA, and this damage may be due to Aβ plaque deposition in these neurons. More importantly, we found that AP39 clearly increased mitochondrial, but not nuclear, DNA integrity. Our results suggest that AP39 may partially contribute to the enhancement of mitochondrial biogenesis, the repair of oxidative damage, and the attenuation of mitochondrial dysfunction in AD. However, we can not exclude the possibility that H_2S may also affect the integrity or activity of various mitochondrial DNA repair proteins in APP/PS1 neurons. This potential relationship remains to be explored in further experiments. Recently, accumulating evidence has suggested that there is an imbalance in mitochondrial fission and fusion in AD progression [62, 63]. Our study showed

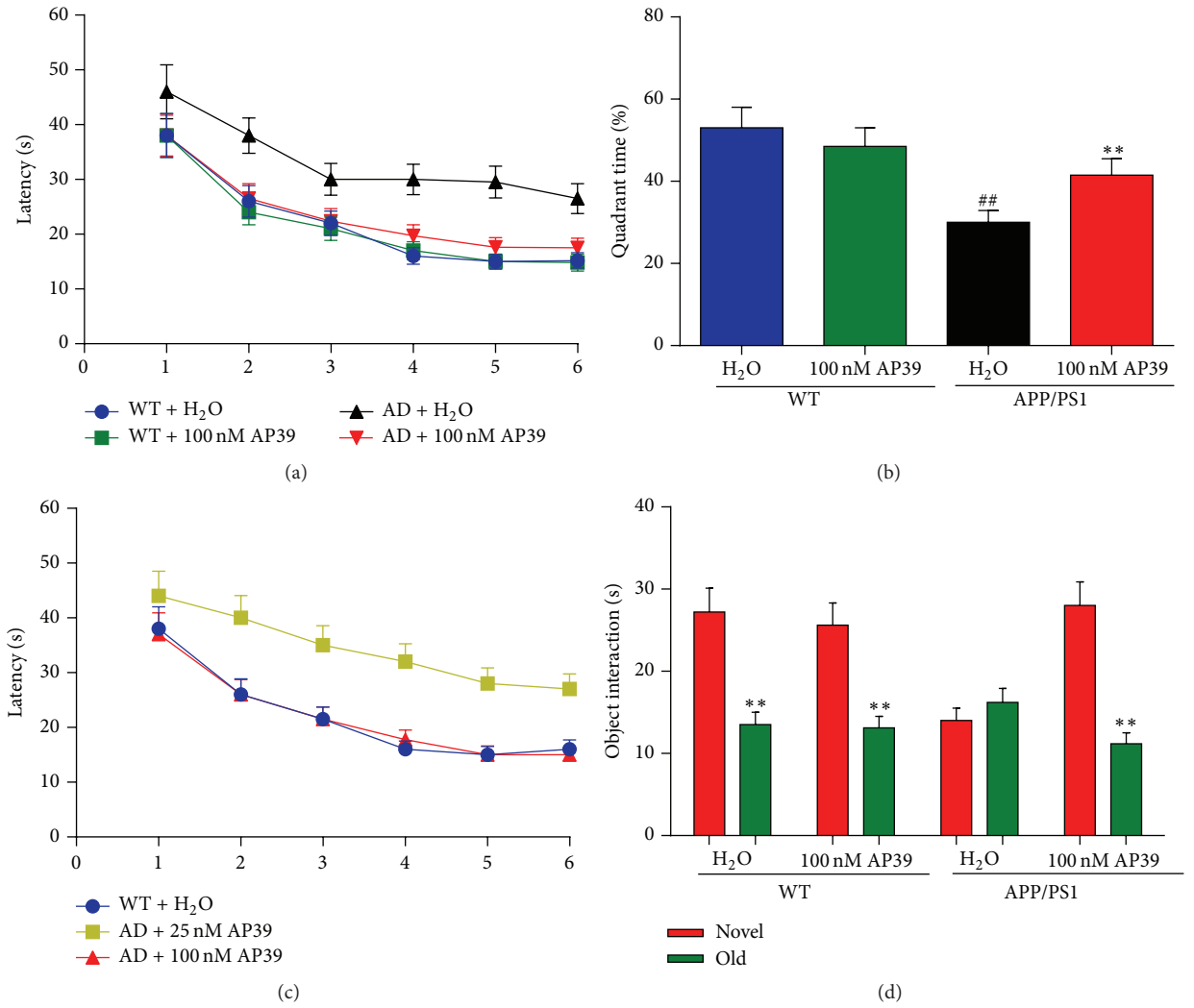

Figure 8: AP39 ameliorated the learning and memory deficits of APP/PS1 mice. WT or AD mice were treated with water or AP39 (100 nM/kg) for 6 weeks, followed by assessment using the Morris water maze and novel object recognition task tests. (a) Spatial learning and memory in AD mice are scored as the latency to locate a hidden platform. (b) After 24 h, a 60-s probe trial was performed. (c) Spatial learning was tested as the latency to locate a hidden platform for the 25 nM/kg AP39-treated mice and scored. (d) Effects of AP39 on the memory performance of 12-month WT or AD mice treated with water or AP39 were tested in the NORT test.

that the levels of the fission proteins Mfn1 and OPA1 were significantly decreased but that the levels of the fusion protein Fis1 were markedly increased in APP/PS1 neurons. These results suggested that mitochondrial fission and fusion were altered in APP/PS1 neurons. However, no apparent changes in the levels of the mitochondrial fusion protein Mfn2 or the mitochondrial fission protein Drp1 were observed in the APP/PS1 neurons. This result was consistent with the observation of mitochondria with increased fission and decreased fusion based on the related mRNA and protein levels in AβPP primary neurons [9]. Importantly, AP39 treatment reversed these changes in APP/PS1 neurons. The molecular basis for the extensive changes in mitochondrial fusion and fission observed in neurons in response to the pathogenesis of mitochondrial-related neurodegenerative diseases has not been described [64]. Interestingly, our data are not consistent with the findings of all previous reports. These inconsistencies may be due to the use of a different experimental model and different environments in vivo and in vitro. Importantly, AP39 treatment reversed these changes in APP/PS1 neurons. Whether the three genes exhibiting altered expression mediate the effects of AP39 on AD is currently under investigation.

To test whether AP39 protects AD model mice against impaired cognitive function, we examined both spatial memory and object recognition memory in APP/PS1 mice. After six weeks of AP39 treatment, the age-dependent memory deficit in the APP/PS1 mice was fully rescued on both memory tests: AP39 ameliorated their spatial learning and memory impairments, as shown by faster movement to the target quadrant of the pool. The reduced swimming time near the periphery of the pool indicated that AP39 can help to relieve anxiety, a common symptom of AD, in mice. In

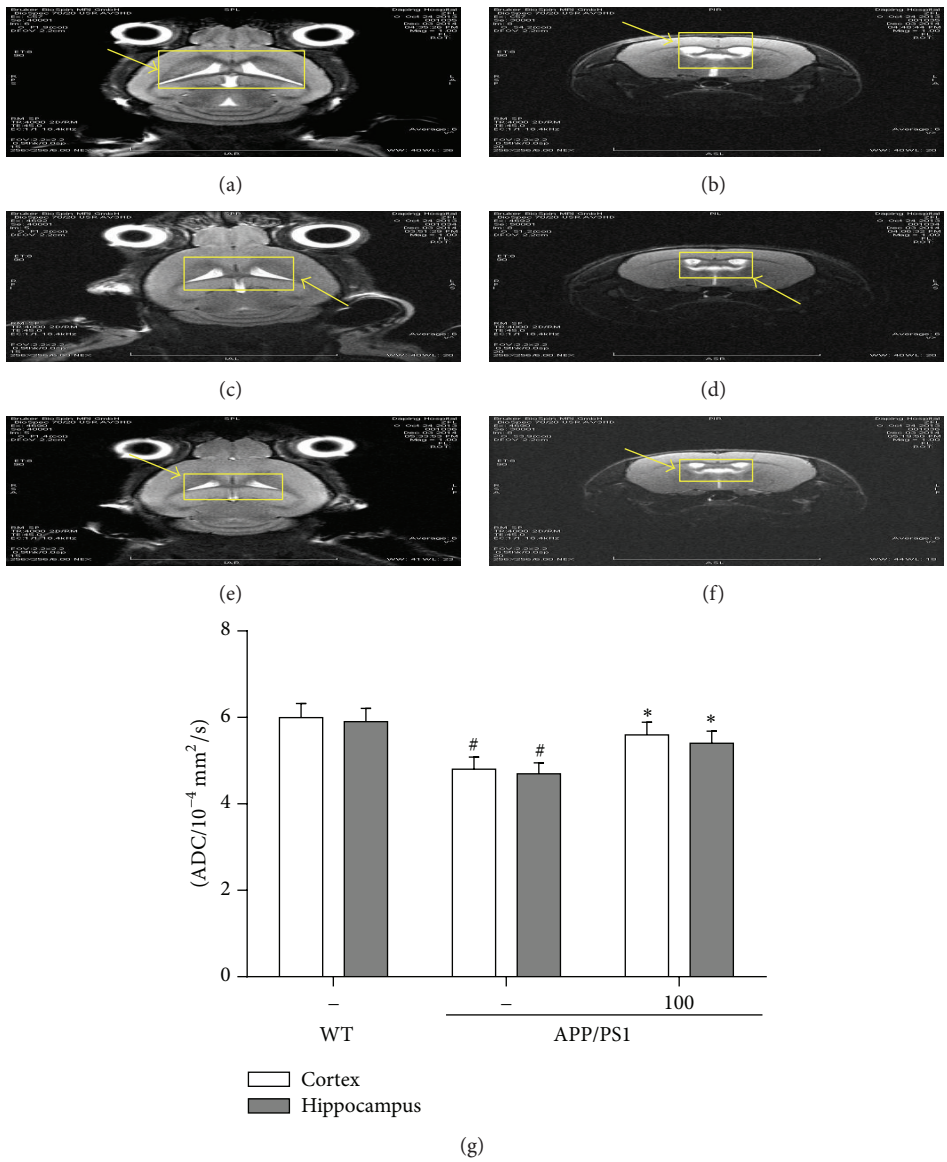

Figure 9: AP39 alleviated the brain atrophy of APP/PS1 mice as observed by brain magnetic resonance imaging (MRI). Brain MRI data were collected at different coronal and axial sections in 12-month-old mice receiving different treatments. Notes: panels (a), (c), and (e) show coronal sections, and panels (b), (d), and (f) show axial sections. The highlighted white regions indicate cerebrospinal fluid (CSF) in the ventricle, and the hippocampus is adjacent to the ventricle. Representative images from brain MRI depict slices of the T2-weighted morphologic images of 12-month-old WT mice treated with water (a)-(b) or AD mice treated with water (c)-(d) or AP39 (e)-(f). (g) ADC value determination of the mouse brains.

the present study, AP39 (100 nM/kg) was a more effective therapeutic concentration than AP39 (25 nM/kg). The dose-dependence of the observed memory improvement implies that an appropriate dose of AP39 is required for its beneficial effects on learning and memory. It remains possible that higher doses of AP39 are deleterious to memory function.

Due to its advantages, such as noninvasiveness and the ability to perform repeated in vivo measurements, MRI has been widely used in AD research [65] and in the auxiliary clinical diagnosis of AD [66]. It was used to directly visualize the inner structure of the intravital cerebrum and to measure the in vivo changes in brain volume [67], amyloid burden [68], and white matter. The hippocampus is a brain area critical for learning and memory and is especially vulnerable to damage in the early stages of AD cases [69]. In our study, the changes in the ventricle, including the deepening and widening of the sulci and the gyri, were clearly observed by MRI. In the water-treated AD mice, we observed asymmetrical ventricles, which indicated the atrophy of regions surrounding the ventricle. However, in the AP39-treated AD mice, we observed that the ventricles were symmetrical and exhibited clear edges. Because the hippocampus is adjacent to the ventricle, we hypothesized that AP39 may partially prevent hippocampal atrophy. However, we must further

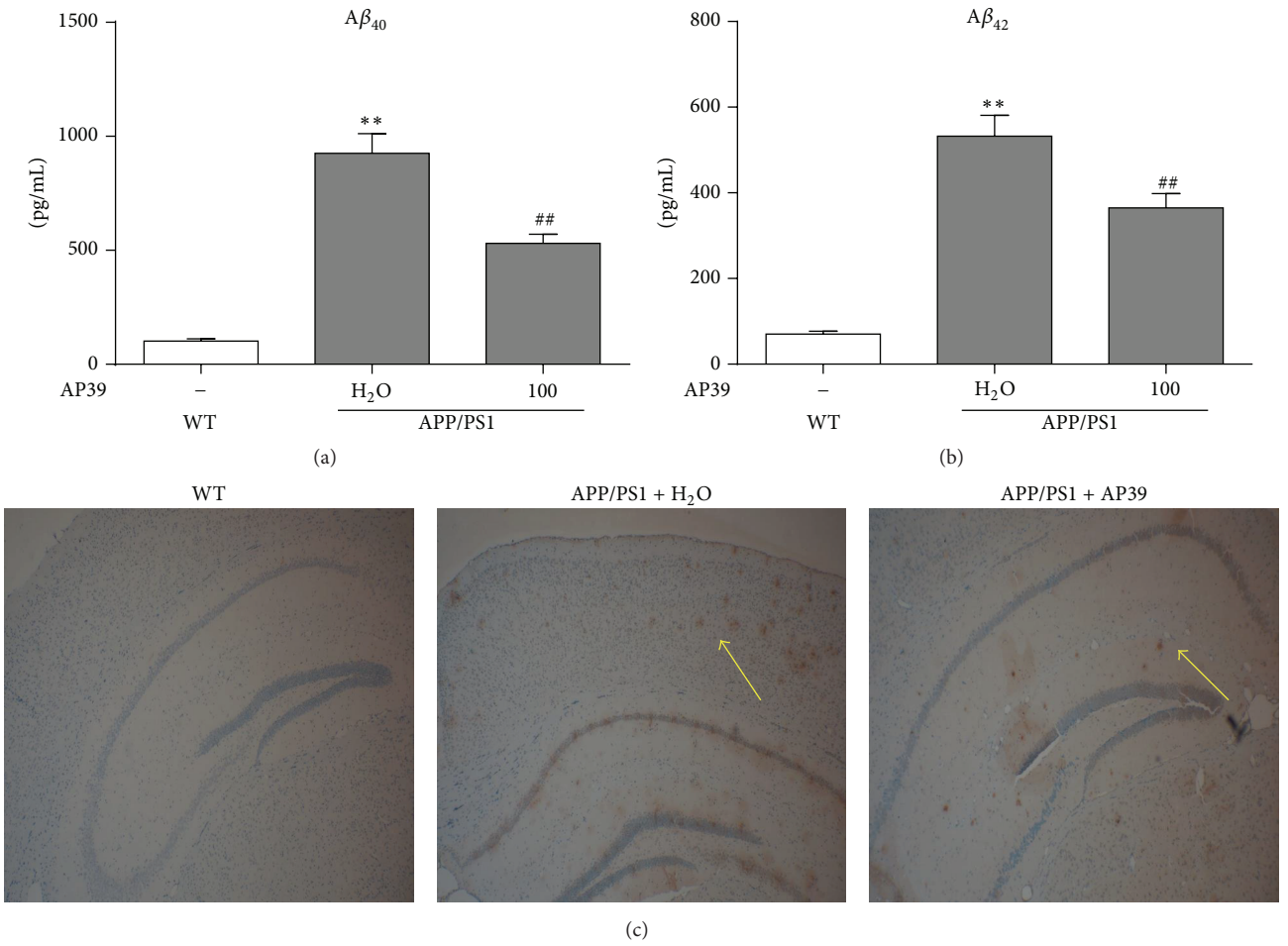

Figure 10: AP39 reduced Aβ production and Aβ deposition in APP/PS1 mice. (a)-(b) After intraperitoneal injection of AP39 for 6 weeks, Aβ_{40} and Aβ_{42} levels in the mouse brains were decreased from 925 pg/mL and 532 pg/mL to 531 pg/mL and 365 pg/mL, respectively. (c) Aβ plaques were detected in the cortex and the hippocampus of the WT and APP/PS1 mouse brains based on 6E10 immunostaining. The statistical results show the area of the Aβ plaques. Original magnification: –40x; scale bars = 100 μm.

investigate this hypothesis. Our data suggest that MRI is a useful tool to observe the dynamic neuropathology changes in AD mouse brains and those changes in aged AD mice observed by MRI correlated with their cognitive dysfunction in the current study.

Interestingly, recent research has indicated that the mitochondrial translocation of H_2S-producing enzymes produces an endogenous protective response to various insults [70].

In our study, AP39 served as a pharmacological tool or potential therapeutic agent that "mimics" this endogenous protective mechanism. However, some limitations of this study should be noted. First, we have not precisely determined the exact cellular metabolism of AP39. It will be necessary to conduct additional studies to establish the dynamics of the cellular metabolism of AP39 in the future. Second, the bell-shaped dose-response properties of AP39 are similar to those observed for authentic H_2S or other H_2S donors, and we must admit that there may be additional pharmacological mechanisms that may be conducive to the detected decrease in cellular bioenergetics at higher concentrations of AP39. The above limitations must be studied in future experiments.

5. Conclusions

Taken together, the results of the current study revealed that the main target of protection by AP39 was mitochondria based on the APP/PS1 model. We showed that AP39 exerts concentration-dependent modulatory effects on cellular bioenergetics in APP/PS1 neurons. In addition, AP39 increased ATP levels, decreased oxidative damage to mtDNA, and reduced ROS levels in APP/PS1 neurons. Moreover, AP39 regulated the balance between mitochondrial fission and fusion. All of these events contribute to an attenuation of mitochondrial dysfunction in APP/PS1 neurons. Based on these data, AP39 exerts multiple protective effects in the APP/PS1 model, including the amelioration of memory deficits, the prevention of brain atrophy, and the decrease of Aβ deposition. Therefore, AP39 represents a good candidate disease-modifying therapy for AD. Despite recent advancements in our understanding of the role of AP39 in mitochondrial bioenergetics and function, whether AP39 is actually beneficial for AD patients remains to be determined and warrants further study.

Conflict of Interests

The authors confirm that this paper content has no conflict of interests.

Acknowledgments

The authors thank Professor Zhang (Associate Professor, Neuroscience Center, the First Affiliated Hospital of Chongqing Medical University) for significant comments and scientific support and Professor Tang for technical assistance. This study was supported by the National Natural Science Foundation of China (Grant no. 81271222).

References

[1] Alzheimer's Association, "2015 Alzheimer's disease facts and figures," *Alzheimer's & Dementia*, vol. 11, no. 3, pp. 332–384, 2015.

[2] W. S. Liang, E. M. Reiman, J. Valla et al., "Alzheimer's disease is associated with reduced expression of energy metabolism genes in posterior cingulate neurons," *Proceedings of the National Academy of Sciences of the United States of America*, vol. 105, no. 11, pp. 4441–4446, 2008.

[3] R. Bowser and M. A. Smith, "Cell cycle proteins in Alzheimer's disease: plenty of wheels but no cycle," *Journal of Alzheimer's Disease*, vol. 4, no. 3, pp. 249–254, 2002.

[4] K. Herrup, M. C. Carrillo, D. Schenk et al., "Beyond amyloid: getting real about nonamyloid targets in Alzheimer's disease," *Alzheimer's & Dementia*, vol. 9, no. 4, pp. 452.e1–458.e1, 2013.

[5] R. H. Swerdlow and S. M. Khan, "A "mitochondrial cascade hypothesis" for sporadic Alzheimer's disease," *Medical Hypotheses*, vol. 63, no. 1, pp. 8–20, 2004.

[6] X. Wang, W. Wang, L. Li, G. Perry, H.-G. Lee, and X. Zhu, "Oxidative stress and mitochondrial dysfunction in Alzheimer's disease," *Biochimica et Biophysica Acta—Molecular Basis of Disease*, vol. 1842, no. 8, pp. 1240–1247, 2014.

[7] H. Xie, J. Guan, L. A. Borrelli, J. Xu, A. Serrano-Pozo, and B. J. Bacskai, "Mitochondrial alterations near amyloid plaques in an Alzheimer'S disease mouse model," *Journal of Neuroscience*, vol. 33, no. 43, pp. 17042–17051, 2013.

[8] O. Benek, L. Aitken, L. Hroch et al., "A direct interaction between mitochondrial proteins and amyloid-beta peptide and its significance for the progression and treatment of Alzheimer's disease," *Current Medicinal Chemistry*, In press.

[9] M. J. Calkins, M. Manczak, P. Mao, U. Shirendeb, and P. H. Reddy, "Impaired mitochondrial biogenesis, defective axonal transport of mitochondria, abnormal mitochondrial dynamics and synaptic degeneration in a mouse model of Alzheimer's disease," *Human Molecular Genetics*, vol. 20, no. 23, Article ID ddr381, pp. 4515–4529, 2011.

[10] S. Rosales-Corral, D. Acuna-Castroviejo, D. X. Tan et al., "Accumulation of exogenous amyloid-beta peptide in hippocampal mitochondria causes their dysfunction: a protective role for melatonin," *Oxidative Medicine and Cellular Longevity*, vol. 2012, Article ID 843649, 15 pages, 2012.

[11] I. Pedrós, D. Petrov, M. Allgaier et al., "Early alterations in energy metabolism in the hippocampus of APPswe/PS1dE9 mouse model of Alzheimer's disease," *Biochimica et Biophysica Acta*, vol. 1842, no. 9, pp. 1556–1566, 2014.

[12] A. C. Rice, P. M. Keeney, N. K. Algarzae, A. C. Ladd, R. R. Thomas, and J. P. Bennett Jr., "Mitochondrial DNA copy numbers in pyramidal neurons are decreased and mitochondrial biogenesis transcriptome signaling is disrupted in Alzheimer's disease hippocampi," *Journal of Alzheimer's Disease*, vol. 40, no. 2, pp. 319–330, 2014.

[13] B. Sheng, X. Wang, B. Su et al., "Impaired mitochondrial biogenesis contributes to mitochondrial dysfunction in Alzheimer's disease," *Journal of Neurochemistry*, vol. 120, no. 3, pp. 419–429, 2012.

[14] C. Szabõ, "Hydrogen sulphide and its therapeutic potential," *Nature Reviews Drug Discovery*, vol. 6, no. 11, pp. 917–935, 2007.

[15] H.-J. Wei, X. Li, and X.-Q. Tang, "Therapeutic benefits of H_2S in Alzheimer's disease," *Journal of Clinical Neuroscience*, vol. 21, no. 10, pp. 1665–1669, 2014.

[16] X. Q. Tang, C. T. Yang, J. Chen et al., "Effect of hydrogen sulphide on β-amyloid-induced damage in PC12 cells," *Clinical and Experimental Pharmacology and Physiology*, vol. 35, no. 2, pp. 180–186, 2008.

[17] A. Xuan, D. Long, J. Li et al., "Hydrogen sulfide attenuates spatial memory impairment and hippocampal neuroinflammation in beta-amyloid rat model of Alzheimer's disease," *Journal of Neuroinflammation*, vol. 9, article 202, 2012.

[18] K. Módis, C. Coletta, K. Erdélyi, A. Papapetropoulos, and C. Szabo, "Intramitochondrial hydrogen sulfide production by 3-mercaptopyruvate sulfurtransferase maintains mitochondrial electron flow and supports cellular bioenergetics," *The FASEB Journal*, vol. 27, no. 2, pp. 601–611, 2013.

[19] B. Szczesny, K. Módis, K. Yanagi et al., "AP39, a novel mitochondria-targeted hydrogen sulfide donor, stimulates cellular bioenergetics, exerts cytoprotective effects and protects against the loss of mitochondrial DNA integrity in oxidatively stressed endothelial cells *in vitro*," *Nitric Oxide*, vol. 41, pp. 120–130, 2014.

[20] S. Le Trionnaire, A. Perry, B. Szczesny et al., "The synthesis and functional evaluation of a mitochondria-targeted hydrogen sulfide donor, (10-oxo-10-(4-(3-thioxo-3H-1,2-dithiol-5-yl)phenoxy)decyl)triphenylphosphonium bromide (AP39)," *MedChemComm*, vol. 5, no. 6, pp. 728–736, 2014.

[21] S. Albers, F. Inthathirath, S. K. Gill et al., "Nuclear 82-kDa choline acetyltransferase decreases amyloidogenic APP metabolism in neurons from APP/PS1 transgenic mice," *Neurobiology of Disease*, vol. 69, pp. 32–42, 2014.

[22] J. L. Jankowsky, D. J. Fadale, J. Anderson et al., "Mutant presenilins specifically elevate the levels of the 42 residue β-amyloid peptide in vivo: evidence for augmentation of a 42-specific γ secretase," *Human Molecular Genetics*, vol. 13, no. 2, pp. 159–170, 2004.

[23] R. Miyamoto, K.-I. Otsuguro, S. Yamaguchi, and S. Ito, "Contribution of cysteine aminotransferase and mercaptopyruvate sulfurtransferase to hydrogen sulfide production in peripheral neurons," *Journal of Neurochemistry*, vol. 130, no. 1, pp. 29–40, 2014.

[24] X.-Q. Tang, H.-R. Fang, C.-F. Zhou et al., "A novel mechanism of formaldehyde neurotoxicity: inhibition of hydrogen sulfide generation by promoting overproduction of nitric oxide," *PLoS ONE*, vol. 8, no. 1, Article ID e54829, 2013.

[25] K. Módis, C. Coletta, A. Asimakopoulou et al., "Effect of S-adenosyl-l-methionine (SAM), an allosteric activator of cystathionine-β-synthase (CBS) on colorectal cancer cell proliferation and bioenergetics *in vitro*," *Nitric Oxide*, vol. 41, pp. 146–156, 2014.

[26] D. A. Ferrick, A. Neilson, and C. Beeson, "Advances in measuring cellular bioenergetics using extracellular flux," *Drug Discovery Today*, vol. 13, no. 5-6, pp. 268–274, 2008.

[27] U. Keil, A. Bonert, C. A. Marques et al., "Amyloid beta-induced changes in nitric oxide production and mitochondrial activity lead to apoptosis," *The Journal of Biological Chemistry*, vol. 279, no. 48, pp. 50310–50320, 2004.

[28] B. Szczesny, G. Olah, D. K. Walker et al., "Deficiency in repair of the mitochondrial genome sensitizes proliferating myoblasts to oxidative damage," *PLoS ONE*, vol. 8, no. 9, Article ID e75201, 2013.

[29] A. C. Kaufman, S. V. Salazar, L. T. Haas et al., "Fyn inhibition rescues established memory and synapse loss in Alzheimer mice," *Annals of Neurology*, vol. 77, no. 6, pp. 953–971, 2015.

[30] R. A. Bevins and J. Besheer, "Object recognition in rats and mice: a one-trial non-matching-to-sample learning task to study 'recognition memory'," *Nature Protocols*, vol. 1, no. 3, pp. 1306–1311, 2006.

[31] J. Zhang, Q. Cao, S. Li et al., "3-Hydroxybutyrate methyl ester as a potential drug against Alzheimer's disease via mitochondria protection mechanism," *Biomaterials*, vol. 34, no. 30, pp. 7552–7562, 2013.

[32] D.-Y. Choi, J. W. Lee, J. Peng et al., "Obovatol improves cognitive functions in animal models for Alzheimer's disease," *Journal of Neurochemistry*, vol. 120, no. 6, pp. 1048–1059, 2012.

[33] R. Wang, "Physiological implications of hydrogen sulfide: a whiff exploration that blossomed," *Physiological Reviews*, vol. 92, no. 2, pp. 791–896, 2012.

[34] C. Szabo, C. Coletta, C. Chao et al., "Tumor-derived hydrogen sulfide, produced by cystathionine-β-synthase, stimulates bioenergetics, cell proliferation, and angiogenesis in colon cancer," *Proceedings of the National Academy of Sciences of the United States of America*, vol. 110, no. 30, pp. 12474–12479, 2013.

[35] K. Módis, E. M. Bos, E. Calzia et al., "Regulation of mitochondrial bioenergetic function by hydrogen sulfide. Part II. Pathophysiological and therapeutic aspects," *British Journal of Pharmacology*, vol. 171, no. 8, pp. 2123–2146, 2014.

[36] M. Whiteman, S. Le Trionnaire, M. Chopra, B. Fox, and J. Whatmore, "Emerging role of hydrogen sulfide in health and disease: critical appraisal of biomarkers and pharmacological tools," *Clinical Science*, vol. 121, no. 11, pp. 459–488, 2011.

[37] L. Tomasova, M. Pavlovicova, L. Malekova et al., "Effects of AP39, a novel triphenylphosphonium derivatised anethole dithiolethione hydrogen sulfide donor, on rat haemodynamic parameters and chloride and calcium Ca_v3 and RyR2 channels," *Nitric Oxide*, vol. 46, pp. 131–144, 2015.

[38] K. Umemura and H. Kimura, "Hydrogen sulfide enhances reducing activity in neurons: neurotrophic role of H_2S in the brain?" *Antioxidants and Redox Signaling*, vol. 9, no. 11, pp. 2035–2041, 2007.

[39] H. Kimura, "Physiological roles of hydrogen sulfide and polysulfides," in *Chemistry, Biochemistry and Pharmacology of Hydrogen Sulfide*, vol. 230 of *Handbook of Experimental Pharmacology*, pp. 61–81, Springer, Basel, Switzerland, 2015.

[40] N. B. Chauhan, "Effect of aged garlic extract on APP processing and tau phosphorylation in Alzheimer's transgenic model Tg2576," *Journal of Ethnopharmacology*, vol. 108, no. 3, pp. 385–394, 2006.

[41] Q.-H. Gong, L.-L. Pan, X.-H. Liu, Q. Wang, H. Huang, and Y.-Z. Zhu, "S-propargyl-cysteine (ZYZ-802), a sulphur-containing amino acid, attenuates beta-amyloid-induced cognitive deficits and pro-inflammatory response: involvement of ERK1/2 and NF-kappaB pathway in rats," *Amino Acids*, vol. 40, no. 2, pp. 601–610, 2011.

[42] D. Giuliani, A. Ottani, D. Zaffe et al., "Hydrogen sulfide slows down progression of experimental Alzheimer's disease by targeting multiple pathophysiological mechanisms," *Neurobiology of Learning and Memory*, vol. 104, pp. 82–91, 2013.

[43] X.-L. He, N. Yan, H. Zhang et al., "Hydrogen sulfide improves spatial memory impairment and decreases production of Aβ in APP/PS1 transgenic mice," *Neurochemistry International*, vol. 67, no. 1, pp. 1–8, 2014.

[44] L. Li, P. Rose, and P. K. Moore, "Hydrogen sulfide and cell signaling," *Annual Review of Pharmacology and Toxicology*, vol. 51, no. 1, pp. 169–187, 2011.

[45] C. Constant-Urban, M. Charif, E. Goffin et al., "Triphenylphosphonium salts of 1,2,4-benzothiadiazine 1,1-dioxides related to diazoxide targeting mitochondrial ATP-sensitive potassium channels," *Bioorganic and Medicinal Chemistry Letters*, vol. 23, no. 21, pp. 5878–5881, 2013.

[46] M. Millard, J. D. Gallagher, B. Z. Olenyuk, and N. Neamati, "A selective mitochondrial-targeted chlorambucil with remarkable cytotoxicity in breast and pancreatic cancers," *Journal of Medicinal Chemistry*, vol. 56, no. 22, pp. 9170–9179, 2013.

[47] H. Yuan, H. Cho, H. H. Chen, M. Panagia, D. E. Sosnovik, and L. Josephson, "Fluorescent and radiolabeled triphenylphosphonium probes for imaging mitochondria," *Chemical Communications*, vol. 49, no. 88, pp. 10361–10363, 2013.

[48] M. Goubern, M. Andriamihaja, T. Nübel, F. Blachier, and F. Bouillaud, "Sulfide, the first inorganic substrate for human cells," *The FASEB Journal*, vol. 21, no. 8, pp. 1699–1706, 2007.

[49] E. Lagoutte, S. Mimoun, M. Andriamihaja, C. Chaumontet, F. Blachier, and F. Bouillaud, "Oxidation of hydrogen sulfide remains a priority in mammalian cells and causes reverse electron transfer in colonocytes," *Biochimica et Biophysica Acta (BBA)—Bioenergetics*, vol. 1797, no. 8, pp. 1500–1511, 2010.

[50] S. Mimoun, M. Andriamihaja, C. Chaumontet et al., "Detoxification of H_2S by differentiated colonic epithelial cells: implication of the sulfide oxidizing unit and of the cell respiratory capacity," *Antioxidants and Redox Signaling*, vol. 17, no. 1, pp. 1–10, 2012.

[51] M. Groeger, J. Matallo, O. McCook et al., "Temperature and cell-type dependency of sulfide effects on mitochondrial respiration," *Shock*, vol. 38, no. 4, pp. 367–374, 2012.

[52] H. Aslami, M. J. Schultz, and N. P. Juffermans, "Potential applications of hydrogen sulfide-induced suspended animation," *Current Medicinal Chemistry*, vol. 16, no. 10, pp. 1295–1303, 2009.

[53] P. Nicholls, "Inhibition of cytochrome c oxidase by sulphide," *Biochemical Society Transactions*, vol. 3, no. 2, pp. 316–319, 1975.

[54] A. A. Khan, M. M. Schuler, M. G. Prior et al., "Effects of hydrogen sulfide exposure on lung mitochondrial respiratory chain enzymes in rats," *Toxicology and Applied Pharmacology*, vol. 103, no. 3, pp. 482–490, 1990.

[55] C. Sturchler-Pierrat, D. Abramowski, M. Duke et al., "Two amyloid precursor protein transgenic mouse models with Alzheimer disease-like pathology," *Proceedings of the National Academy of Sciences of the United States of America*, vol. 94, no. 24, pp. 13287–13292, 1997.

[56] Z. Qiu, D. L. Naten, J. C. Liston, J. Yess, and G. W. Rebeck, "A novel approach for studying endogenous abeta processing using cultured primary neurons isolated from APP transgenic mice," *Experimental Neurology*, vol. 170, no. 1, pp. 186–194, 2001.

[57] S. Bürger, Y. Yafai, M. Bigl, P. Wiedemann, and R. Schliebs, "Effect of VEGF and its receptor antagonist SU-5416, an inhibitor of angiogenesis, on processing of the β-amyloid precursor protein in primary neuronal cells derived from brain tissue of Tg2576 mice," *International Journal of Developmental Neuroscience*, vol. 28, no. 7, pp. 597–604, 2010.

[58] R. H. Takahashi, C. G. Almeida, P. F. Kearney et al., "Oligomerization of Alzheimer's beta-amyloid within processes and synapses of cultured neurons and brain," *Journal of Neuroscience*, vol. 24, no. 14, pp. 3592–3599, 2004.

[59] M.-H. Wu and C.-Y. Kuo, "Application of high throughput perfusion micro 3-D cell culture platform for the precise study of cellular responses to extracellular conditions—effect of serum concentrations on the physiology of articular chondrocytes," *Biomedical Microdevices*, vol. 13, no. 1, pp. 131–141, 2011.

[60] G. J. Tranah, J. S. Yokoyama, S. M. Katzman et al., "Mitochondrial DNA sequence associations with dementia and amyloid-beta in elderly African Americans," *Neurobiology of Aging*, vol. 35, no. 2, pp. 442.e1–442.e8, 2014.

[61] M. P. Mattson, "Mother's legacy: mitochondrial DNA mutations and Alzheimer's disease," *Trends in Neurosciences*, vol. 20, no. 9, pp. 373–375, 1997.

[62] X. Wang, B. Su, H.-G. Lee et al., "Impaired balance of mitochondrial fission and fusion in Alzheimer's disease," *The Journal of Neuroscience*, vol. 29, no. 28, pp. 9090–9103, 2009.

[63] P. H. Reddy, "Amyloid beta, mitochondrial structural and functional dynamics in Alzheimer's disease," *Experimental Neurology*, vol. 218, no. 2, pp. 286–292, 2009.

[64] M. Cagalinec, D. Safiulina, M. Liiv et al., "Principles of the mitochondrial fusion and fission cycle in neurons," *Journal of Cell Science*, vol. 126, no. 10, pp. 2187–2197, 2013.

[65] M. R. Brier, J. B. Thomas, A. Z. Snyder et al., "Loss of intranetwork and internetwork resting state functional connections with Alzheimer's disease progression," *Journal of Neuroscience*, vol. 32, no. 26, pp. 8890–8899, 2012.

[66] M. J. de Leon, S. Desanti, R. Zinkowski et al., "MRI and CSF studies in the early diagnosis of Alzheimer's disease," *Journal of Internal Medicine*, vol. 256, no. 3, pp. 205–223, 2004.

[67] J. Yin, G. H. Turner, S. W. Coons, M. Maalouf, E. M. Reiman, and J. Shi, "Association of amyloid burden, brain atrophy and memory deficits in aged apolipoprotein ε4 mice," *Current Alzheimer Research*, vol. 11, no. 3, pp. 283–290, 2014.

[68] T. M. Wengenack, C. R. Jack Jr., M. Garwood, and J. F. Poduslo, "MR Microimaging of amyloid plaques in Alzheimer's disease transgenic mice," *European Journal of Nuclear Medicine and Molecular Imaging*, vol. 35, supplement 1, pp. S82–S88, 2008.

[69] Y. Mu and F. H. Gage, "Adult hippocampal neurogenesis and its role in Alzheimer's disease," *Molecular Neurodegeneration*, vol. 6, article 85, 2011.

[70] H. Teng, B. Wu, K. Zhao, G. Yang, L. Wu, and R. Wang, "Oxygen-sensitive mitochondrial accumulation of cystathionine β-synthase mediated by Lon protease," *Proceedings of the National Academy of Sciences of the United States of America*, vol. 110, no. 31, pp. 12679–12684, 2013.

Hindawi Publishing Corporation
Oxidative Medicine and Cellular Longevity
Volume 2016, Article ID 8296150, 10 pages
http://dx.doi.org/10.1155/2016/8296150

Research Article

Proliferation of Human Primary Myoblasts Is Associated with Altered Energy Metabolism in Dependence on Ageing *In Vivo* and *In Vitro*

Reedik Pääsuke,[1,2,3] Margus Eimre,[1] Andres Piirsoo,[1] Nadežda Peet,[1] Liidia Laada,[1] Lumme Kadaja,[1] Mart Roosimaa,[1] Mati Pääsuke,[4] Aare Märtson,[2,3] Enn Seppet,[1] and Kalju Paju[1]

[1]*Institute of Biomedicine and Translational Medicine, University of Tartu, Ravila 19, 50411 Tartu, Estonia*
[2]*Department of Traumatology and Orthopaedics, Tartu University Hospital, L. Puusepa 8, 51014 Tartu, Estonia*
[3]*Department of Traumatology and Orthopaedics, University of Tartu, L. Puusepa 8, 51014 Tartu, Estonia*
[4]*Institute of Exercise Biology and Physiotherapy, University of Tartu, Ravila 14a, 50411 Tartu, Estonia*

Correspondence should be addressed to Reedik Pääsuke; reedik.paasuke@gmail.com

Received 24 September 2015; Accepted 8 December 2015

Academic Editor: Rebeca Acín-Pérez

Copyright © 2016 Reedik Pääsuke et al. This is an open access article distributed under the Creative Commons Attribution License, which permits unrestricted use, distribution, and reproduction in any medium, provided the original work is properly cited.

Background. Ageing is associated with suppressed regenerative potential of muscle precursor cells due to decrease of satellite cells and suppressive intramuscular milieu on their activation, associated with ageing-related low-grade inflammation. The aim of the study was to characterize the function of oxidative phosphorylation (OXPHOS), glycolysis, adenylate kinase (AK), and creatine kinase (CK) mediated systems in young and older individuals. *Materials and Methods*. Myoblasts were cultivated from biopsies taken by transcutaneous conchotomy from vastus lateralis muscle in young (20–29 yrs, $n = 7$) and older (70–79 yrs, $n = 7$) subjects. Energy metabolism was assessed in passages 2 to 6 by oxygraphy and enzyme analysis. *Results*. In myoblasts of young and older subjects the rate of OXPHOS decreased during proliferation from passages 2 to 6. The total activities of CK and AK decreased. Myoblasts of passage 2 cultivated from young muscle showed higher rate of OXPHOS and activities of CK and AK compared to myoblasts from older subjects while hexokinase and pyruvate kinase were not affected by ageing. *Conclusions*. Proliferation of myoblasts *in vitro* is associated with downregulation of OXPHOS and energy storage and transfer systems. Ageing *in vivo* exerts an impact on satellite cells which results in altered metabolic profile in favour of the prevalence of glycolytic pathways over mitochondrial OXPHOS of myoblasts.

1. Introduction

Ageing is associated with a progressive loss of skeletal muscle mass and strength referred to as sarcopenia [1, 2]. It is characterized by a decline in the total number of muscle fibers with prevalent atrophy of the type II fibers [3–6]. Despite intensive studies the cellular and molecular mechanisms underlying sarcopenia are still under considerable debate.

Sarcopenia can also be envisaged as an age-dependent impairment of processes responsible for maintenance and repair of the muscle in response to contraction-induced injury [7–10]. These functions largely rely on myogenic stem cells, that is, satellite cells located between the sarcolemma and basal lamina. In response to muscle damage or under increased workload these cells activate, migrate into damaged sites, proliferate, and fuse with existing myofibers or with each other to form new myofibers, whereas a small portion of these cells returns into quiescence [11, 12]. One line of evidence suggests that with ageing the capacities of stem cells to produce their reserve progeny diminish [13]. As a result, the satellite cell number decreases thereby promoting loss of muscle mass [14–23]. Alternatively, ageing modulates the intrinsic properties of the satellite cells characterized by disability to execute the differentiation program [24–27]. It has been demonstrated that aged satellite cells express S100B, an antimyogenic protein stimulating proliferation but inhibiting

differentiation [28]. Also, aged satellite cells lose their ability to upregulate the factors involved in the early phases of myogenic differentiation (e.g., MyoD and myogenin) [24]. In contrast to counterparts from young subject's muscle, the satellite cells from aged muscle exhibit the gene expression pattern which favours oxidative damage, altered turnover of cytoskeleton, activation of FOXO-dependent atrophy programs, suppressed myotube formation, and impairment of Ca^{2+}-mediated signaling [25–27, 29, 30]. Thus, the increasing evidence indicates resetting of the regulatory systems that lead to altered phenotype of satellite cells in aged muscles.

Interestingly, satellite cells from old muscles also display dysregulation of genes controlling mitochondrial and glycolytic enzymes [31]. The functional consequences of these changes are unclear. Up to now, only the effects of *in vitro* ageing on energy metabolism of cultured myoblasts have been addressed [32, 33]. The results show that replicative senescence results in reduced capacities of myoblasts to differentiate, in association with defective glycose and lipid metabolism, decreased cellular mitochondrial and ATP contents, and increased ROS production, these changes accompanied with normal-to-increased ATP synthesis capacities of mitochondria [32, 33]. These data were recorded in conditions of differentiation of myoblasts, though. It is not clear how ageing *in vitro* affects the energy metabolism in the phase of myoblast proliferation. Also, no study has addressed the status of energy metabolism comparatively in myoblasts cultured from muscle biopsies of older and young subjects. Therefore, the aim of the present study was to investigate the energy metabolism in primary myoblasts derived from muscle biopsies taken from vastus lateralis of young and older subjects. Specifically, the function of the respiratory chain complexes and the system of oxidative phosphorylation (OXPHOS) was assessed in permeabilized myoblasts. Also, the expression and function of various enzymes participating in glycolysis and intracellular energy transfer were investigated.

2. Materials and Methods

2.1. Chemicals and Reagents. K-Lactobionate, EGTA, and taurine were from Fluka, NADH, pyruvate, and saponin were from SERVA, $MgCl_2$ and KCl were from ACROS, and leupeptin was from Roche.

Other reagents, adenine nucleotides (ATP, ADP, and AMP), bovine serum albumin, enzymes (hexokinase, glucose-6-phosphate dehydrogenase, and lactate dehydrogenase), DTT, KH_2PO_4, HEPES, L-glutamate, DL-malate, rotenone, succinate, atractyloside, antimycin A, TMPD, ascorbate, EDTA, glucose, Triton X-100, tris, PEP, and NADP were from Sigma.

2.2. Human Study Subjects. Seven young subjects (mean age 22.9 ± 1.0 yrs) and 7 older subjects (mean age 76.0 ± 1.8 yrs) were enrolled in the study. Young subjects did not have any record of muscular diseases, traumatic lesions, cardiovascular diseases, or diabetes and were physically active performing some recreational activities but did not train for any specific discipline. Their mean body mass index (BMI) was 22.8 ± 1.0 kg/m^2. Older subjects also did not have any record of muscular diseases, traumatic lesions, cardiovascular diseases, or diabetes and their mean body mass index (BMI) was 27.4 ± 1.8 kg/m^2. All investigations were approved by the Research Ethics Committee of the University of Tartu in accordance with the principles of the Declaration of Helsinki (WMA 1997). All subjects signed informed consent based on their voluntary decision and agreement to undergo the procedures. The muscle biopsies were obtained from the vastus lateralis muscle by conchotome technique 10 cm cranially from the superior apex of the patella.

2.3. Primary Cultures of Human Myoblasts. Primary cultures of myoblasts were made from human skeletal muscle biopsies using explant culture technique. After 7 to 9 days, cells surrounding the explants were removed with trypsin and propagated in medium (1 vol. DMEM/4 vol. 199 Medium) supplemented with 20% FCS, penicillin (50 units/mL)/streptomycin (50 μg/mL), and 5 ng/mL recombinant human hepatocyte growth factor (HGF) (Pepro Tech). The myoblasts were plated and allowed to proliferate in this medium at 37°C in 5% CO_2 atmosphere with changing the medium every second day in 100 mm dish. The myoblast purity of human skeletal muscle culture was determined by immunostaining for desmin expression and cultures with purity more than 70% desmin positive cells were used for experiments. After reaching 70–80% confluency the cell populations were trypsinized to establish the next passage. The passages of 2 to 6 were mainly used in the studies of bioenergetic parameters. For these assessments, the cells were removed by trypsin, washed with the medium, counted with hemocytometer, and resuspended in the culture medium supplemented with 10% FCS. The mean doubling time was calculated by counting cell numbers at the beginning (N_0) and end (N_t) of the observation period (t) and calculated applying the equation $dt = t/\log_2(N_t/N_0)$, where dt is doubling time and $\log_2$ is logarithm to base 2.

2.4. Determination of Activities of the Respiratory Chain Complexes. The activities of the mitochondrial respiratory chain segments in myoblasts were assessed by polarographic method (Oroboros, Austria) as respiration rates (VO_2) in Mitomed solution containing (in mM) sucrose 110, K-lactobionate 60, CaK_2EGTA 0.138, K_2EGTA 0.362, $MgCl_2$ 3, dithiothreitol 0.5, taurine 20, KH_2PO_4 3, K-HEPES 20, pH 7.1, and 1 mg/mL fatty acid free bovine serum albumin (BSA), glutamate, or pyruvate 10 and malate 2, pH 7.1, at 25°C. For permeabilization of the cell membrane, 50 μg/mL saponin was added and the cells were incubated during the 15 min. After addition of 1 mM ADP the respiration was titrated with 10 μM rotenone (Rot) to inhibit complex I, 10 mM succinate (Succ) to activate the complex II dependent respiration, 0.1 mM atractyloside (Atr) to assess the function of adenine nucleotide translocase (ANT), and 10 μM antimycin A (Ant) to inhibit complex III and thereby block the electron flow from complex II to cytochrome c. To activate cytochrome c oxidase 0.5 mM TMPD and 2 mM ascorbate were applied. The rotenone sensitive portion of the NADH-linked ADP-dependent respiration ($V_{ADP} - V_{Rot}$) was considered to represent the activity of complex I and increment of respiration by succinate ($V_{Succ} - V_{Rot}$) was taken to represent the complex II

activity. The antimycin-sensitive respiration in the presence of atractyloside ($V_{atr} - V_{ant}$) was considered to represent the proton leak. The COX activity (V_{Cytox}) was measured as the NaN_3-sensitive portion of the TMPD-dependent VO_2.

2.5. Determination of the Activities of Kinases. Myoblasts were homogenized by sonication (Bandelin Sonopuls HD 2200, probe MS 72) in homogenization solution containing (in mM) EDTA 1, DTT 1, glucose 10, $MgCl_2$ 5, HEPES 5 (pH 8 with NaOH), Triton X-100 0.1%, and leupeptin 5 μg/mL. PK activity measurements were performed in a spectrophotometric cuvette in stirring conditions in solution containing (in mM) tris-HCl 20 (pH 8, 25°C), KCl 15, DTT 0.33, NADH 0.24, PEP 5, ADP 2, and 1 IU/mL LDH. After registration of baseline the reaction was started by addition of the homogenate and from the following changes in NADH oxidation rates at 340 nm the PK activity was calculated. For measurements of AK activity the same solution was used except that ADP was absent and the solution contained 6 IU/mL PK, 0.8 mM PEP, and 3 IU/mL of LDH. After registration of basal CaMgATPase activity in the presence of 1 mM MgATP, 1.3 mM AMP was added to determine the AK activity. For CK activity measurements the homogenates were incubated in a spectrophotometric cuvette in stirring conditions in solution containing (in mM) glucose 20, AMP 20, DTT 0.3, magnesium acetate 3, MgADP 1, NADP 1, tris-HCl 50 (pH 7.4, 25°C), supplemented with 2 IU/mL hexokinase (HK), and 2 IU/mL glucose-6-phosphate dehydrogenase (G6PDH) at 25°C. After stabilization of the optical density, the reaction was started by addition of 20 mM PCr and the rate of NADPH formation was registered. The HK activity was measured in the presence of 2 mM MgATP, 0.6 mM NADP, and 2 IU/mL G6PDH, and the rate of NADPH generation was monitored spectrophotometrically (Perkin-Elmer Lambda 900) after addition of homogenate at 340 nm, 25°C.

2.6. Gene Expression Study. In order to study the expression of different isoforms of kinases (CK, AK, and HK), the real-time PCR method was applied. At first, total RNA from 1×10^6 cultured cells (frozen and stored at −80°C) originated from vastus lateralis of older and young subjects was isolated and purified by the RNeasy Plus Mini Kit (Qiagen, Germany) using QIAshredders (Qiagen, Germany) for cell lysate homogenization. To convert RNA (1 μg per reaction) to cDNA, the QuantiTect Reverse Transcription Kit (Qiagen, Germany) that includes genomic DNA elimination reagent was used. Real-time PCR amplification was carried out by using gene-specific primers (Proligo, France, and Oligomer OY, Finland) in QuantiTect SYBR Green PCR Kit (Qiagen, Germany). The process of collecting fluorescence data during PCR was performed by StepOnePlus Real-Time PCR Instrument (Applied Biosystems, USA) using intercalator-based method, also well-known as SYBR Green method. An identical PCR cycle profile was used for all genes. The amplification started by heat activation of HotStarTaq DNA polymerase at 95°C for 15 min. The following 35 cycles of PCR consisted of denaturation step for 15 s at 94°C and primer annealing step for 30 s at 56°C and for 30 s extension phase at 72°C. PCR runs were performed in duplicate or in triplicate and the volume for one reaction was 20 μL.

Determination of relative target quantity in samples was done by the comparative threshold cycle (ΔCT, ΔΔCT) method using StepOne software. Measurements were normalized to multiple endogenous control genes: ACTB, B2M, and HPRT1. The relative quantity of target in each sample was assessed by comparing normalized target quantity in each sample to normalized target quantity in the reference sample. The amplified double-stranded DNA sequences were separated in a 2.4% agarose gel to verify amplicons by length using DNA size marker (100 bp GeneRuler, Fermentas, Lithuania).

2.7. Statistical Analysis. Data are given as mean ± SEM. One-way analysis of variance (ANOVA) followed by Scheffe post hoc comparisons was used to test for differences between groups. A level of $p < 0.05$ was selected to indicate statistical significance.

3. Results

3.1. Characterization of Myoblast Culture Growth. Figure 1(a) shows a typical morphology of the myoblast culture in proliferation medium in the end of passage 2. Since the medium contained HGF the fibroblasts contamination was maximally suppressed and more than 70% of cells were desmin positive indicating the myogenic nature of the cells. The myogenic purity was similar in the cells obtained from young and older subjects (not shown).

In our conditions the myoblasts reached the 75% confluence during 3–5 days after which they were trypsinized and plated on a new dish. Interestingly, within the given passage the growth rate of the myoblasts was maximum during the first day of cultivation when the number of the cells doubled. Thereafter the growth gradually declined, so that the doubling rate increased twice by the end of incubation. Interestingly, the myoblasts isolated from the older and young subjects grew with similar rate in the beginning of the cultivation. After 3 days the old cells tended to grow slower compared to young ones, but no statistical significance was observed between the groups.

3.2. Effect of In Vitro and In Vivo Ageing on Mitochondrial Function. The function of different respiratory chain complexes in saponin skinned myoblasts was assessed by using a substrate/inhibitor titration protocol (Figure 2(a)). It can be seen that mitochondrial respiration in permeabilized myoblasts strongly increased over the basal levels after addition of ADP in the presence of glutamate and malate. This change indicates tight coupling of complex I dependent respiration to phosphorylation of ADP and effective permeabilization of cell membrane, as ADP exerted only insignificant effect on cellular respiration in the absence of saponin (not shown). In separate experiments (not shown) the concentration of ADP was increased by small increments (cumulatively) to assess the apparent affinity of mitochondria inside the cells. We found that the apparent Km for regulation of OXPHOS with ADP was below 10 μM which corresponds

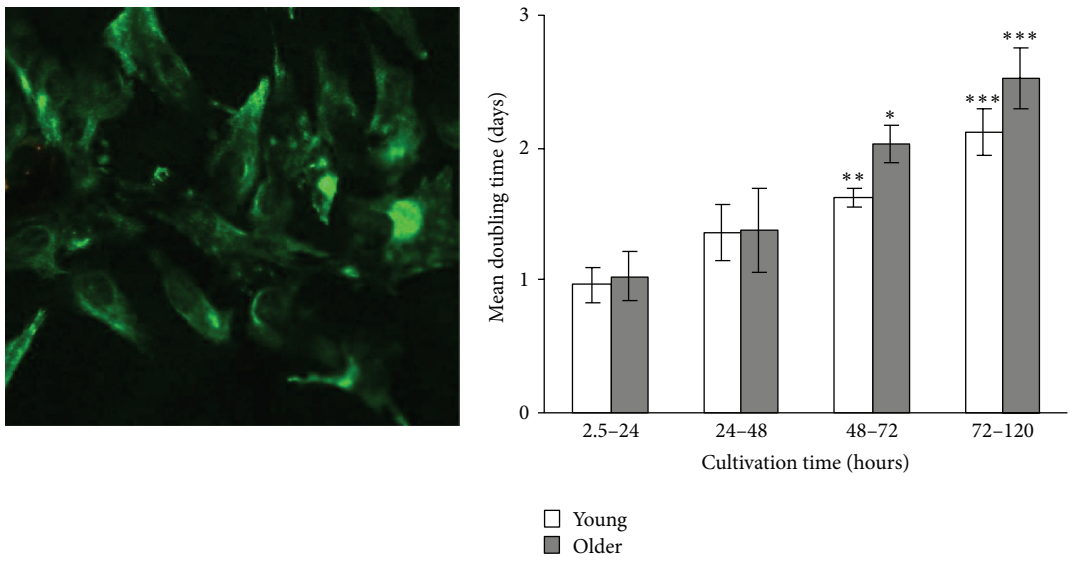

Figure 1: (a) Morphology of desmin-specific (green) skeletal muscle myoblasts of passage 2 in the culture (40x). (b) Proliferation of skeletal muscle myoblasts in culture throughout a single passage for young ($n = 5$) and older ($n = 7$) subjects. The data (mean ± SEM) for cells from passages 3, 5, and 6 were combined, as the dynamics of cell growth was similar within each of the passages. $^{*}p < 0.05$; $^{**}p < 0.01$; $^{***}p < 0.001$ compared to the first day of cultivation.

to that parameter in isolated mitochondria [34]. Thus, mitochondria in permeabilized myoblasts were characterized by very high apparent sensitivity towards exogenous ADP which indicates lack of intracellular diffusion restrictions for adenine nucleotides, a property registered earlier for mice cardiac myoblasts [35]. After registration of the respiration in the presence of ADP and NADH-linked substrates (Figure 2(a)) rotenone was added to inhibit complex I. The following addition of succinate reestablished the respiration, now being totally complex II dependent. Next, atractyloside was added that almost totally abolished the succinate dependent respiration. Such a strong control of respiration by atractyloside, an inhibitor of ANT, indicates that the mitochondrial inner membrane remained intact despite the sarcolemmal permeabilization by saponin in myoblasts. In a following step the cytochrome c oxidase was maximally activated by reduction of cytochrome c with TMPD and ascorbic acid and the NaN_3-insensitive portion of stimulation was used to indicate complex IV dependent respiration. Figures 2(b) and 2(c) show that replicative ageing *in vitro* (from passage 2 to passage 6) is associated with significant decline in the rates of complex I and IV dependent respiration (normalized for cell protein content) in myoblasts cultivated either from young or from older subjects. Similar change was observed also for complex II dependent respiration in young myoblasts, but not in myoblasts from older subjects where only a tendency for decrease was observed. Comparison of the myoblasts from young and older subjects revealed a tendency for decreased respiration rate in the latter group for both complex I and complex II and also for complex IV dependent respiration. In passage 2 these respiration rates in myoblasts from young subjects were 3.12 ± 0.25, 2.99 ± 0.25, and 5.87 ± 0.39 μmoles/min/mg protein, respectively. In myoblasts from older subjects respiration rates were 2.80 ± 0.06, 2.53 ± 0.12, and 5.67 ± 0.41 μmoles/min/mg protein, respectively. In passage 6 the complex I, complex II, and complex IV dependent respiration rates in myoblasts from young subjects were 2.54 ± 0.18, 2.27 ± 0.26, and 4.73 ± 0.30 μmoles/min/mg protein, respectively. In myoblasts from older subjects the respiration rates were 2.40±0.15, 2.07±0.29, and 4.68 ± 0.37 μmoles/min/mg protein, respectively. Proton leak was unaffected by ageing either *in vitro* or *in vivo*.

Principally, alterations in ADP-dependent respiration demonstrated in Figure 2(b) may be related to changes in cellular mitochondrial contents or inhibition of the processes of OXPHOS. Assessment of citrate synthase (CS) activity which is proportional to content of mitochondria enables evaluating the role of mitochondrial mass. We found that changes in CS activity roughly paralleled the alterations in respiration; in both young and old cells a decrease during transition from passages 2 to 6 was observed, although statistical significance was observed only in young cells. Normalization of respiration for CS activity (Figure 2(c)) abolished differences due to replicative *in vitro* ageing (not shown).

3.3. Effects of Ageing on Expression of Enzymes in Myoblasts. It is plausible that chronological ageing or ageing *in vitro* results in altered balance between the oxidative and glycolytic capacities or between the systems of energy transfer from mitochondria to ATPases. With this assumption the expression of several enzymes at gene and activity levels was determined. Qualitative data of expressions normalized to multiple endogenous control genes, ACTB, B2M, and HPRT1, showed that, in the young passage 2 myoblasts, pyruvate kinase type M2 (PKM2) isoform is most abundantly expressed (1722, $n = 2$). Other enzymes, like cytosolic and

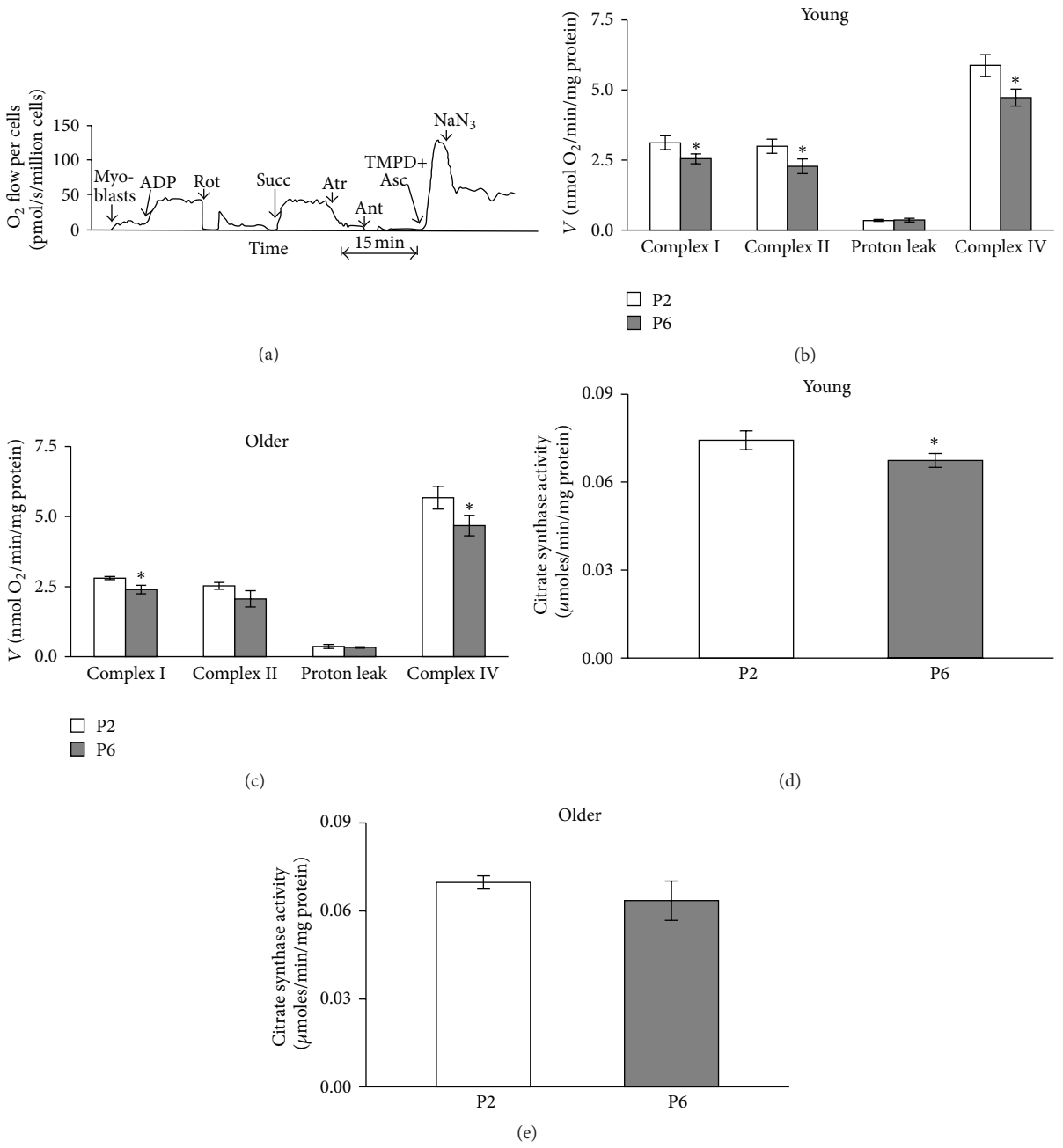

Figure 2: (a) Original recording of the assessment of the respiratory chain function in myoblasts. Myoblasts were incubated in Mitomed medium at 25°C in the presence of 50 μg/mL saponin. Further additions: ADP 1 mM, Rot: 10 μM rotenone, Succ: 10 mM succinate, Atr: 0.1 mM atractyloside, Ant: 10 μM antimycin A, TMPD+Asc: 0.5 mM TMPD with 2 mM ascorbate, and NaN_3: 5 mM sodium azide. (b, c) Summary of results shown in (a) in groups of cells cultured from young subjects. Complex I: ADP-dependent complex I activity, complex II: ADP-dependent complex II activity, complex IV: complex IV activity, and (d, e) citrate synthase activities in myoblast samples assessed in panel (b). Data are mean ± SEM. $^*p < 0.05$ differences compared to passage 2. P2: passage 2; P6: passage 6.

mitochondrial AK (qualitative data, 164 and 27, $n = 2$, resp.), brain type CK (105, $n = 2$), and HK isoforms (HK1, 8, $n = 2$, HK2, 11, $n = 2$), are much less expressed. We found that the mitochondrial CK isoenzyme practically is not expressed in myoblasts. At gene levels we could not see significant differences in aged *in vitro* or *in vivo* groups compared to young group.

Quantitative assessment of the enzyme activities (Figure 3) revealed that in myoblasts the PK was represented with the highest activity, followed by the activities of AK, CK, and HK, this decreasing order corresponding to the gene expression levels. Nevertheless the activities of PK and AK were ~4 times lower and the activity of HK was ~4 times higher than in muscle cells [36–38].

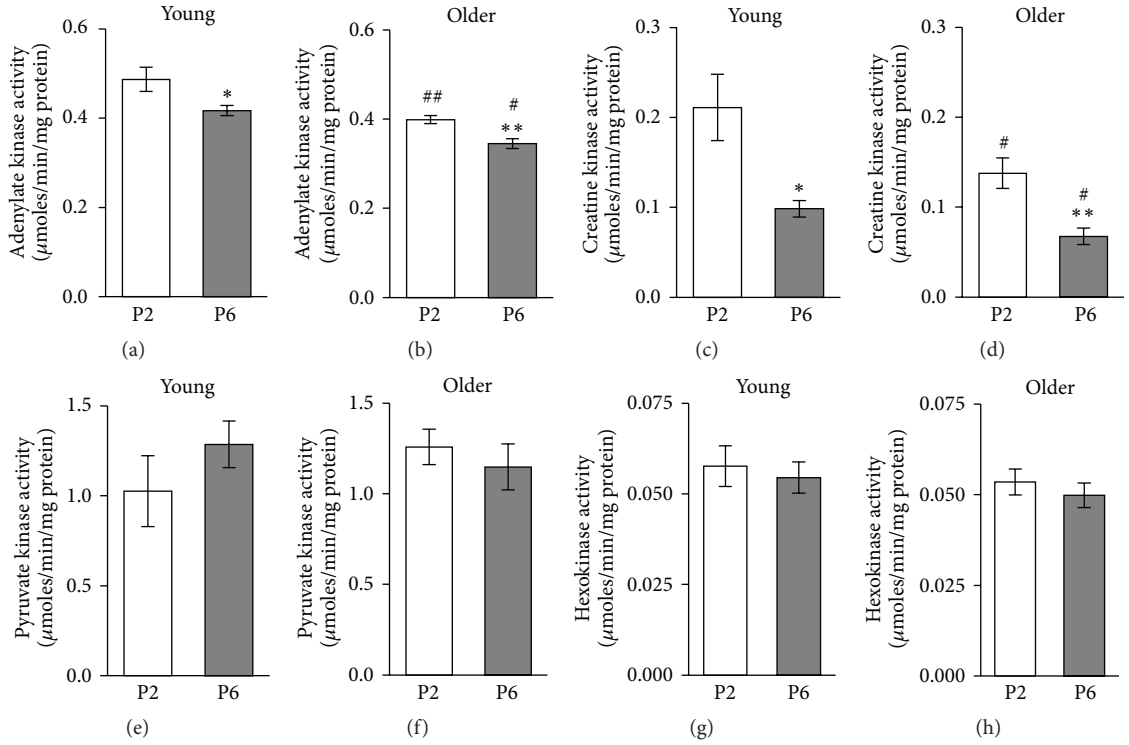

Figure 3: The assessment of the influence of ageing on adenylate kinase (a, b); creatine kinase (c, d); pyruvate kinase (e, f); and hexokinase (g, h) activities in myoblasts of passage 2 (P2) and passage 6 (P6). The myoblasts were derived from the vastus lateralis bioptates taken from young and old subjects. Data are mean ± SEM. $^{*}p < 0.05$; $^{**}p < 0.01$ compared to passage 2 of myoblasts. $^{\#}p < 0.05$; $^{\#\#}p < 0.01$ compared to young subjects.

Based on gene expression data it is conceivable that in myoblasts the high PK activity stems from relatively high expression of PKM2, the AK activity is based mainly on AK1 isoform, and CK activity is based mainly on CKB isoform, whose activity was ~90 times lower than in muscle cells from *m. vastus lateralis* (Linossier et al., 1997). HK activity results from expression of both HK1 and HK2 isoforms.

Interestingly, the activities of AK and CK significantly decreased during replicative senescence of myoblasts from passage 2 to passage 6 in both young and older subjects. Ageing *in vivo* also affected these enzymes as the myoblasts from older subjects exhibited lower AK activity in both passage 2 and passage 6 cells compared to young counterparts (0.399 ± 0.009 and 0.487 ± 0.027 μmoles/min/mg protein in passage 2, $p < 0.05$, resp., and 0.345 ± 0.011 and 0.417 ± 0.025 μmoles/min/mg protein in passage 6, $p < 0.05$, resp.). Similar *in vivo* ageing effect was observed in CK activity (0.138 ± 0.017 and 0.211 ± 0.027 μmoles/min/mg protein, in passage 2, $p < 0.05$, resp., and 0.068 ± 0.009 and 0.098 ± 0.010 μmoles/min/mg protein in passage 6, $p < 0.05$, resp.). In contrast, the activities of PK and HK were not influenced by ageing *in vitro* or *in vivo*. However, it is noticeable that the PK activity in myoblasts from young and older subjects responded differently to replicative senescence, with increase and decrease, respectively. As we also have seen a trend to decrease respiratory parameters in *in vivo* aged group of myoblasts we hypothesized that ageing *in vivo* may alter the metabolic profile of the myoblasts. One way to measure this is to assess the ratio of glycolytic to oxidative capacity [39]. Therefore, we have examined the ratios of cellular PK activities as a strongly expressed marker of glycolysis to the maximum OXPHOS activity measured as respiration rate at saturating ADP in conditions of function of different complexes of the respiratory chain (Figure 2).

As Figure 4 shows this index increased during *in vitro* ageing in young passage 6 group of cells, but not in the cells from older subjects, because the ratio of PK activity/complex I in the myoblasts from older subjects was already increased ($p < 0.05$) in passage 2 compared to myoblasts from young subjects. Similar differences were observed in the PK/CS ratio (Figures 4(c) and 4(d)).

4. Discussion

The present study demonstrated that replicative *in vitro* ageing is associated with significant decline in the rate of ADP-dependent respiration in myoblasts cultivated either from young or from older subjects. The decrease of CS activity was associated with decreased respiration in myoblasts. Minet and Gaster [32] demonstrated that replicative senescence results in decreased mitochondrial mass and ATP content in myotubes while mitochondrial ATP synthesis rate normalized to mitochondrial protein was unchanged. Comparison of the myoblasts from young and older subjects revealed

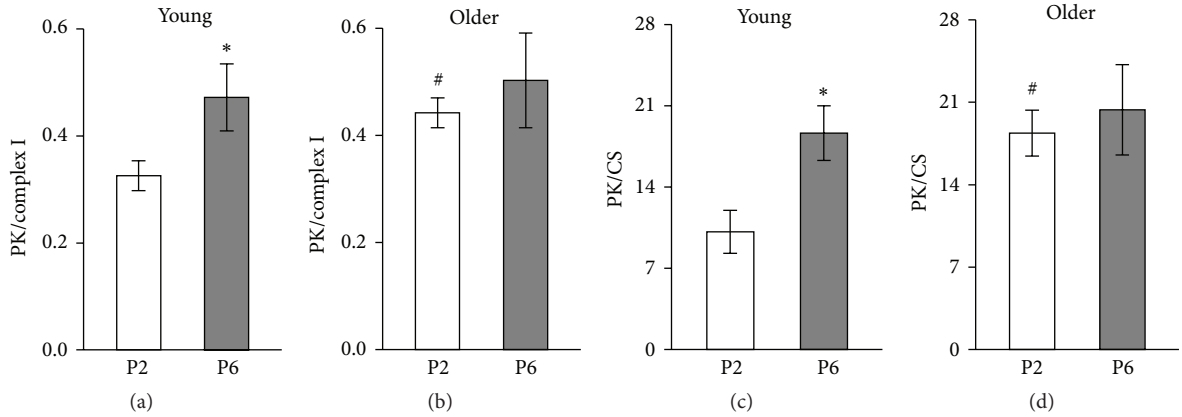

Figure 4: Influence of ageing on activity of pyruvate kinase (PK) normalized for complex I dependent respiration (PK/complex I) in myoblasts of passage 2 (P2) and passage 6 (P6) of young (a) and older (b) subjects. (c-d) Influence of ageing on ratio of activity of PK to citrate synthase (CS) of P2 and P6 of young and older subjects. Data are mean ± SEM. $^{*}p < 0.05$ compared to passage 2. $^{\#}p < 0.05$ compared to young subjects.

a tendency for decreased respiration rate and CS activity in the latter group. These changes were specifically evident in the earlier passage (2) but disappeared in the later passage (6). Thus, it seems that ageing of subject affects the properties of the satellite cells which determine the function of mitochondria in myoblasts. It is evident that decreased respiratory capacity associated with replicative or *in vivo* senescence of myoblasts resulted from reduced mitochondrial content of the myoblasts.

Gene expression study shows absence of mRNA of the mitochondrial CK isoenzyme, but considerable mRNA level of the mitochondrial isoenzyme AK2 which accounted for 14% of total level of sum of both AK isoforms in myoblasts. These findings suggest that, similarly to the HL-1 cells, myoblasts do not have the energy transport system of CK isoforms; instead AK isoforms participate significantly in energy transport [35]. Our data presents that the activity of AK decreased significantly during replicative senescence of myoblasts, which has not been shown before. Ageing *in vivo* also affected this enzyme as the myoblasts from older subjects exhibited lower AK activity compared to young counterparts. Borges and Essen-Gustavsson [40] and Lanza with coworkers [41] have previously shown that AK activity is decreased also in muscle fibers from older subjects compared to young subjects. As AK also conveys information about the cellular energy state to AMP signal and accordingly metabolic sensors reduce ATP-consuming and activate ATP-generating pathways to adjust energy metabolism and functional activity [42], AK can be an important intermediate step in the mechanism for developing age-related muscle weakness. As AMP signaling can via AMP-activated protein kinase (AMPK) and phosphorylation of PGC-1alpha [43, 44] regulate mitochondrial biogenesis, it is possible that deficit of AK is associated with decrease in the amount of mitochondria of muscle cells in older persons both in ageing *in vivo* and in replicative senescence. Ageing also decreases the differentiation potential of human myoblasts [25]; since the results have already shown that AK-AMPK metabolic signaling axis supports stem cell differentiation [45] our results show significant decrease in AK activity. The decreased AK activity is a significant cause for decreased satellite cell differentiation and hence sarcopenia. Unlike AK-AMPK metabolic signaling, the upstream pathways for expression and activity regulation of AK still remain to be elucidated.

The low CK activities we measured and dominance of BB-CK in myoblasts are consistent with the results of other investigators [46, 47]. In accordance with [48–52] we were unable to show the presence of sarcomeric mitochondrial CK isoenzyme in myoblasts; therefore, we can assume that the CK energy transport system is not developed there. However it is possible that CK is necessary in myoblasts for creating PCr reserve as an energy source for differentiation [51]. Low CK activity still significantly decreased during *in vitro* replicative and *in vivo* senescence, which could also result in decrease in the concentration of PCr and thereby worsening differentiation quality of the muscle fibers.

In Figure 1(b), proliferation of young and older human skeletal muscle myoblasts in culture throughout a single passage showed tendency for longer doubling time, in cultivation times of 48–72 and 72–120 hours, which might be caused by impairment of energy transfer by AK and CK systems as total activities of both enzymes were decreased in *in vivo* aged groups in passage 2 and also in passage 6.

Activity of PK in myoblasts was not influenced by ageing *in vitro* or *in vivo* (Figure 3(e)). But a decline in the activity of PK in human muscles has been reported by several investigators [36, 41]. Also the mitochondrial ATP production capacity and CS activity, indicating number of mitochondria in muscles, become smaller with age [41] but less compared to glycolytic enzymes; hence the muscle becomes more oxidative. It would be interesting to know whether the metabolic profile will change with age, similarly in muscle myogenic cells. We used the ratio of activities of PK and CS as an indicator of metabolic profile. Mean PK activity in dog heart is ~6 times and in vastus lateralis muscle

~26 times higher compared to mean CS activity [52]; human vastuslateralis muscle seems to be somewhat less glycolytic; ratio of mean activities of the abovementioned enzymes is ~17 [53]. Values of PK/CS ratios were similar to PK/CS ratio of human muscle. In young myoblasts from passage 2 PK/CS ratio was 10.1 ± 1.85 and increased significantly during replicative senescence of myoblasts to 18.6 ± 2.35 in passage 6; ageing *in vivo* also affected PK/CS ratio as the myoblasts from older subjects exhibited also a higher PK/CS ratio, 18.4 ± 1.95, in passage 2 compared to young counterparts. For the second measure for evaluation of metabolic profile we used ratio of PK activity/complex I, which, to our knowledge, has not previously been used. The results (Figure 4) show that this ratio in the myoblasts of passage 2 cultivated from older subject's muscle increased compared to myoblasts from young subjects of the same passage. Also the increase in this index was detected during *in vitro* ageing in young passage 6 group of cells, but not in the cells from older subjects. Similarly increased PK activity and glycolysis are shown in cultured human diploid fibroblasts ageing *in vitro* [54]. The most well-known cause for metabolic shift to glycolysis is hypoxia, resulting in binding a nuclear protein, hypoxia-inducible factor 1 (HIF-1), to DNA and increased expression of pyruvate kinase and other glycolytic enzymes [55]. HIF-1 may, however, also cause reprogramming of metabolism to favour glycolysis even under aerobic conditions [56–59]. In H_2O_2-induced senescent skin fibroblasts, was observed a decrease in the expression of pyruvate dehydrogenase, activity of cytochrome c oxidase, and the rate of oxygen consumption. The mRNA level of HIF-1 and activities of PDH kinase and lactate dehydrogenase were increased in the senescent skin fibroblasts. These changes in the expression of enzymes suggest a metabolic shift from mitochondrial respiration to glycolysis as a major supply of ATP in these cells [60]. Differently from PK, ratios of HK/complex I and HK/CS in myoblasts were not influenced by ageing *in vitro* nor *in vivo* (data not shown). Likely reason for the lack of change of these ratios is the lower sensitivity of expression of HK to HIF-1.

5. Conclusions

The results of the current study demonstrated that proliferation of myoblasts *in vitro* is associated with downregulation of OXPHOS and CK and AK mediated systems of energy storage and transfer. The myoblasts cultivated from older subjects showed lower rate of activities of CK and AK compared to myoblasts from young subjects. The total activities of HK and PK were not affected by ageing *in vivo* or *in vitro*; however there is an uptrend for PK and significantly increased ratio of PK/complex I dependent respiration. Ageing *in vivo* exerts an impact on satellite cells which results in altered metabolic profile in favour of the prevalence of glycolytic pathways over mitochondrial OXPHOS of myoblasts.

Conflict of Interests

The authors declare that they have no conflict of interests.

Acknowledgments

This work was supported by Institutional Research Funding IUT20-46 of the Estonian Ministry of Education and Research and by the grant of Estonian Science Foundation no. 8736 and by EUFP7 project MYOAGE (HEALTH-2007-2.4.5-10).

References

[1] W. J. Evans and W. W. Campbell, "Sarcopenia and age-related changes in body composition and functional capacity," *The Journal of Nutrition*, vol. 123, no. 2, pp. 465–468, 1993.

[2] T. Rantanen, K. Masaki, D. Foley, G. Izmirlian, L. White, and J. M. Guralnik, "Grip strength changes over 27 yr in Japanese-American men," *Journal of Applied Physiology*, vol. 85, no. 6, pp. 2047–2053, 1998.

[3] G. Grimby, "Muscle performance and structure in the elderly as studied cross-sectionally and longitudinally," *The Journals of Gerontology A: Biological Sciences and Medical Sciences*, vol. 50, pp. 17–22, 1995.

[4] L. Larsson, B. Sjodin, and J. Karlsson, "Histochemical and biochemical changes in human skeletal muscle with age in sedentary males, age 22–65 yrs," *Acta Physiologica Scandinavica*, vol. 103, no. 1, pp. 31–39, 1978.

[5] J. Lexell, C. C. Taylor, and M. Sjöström, "What is the cause of the ageing atrophy? Total number, size and proportion of different fiber types studied in whole vastus lateralis muscle from 15- to 83-year-old men," *Journal of the Neurological Sciences*, vol. 84, no. 2-3, pp. 275–294, 1988.

[6] L. B. Verdijk, R. Koopman, G. Schaart, K. Meijer, H. H. C. M. Savelberg, and L. J. C. Van Loon, "Satellite cell content is specifically reduced in type II skeletal muscle fibers in the elderly," *The American Journal of Physiology—Endocrinology and Metabolism*, vol. 292, no. 1, pp. E151–E157, 2007.

[7] M. A. Alnaqeeb and G. Goldspink, "Changes in fibre type, number and diameter in developing and ageing skeletral muscle," *Journal of Anatomy*, vol. 153, pp. 31–45, 1987.

[8] S. V. Brooks and J. A. Faulkner, "Skeletal muscle weakness in old age: underlying mechanisms," *Medicine & Science in Sports & Exercise*, vol. 26, no. 4, pp. 432–439, 1994.

[9] S. V. Brooks and J. A. Faulkner, "The magnitude of the initial injury induced by stretches of maximally activated muscle fibres of mice and rats increases in old age," *The Journal of Physiology*, vol. 497, no. 2, pp. 573–580, 1996.

[10] R. N. Cooper, G. S. Butler-Browne, and V. Mouly, "Human muscle stem cells," *Current Opinion in Pharmacology*, vol. 6, no. 3, pp. 295–300, 2006.

[11] M. D. Grounds and Z. Yablonka-Reuveni, "Molecular and cell biology of skeletal muscle regeneration," *Molecular and Cell Biology of Human Diseases Series*, vol. 3, pp. 210–256, 1993.

[12] Z. Yablonka-Reuveni, K. Day, A. Vine, and G. Shefer, "Defining the transcriptional signature of skeletal muscle stem cells," *Journal of Animal Science*, vol. 86, no. 14, pp. E207–E216, 2008.

[13] K. Day, G. Shefer, A. Shearer, and Z. Yablonka-Reuveni, "The depletion of skeletal muscle satellite cells with age is concomitant with reduced capacity of single progenitors to produce reserve progeny," *Developmental Biology*, vol. 340, no. 2, pp. 330–343, 2010.

[14] V. Renault, E. Rolland, L.-E. Thornell, V. Mouly, and G. Butler-Browne, "Distribution of satellite cells in the human vastus

lateralis muscle during aging," *Experimental Gerontology*, vol. 37, no. 12, pp. 1511–1512, 2002.

[15] V. Renault, L.-E. Thorne, P.-O. Eriksson, G. Butler-Browne, and V. Mouly, "Regenerative potential of human skeletal muscle during aging," *Aging Cell*, vol. 1, no. 2, pp. 132–139, 2002.

[16] Š. Sajko, L. Kubínová, E. Cvetko, M. Kreft, A. Wernig, and I. Eržen, "Frequency of M-cadherin-stained satellite cells declines in human muscles during aging," *Journal of Histochemistry & Cytochemistry*, vol. 52, no. 2, pp. 179–185, 2004.

[17] A. S. Brack, H. Bildsoe, and S. M. Hughes, "Evidence that satellite cell decrement contributes to preferential decline in nuclear number from large fibres during murine age-related muscle atrophy," *Journal of Cell Science*, vol. 118, no. 20, pp. 4813–4821, 2005.

[18] E. Schultz and B. H. Lipton, "Skeletal muscle satellite cells: changes in proliferation potential as a function of age," *Mechanisms of Ageing and Development*, vol. 20, no. 4, pp. 377–383, 1982.

[19] M. H. Snow, "The effects of aging on satellite cells in skeletal muscles of mice and rats," *Cell and Tissue Research*, vol. 185, no. 3, pp. 399–408, 1977.

[20] F. Kadi, N. Charifi, C. Denis, and J. Lexell, "Satellite cells and myonuclei in young and elderly women and men," *Muscle & Nerve*, vol. 29, no. 1, pp. 120–127, 2004.

[21] C. A. Collins, P. S. Zammit, A. Pérez Ruiz, J. E. Morgan, and T. A. Partridge, "A population of myogenic stem cells that survives skeletal muscle aging," *Stem Cells*, vol. 25, no. 4, pp. 885–894, 2007.

[22] G. Shefer, D. P. Van de Mark, J. B. Richardson, and Z. Yablonka-Reuveni, "Satellite-cell pool size does matter: defining the myogenic potency of aging skeletal muscle," *Developmental Biology*, vol. 294, no. 1, pp. 50–66, 2006.

[23] G. Shefer, G. Rauner, Z. Yablonka-Reuveni, and D. Benayahu, "Reduced satellite cell numbers and myogenic capacity in aging can be alleviated by endurance exercise," *PLoS ONE*, vol. 5, no. 10, Article ID e13307, 2010.

[24] A. Bigot, V. Jacquemin, F. Debacq-Chainiaux et al., "Replicative aging down-regulates the myogenic regulatory factors in human myoblasts," *Biology of the Cell*, vol. 100, no. 3, pp. 189–199, 2008.

[25] P. Lorenzon, E. Bandi, F. de Guarrini et al., "Ageing affects the differentiation potential of human myoblasts," *Experimental Gerontology*, vol. 39, no. 10, pp. 1545–1554, 2004.

[26] S. Beccafico, C. Puglielli, T. Pietrangelo, R. Bellomo, G. Fanò, and S. Fulle, "Age-dependent effects on functional aspects in human satellite cells," *Annals of the New York Academy of Sciences*, vol. 1100, pp. 345–352, 2007.

[27] T. Pietrangelo, C. Puglielli, R. Mancinelli, S. Beccafico, G. Fanò, and S. Fulle, "Molecular basis of the myogenic profile of aged human skeletal muscle satellite cells during differentiation," *Experimental Gerontology*, vol. 44, no. 8, pp. 523–531, 2009.

[28] S. Beccafico, F. Riuzzi, C. Puglielli et al., "Human muscle satellite cells show age-related differential expression of S100B protein and RAGE," *Age*, vol. 33, no. 4, pp. 523–541, 2011.

[29] S. Fulle, S. Di Donna, C. Puglielli et al., "Age-dependent imbalance of the antioxidative system in human satellite cells," *Experimental Gerontology*, vol. 40, no. 3, pp. 189–197, 2005.

[30] E. Luin, P. Lorenzon, A. Wernig, and F. Ruzzier, "Calcium current kinetics in young and aged human cultured myotubes," *Cell Calcium*, vol. 44, no. 6, pp. 554–566, 2008.

[31] S. Bortoli, V. Renault, R. Mariage-Samson et al., "Modifications in the myogenic program induced by *in vivo* and *in vitro* aging," *Gene*, vol. 347, no. 1, pp. 65–72, 2005.

[32] A. D. Minet and M. Gaster, "Cultured senescent myoblasts derived from human vastus lateralis exhibit normal mitochondrial ATP synthesis capacities with correlating concomitant ROS production while whole cell ATP production is decreased," *Biogerontology*, vol. 13, no. 3, pp. 277–285, 2012.

[33] J. O. Nehlin, M. Just, A. C. Rustan, and M. Gaster, "Human myotubes from myoblast cultures undergoing senescence exhibit defects in glucose and lipid metabolism," *Biogerontology*, vol. 12, no. 4, pp. 349–365, 2011.

[34] B. Chance and G. R. Williams, "The respiratory chain and oxidative phosphorylation," *Advances in Enzymology and Related Subjects of Biochemistry*, vol. 17, pp. 65–134, 1956.

[35] M. Eimre, K. Paju, S. Pelloux et al., "Distinct organization of energy metabolism in HL-1 cardiac cell line and cardiomyocytes," *Biochimica et Biophysica Acta*, vol. 1777, no. 6, pp. 514–524, 2008.

[36] C. E. Shonk, B. J. Koven, H. Majima, and G. E. Boxer, "Enzyme patterns in human tissues. II. Glycolytic enzyme patterns in nonmalignant human tissues," *Cancer research*, vol. 24, pp. 722–731, 1964.

[37] E. A. Newsholme and C. Start, *Regulation in Metabolism*, Wiley, London, UK, 1973.

[38] M.-T. Linossier, D. Dormois, C. Perier, J. Frey, A. Geyssant, and C. Denis, "Enzyme adaptations of human skeletal muscle during bicycle short-sprint training and detraining," *Acta Physiologica Scandinavica*, vol. 161, no. 4, pp. 439–445, 1997.

[39] C. Stockmar, H. Lill, A. Trapp, C. Josten, and K. Punkt, "Fibre type related changes in the metabolic profile and fibre diameter of human vastus medialis muscle after anterior cruciate ligament rupture," *Acta Histochemica*, vol. 108, no. 5, pp. 335–342, 2006.

[40] O. Borges and B. Essen-Gustavsson, "Enzyme activities in type I and II muscle fibres of human skeletal muscle in relation to age and torque development," *Acta Physiologica Scandinavica*, vol. 136, no. 1, pp. 29–36, 1989.

[41] I. R. Lanza, D. K. Short, K. R. Short et al., "Endurance exercise as a countermeasure for aging," *Diabetes*, vol. 57, no. 11, pp. 2933–2942, 2008.

[42] P. Dzeja and A. Terzic, "Adenylate kinase and AMP signaling networks: metabolic monitoring, signal communication and body energy sensing," *International Journal of Molecular Sciences*, vol. 10, no. 4, pp. 1729–1772, 2009.

[43] S. Jäer, C. Handschin, J. St Pierre, and B. M. Spiegelman, "AMP-activated protein kinase (AMPK) action in skeletal muscle via direct phosphorylation of PGC-1α," *Proceedings of the National Academy of Sciences of the United States of America*, vol. 104, no. 29, pp. 12017–12022, 2007.

[44] D. Knutti, D. Kressler, and A. Kralli, "Regulation of the transcriptional coactivator PGC-1 via MAPK-sensitive interaction with a repressor," *Proceedings of the National Academy of Sciences of the United States of America*, vol. 98, no. 17, pp. 9713–9718, 2001.

[45] P. P. Dzeja, S. Chung, R. S. Faustino, A. Behfar, and A. Terzic, "Developmental enhance-ment of adenylate kinase-AMPK metabolic signaling axis supports stem cell cardiac differentiation," *PLoS ONE*, vol. 6, no. 4, Article ID e19300, 2011.

[46] J. S. Chamberlain, J. B. Jaynes, and S. D. Hauschka, "Regulation of creatine kinase induction in differentiating mouse

myoblasts," *Molecular and Cellular Biology*, vol. 5, no. 3, pp. 484–492, 1985.

[47] J. C. Perriard, "Developmental regulation of creatine kinase isoenzymes in myogenic cell cultures from chicken. Levels of mRNA for creatine kinase subunits M and B," *Journal of Biological Chemistry*, vol. 254, no. 15, pp. 7036–7041, 1979.

[48] R. C. Haas, C. Korenfeld, Z. F. Zhang, B. Perryman, D. Roman, and A. W. Strauss, "Isolation and characterization of the gene and cDNA encoding human mitochondrial creatine kinase," *Journal of Biological Chemistry*, vol. 264, no. 5, pp. 2890–2897, 1989.

[49] S. C. Klein, R. C. Haas, M. B. Perryman, J. J. Billadello, and A. W. Strauss, "Regulatory element analysis and structural characterization of the human sarcomeric mitochondrial creatine kinase gene," *Journal of Biological Chemistry*, vol. 266, no. 27, pp. 18058–18065, 1991.

[50] R. M. Payne and A. W. Strauss, "Expression of the mitochondrial creatine kinase genes," *Molecular and Cellular Biochemistry*, vol. 133-134, no. 1, pp. 235–243, 1994.

[51] R. S. O'connor, C. M. Steeds, R. W. Wiseman, and G. K. Pavlath, "Phosphocreatine as an energy source for actin cytoskeletal rearrangements during myoblast fusion," *The Journal of Physiology*, vol. 586, no. 12, pp. 2841–2853, 2008.

[52] S. R. Stuewe, P. A. Gwirtz, N. Agarwal, and R. T. Mallet, "Exercise training enhances glycolytic and oxidative enzymes in canine ventricular myocardium," *Journal of Molecular and Cellular Cardiology*, vol. 32, no. 6, pp. 903–913, 2000.

[53] H. J. Green, E. B. Bombardier, T. A. Duhamel, G. P. Holloway, A. R. Tupling, and J. Ouyang, "Acute responses in muscle mitochondrial and cytosolic enzyme activities during heavy intermittent exercise," *American Journal of Physiology: Regulatory, Integrative and Comparative Physiology*, vol. 104, no. 4, pp. 931–937, 2008.

[54] A. H. Bittles and N. Harper, "Increased glycolysis in ageing cultured human diploid fibroblasts," *Bioscience Reports*, vol. 4, no. 9, pp. 751–756, 1984.

[55] G. L. Semenza, P. H. Roth, H.-M. Fang, and G. L. Wang, "Transcriptional regulation of genes encoding glycolytic enzymes by hypoxia-inducible factor 1," *Journal of Biological Chemistry*, vol. 269, no. 38, pp. 23757–23763, 1994.

[56] G. L. Semenza, "Regulation of metabolism by hypoxia-inducible factor 1," *Cold Spring Harbor Symposia on Quantitative Biology*, vol. 76, pp. 347–353, 2011.

[57] R. H. Wenger, "Cellular adaptation to hypoxia: O_2-sensing protein hydroxylases, hypoxia-inducible transcription factors, and O_2-regulated gene expression," *The FASEB Journal*, vol. 16, no. 10, pp. 1151–1162, 2002.

[58] M. Ohh, "Tumor strengths and frailties: cancer SUMmOns Otto's metabolism," *Nature Medicine*, vol. 18, no. 1, pp. 30–31, 2012.

[59] S. N. Greer, J. L. Metcalf, Y. Wang, and M. Ohh, "The updated biology of hypoxia-inducible factor," *The EMBO Journal*, vol. 31, no. 11, pp. 2448–2460, 2012.

[60] Y.-H. Wei, S.-B. Wu, Y.-S. Ma, and H.-C. Lee, "Respiratory function decline and DNA mutation in mitochondria, oxidative stress and altered gene expression during aging," *Chang Gung Medical Journal*, vol. 32, no. 2, pp. 113–132, 2009.

Hindawi Publishing Corporation
Oxidative Medicine and Cellular Longevity
Volume 2016, Article ID 6705621, 12 pages
http://dx.doi.org/10.1155/2016/6705621

Research Article

Resveratrol Regulates Mitochondrial Biogenesis and Fission/Fusion to Attenuate Rotenone-Induced Neurotoxicity

Kaige Peng,[1] Yuan Tao,[2] Jun Zhang,[2] Jian Wang,[1] Feng Ye,[1] Guorong Dan,[1] Yuanpeng Zhao,[1] Ying Cai,[1] Jiqing Zhao,[1] Qiang Wu,[2] Zhongmin Zou,[1] Jia Cao,[1] and Yan Sai[1]

[1]*Institute of Toxicology, College of Preventive Medicine, Third Military Medical University, Chongqing 400038, China*
[2]*College of Preventive Medicine, Third Military Medical University, Chongqing 400038, China*

Correspondence should be addressed to Yan Sai; sytmmu@126.com

Received 15 April 2015; Revised 2 August 2015; Accepted 31 August 2015

Academic Editor: David Sebastián

Copyright © 2016 Kaige Peng et al. This is an open access article distributed under the Creative Commons Attribution License, which permits unrestricted use, distribution, and reproduction in any medium, provided the original work is properly cited.

It has been confirmed that mitochondrial impairment may underlie both sporadic and familial Parkinson's disease (PD). Mitochondrial fission/fusion and biogenesis are key processes in regulating mitochondrial homeostasis. Therefore, we explored whether the protective effect of resveratrol in rotenone-induced neurotoxicity was associated with mitochondrial fission/fusion and biogenesis. The results showed that resveratrol could not only promote mitochondrial mass and DNA copy number but also improve mitochondrial homeostasis and neuron function in rats and PC12 cells damaged by rotenone. We also observed effects with alterations in proteins known to regulate mitochondrial fission/fusion and biogenesis in rotenone-induced neurotoxicity. Therefore, our findings suggest that resveratrol may prevent rotenone-induced neurotoxicity through regulating mitochondrial fission/fusion and biogenesis.

1. Introduction

Resveratrol (trans-3,4′,-5-trihydroxystilbene) is a nature-derived compound found in red grapes, peanuts, and red wine [1]. The protective effects of resveratrol have been extensively investigated in both in vivo and in vitro models. A wide range of biological and pharmacological properties have been shown, including antioxidant, anti-inflammatory, antimutagenic, and anticarcinogenic activities [2–5]. The neuroprotective potential of resveratrol against dopamine- (DA-) induced apoptosis in neuronal SH-SY5Y cells, the 6-OHDA-treated rat model of Parkinson's disease (PD), and the MPTP-treated mouse model of PD has also been confirmed [1, 6, 7]. However, the mechanism of resveratrol protection in cellular and animal PD models has not been clearly elaborated in detail.

PD is the second most common neurodegenerative disease, characterized by a progressive loss of DA neurons in the substantia nigra (SN) [8]. Although the etiology of dopaminergic neurodegeneration remains unknown, it has been accepted that PD-related neurodegeneration is the result of environmental and genetic interactions [8]. Rotenone, one of the most widely used pesticides, has been suggested as the primary environmental risk factor for PD [9, 10]. Long-term and low-dose exposure to rotenone leads to a systemic defect in mitochondrial complex I and oxidative stress, the main contributors to the etiology of PD [9, 11]. Therefore, mitochondria are believed to play an important role in rotenone-induced dopaminergic neurodegeneration [12].

Mitochondria are dynamic organelles, continuously undergoing fission/fusion and biogenesis to form a network that spans the entire area of neuron to meet the demands of cellular function [13]. These processes not only determine the structure of the entire mitochondrial population in the neurons but also influence nearly every aspect of mitochondrial function, such as the formation of reactive oxygen species (ROS), ATP production, and respiration [13, 14]. Apart from maintaining normal mitochondrial functions and integrity, mitochondrial fusion/fission, as well as mitochondrial biogenesis, has also been associated with cell death mechanisms [15]. The dysfunction of mitochondrial fission/fusion and

biogenesis is associated with many diseases, in particular, neurodegenerative diseases such as Huntington's disease, Alzheimer's disease, and PD [15–17]. In recent years, there have been reports that resveratrol could increase the activity of mitochondria, thereby conferring resistance to mitochondrial dysfunction in various disease states [18]. To date, accumulated evidence suggests clinical potential for resveratrol, but the precise molecular mechanism for biological activity in the mitochondria remains poorly understood.

In the present study, we explored the protective effect of resveratrol on rotenone-induced dopamine neurotoxicity and its action in mitochondrial fission/fusion and biogenesis. We intend to clarify the mechanism of resveratrol in mitochondrial dynamics in dopamine neurotoxicity induced by rotenone. This research will be helpful in explaining the diverse biological and pharmacological properties of resveratrol.

2. Materials and Methods

2.1. Materials. Healthy male Sprague-Dawley rats (5–7 weeks old) weighing 180–220 g are obtained from the Animal Center of the Third Military Medical University (Chongqing, China). PC12 cells (adrenal gland; pheochromocytoma) were provided by Shanghai Cell Bank, Institute of Biochemistry and Cell Biology, Chinese Academy of Sciences. Rotenone, dimethyl sulfoxide (DMSO), resveratrol, and adenosine triphosphate (ATP) were purchased from Sigma (St. Louis, MO, USA). Except for antibodies of mitochondrial transcription factor A (mtTFA, Santa Cruz, USA), antibodies of optic atrophy 1 (OPA1), mitofusin 2 (MFN2), mitochondrial fission 1 (Fis1), dynamin-1-like protein (Drp1), peroxisome proliferator-activated receptor gamma, and coactivator 1 alpha (PGC-1α) were purchased from Abcam (USA). All other reagents used were of the highest grade available.

2.2. Animal Care and Treatment. The male Sprague-Dawley rats were housed in climate-controlled rooms at 23 ± 2°C housing temperature on a reverse 12 : 12 h light/dark cycle with lights on at 8:00. Animals were allowed free access to food and water during the experimental period. Animals were divided into three groups: control, rotenone-exposed, and rotenone plus resveratrol treated. Between 1 and 5 animals per cage were acclimated for 1 week in our temperature-controlled animal room prior to drug treatment. The rotenone-exposed group (R group) was treated with subcutaneous injections of rotenone (first: 2 mg/kg, every day for three days; second: 1 mg/kg, every day for seven days; and then 0.5 mg/kg, every day for twenty days). The control group was injected with an equal volume of dimethyl sulfoxide for thirty days. The resveratrol protection group (R + RSV group) was treated first with intraperitoneal injection of resveratrol (50 mg/kg, every day for thirty days), and then thirty minutes later, animals were treated the same as in the rotenone exposure group. All animal procedures were conducted per the guidelines of the care and use of laboratory animals and China's laws on animal experimentation.

2.3. Neurobehavioral Tests: Rotarod Performance Test. The rotarod test has been used to assess motor coordination and balance alterations in rodents. This test measured the ability of the rat to preserve balance by holding itself on the rotating rod [19]. Thirty days after drug treatments, we performed this locomotor activity, which measured motor coordination in rats. The rats were adapted to the bar. When all rats could remain on the rotating rod for approximately 3 min, each rat was placed on a horizontal rod rotating at a speed of 12 rpm for a maximum of 3 min. The duration of time during which each rat was able to maintain its balance walking on the top of the rod was measured. The number of rats that fell was recorded.

2.4. Tissue Preparation. After completion of the behavioral tests on day 31, the rats were sacrificed by decapitation. Whole brains were removed quickly and prepared for assay. The brain was rinsed with chilled saline, and the corpus striatum was dissected on ice according to coordinates indicated in the rat brain atlas. A portion of the tissues was used for measuring the levels of ROS and ATP. Another portion of the tissues was used for detecting the gene and protein expression levels of mitochondrial fission/fusion and biogenesis.

2.5. Cell Culture and Treatment. PC12 cells were cultured at 37°C under an atmosphere of 5% CO_2 in Dulbecco's Modified Eagle's Medium (DMEM, Invitrogen, USA) containing 10% horse serum and 5% fetal bovine serum (Hyclone, USA). Cells were divided into three groups. The rotenone-exposed group (R group) was treated with the indicated concentration of rotenone dissolved in DMSO for 24 h. The control group was administered equivalent amounts of DMSO for 24 h. The resveratrol protection group (RSV + R group) was pretreated with resveratrol for 24 h and then exposed to rotenone for 24 h.

2.6. Transfection of siRNA of PGC-1α. PC12 cells (1×10^5/well) were seeded into 12-well plates containing 500 μL of complete medium and were incubated for 24 h. Then transfection with siRNA was conducted using a Lipofectamine 2000 reagent as per user's guide. After 6 hours, the medium was changed to a normal culture medium. After another 48 hours, the cells were harvested and sent for isolation of RNA and analysis of PGC-1α expression by real-time PCR. The sequences are as follows: 5-AAGACGGATTGCCCTCATTTG-3 (siPGC-1α) and 5-AACGUGACACGUUCG GAGAATT-3 (negative control).

2.7. CCK-8 Assay to Evaluate PC12 Cell Viability. PC12 cell viability was assayed with the Cell Counting Kit-8 (DOJINDO, Japan), according to the manufacturer's instructions. All results were normalized to optical density values measured from an identically conditioned well without medium.

2.8. Annexin V-FITC to Evaluate PC12 Cell Apoptosis. According to the instructions of the manufacturer of Annexin V-FITC Apoptosis Detection Kit (BD, USA), the cells were

Table 1

	Sense primer	Antisense primer
mtTFA	5′-CGCCTGTCAGCCTTAT-3′	5′-GACTCATCCTTAGCCTCC-3′
PGC-1α	5′-GACCGTCCAAAGCATTCA-3′	5′-GGTTCTTGTCCACGCCTC-3′
Fis1	5′-ATCCGTAGAGGCATCGTG-3′	5′-GGGAGGAGGAAGAGCAGA-3′
Drp1	5′-TCTCCGAGTCCTTTATTG-3′	5′-TCTGACCACTTCTTACCG-3′
OPA1	5′-AAGAGGCACTTCAAGGTCG-3′	5′-TGTATTCGCCAGAACAGGA-3′
MFN2	5′-CGTCAAGAAGGATAAGCGACAC-3′	5′-CAACCCGCAGGAAGCAAT-3′
β-actin	5′-TGGTGAAGCAGGCATCTGA-3′	5′-TGCTGTTGAAGTCGCAGGAG-3′

harvested for apoptosis analysis. After centrifugation and resuspension in staining buffer, cells were incubated in Annexin V-FITC and propidium iodide (PI) for 20 min at room temperature. Fluorescence was detected with a FC500 flow cytometer (Beckman, USA), and data were analyzed using CXP analysis software (Beckman, USA).

2.9. Mito Tracker Green to Observe the Mitochondrial Mass. Mito Tracker Green (Invitrogen, USA) is a mitochondria-selective membrane potential-independent probe [20]. Thus, mitochondria in cells stained with MitoTracker Green dye display bright green fluorescence, making it a tool for determining mitochondrial mass [20–22]. After treatment, PC12 cells were rinsed with phosphate-buffered saline (PBS). Then, a working solution of the Mito Tracker Green probe was added and incubated for 45 min while avoiding light. PC12 cells were then rinsed three times with PBS. A confocal laser microscope (Leica TCS SP5) was used to observe and photograph the mitochondrial fluorescence intensity, with the same excitation and emission wavelengths. The fluorescence intensity was quantified and analyzed with confocal microscopy image analysis software. Mitochondria were classified into fragmented (<0.5 μm), intermediate (0.5–5 μm), and tubular (>5 μm) mitochondria. The cells showing 70% fragmented or intermediate mitochondria were classified as fragmented cells. Several random fields (≥200 cells per dish) were selected from each sample and analyzed by ImageJ.

2.10. RNA Isolation and RT-PCR. Total RNA was isolated according to the manufacturer's instructions of TRIZOL (Invitrogen, USA). The quantity and purity of isolated RNA were analyzed with a NanoDrop ND-1000 spectrophotometer. The samples of RNA were stored at −80°C until analysis. All first-strand cDNA samples were synthesized from 2.5 μg total RNA per 20 μL reaction using the ReverTra Ace Qpcr RT Kit (ToYoBo, Japan). Primers against each of the rat genes were designed using Primer 5.0, which are shown in Table 1.

Real-time PCR (RT-PCR) was performed, and the key parameters were as follows: initial denaturation at 94°C for 5 min; denaturation at 94°C for 40 seconds; annealing at the appropriate annealing temperature for 30 seconds (mtTFA: 53.5°C, PGC-1α: 55°C, Fis1: 54°C, Drp1: 53.5°C, OPA1: 54.5°C, and MFN2: 56.5°C); extension at 72°C for 45 seconds. The above three steps ran for 35 cycles, followed by 72°C for 5 min. β-actin was used to normalize the RT-PCR results. The annealing temperature of β-actin was 55°C. The amplified fragments were analyzed by electrophoresis using 0.8% and 1.2% agarose gels with ethidium bromide.

2.11. Western Blot. Western blot analysis was performed to investigate the protein expression of MFN2, OPA1, Drp1, and Fis1. Samples of the rat tissue and PC12 cells were sonicated in ice-cold lysis buffer and centrifuged at 12000 g for 10 min. The supernatants were collected. Protein concentrations were measured using the Bradford Protein Assay Kit. Samples were boiled in sample loading buffer. Equivalent amounts of proteins (10–25 mg) were loaded in each well of a 15% SDS-PAGE gel, and the separated proteins were transferred onto PVDF membranes after electrophoresis. Blots were blocked in 5% nonfat dry milk and then incubated overnight with primary mouse monoclonal antibody against OPA1 (1 : 500), mouse monoclonal antibody against MFN2 (1 : 1000), mouse monoclonal antibody against Drp1 (1 : 1000), mouse monoclonal antibody against Fis1 (1 : 1000), or mouse monoclonal antibody against β-actin (1 : 1000). After washes in TBST, blots were incubated with HRP-conjugated goat anti-mouse secondary antibody. The blots were then developed using electrochemiluminescence (ECL). The intensities of individual bands of the proteins of interest were then analyzed using the BioImaging System. The grayscale value of MFN2, OPA1, Drp1, and Fis1 was normalized to the value of the standard protein marker (β-actin) band to determine the expression level of the protein. The experiments were repeated at least three times independently.

2.12. Mitochondrial DNA Copy Number by Real-Time PCR. Total DNA from PC12 cells was separately isolated by phenol-chloroform extraction with Promega DNA Isolation Kits using standard methods. To determine mitochondrial DNA (mtDNA) copy number, mtDNA was quantified by normalizing the mitochondrial-encoded gene mtCol (mitochondrially encoded cytochrome c oxidase 1) to the nuclear-encoded gene Ndufv1 (NADH dehydrogenase (ubiquinone) flavoprotein 1) using RT-PCR and the ΔΔct method. The sequences of primer pairs designed to amplify mtCo1 as well as the nuclear DNA-encoded internal control gene Ndufv1 were as follows: 5′-ACCCCCGCTATAACCCAATATCAGAC-3′ (F, mtco1); 5′-TGGGTGTCCGAAGAATCAAAATAG-3′ (R, mtco1); 5′-CGCCATGACTGGAGGTGAGGXAG-3′ (F, Ndufv1); and 5′-GGCCCCGTAAACCCGATGTCTTC-3′ (R, Ndufv1). The copy number

of mtDNA was then normalized against that of Ndufv1 to calculate the relative value of mtDNA copy number.

2.13. Detection of Mitochondrial ATP Levels in PC12 Cells. Mitochondria were extracted from the PC12 cells on ice with Mitochondrial Extraction Kits (Beyotime, China). The extracted mitochondria were incubated with 1 mL of chilled 0.6 M perchloric acid at 0°C for 5 min. The homogenate was centrifuged at 20000 g for 10 min, and the pH of the supernatant was adjusted to pH 6.5–6.8 using 2.5 M K_2CO_3 solutions. Next, the mixture was centrifuged at 20000 g for 10 min after standing at 4°C for 10 min. The final supernatant was collected and removed by filtration through Whatman membrane filter paper. The samples were stored at −80°C until analyzed. Samples were analyzed with an ODS C18 column kept at room temperature with a flow rate of 1.0 mL/min and injected with 20 μL of sample. The UV detection wavelength was 254 nm. The external standard method was used in the experiments. The ATP content was calculated with the injection volume and the measured peak area. The concentration of ATP was expressed as micrograms per gram of protein. The Bradford protein assay kit was used to determine the protein concentration of the samples.

2.14. Determination of ROS Production in PC12 Cells. ROS production was measured by the oxidation-sensitive fluorescent probe 2′,7′-dichlorofluorescein diacetate (DCFH-DA) as manufacturer's instructions. Briefly, at the end of treatment, DCFH-DA (10 μM) was added and incubated in the dark at 37°C for 30 min. Fluorescence was monitored by flow cytometry with excitation at 485 nm and emission at 530 nm. The results were expressed as intensity of DCF-fluorescence of the control group.

2.15. Statistical Analysis. Data are expressed as the mean ± S.E.M and were analyzed using SPSS (V13.0.0). Statistical comparisons between all groups were performed using One-Way Analysis of Variance (ANOVA), and post hoc comparisons between groups were completed using Tukey's test. $P < 0.05$ were considered statistically significant.

3. Results

3.1. Effects of Resveratrol on the Mortality and Rotarod Performance of Rats. The survival rate of rats in the R group was significantly decreased compared with that of the control group ($P < 0.01$). However, resveratrol pretreatment enhanced survival rate, which was statistically significant relative to that of the R group (Figure 1(a)). Additionally, as observed in Figures 1(b) and 1(c), all rats in the control group endured 80 s on the rotating rod without falling. However, rotenone treatment caused disturbance of motor coordination in rats. The duration of time maintaining balance walking on the top of the rod was decreased, and the number of rats unable to stand on the rotating rod even during the first set of trials was increased. However, resveratrol pretreatment decreased the disturbance of motor coordination, with the rate and duration of motion enhanced significantly. Therefore, resveratrol has a protective effect in the substantia nigra of rats subjected to rotenone-induced Parkinson's disease.

3.2. Effects of Resveratrol on the Viability, Apoptosis, and Morphology of PC12 Cells. Whether the viability of PC12 cells exposed to rotenone was protected by resveratrol pretreatment was investigated using CCK-8 Kits. The results showed that cell viability was significantly decreased in the rotenone-exposed group compared with that of the control group. However, resveratrol pretreatment of PC12 cells exposed to rotenone influenced viability in a concentration-dependent manner. In our experiment, at resveratrol concentrations of 1.0 μM and 5.0 μM, there was no difference in PC12 cell viability between the R group and the R + RSV group. When the concentration increased to 10.0 μM, 50 μM, and 60 μM, resveratrol demonstrated a statistically significant protective effect ($^{\#\#}P < 0.01$). However, the protective effect disappeared at a resveratrol concentration of 100.0 μM (Figure 2(a)).

The morphology of PC12 cells in the control group was similar to primary sympathetic neurons in shape, with an integral cell body and long processes. When PC12 cells were exposed to rotenone, the cells were damaged, the processes became shorter, and some of the cells became round and polygonal in shape. However, pretreatment of PC12 cells with resveratrol significantly influenced morphology and the processes appeared obviously longer compared to cells treated with rotenone alone (Figures 2(b), 2(c), and 2(d)).

To further confirm the apoptosis of rotenone, PC12 cells were incubated with Annexin V/PI and were analyzed by flow cytometry. As shown in Figure 2(e), the percentage of apoptotic cells was increased in the rotenone-exposed group compared with the control group, while the number of apoptotic cells was significantly decreased in the R + RSV group compared with that of the R group. Resveratrol could obviously alleviate rotenone-induced PC12 cell apoptosis (Figure 2(e)).

3.3. Effects of Resveratrol on Mitochondrial Mass and Mitochondrial Fission/Fusion. Mitochondrial mass was quantified using MitoTracker Green. Staining was typically observed in perinuclear regions and processes; the nucleus was typically devoid of staining (Figure 3(a)). MitoTracker Green demonstrated a statistically significant decrease in fluorescence intensity following treatment with rotenone. However, there was a small increase in the fluorescence intensity of PC12 cells pretreated with resveratrol compared to the rotenone-exposed group ($P < 0.05$) (Figure 3(b)). Furthermore, high definition images show that mitochondria of control group were filamentous with a tubular or thread-like appearance. In comparison, rotenone treatment led to a significant increase in the number of fragmented mitochondria with small ring-shapes. However, resveratrol reversed the morphological changes of mitochondria (Figure 3(a)). The cells showing 70% fragmented or intermediate mitochondria were classified as fragmented cells. The results showed that rotenone treatment led to a significant increase in the number of fragmented

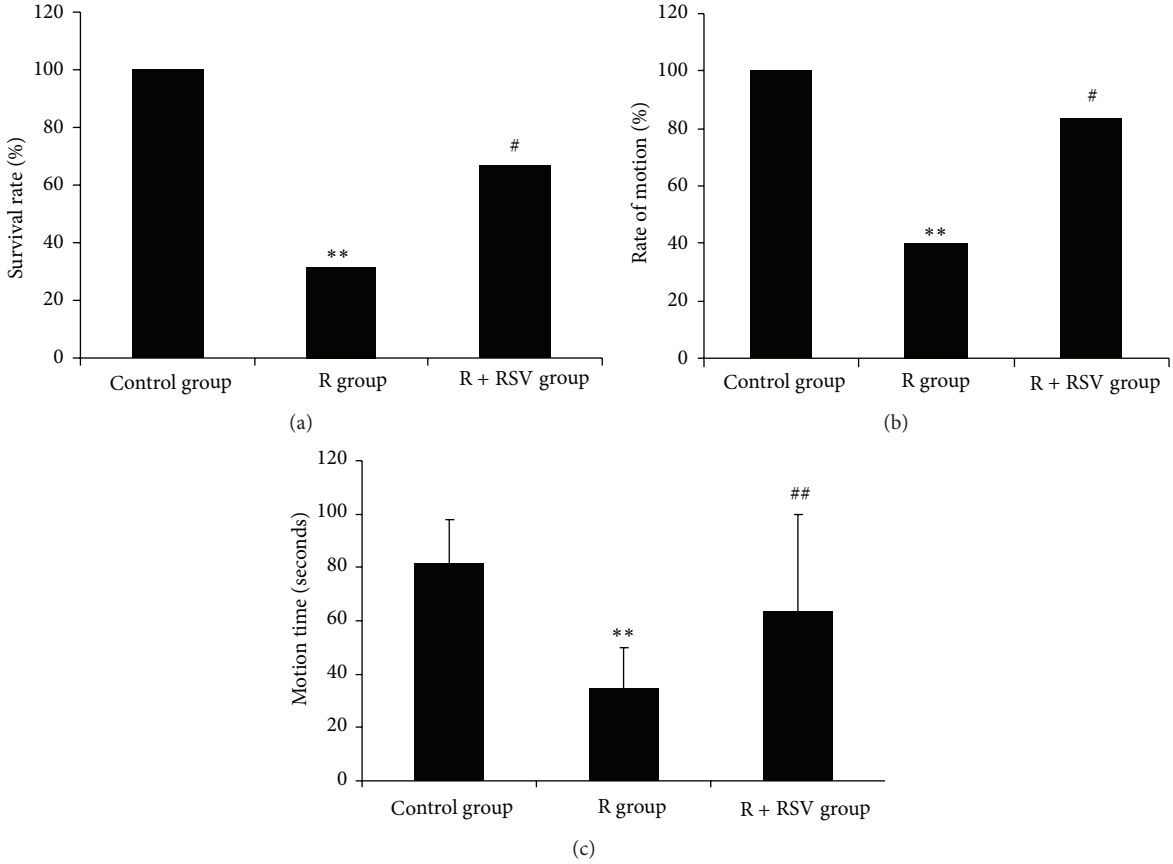

Figure 1: RSV improved survival rate and motor ability of rats decreased by rotenone. (a) The survival rate of rats in the R group is reduced significantly compared to the control, and resveratrol pretreatment significantly improves the survival rate of rats exposed to rotenone compared to the R group. (b) The rate of motion is decreased in rats exposed to rotenone; however, the rate of motion is significantly increased in rats pretreated with resveratrol. (c) Rotenone leads to a decrease in motion time, and resveratrol pretreatment improved the decrease in motion time induced by rotenone. The results are presented as the mean ± S.E.M. ($n = 20$/group for survival rate; $n = 6$/group for motion ability). $^{**}P < 0.01$ versus control group; $^{\#}P < 0.05$ versus R group; $^{\#\#}P < 0.01$ versus R group.

cells compared with control group. Resveratrol significantly reduced the number of fragmented cells compared with R group (Figure 3(c)).

The mitochondrial mass was determined by mitochondrial fission and fusion. Therefore, the regulating signals in mitochondrial fission and fusion were also investigated. The results showed that rotenone exposure induced an inhibition of mitochondrial fission and fusion, leading to a decrease in expression of both mRNA and protein levels of genes responsible for mitochondrial fission and fusion. However, resveratrol pretreatment could improve the ability of mitochondrial fission and fusion, by promoting expression of Drp1, Fis1, OPA1, and MFN2 mRNA and protein associated with mitochondrial fission and fusion (Figures 3(d), 3(e), 3(f), and 3(g)). Thus, resveratrol demonstrated a protective effect in mitochondria via enhanced mitochondrial fission and fusion ability.

3.4. Effects of Resveratrol on mtDNA Copy Number and the Expression and Transcriptional Activity of PGC-1α. Mitochondrial DNA (mtDNA) copy number is a critical component of overall mitochondrial health. The results showed that the relative mtDNA copy number was decreased significantly compared to that of the control group. When PC12 cells were pretreated with resveratrol, the mtDNA copy number increased compared to the mean value of the PC12 cells exposed to rotenone alone (Figure 4(f)).

Resveratrol-mediated increases in mitochondrial DNA copy number may be attributed to the promotion of mitochondrial fission and fusion. However, the increase may also be attained through the regulation of a number of transcriptional factors and cofactors. To assess whether resveratrol would enhance expression and activity of PGC-1α, we analyzed the transcription and protein level of the PGC-1α gene and its target gene mtTFA, which is directly involved in mitochondrial biogenesis. The results revealed a significant decrease in mRNA transcripts and protein levels of PGC-1α and in its downstream target gene (mtTFA) in rotenone-exposed rats (Figures 4(a) and 4(b)) and PC12 cells (Figures 4(c) and 4(d)) compared to the control groups. The results further confirmed that PGC-1α activity and transcriptional deregulation of its target gene were altered in rats and PC12 cells exposed to rotenone. Moreover, resveratrol pretreatment could reverse the inhibition of PGC-1α

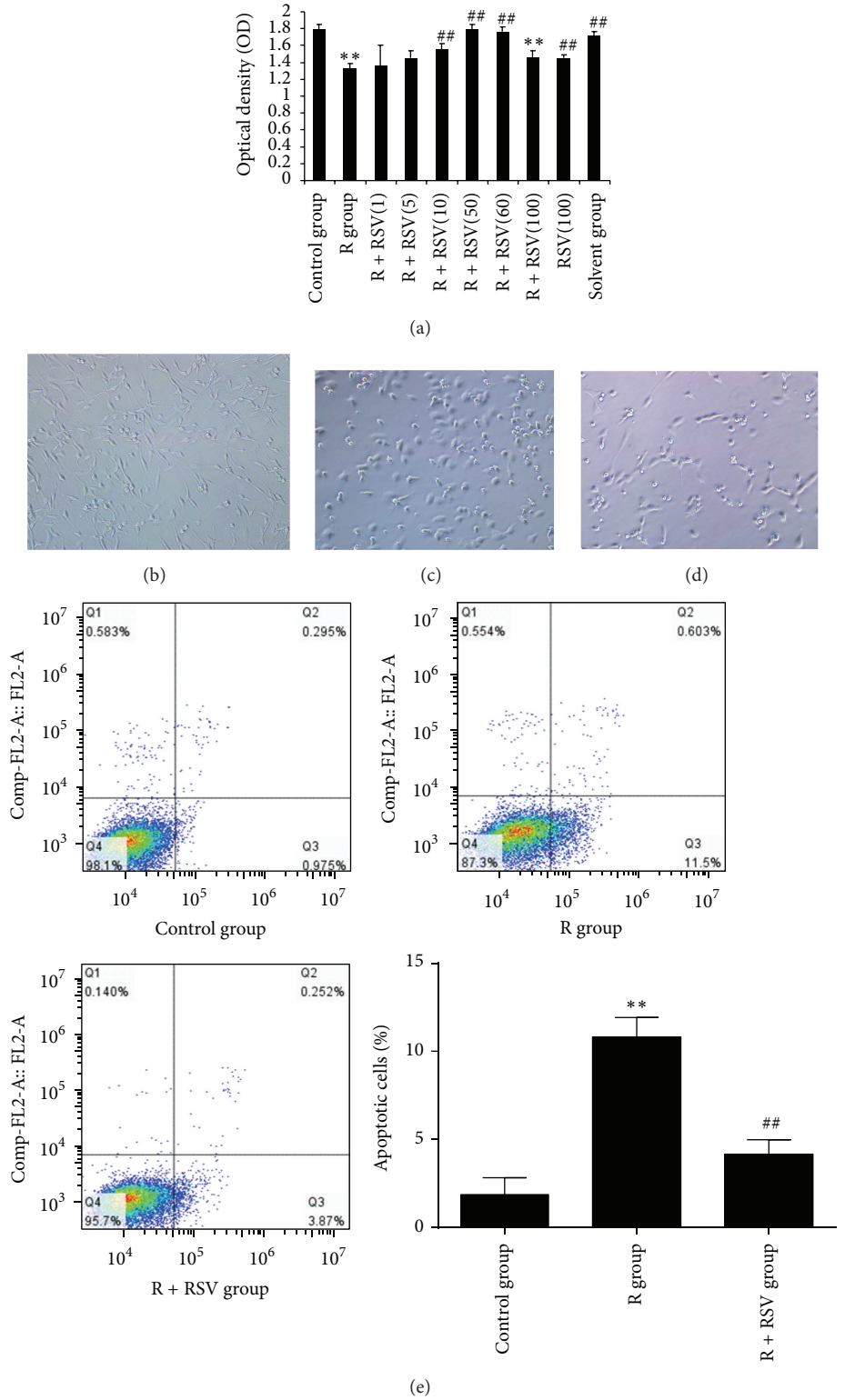

Figure 2: Effects of resveratrol on PC12 cell viability, apoptosis, and morphology. (a) The results show that rotenone induces a statistically significant decrease in cell viability. Resveratrol significantly relieves the damage to PC12 cells induced by rotenone within a concentration range (5–100 μM). When the concentration is under 5 μM, the protective effect is not significant. Protection is concentration-dependent; however, at a concentration of 100 μM, the protective effect of resveratrol on PC12 cell viability was decreased compared to 60 μM. (b) The normal (control) morphology of PC12 cells with long processes. (c) The processes of PC12 cells in the R group appear much shorter compared with that of the control group. (d) The injury to PC12 cell morphology was alleviated with resveratrol pretreatment. (e) Results show that rotenone induces an increase of cell apoptosis with statistical significance. Resveratrol pretreatment decreases the number of apoptotic cells induced by rotenone with significant difference. The results are presented as the mean ± S.E.M. $^{**}P < 0.01$ versus control group; $^{\#\#}P < 0.01$ versus R group.

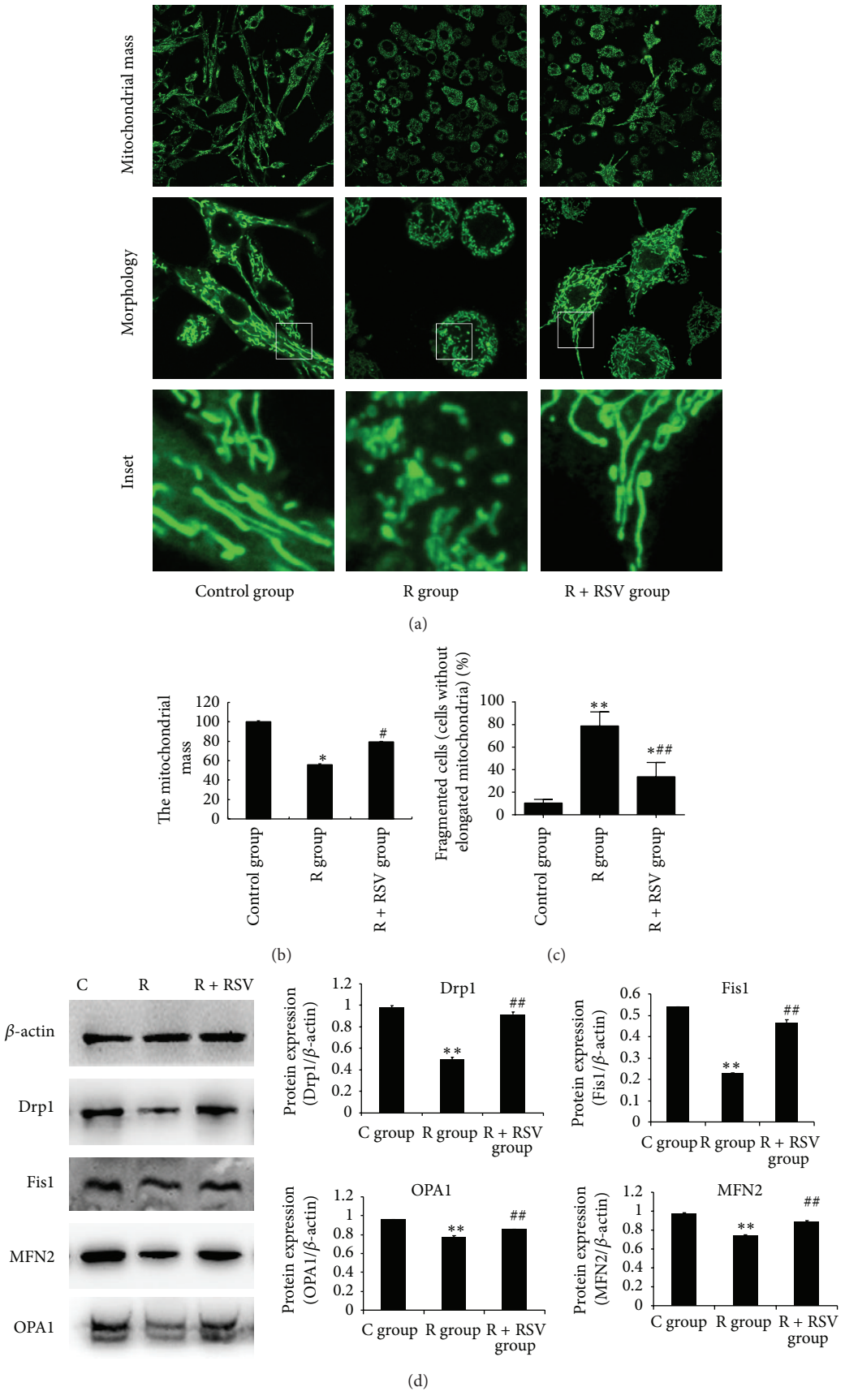

Figure 3: Continued.

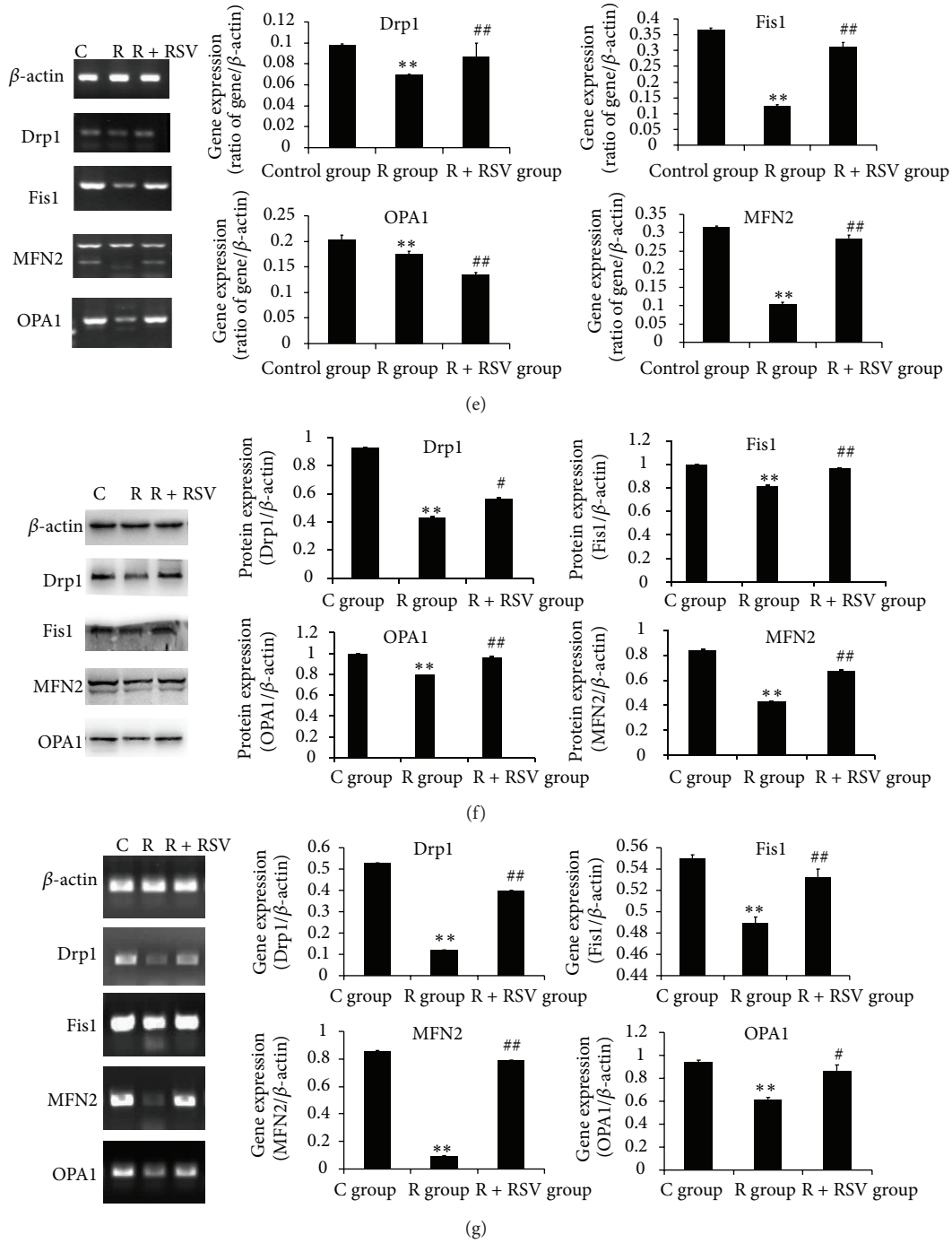

Figure 3: The protective effect of resveratrol against rotenone-induced mitochondrial fission and fusion in SD rats and PC12 cells. (a, b) The fluorescence intensity indicating mitochondrial mass was calculated and analyzed. The results show that rotenone induced a reduction in mitochondrial mass and an increase in the number of fragmented mitochondria with small ring-shapes compared with that in the control group. However, the decrease in mitochondrial mass and mitochondrial fragmentation is improved by resveratrol pretreatment of PC12 cells prior to rotenone exposure. (c) The number of fragmented cells is significantly increased in R group compared with that in control group. Resveratrol pretreatment significantly reduced the number of fragmented cells compared with R group. (d, e) In the in vivo model, the quantification analysis of Drp1. Fis1, OPA1, and MFN2 protein and mRNA levels involved in mitochondrial fission and fusion reveals a significant decrease in the R groups compared with the control group and an increase in the RSV-pretreated groups exposed to rotenone, showing resveratrol's protective effect in rotenone-induced neurotoxicity. (f, g) Protein and mRNA levels are reduced significantly following rotenone exposure in vitro, and resveratrol significantly increased expression compared to the control group. Representative immunoblots of proteins and electrophoretic bands of genes associated with mitochondrial fission and fusion. β-actin served as the internal control to normalize the amount of protein and mRNA. The results are presented as the mean ± S.E.M. The values were generated from three independent experiments. $^{*}P < 0.05$ versus control group; $^{**}P < 0.01$ versus control group; $^{\#}P < 0.05$ versus R group; $^{\#\#}P < 0.01$ versus R group.

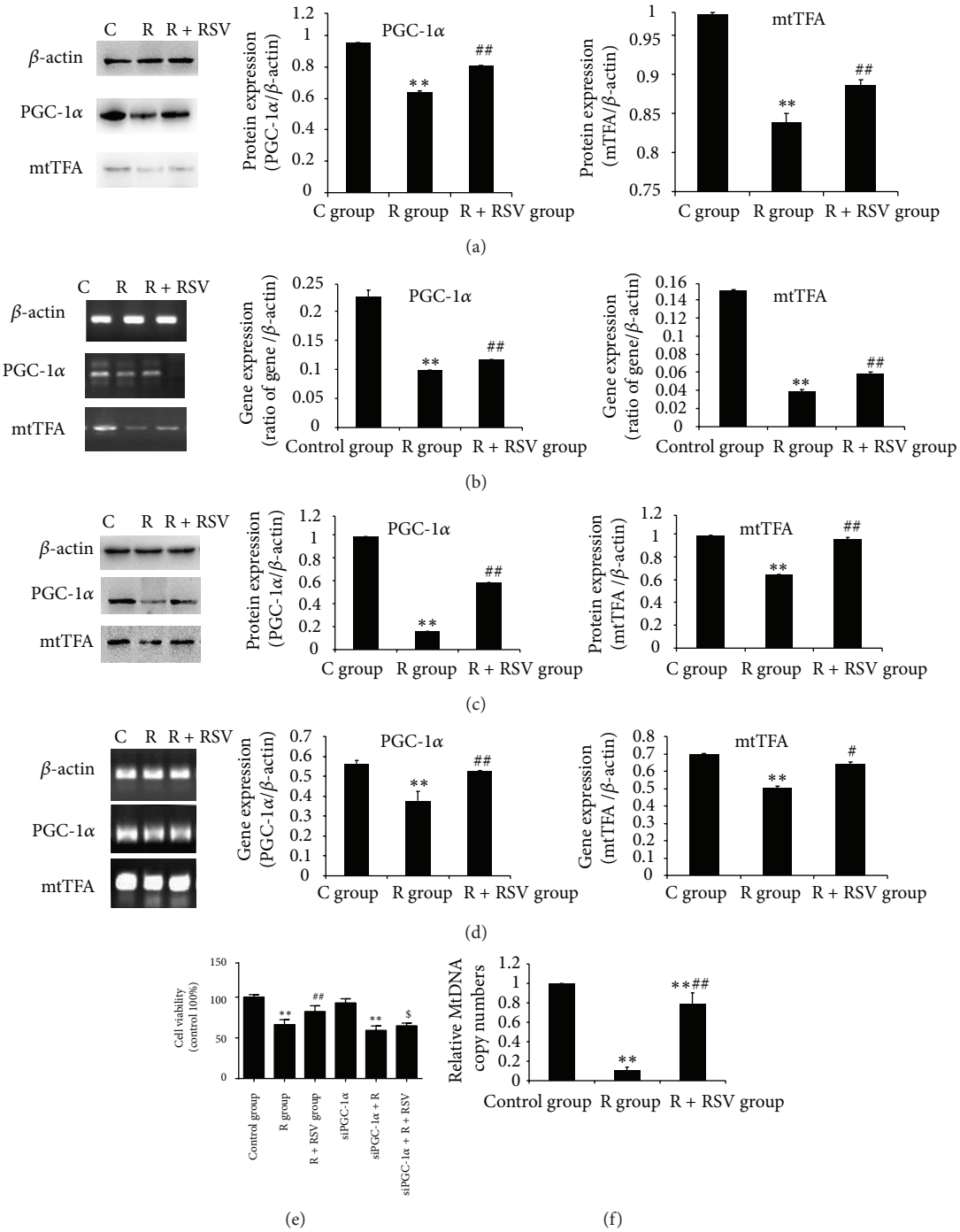

Figure 4: Resveratrol improves mitochondrial biogenesis inhibited by rotenone. Representative immunoblots of proteins and electrophoretic bands of genes involved in mitochondrial biogenesis. β-actin is used as an internal control to normalize the amount of proteins and mRNA. (a, b) In vivo model results show that protein and mRNA expression of PGC-1α and mtTFA are reduced in rotenone-exposed rats compared to the control group. Resveratrol pretreatment significantly increased protein and mRNA expression of PGC-1α and mtTFA, which were suppressed by rotenone treatment. (c, d) Western blot and RT-PCR analysis show that rotenone inhibited mitochondrial biogenesis in vitro and that resveratrol could relieve the suppression of the two proteins and genes. (e) Results show that rotenone induces a decrease of cell viability with statistical significance. Resveratrol restores the damage of PC12 cells induced by rotenone with significant difference. However, after all three treatments, there is no significant change in viability of PC12 cells with PGC-1α knocked down compared with that of wild PC12 cells. (f) The mitochondrial DNA copy number is significantly lower in the R group compared with that in the control group. Resveratrol significantly enhances mitochondrial DNA copy number in PC12 cells exposed to rotenone. The results are presented as the mean ± S.E.M. The values were generated from three independent experiments. $^{**}P < 0.01$ versus control group; $^{\#}P < 0.05$ versus R group; $^{\#\#}P < 0.01$ versus R group; $^{\$}P < 0.05$ versus R + RSV group.

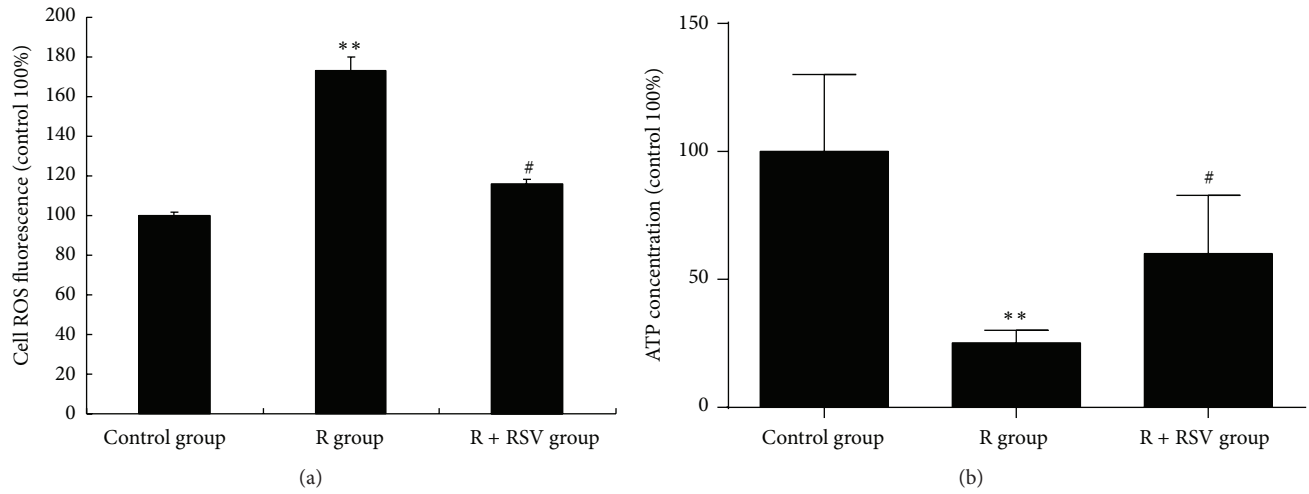

Figure 5: Effects of resveratrol pretreatment on ROS and ATP concentrations in PC12 cells exposed to rotenone. (a) ROS formation is induced in PC12 cells exposed to rotenone with high fluorescence intensity compared to the control group. Resveratrol pretreatment could significantly suppress ROS formation induced by rotenone. (b) Rotenone exposure leads to a significant reduction in the ATP concentration in PC12 cells. There was an increase in ATP concentration in PC12 cells with resveratrol pretreatment compared to the control group. The results are presented as the mean ± S.E.M. $^{**}P < 0.01$ versus control group; $^{\#}P < 0.05$ versus R group.

and mtTFA protein and mRNA expression caused by rotenone (Figure 4) To investigate the role of PGC-1α in resveratrol's protection in PC12 cells, PGC-1α were further knocked down. Results showed that the viability of PC12 cells was decreased significantly in siPGC-1α + R + RSV group compared with that of the R + RSV group (Figure 4(e)). It is indicated that PGC-1α downregulation seriously affected the protective effect of resveratrol on PC12 cell viability. Together, the results presented here indicate a resveratrol-mediated increase in PGC-1α transcriptional activity, as shown by the upregulation of its target gene. This not only was related to PGC-1α expression but also suggested a possible effect at a posttranslational level.

3.5. Effects of Resveratrol on ROS Formation and ATP Production. PGC-1α is a transcriptional coactivator known as the master regulator of mitochondrial functions and oxidative metabolism. Because resveratrol can promote the expression and activity of PGC-1α, we evaluated the role of resveratrol on oxidative stress and ATP production in PC12 cells exposed to rotenone. The results showed that the ROS level (Figure 5(a)) was increased and that ATP production (Figure 5(b)) was decreased significantly when PC12 cells were treated with rotenone compared with the control group. However, if PC12 cells were pretreated with resveratrol, the ROS production decreased (Figure 5(a)) and ATP production (Figure 5(b)) increased significantly compared with those of the R group. Therefore, resveratrol could reduce oxidative stress and promote ATP production in PC12 cells exposed to rotenone.

4. Discussion

Although the etiology of dopaminergic neuronal degeneration of PD remains unknown, mitochondrial dysfunction has been the focus of studies into the etiology of familial and sporadic PD [8]. Mitochondria are now known to constitute a population of organelles requiring careful balance and integration of numerous processes, including fission-fusion machinery, the regulation of biogenesis, migration throughout the cell, shape remodeling, and autophagy [15, 23–25].

Here, we used in vitro and in vivo PD models to show rotenone-induced loss of dopaminergic neurons and oxidative damage in mitochondria, decreases in mitochondrial mass and mitochondrial DNA copy number, and increases in impaired mitochondrial fission/fusion and biogenesis. Thus, we concluded that rotenone exposure leads to dopaminergic neurodegeneration, which is associated with an imbalance of mitochondrial homeostasis and organelle damage.

In the present study, we also have demonstrated that resveratrol could significantly ameliorate the motor dysfunction and attenuate the damage of substantia nigra dopaminergic-induced Parkinson's disease rats. It is known that a decrease in athletic ability is positively correlated with the damage of dopaminergic neurons in the substantia nigra. Thus, it is suggested that resveratrol pretreatment has a protective effect on dopaminergic neurons in rat substantia nigra. Furthermore, the study also showed that resveratrol treatment could significantly relieve rotenone-induced increases in ROS and improve rotenone-induced decreases in ATP production in PC12 cells. All of these data provide a mechanistic basis for resveratrol in the clinical treatment of Parkinson's disease. Thus, the potential application of resveratrol in the treatment of Parkinson's disease deserves further investigation.

Therefore, combined with other unpublished results collected by our lab, we have explored the effects of resveratrol on mitochondrial fission/fusion and biogenesis of dopamine neurons in rats and PC12 cells exposed to rotenone. It is known that PGC-1α and mtTFA are two key signaling factors regulating mitochondrial biogenesis, which has been

confirmed in many other studies [26, 27]. Our results showed that rotenone suppressed the expression of PGC-1α and mtTFA. However, resveratrol pretreatment could obviously improve mRNA and protein expression of PGC-1α and mtTFA in the substantia nigra and in PC12 cells, which was inhibited by rotenone. In addition, we further used PGC-1α siRNA to knock down its expression to explore whether the effect of resveratrol on cell viability is affected. Results showed that cell viability was affected, which proved that resveratrol protection in cells induced by rotenone might be associated with PGC-1α. Therefore, a decrease in mitochondrial DNA copy number and mitochondrial mass in rotenone-induced neurotoxicity could be the result of a reduction of mitochondrial biogenesis. Inhibition of mitochondrial biogenesis may contribute to the development of rotenone-induced neurotoxicity. Furthermore, resveratrol could prevent rotenone-induced neurotoxicity by promoting mitochondrial biogenesis. In addition, OPA1, MFN2, Drp1, and Fis1 proteins were involved in regulating mitochondrial fission and fusion [28]. Our results further showed that rotenone could result in a decrease in OPA1, MFN2, Drp1, and Fis1 expression, leading to dysfunction in mitochondrial fission/fusion. The dysfunction in mitochondrial fission and fusion promoted a decrease in mitochondrial mass, which may further promote increased ROS formation and decreased ATP production in rotenone-induced neurotoxicity. In our experiments, the dysfunction of mitochondrial fission and fusion could be alleviated with resveratrol pretreatment through improving the expression of OPA1, MFN2, Drp1, and Fis1, which were inhibited by rotenone. Thus, the observed resveratrol-mediated increase in mitochondrial fusion likely acted to increase mitochondrial DNA copy number and mitochondrial mass, which were inhibited by the mitochondrial complex I inhibitor rotenone. We conclude that resveratrol likely increased mitochondrial fusion, not solely through increased mitochondrial biogenesis, to increase mitochondrial DNA copy number and mitochondrial mass to maintain mitochondrial homeostasis. Thus, the neuroprotective effects of resveratrol on rotenone-induced neurotoxicity were mediated through regulation of mitochondrial fission/fusion and biogenesis. Similar results were obtained in a recent study that demonstrated that MPTP increased vulnerability with aging by the mechanisms underlying mitochondrial dynamics [29]. Therefore, these data suggested that resveratrol alleviation of rotenone-induced damage of dopaminergic neurons could be mediated through regulating the balance of mitochondrial dynamics.

It is worth noting that despite using higher doses than the present study, resveratrol was reported to have no protective effects on rotenone-induced apoptosis in SH-SY5Y cells in a previous study [30]. First, we postulated that the difference in protective effects may be related to the use of different cell lines. Through further analysis, we found that SH-SY5Y cells were pretreated with resveratrol for 1 h prior to rotenone exposure, as opposed to 24 h in our study. Furthermore, a paper published recently also reported that resveratrol had protective effects in SH-SY5Y cells following 24 h pretreatment by inducing treatment-dependent autophagy [31]. Thus, a sufficient pretreatment time is required to enable expression of critical neuroprotective genes and proteins. In addition to sufficient time, based on our experiments, the protection by resveratrol on the viability of PC12 cells exposed to rotenone is more likely confined to a concentration range. In support of this hypothesis, we demonstrated that increased fission/fusion and biogenesis protein expression in response to resveratrol conferred neuroprotective effects in a concentration- and time-dependent manner. Therefore, our results demonstrated that resveratrol attenuated rotenone-induced neurotoxicity through increased mitochondrial biogenesis and maintained the balance of mitochondrial fission and fusion, which may limit ROS production and promote ATP content and thereby acted as a protective agent in rotenone-induced neuronal toxicity.

Mitochondrial fission/fusion and biogenesis are dynamic processes, which regulate mitochondrial homeostasis [15]. Recently, mitochondrial fission/fusion and biogenesis dysfunction have been linked to PD development [8, 15]. Mitochondrial fission/fusion and biogenesis are active at a basal level in most cells in the body. The processes not only determine the structure of the entire mitochondrial population but also influence nearly every aspect of mitochondrial function, thereby acting as a protective mechanism in cells [32–34]. Herein, we provided evidence that resveratrol induced PGC-1α and mtTFA expression to augment mitochondrial biogenesis and influence OPA1/MFN2 and Fis1/Drp1 expression to regulate the balance of mitochondrial fission/fusion, thus maintaining mitochondrial homeostasis and preventing rotenone-induced neuronal degeneration. Of course, we could not exclude mitophagy, also regulating the mitochondrial homeostasis, which we should do some work on in the future. Furthermore, resveratrol attenuated rotenone-induced intracellular ROS generation, which also corresponded to increased ATP production. This study provides novel insight into the cellular mechanisms of resveratrol in preventing neurodegeneration and elucidates potential downstream targets for future therapeutic strategies.

Conflict of Interests

The authors declare no conflict of interests.

Acknowledgments

This work was supported by grants from the NSFC (Natural Science Foundation of China) (81473006, 81273106) to Yan Sai and the Natural Science Foundation of Chongqing (cstc2012jjA10028) to Yan Sai.

References

[1] J. Blanchet, F. Longpré, G. Bureau et al., "Resveratrol, a red wine polyphenol, protects dopaminergic neurons in MPTP-treated mice," *Progress in Neuro-Psychopharmacology & Biological Psychiatry*, vol. 32, no. 5, pp. 1243–1250, 2008.

[2] R. Pangeni, J. K. Sahni, J. Ali, S. Sharma, and S. Baboota, "Resveratrol: review on therapeutic potential and recent advances in drug delivery," *Expert Opinion on Drug Delivery*, vol. 11, no. 8, pp. 1285–1298, 2014.

[3] V. W. Dolinsky, A. Y. M. Chan, I. R. Frayne, P. E. Light, C. Des Rosiers, and J. R. B. Dyck, "Resveratrol prevents the prohypertrophic effects of oxidative stress on LKB1," *Circulation*, vol. 119, no. 12, pp. 1643–1652, 2009.

[4] K.-F. Hsu, C.-L. Wu, S.-C. Huang et al., "Cathepsin L mediates resveratrol-induced autophagy and apoptotic cell death in cervical cancer cells," *Autophagy*, vol. 5, no. 4, pp. 451–460, 2009.

[5] M. Lagouge, C. Argmann, Z. Gerhart-Hines et al., "Resveratrol improves mitochondrial function and protects against metabolic disease by activating SIRT1 and PGC-1alpha," *Cell*, vol. 127, no. 6, pp. 1109–1122, 2006.

[6] D. D. Lofrumento, G. Nicolardi, A. Cianciulli et al., "Neuroprotective effects of resveratrol in an MPTP mouse model of Parkinson's-like disease: possible role of SOCS-1 in reducing pro-inflammatory responses," *Innate Immunity*, vol. 20, no. 3, pp. 249–260, 2014.

[7] F. Jin, Q. Wu, Y.-F. Lu, Q.-H. Gong, and J.-S. Shi, "Neuroprotective effect of resveratrol on 6-OHDA-induced Parkinson's disease in rats," *European Journal of Pharmacology*, vol. 600, no. 1–3, pp. 78–82, 2008.

[8] J.-H. Shin, V. L. Dawson, and T. M. Dawson, "SnapShot: pathogenesis of Parkinson's disease," *Cell*, vol. 139, no. 2, pp. 440.e1–440.e2, 2009.

[9] C. Perier, J. Bové, M. Vila, and S. Przedborski, "The rotenone model of Parkinson's disease," *Trends in neurosciences*, vol. 26, no. 7, pp. 345–346, 2003.

[10] C. M. Tanner, F. Kame, G. W. Ross et al., "Rotenone, paraquat, and Parkinson's disease," *Environmental Health Perspectives*, vol. 119, no. 6, pp. 866–872, 2011.

[11] A. Spivey, "Rotenone and paraquat linked to Parkinson's disease: human exposure study supports years of animal studies," *Environmental Health Perspectives*, vol. 119, no. 6, article A259, 2011.

[12] A. Abeliovich, "Parkinson's disease: mitochondrial damage control," *Nature*, vol. 463, no. 7282, pp. 744–745, 2010.

[13] J. R. Friedman and J. Nunnari, "Mitochondrial form and function," *Nature*, vol. 505, no. 7483, pp. 335–343, 2014.

[14] J. Nunnari and A. Suomalainen, "Mitochondria: in sickness and in health," *Cell*, vol. 148, no. 6, pp. 1145–1159, 2012.

[15] D. C. Chan, "Mitochondria: dynamic organelles in disease, aging, and development," *Cell*, vol. 125, no. 7, pp. 1241–1252, 2006.

[16] L. Cui, H. Jeong, F. Borovecki, C. N. Parkhurst, N. Tanese, and D. Krainc, "Transcriptional repression of PGC-1alpha by mutant huntingtin leads to mitochondrial dysfunction and neurodegeneration," *Cell*, vol. 127, no. 1, pp. 59–69, 2006.

[17] M. Milone, "Mitochondria, diabetes, and Alzheimer's disease," *Diabetes*, vol. 61, no. 5, pp. 991–992, 2012.

[18] R. Wang, Y. Y. Liu, X. Y. Liu et al., "Resveratrol protects neurons and the myocardium by reducing oxidative stress and ameliorating mitochondria damage in a cerebral ischemia rat model," *Cellular Physiology and Biochemistry*, vol. 34, no. 3, pp. 854–864, 2014.

[19] J. S. Franzone and M. C. Reboani, "Stimulating action of hematoporphyrin on motor coordination and resistance to fatigue in rats," *Archivio per le Scienze Mediche*, vol. 134, no. 4, pp. 403–406, 1977.

[20] J. F. Buckman, H. Hernandez, G. J. Kress, T. V. Votyakova, S. Pal, and I. J. Reynolds, "MitoTracker labeling in primary neuronal and astrocytic cultures: influence of mitochondrial membrane potential and oxidants," *Journal of Neuroscience Methods*, vol. 104, no. 2, pp. 165–176, 2001.

[21] M. Agnello, G. Morici, and A. M. Rinaldi, "A method for measuring mitochondrial mass and activity," *Cytotechnology*, vol. 56, no. 3, pp. 145–149, 2008.

[22] L. F. Marques-Santos, J. G. P. Oliveira, R. C. Maia, and V. M. Rumjanek, "Mitotracker green is a P-glycoprotein substrate," *Bioscience Reports*, vol. 23, no. 4, pp. 199–212, 2003.

[23] S. Hoppins and J. Nunnari, "Mitochondrial dynamics and apoptosis—the ER connection," *Science*, vol. 337, no. 6098, pp. 1052–1054, 2012.

[24] M. O. Dietrich, Z.-W. Liu, and T. L. Horvath, "Mitochondrial dynamics controlled by mitofusins regulate Agrp neuronal activity and diet-induced obesity," *Cell*, vol. 155, no. 1, pp. 188–199, 2013.

[25] Y. Tamura, K. Itoh, and H. Sesaki, "SnapShot: mitochondrial dynamics," *Cell*, vol. 145, no. 7, pp. 1158–1158.e1, 2011.

[26] Z. Wu, P. Puigserver, U. Andersson et al., "Mechanisms controlling mitochondrial biogenesis and respiration through the thermogenic coactivator PGC-1," *Cell*, vol. 98, no. 1, pp. 115–124, 1999.

[27] L. Z. Agudelo, T. Femenia, F. Orhan et al., "Skeletal muscle PGC-1α1 modulates kynurenine metabolism and mediates resilience to stress-induced depression," *Cell*, vol. 159, no. 1, pp. 33–45, 2014.

[28] R. J. Youle and A. M. van der Bliek, "Mitochondrial fission, fusion, and stress," *Science*, vol. 337, no. 6098, pp. 1062–1065, 2012.

[29] N. Jiang, H. Bo, C. Song et al., "Increased vulnerability with aging to MPTP: the mechanisms underlying mitochondrial dynamics," *Neurological Research*, vol. 36, no. 8, pp. 722–732, 2014.

[30] G. Filomeni, I. Graziani, D. De Zio et al., "Neuroprotection of kaempferol by autophagy in models of rotenone-mediated acute toxicity: possible implications for Parkinson's disease," *Neurobiology of Aging*, vol. 33, no. 4, pp. 767–785, 2012.

[31] T.-K. Lin, S.-D. Chen, Y.-C. Chuang et al., "Resveratrol partially prevents rotenone-induced neurotoxicity in dopaminergic SH-SY5Y cells through induction of heme oxygenase-1 dependent autophagy," *International Journal of Molecular Sciences*, vol. 15, no. 1, pp. 1625–1646, 2014.

[32] D. M. Arduíno, A. R. Esteves, and S. M. Cardoso, "Mitochondrial fusion/fission, transport and autophagy in Parkinson's disease: when mitochondria get nasty," *Parkinson's Disease*, vol. 2011, Article ID 767230, 13 pages, 2011.

[33] B. Westermann, "Mitochondrial fusion and fission in cell life and death," *Nature Reviews Molecular Cell Biology*, vol. 11, no. 12, pp. 872–884, 2010.

[34] B. Westermann, "Bioenergetic role of mitochondrial fusion and fission," *Biochimica et Biophysica Acta: Bioenergetics*, vol. 1817, no. 10, pp. 1833–1838, 2012.